University of Novi Sad
FACULTY OF TECHNICAL SCIENCES
DEPARTMENT OF PRODUCTION ENGINEERING
21000 NOVI SAD, Trg Dositeja Obradovica 6, SERBIA

UDK 621 ISSN 1821-4932

JOURNAL OF

PRODUCTION ENGINEERING

Volume 19 Number 1

Novi Sad, June 2016

Journal of Production Engineering, Vol.19 (2016), Number 1

Publisher: FACULTY OF TECHNICAL SCIENCES
DEPARTMENT OF PRODUCTION ENGINEERING
21000 NOVI SAD, Trg Dositeja Obradovica 6
SERBIA

Manuscript submitted for publication: June 30, 2016.
Printing: 1st
Circulation: 300 copies

CIP classification:

CIP – Катаголизација у публикацији
Библиотека Матице српске, Нови Сад

621

JOURNAL of Production Engineering / editor in chief Pavel Kovač. – Vol. 12, No. 1 (2009)- . – Novi Sad : Faculty of Technical Sciences, Department for Production Engineering, 2009-. – 30 cm

Dva puta godišnje (2012-). Je nastavak: Časopis proizvodno mašinstvo = ISSN
0354-6446
ISSN 1821-4932

Printing by: FTN, Graphic Center ***GRID,*** *Novi Sad*

ISSN: 1821-4932

INTERNATIONAL EDITORIAL BOARD

Editorial

The ***Journal of Production Engineering*** *dates back to 1984, when the first issue of the* ***Proceedings of the Institute of Production Engineering*** *was published in order to present its accomplishments. In 1994, after a decade of successful publication, the Proceedings changed the name into Production Engineering, with a basic idea of becoming a Yugoslav journal which publishes original scientific papers in this area.*

In 2009 year, our Journal finally acquires its present title - ***Journal of Production Engineering****. To meet the Ministry requirements for becoming an international journal, a new international editorial board was formed of renowned domestic and foreign scientists, refereeing is now international, while the papers are published exclusively in English. From the year 2011 Journal is in the data base COBISS and KoBSON presented.*

The Journal is distributed to a large number of recipients home and abroad, and is also open to foreign authors. In this way we wanted to heighten the quality of papers and at the same time alleviate the lack of reputable international and domestic journals in this area.

In this journal are published, reviewed papers from International Conference "MMA 2015" which was in Novi Sad, Serbia and certain number of new scientific papers as well.

Editor in Chief

Professor Pavel Kovač, PhD,

Journal of Production Engineering
Vol.19 No.1

Contents

REVIEW PAPER

ORIGINAL SCIENTIFIC PAPER

Journal of Production Engineering
Vol.19 No.1
JPE (2016) Vol. 19 (1) Review Paper
Gostimirović, M. , Kovač, P., Sekulić, M., Rodić, D., Pucovsky, V.

MACHINING CHARACTERISTICS OF ELECTRICAL DISCHARGE MACHINING – A REVIEW

Received: 10 January 2016 / Accepted: 22 April 2016

Abstract: *In electrical discharge machining (EDM) the machining characteristics of the process directly depend on the discharge energy which is transformed into heat in the machining area. The generated thermal energy leads to high temperatures which result in local melting and evaporation of workpiece material. However, the high temperature also impacts various physical and chemical properties of tool and workpiece. Process parameters and machining characteristics of EDM are identified in this paper. Based on the previous investigations, an analytical dependence was established between the parameters of discharge energy and technological performance. In addition, properties of discharge energy were experimentally investigated and their influence on productivity, accuracy and quality of EDM was established. Mathematical and experimental researches conducted in this paper allow development of intelligent modeling approaches for efficient selection of relevant parameters of EDM discharge energy. The results obtained represent a technological knowledge base for the selection of optimal conditions of EDM process.*
Key words*: EDM, machining parameters, technological performance, modeling, optimization*

Pregled tehnoloških karakteristika procesa elektroerozivne obrade. *Kod elektroerozivne obrade (EDM) tehnološke karakteristike procesa direktno zavise od energije pražnjenja koja se u zoni obrade pretvara u toplotu. Generisana toplotna energija dovodi do pojave ekstremno visokih temperatura usled čega dolazi do trenutnog rastapanja i isparavanja lokalnog dela materijala obratka. Međutim, visoka temperatura istovremeno uslovljava i niz fizičko-hemijskih promena u površinskom sloju materijala alata i obratka. U ovom radu se sistematizuju parametri obrade i tehnološke karakteristike EDM procesa. Na osnovu prethodnih istraživanja, uspostavljena je analitička zavisnost između parametara energije pražnjenja i tehnoloških pokazatelja procesa. Pored toga, eksperimentalno su istražene specifičnosti energije pražnjenja i njihov uticaj na proizvodnost, tačnost i kvalitet EDM obrade. Sprovedena matematička i eksperimentalna istraživanja omogućila su razvoj inteligentnog modela i pristupa za efikasnu selekciju relevantnih parametara EDM energije pražnjenja. Tako dobijeni rezultati predstavljaju adekvatnu tehnološku bazu znanja pri izboru optimalnih uslova procesa elektroerozivne obrade.*
Ključne reči*: elektroerozivna obrada, parametri obrade, tehnološki pokazatelji procesa, modeliranje, optimizacija*

1. INTRODUCTION

Modern manufacturing is facing complex demands on a daily basis. Manufacturing flexibility, productivity and quality are the most vital demands facing the market oriented industrial systems. Only modern equipped industrial systems will be able to adjust their manufacturing process to these high market demands. In this context, there can be little doubt that the machining processes shall remain important integral part of the technological process of product manufacturing and assembly. Basic advantages of machining process are high technological performance (efficiency, precision and quality) with the ability to cope with hard materials and complex surfaces [1-4].

On the basis of the current research and future projections, one can expect increased application of electrical discharge machining (EDM) in comparison with others available conventional and non-conventional machining processes [5-7]. EDM is one of the most important non-conventional machining processes that is used for complex machining of many different classes of electrically conductive materials, regardless of their physical and metallurgical properties [8].

Clearly, the benefits of EDM are considerable. It is often appropriate to EDM instead of using conventional machining processes, but not always, because the EDM has certain technological drawbacks. EDM process includes machining of materials that offers minimum 0,01 S/cm of electrical conductivity [9]. Productivity is relatively low compared to conventional machining. Tool wear affects the accuracy of the machined features. The machining accuracy of the EDM is limited to about ±0.001 mm. Minimum surface roughness average is about 0,1 μm. EDM induces thermal stress in machined surfaces. Surface integrity can be as good as or better than a ground surface [10,11].

2. BASICS OF ELECTRICAL DISCHARGE MACHINING

The origin of electrical discharge machining goes back to 1770, when J. Priestly discovered the effect of

electrical discharges. In 1943, B. Lazarenko and N. Lazarenko have developed the controlled EDM process for machining materials. The evolution of EDM since the 1970 was due to the numerical control, powerful generators, new wire tool electrodes, improved machine intelligence and better technological aspects. In recent times, the incorporation of EDM within a computer integrated manufacturing resulting in significantly reduced machining costs and competitiveness.

The EDM is basically a complex process which is based on periodical transformation of electrical energy into thermal energy [12-14]. Thermoelectric energy is created between the tool and workpiece with the passage of electric current. Both the tool and workpiece electrode materials have to be conductors of electricity and submerged in a dielectric fluid. A specific small gap is maintained between the tool and the workpiece. A power supply controls the timing and intensity of the electrical discharges and the movement of the tool in relation to the workpiece. Shown in Fig. 1 is schematically the basic working principle of EDM, input process parameters (workpiece, tool, machine and dielectric) and output technological performances (productivity, machining accuracy and surface integrity).

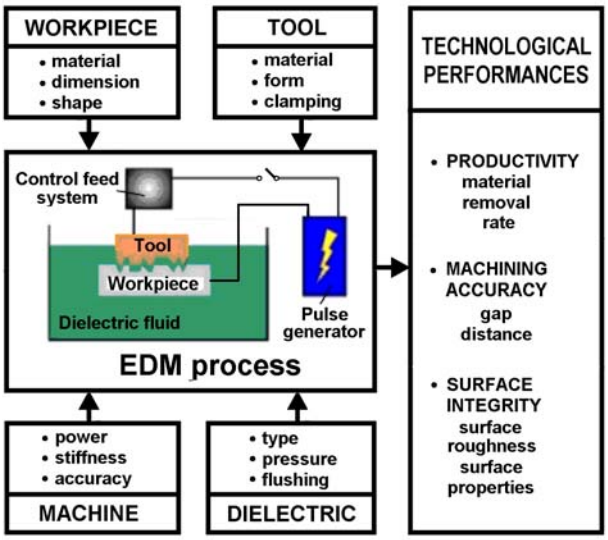

Fig.1. EDM process with machining characteristics

2.1 Working principle of EDM process

The working principle of EDM process is based on a series of non-stationary electrical discharge which remove material from a workpiece [15,16]. Material removal rate occurs at the spot where the electric field is strongest. Upon establishing the voltage, a strong magnetic field is established between the tool and workpiece (ignition phase). Due to attractive force of the magnetic field, at the shortest local distance between the tool and workpiece there is a build-up of particles from the machining process which float in the dielectric fluid. This forms the electrical circuit and the electrons begin to move towards the positively charged electrode. On their way, the accelerated electrons collide with the neutral particles from the machining process and the dielectric fluid. There is a chain reaction in which a large number of negative and positive ions are generated (discharge phase). The ionization initiates creation of electro-conductive zone between the workpiece and tool, thus causing electrical discharge. In electrical discharge, electrical energy is transformed into thermal energy. A discharge zone is formed at temperatures as high as 40.000 °C. Such high temperature cause local heating, melting, evaporation, and incineration of workpiece material. High temperatures also produce lower machining quality, tool wear, thermal dilatations, etc. The disruption of current supply annihilates the discharge zone, causing abrupt cooling which results in an explosive flushing of melted matter and solid particles off the workpiece surface (ejection phase). Fig. 2 shows a single electrical discharge of the EDM process with electrical pulse parameters [17,18].

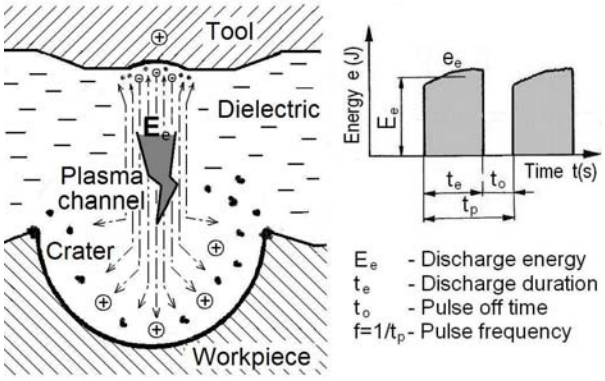

Fig. 2. Mechanism of a single discharge in EDM

Between the periodical discharges there is a deionization of dielectric liquid and the products of machining are evacuated from the work zone. This process provides stability of pulse discharge by preventing the continuous current flow and generation of electric arc or a short circuit.

During an electrical discharge there are the voltage and current pulses which vary in time, Fig. 2. Electrical pulses are interdependent, and are determined by following parameters: U_e – discharge voltage, I_e – discharge current, t_e – discharge duration, t_o – pulse off time and t_p – pulse cycle time. The derived parameters are: $E_e=U_e \cdot I_e \cdot t_e$ – discharge energy, $f=1/t_p$ – pulse frequency and $\tau=t_e/t_p$ – duty factor.

The most important parameter of EDM is the discharge energy. The discharge energy is the mean value of electric parameter which is transformed into heat during discharge. It is directly influenced by the characteristics of electric pulses. Their influences are interconnected and depend on the rest of the machining parameters [19,20].

The discharge voltage depends on the paired electrode materials and machining conditions. It ranges between 15 and 30 V [21]. For proper machining conditions, electrical discharge occurs instantaneously and is independent from other electrical pulse parameters. Therefore, the most important electrical pulse parameters of EDM are discharge current and discharge duration. However, the impact of discharge current is limited by the tool surface which is

interfacing the workpiece, i.e. the current density [22,23]. In case when the current density oversteps the limit for the given machining conditions, the process of deionization of the discharge zone deteriorates, thus reducing the efficiency of EDM. The independent regulation of the discharge duration is also limited. It is known from experience that discharge duration must be limited for a particular discharge current. Otherwise, an electrical arcing occurs which damages both tool and workpiece.

Besides the electric parameters described above, the polarity (±) of electrodes, has important effects on the EDM results. The polarity can be either positive or negative and it depends on tool material, workpiece material, current density and discharge duration. Because the plasma channel is made of ion and electron flows, and electrons have mass smaller than anions, for that reason electrode polarity is usually positive, allowing attaining good material removal rate and the minimum relative tool wear ratio [24,25].

2.2 Machining characteristics

Similar to other machining processes, the most important EDM machining characteristics are: productivity, machining accuracy and surface integrity, Fig. 1. Productivity is expressed as the material removal rate and refers to how fast is workpiece material removed per time unit. Machining accuracy is defined by tolerances on dimension and shape of the workpiece. Surface integrity is expressed through surface roughness and surface layer properties. The importance of machining performance is relative and depends on machining conditions and the desired function of parts. Together with machining costs, productivity determines the overall cost-effectiveness of the machining process, while accuracy and quality impact the functional value of product.

The material removal process in EDM is associated with the erosive effects which occur as a result of an extremely high temperature due to the high intensity of discharge energy through the plasma channel, Fig. 2. The material removal rate and the surface integrity correspond to the adjusted crater profile that is defined through the radius. The crater radius is assumed to be a function of discharge energy [17,26,27].

Now it can be logically assumed that the material removed volume of a single electric pulse would be proportional to the discharge energy:

$$V_e = C_V \cdot E_e \tag{1}$$

where C_V is the constant that depends on the workpiece material.

The material removal rate represents the average volume of material removed over the machining time and there follows the expression for material removal rate:

$$V_w = V_e \cdot f = C_V \cdot U_e \cdot I_e \frac{t_e}{t_e + t_o} \tag{2}$$

On the other hand, the material removal in a single pulse discharge is determined by computing the volume of the crater, under the assumption of hemispherical shape with a radius equal to R_{max}:

$$V_e = \frac{2}{3}\pi \cdot R_{\max}^3 \tag{3}$$

In Eq (3), R_{max} is defined as the maximum surface roughness observed over maximum height of irregularities.

From the Eq. (3) also using Eq. (1), one derives expression for maximum height of irregularities:

$$R_{\max} = \left(\frac{3}{2\pi} C_V \cdot E_e \right)^{1/3} \tag{4}$$

In practice, the surface quality is defined over the surface roughness $R_a \cong R_{max}/4$. The surface roughness is defined as the arithmetic average deviation of the assessed profile (ISO 4287).

Theoretically, dependence of the gap distance and the discharge energy is given by equation:

$$a_e = C_a \cdot E_e^m \tag{5}$$

where C_a and m are the constants that depend on the machining conditions.

2.3 Different types of EDM

EDM system comes in two basic types (Fig. 3): die-sinking and wire-cut. Die-sinking EDM, also known as ram EDM or standard EDM, is the oldest form of EDM machining. The wire-cut EDM, also known as WEDM or spark EDM**,** is controlled by CNC following the assigned geometry for the part to be produced [5-7,28,29].

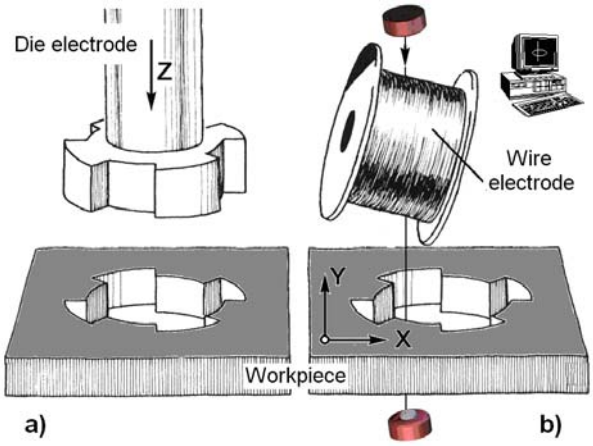

Fig.3. Different types of EDM
a) Die-sinking EDM, b) Wire-cut EDM

Die-sinking EDM reproduces the shape of the tool into the part or assembly. Die-sinking EDM are generally used for complex geometries where the machine uses a shaped graphite or copper electrode. Many die-sinking EDM machine with CNC control, can rotate the electrodes around more axis allowing machining of internal cavities. This makes die-sinking EDM a highly capable manufacturing process.

In wire-cut EDM a wire electrode is used to cut a programmed outline into the workpiece. Wire-cut EDM is used for shapes cutout of a flat sheet or plate. With a

wire-cut EDM machine, an initial hole must first be drilled in the material, and then the wire can be fed through the hole to complete the machining assembly. The wire-cut EDM can produce all sorts of complex shapes that are very difficult with other processes.

2.4 EDM applications

EDM has become an indispensable process in the modern manufacturing industry. The use of EDM is especially essential for machining difficult-to-machine materials (hardened alloy steel, high speed steel, superalloy, cemented carbide) and complex geometry parts for which traditional techniques are not applicable [1,5].

It is primarily used for production of subtle cavities in forming tools or polymer injection, prototype parts and other highly specialized products. With the increased capability of EDM controls, new processes use simple-shaped electrodes to 3D EDM complex shapes. Since the tool does not touch the workpiece there are no cutting forces, therefore, very fragile parts can be EDM machined [30,31]. Also, there is a great importance of EDM on the production of very accurate small and micro parts. Some of the applications made by EDM process are shown in Fig. 4.

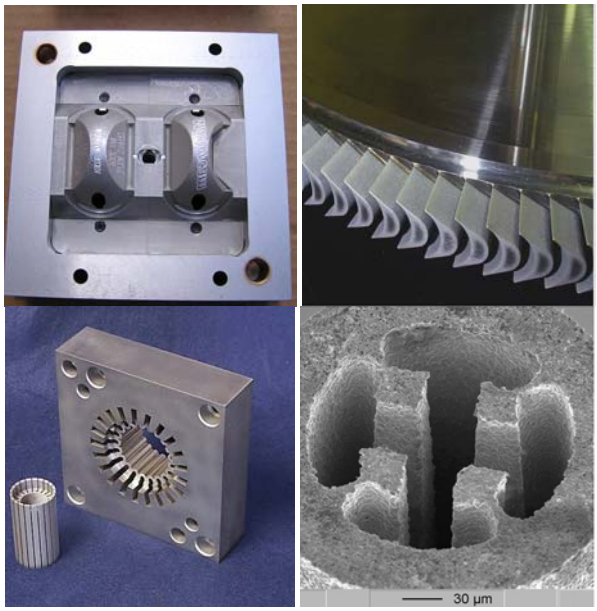

Fig.4. Applications of EDM

3. EXPERIMENTAL APPROACH

As analysed in section 2.2, the machining characteristics of EDM mostly depend on the discharge energy, i.e. discharge current and duration time [32-34].

Fig. 5. shows the effect of the most important electrical pulse parameters on the material removal rate of tool steel using copper tool electrode. The diagram shows dependence of material removal rate on discharge duration for various discharge currents. The results of experimental investigation show that for every discharge current there is a corresponding optimal discharge duration $t_{e(opt)}$ which allows maximum material removal rate. This value increases with the increase of discharge current [13,21].

This efficiently precludes us from unambiguous determination of the influence of the discharge current and pulse duration on material removal rate. The experimentally established optimal influence of the electrical pulse parameters on material removal rate, does not agree with the expected influence. In real conditions, discharge current and discharge duration increase material removal rate, as well as the increase of gas bubbles in the discharge zone. Due to impaired evacuation of machining products, a portion of the discharge energy is spent on re-melting and evaporation of solidified metal particles. Also, larger portion of discharge energy takes place in a gaseous environment, thus being lost irreversibly. Such impaired process stability affects the EDM productivity.

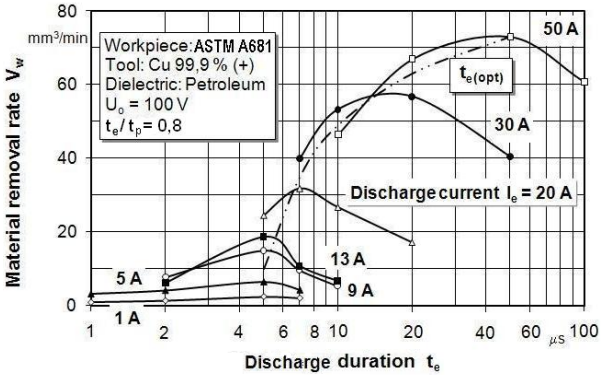

Fig. 5. Dependence of material removal rate on discharge duration for various discharge currents

Fig. 6 shows the influence of discharge current and duration time on gap distance. The diagram shows that the increase of electrical pulse parameters results in increased gap distance [13,21]. Although the influence of discharge current and discharge duration on gap distance is uniform, the discharge current has a somewhat larger influence on the gap distance. It is evident that the gap distance follows the electrical pulse parameters in order to maintain stability of EDM. Otherwise, the deionization of the discharge zone would be affected, which could result in either low or uncontrolled material removal rate.

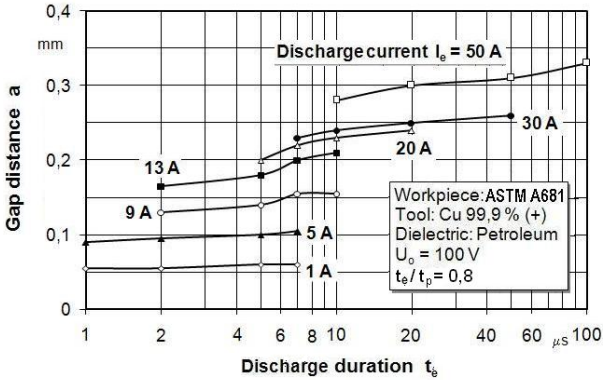

Fig. 6. Influence of the discharge parameters on gap distance

The relationship between the surface roughness and electrical pulse parameters is shown in Fig. 7. The results of experimental investigation show a slight increase of surface roughness with the increase of discharge duration, while the discharge current has a more pronounced influence on surface roughness. As the discharge current increases, so do the discharge heat concentration on the workpiece surface, which results in larger craters, i.e. greater surface roughness. Shown in Fig. 7 are typical images of machined surfaces at various electrical pulse parameters. The EDM surface consists of a number of craters of various dimensions, while the roughness is even in all directions [13,21].

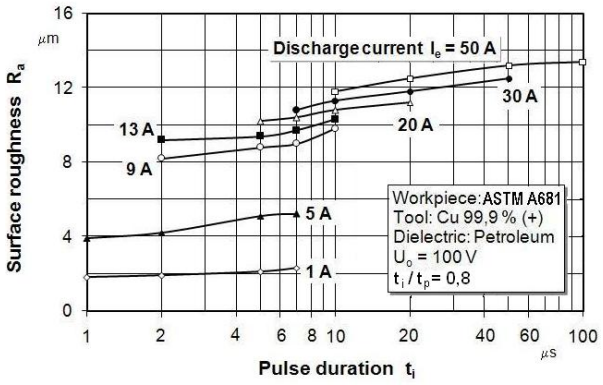

Fig. 7. Influence of the discharge parameters on surface roughness

As EDM generates extremely high temperatures in machining area, thermal defects are to be expected in the workpiece surface layer. Shown in Fig. 8 is metallographic image of the surface layer of hardened tool steel, which was eroded by a copper tool with a certain parameters of discharge energy.

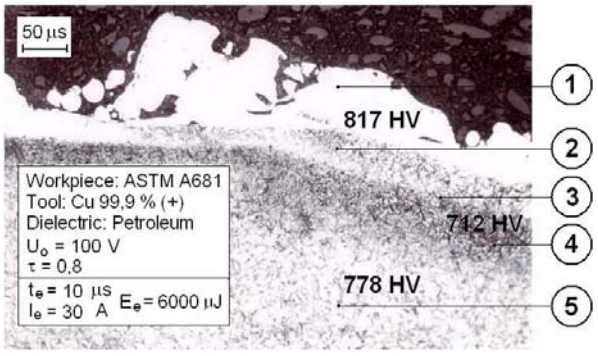

Fig. 8. Metallographic image of the surface layer of tool steel after EDM [18]
1. melted layer, 2. hardened layer, 3. interface layer, 4. tempered layer, 5. basic layer

Metallographic investigations shows that there was a change in workpiece surface layer. The changes manifest as uneven thickness, microstructure transformations, and a modified microhardness compared to the initial state of workpiece material. Fig. 9. shows the dependence of recast layer thickness on discharge energy [18,35-37].

The analysis of metallographic images reveals four characteristic secondary-changed workpiece surface layers: melted metal layer, hardened layer, interface layer, and tempered layer.

The melted layer is a sludge of lightly welded particles which is a residue left after ejection of melted material from the crater. The hardened layer consists of martensite, residual austenite with extremely pronounced grains, and cementite. The interface layer consists of martensitic-austenitic grid, and cementite, where the ratio of austenite diminishes with the distance from the tempered layer. The microstructure of the tempered layer is tempered martensite, and cementite, martensite, and cementite, which gradually phase into basic microstructure consisting of martensite with fine globular cementite.

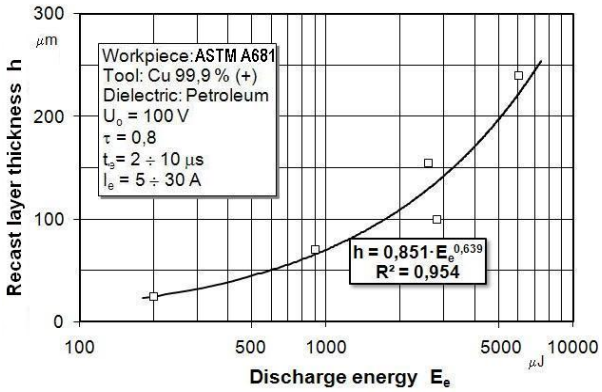

Fig. 9. Dependence of recast layer thickness on discharge energy [18]

Compared to the initial material condition, the secondary-hardened layer has higher, while the tempered layer has lower microhardness, Fig. 8. Higher microhardness of the hardened layer is the result of the austenitic-martensitic phase transition, while the lower microhardness of the tempered layer occurs around the highly tempered grains in the martensitic-austenitic grid.

4. MATHEMATICAL MODELING OF EDM

The mathematical modeling of the EDM process based on the electro-thermal model is conducted using analytical-numerical procedures. It is well known that thermal modeling of EDM processes is very difficult. The role of modeling behind thermal phenomena in the EDM is to adopt the most adequate mathematical model of factors in the discharge zone and their inter-relationships [38-40].

For defined thermal model of EDM, the partial differential equation of heat conduction in two-dimensional cylindrical coordinate system for the workpiece and tool is given as follows:

$$\rho c \frac{\partial T}{\partial t} = k\left(\frac{1}{r}\frac{\partial T}{\partial r} + \frac{\partial^2 T}{\partial r^2} + \frac{\partial^2 T}{\partial z^2}\right) \qquad (6)$$

Differential Eq. (6) should be considered in conjunction with the initial temperature which can be taken as normal room temperature of the dielectric in which the electrodes are completely dipped:

$$T(r,z,t)\big|_{t=0} = T_0 \tag{7}$$

and the boundary conditions of the system:

$$\begin{aligned} -k\frac{\partial T(r,z,t)}{\partial z}\bigg|_{z=0} &= q(r,t) \\ -k\frac{\partial T(r,z,t)}{\partial z}\bigg|_{z=\infty} &= 0 \\ -k\frac{\partial T(r,z,t)}{\partial r}\bigg|_{r=\infty} &= 0 \end{aligned} \tag{8}$$

where T is the temperature, r is the radial cylindrical coordinate, z is the axial cylindrical coordinate, t is the time, k is the thermal conductivity, ρ is the material density, c is the specific heat and q is the heat flux density.

The finite element method (FEM) that is used to solve partial differential equations of heat conduction (Eq. 6) using the Galerkin's method can be expressed in matrix form as:

$$[k]\{T\} + [c]\left\{\frac{\partial T}{\partial t}\right\} = \{q\} \tag{9}$$

where $[k]$ is the thermal conductivity matrix; $[c]$ is the specific heat matrix; $\{T\}$ is the temperature vector and $\{q\}$ is the heat flux vector [41-43].

Example 3D axisymmetric finite element model of the EDM electrical pulse discharge process is shown on Fig. 10.

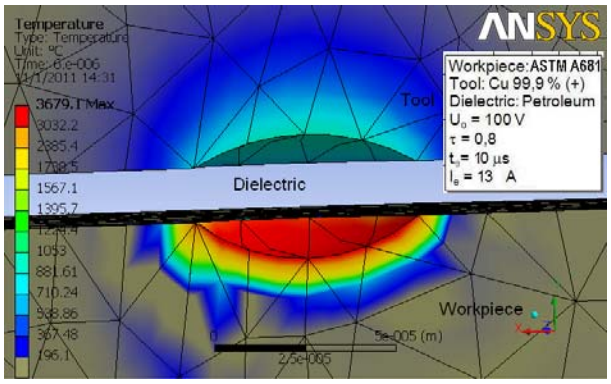

Fig. 10. FEM model of EDM process of a single electrical pulse

The results of FEM modeling of the volume of material removed was compared with the experimental results as shown in Fig. 11. The diagram show that the increase of discharge energy, results in increased radius and depth of the crater, which ultimately leads to higher volume of material removed from the workpiece. The average volume of material removed from the workpiece is calculated using numerical estimated value geometry of the crater.

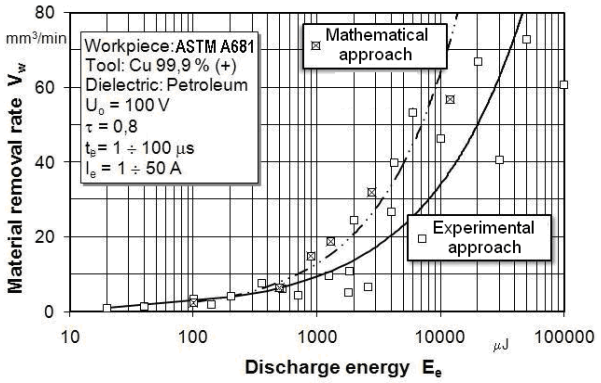

Fig. 11. Comparison of FEM modeling and experimental results of the material removed volume

5. MODELING OF EDM PROCESS USING ARTIFICIAL INTELLIGENCE

Recently, some initial investigations in applying the basic artificial intelligence approach to model machining processes, have been realized. To generalize the experimental results and develop the system model accurately, neural networks, fuzzy systems, evolutionary computation etc, are reported as an alternative approach. From the review of literature, it is observed that artificial intelligence techniques have found wide applications in modelling of process parameters and controlling the EDM system also [44-47].

Evolutionary algorithms, as their name is suggesting are based on principles of evolution and natural selection. Each solution to the problem is considered to be one individual who is evaluated by fitness function. Results of evaluation are directly determining each individual's probability of mating and thus transferring his genetic material onto next generation [48-50].

Evolutionary algorithms are a larger group of algorithms based on evolution but often only genetic algorithms (GA) and genetic programming (GP) are represented. Both of these algorithms are inspired by nature in same way: they apply evolutionary characteristics of selection, crossover and mutation on problem solutions while respecting main law of evolution, survival of the fittest, gradually progress towards optimal solution. In genetic algorithms, results are individuals while in genetic programming solutions are whole computer programs.

Example for a model of the genetic algorithms for material removal rate V_w, gap distance a and surface roughness R_a, depending on the discharge currents I_e and discharge duration t_e, is given by equations:

$$\begin{aligned} V_w &= 0.86 \cdot I_e^{0.9} \cdot t_e^{0.202} \\ a &= 0.054 \cdot I_e^{0.4} \cdot t_e^{0.054} \\ R_a &= 2.125 \cdot I_e^{0.468} \cdot t_e^{0.041} \end{aligned} \tag{10}$$

In the text below is presents the development and application of an ANFIS (adaptive neuro-fuzzy inference system) in electrical discharge machining for

prediction of surface roughness. In this ANFIS system, discharge current and discharge duration are the input variables and output is surface roughness, Fig. 12. The proposed ANFIS model in this study provides a more precise and easy selection of EDM input parameters, leads to better machining conditions and decreases the machining costs [52,55].

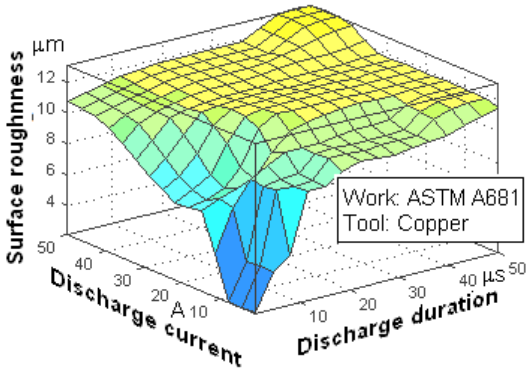

Fig. 12. ANFIS modeling of surface roughness in EDM process [55]

The ANFIS modeling of EDM was able to predict the experimental results and have shown the predictions on the surface roughness with a very small average error. ANFIS gives the mapping relation between the input and output data by using hybrid learning method to determine the optimal distribution of membership functions [53]. Both artificial neural network (ANN) and fuzzy logic (FL) are used in ANFIS architecture [54].

Fig. 13 describes the comparison of experimental, ANFIS ANN and GP predicted results for the surface roughness. It proved that the methods used in this paper are feasible and could be used to predict the surface roughness in an acceptable error rate for EDM. The compared lines seem to be close to each other indicating with good agreement. Comparative observation showed that the genetic algorithms gives slightly smaller deviation of the measured values of model than neuro-fuzzy model [51,55,56].

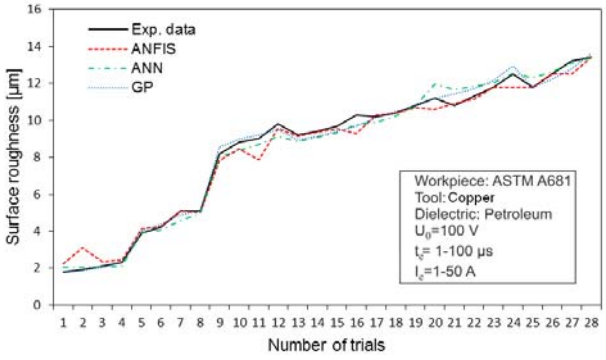

Fig. 13. Correlation between experimental, ANFIS, ANN and GP surface roughness value [46]

6. APPLICATION FOR SELECTION OF EDM PARAMETERS

Based on the summary of results of experimental investigation [13, 18, 21, 57], realised the model for selection of the optimal electrical pulse parameters in EDM. The Fig. 14 shows mutual dependence of material removal rate, tool wear ratio, gap distance and surface roughness for optimal electrical pulse parameters. Selected tool surface or surface roughness enables to choose discharge current and pulse duration which results in maximum material removal rate, and the corresponding gap distance and tool wear ratio.

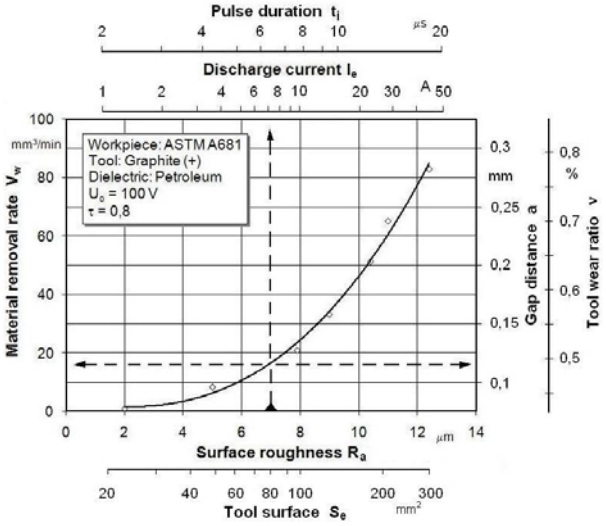

Fig. 14. Model for selection of the optimal electrical pulse parameters in EDM [21]

Fig. 15 shows application form for automatic selection of input parameters in electrical discharge machining.

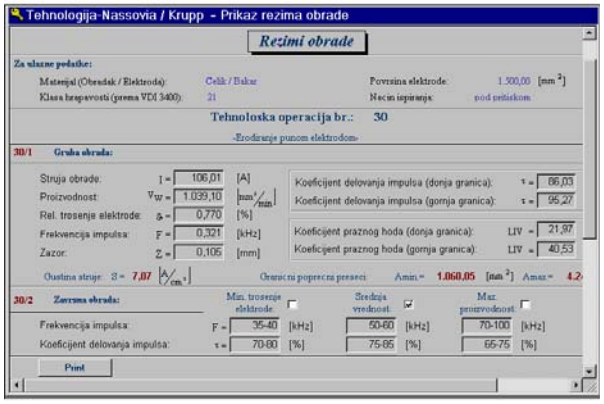

Fig. 15. Application for selection of EDM parameters

5. CONCLUSIONS

Based on the literature review, it follows that the electrical discharge machining (EDM) is a very common type of machining in manufacturing industries. Thereby, the machining characteristics of EDM mainly depend on generation and distribution of discharge energy within the machining zone. The energy generated depends on the discharge current and discharge duration, while the distribution of energy depends on physical and chemical characteristics of the discharge zone. Since the EDM process is complex and stochastic in nature, most attempts to model the

technological performance of EDM process in literature, has been reported to be based on electro-thermal concepts. Thereby, for the modeling of EDM the experimental, mathematical, empirical or intelligent methods are used, with different characteristics and approximation results.

Conducted theoretical approach and experimental investigation of the machining characteristics of EDM, yields following conclusions:

- Technological performance of EDM directly depends on the discharge energy which is transformed into thermal energy in the discharge zone;
- An existence of optimal discharge energy which yields optimal productivity and machining quality;
- The analytical-numerical modeling of EDM is a practical way to reliably determine the mechanism of generation and distribution of thermal energy in the discharge zone and be estimate the material removal rate and surface roughness;
- Research showed that intelligent models give accurate prediction on technological performance in EDM;
- Values predicted by the mathematical and intelligent model largely agree with the experimental results and the difference between the modeling and experimental results are primarily due to the difficulity to incorporate all effects in the electro-thermal model of EDM process.

6. REFERENCES

[1] Rao R.V.: Advanced modeling and optimization of manufacturing processes, Springer-Verlad, London, 2011.

[2] Kovač P., Gostimirović M., Sekulić M., Savković B.: A rewiev of research related to advancing manufacturing technology, Journal of Production Engineering, Vol. 12/1, 2009, pp. 9-16.

[3] Delgado Sobrino D.R., Holubek R., Ružarovský R.: On the Analysis and a Few Optimization Issues of a New iCIM 3000 System at an Academic-Research Oriented Institution, International Journal of Mechanical, Aerospace, Industrial, Mechatronic and Manufacturing Engineering, Vol. 7/6, 2013, pp. 1033-1038.

[4] Gostimirović M., Kovač P., Radovanović M., Madić M., Krajny Z.: Modular design of unconventional cutting machine tools, Journal of Production Engineering, Vol. 18/1, 2015, pp. 27-30.

[5] El-Hofy H.: Advanced machining processes, Nontraditional and hybrid machining processes, McGraw-Hill Professional, 2005.

[6] Lazarević D., Radovanović M.: Nekonvencionalne metode – obrada materijala odnošenjem, Mašinski fakultet, Niš, 1994.

[7] Lazić M.: Nekonvencionalni postupci obrade, Naučna knjiga, Beograd, 1990.

[8] Abbas N.M., Solomon D.G., Bahari M.F.: A review on current research trends in electrical discharge machining (EDM), Int J Mach Tools Manuf, Vol. 47, 2007, pp. 1214-1228.

[9] Amorim F.L., Weingaertner W.L.: The influence of generator actuation mode and process parameters on the performance of finish EDM of a tool steel, J Mater Process Tech., Vol. 166/3, 2005, pp. 411-416.

[10] Grigor'ev S.N., Kuzin V.V., Fedorov S.Y, Szalay T., Farkas B.: Technological aspects of the electrical-discharge machining of small-diameter holes in a high-density ceramic. Part 1, Refractories and Industrial Ceramics, Vol. 55/4, 2014, pp. 330-334.

[11] Singh S., Maheshwari S., Pandey P.C.: Some investigations into the electric discharge mchining of hardened tool steel using different electrode materials, J. Mater. Process. Technol, Vol. 149, 2004, pp. 272-277.

[12] Gostimirović M., Kovac P., Sekulić M., Savković B.: The research of discharge energy in EDM process, Proceedings of the 34th international conference on production engineering, Niš, 2011, pp. 28-30.

[13] Gostimirović M., Kovac P., Sekulić M., Savković B.: Influence of discharge parameters on the performance of electrical discharge machining, 8th Internacional Scientific Conference Development and Modernization of Production – RIM 2011, V. Kladuša, BiH, 2011, pp. 1-4.

[14] Kovač P., Gostimirović M., Sekulić M., Savković B.: A rewiev to advanced modeling and simulation of machining process, Journal of Production Engineering, Vol. 12/1, 2009, pp. 17-22.

[15] Erden A., Kaftanoglou B.: Thermo-mathematical modelling and optimization of energy pulse forms in Electric Discharge Machining (EDM), Int. J. Mach. Tool Des. Res., Vol. 21/1, 1981, pp. 11-22.

[16] DiBitonto D.D., Eubank P.T., Patel M.R., Barrufet M.A.: Theoretical models of the electrical discharge machining process: I. A simple cathode erosion model, J. Appl. Phys., Vol. 66/9, 1989, pp. 4095–4103.

[17] Gostimirović M., Kovač P., Sekulić M., Savković B.: A study of discharge pulse energy in electrical discharge machining, Journal of Production Engineering, Vol. 15/1, 2012, pp. 7-10.

[18] Gostimirović M., Kovač P., Sekulić M., Škorić B.: Influence of discharge energy on machining characteristics in EDM, Journal of Mechanical Science and Technology, Vol.26/1, 2012, pp. 173-179.

[19] Lin Y.C., Hwang L.R., Cheng C.H., Su P.L.: Effects of electrical discharge energy on machining performance and bending strength of cemented tungsten carbides, J Mater Process Tech., Vol. 206, 2008, pp. 491-499.

[20] Rebelo J.C., Morao Dias A., Kremer D., Lebrun J.L.: Influence of EDM pulse energy on the

surface integrity of martensitic steels, J Mater Process Tech, Vol. 84, 1998, pp. 90-96.
[21] Gostimirović M., Kovač P., Škorić B., Sekulić M.: Effect of electrical pulse parameters on the machining performance in EDM, Indian Journal of Engineering & Materials Sciences, Vol. 18/6, 2011. pp. 411-415.
[22] Pandey P.C., Jilani S.T.: Plasma channel growth and the resolidified layer in EDM, Precision Eng., Vol. 8/2, 1986, pp. 104-110.
[23] Singh A., Ghosh A.: Thermo-electric model of material removal during electric discharge machining, Int. J. Machine Tools Manufact., Vol. 39/4, 1999, pp. 669-682.
[24] Snoeys R., Van Dijck F.: Investigation of electro discharge machining operations by means of thermo-mathematical model, CIRP Ann., Vol. 20/1, 1971, pp. 35-36.
[25] Wang P.J., Tsai K.M.: Semi-empirical model on work removal and tool wear in electrical discharge machining, J Mater Process Tech., Vol. 114/1, 2001, pp. 1-17.
[26] Ekmekcil B., Sayar A., Opoz T., Erden A.: Geometry and surface damage in micro electrical discharge machining of micro-holes, J Micromech. Microeng., Vol. 19, 2009, pp. 1-16.
[27] Salonitis K., Stournaras A., Stavropoulos P., Chryssolouris G.: Thermal modeling of the material removal rate and surface roughness for die-sinking EDM, Int J Adv Manuf Technol., Vol. 40/3-4, 2009, pp. 316-323.
[28] Tarng Y.S., Ma S.C., Chung L.K.: Determination of optimal cutting parameters in wire electrical discharge machining, Int. J. Mach. Tools Manuf., Vol. 35/12, 1995, pp. 1693–1701.
[29] Ho K.H., Newman S.T.: State of the art in wire electrical discharge machining (WEDM), Int J Mach Tools Manuf, Vol. 44, 2004, pp. 1247-1259.
[30] Heckele M., Schomburg W.K.: Review on micro molding of thermoplastic polymers, J. Micromech. Microeng., Vol. 14, 2004, pp. 1-14.
[31] Liu K., Lauwers B., Reynaerts D.: Process capabilities of Micro-EDM and its applications, Int J Adv Manuf Technol, Vol. 47, 2010, pp. 11-19.
[32] Jilani S.T., Pandey P.C.: Analysis of surface erosion in electrical discharge machining, Wear, Vol. 843, 1983, pp. 275-284.
[33] Tsai Y.Y., Lu C.T.: Influence of current impulse on machining characteristics in EDM, J Mech Sci Technol, Vol. 21/10, 2007, pp. 1617-1621.
[34] Lin Y.C., Hwang L.R., Cheng C.H., Su P.L.: Effects of electrical discharge energy on machining performance and bending strength of cemented tungsten carbides, J Mater Process Technol, Vol. 206, 2008, pp. 491-499.
[35] Gostimirovic M., Kovac P., Ješić D., Škorić B., Savković B.: Surface layer properties of the workpiece material in high performance grinding, Metalurgija, Vol. 51/1, 2012, pp. 105-108.
[36] Yadav V., Jain V.K., Dixit P.M.: Thermal stresses due to electrical discharge machining, Int J Mach Tool Manuf., Vol. 42/8, 2002, pp. 877-888.
[37] Madic M., Radovanovic M., Gostimirović M.: ANN modeling of kerf taper angle in CO_2 laser cutting and optimization of cutting parameters using Monte Carlo method, International Journal of Industrial Engineering Computations, Vol. 6/1, 2015, pp. 33-42.
[38] Gostimirović M., Kovač P., Sekulić M.: An inverse heat transfer problem for optimization of the thermal process in machining, Sadhana, Vol 36/4, 2011, pp. 489-504.
[39] Gostimirović M., Pucovsky V., Kovač P., Sekulić M., Savković B.: An Analytical Study of Energy Partition in Grinding, Key Engineering Materials, Vol. 686, 2016, pp. 80-85.
[40] Yeo S.H., Kurnia W., Tan P.C.; Critical assessment and numerical comparison of electro-thermal models in EDM, J Mater Process Tech., Vol. 203, 2008, pp. 41-251.
[41] Brenner S., Scott R.L.: The Mathematical Theory of Finite Element Methods. Springer-Verlag, New York, 1994.
[42] Kovacevic D., Budak I., Antic A., Kosec B.: Special Finite Elements: Theoretical Background and Application, Teh Vjesn., Vol. 18/4, 2011, pp. 649-655.
[43] Marafona J., Chousal J.A.G.: A finite element model of EDM based on the Joule effect, Int J Mach Tool Manuf., Vol. 46/6, 2006, pp. 595-602.
[44] Kovac, P., Rodic, D., Pucovsky, V., Savkovic, B., Gostimirovic, M.: Application of fuzzy logic and regression analysis for modeling surface roughness in face milliing, Journal of Intelligent Manufacturing, Vol. 24/4, 2013, pp.755-762.
[45] Madić M., Radovanović M., Ćojbašić Ž., Nedić B., Gostimirović M.: Fuzzy Logic Approach for the Prediction of Dross Formation in CO_2 Laser Cutting of Mild Steel, Journal of Engineering Science and Technology Review, Vo.l 8/3, 2015, pp. 143-150.
[46] Rodic D., Gostimirovic M., Kovac P., Mankova I., Pucovsky V.: Predicting of machining quality in electric discharge machining using intelligent optimization techniques, International Journal of Recent advances in Mechanical Engineering (IJMECH), Vol. 3/2, 2014, pp. 1-9.
[47] Wang K., Gelgele H.L., Wang Y., Yuan Q., Fang M.: A hybrid intelligent method for modelling the EDM process, International Journal of Machine Tools and Manufacture, Vol. 43, 2003, pp. 995-999.
[48] Kovač P., Rodić D., Pucovski V., Mankova I., Savković B., Gostimirović M.: A review of artificial inteligence approaches applied in inteligent processes, Journal of Production Engineering, Vol. 15/1, 2012, pp. 1-6.
[49] Golshan A., Gohari S., Ayob A.: Multi-objective optimization of electrical discharge machining of metal matrix composite Al/SiC using non-dominated sorting genetic algorithm, International Journal of Mechatronics and Manufacturing Systems, Vol. 5, 2012, pp. 385-398.
[50] Delgado Sobrino D.R., Moravčík O.: A Selection and Application Scheme of Local Search

Neighborhood Operators for the Vehicle Routing Problem. Proceedings of the World Congress on Engineering and Computer Science, Vol I, WCECS 2010, October 20-22, 2010, San Francisco, USA, pp. 113-116, ISBN 978-988-17012-0-6.
[51] Gostimirovic M., Pucovsky V., Kovac P., Rodic D., Savković, B.: Modeling of discharge energy in electrical discharge machining by the use of genetic programming, Journal of Production Engineering, Vol. 15/2, 2012, pp. 15-18.
[52] Gostimirovic M., Rodic D., Kovac P., Pucovsky V., Sekulic M.: Modeling of material removal rate in EDM using neural fuzzy systems, Journal of Production Engineering, Vol. 16/1, 2013, pp. 1-4.
[53] Ying L. C., Pan M. C.: Using adaptive network based fuzzy inference system to forecast regional electricity loads, Energy Conversation and Management, Vol. 49, 2008, pp. 205–211.
[54] Avci E.: Comparison of wavelet families for texture classification by using wavelet packet entropy adaptive network based fuzzy inference system, Applied Soft Computing, Vol 8, 2008, pp. 225–231.
[55] Rodic D., Gostimirovic M., Kovac P., Radovanovic M., Savkovic B.: Comparison of fuzzy logic and neural network for modelling surface roughness in EDM, International Journal of Recent advances in Mechanical Engineering (IJMECH), Vol. 3/3, 2014, pp. 69-78.
[56] Gostimirovic M., Rodic D., Kovac P., Pucovski V., Savkovic B.: Application of neuro-fuzzy systems and genetic programming for modelling surface roughness in electrical discharge machining, Annals of Faculty Engineering Hunedoara – International Journal of Engineering, Vol. 12/1, 2014, pp. 137-140.
[57] Gostimirović M.: Nekonvencionalni postupci obrade, Univerzitet u Novom Sadu, Fakultet tehničkih nauka, Novi Sad, 2013.

Authors: **Prof. Dr. Marin Gostimirovic, Prof. Dr. Pavel Kovac, Prof. Dr. Milenko Sekulic, M.Sc. Dragan Rodic, M.Sc. Vladimir Pucovsky**

University of Novi Sad, Faculty of Technical Sciences, Department of Production Engineering, Trg Dositeja Obradovica 6, 21000 Novi Sad, Serbia, Phone: +381 21 450-366, Fax: +381 21 454-495.

E-mail: maring@uns.ac.rs
pkovac@uns.ac.rs
milenkos@uns.ac.rs
rodicdr@uns.ac.rs
pucovski@uns.ac.rs

Note**: This paper presents a part of researching at the Project number TR 35015, financed by Ministry of Education, Science and Technological Development of the Republic of Serbia.**

Journal of Production Engineering
Vol.19 No.1
JPE (2016) Vol.19 (1) Original Scientific Paper
Mithilesh K. Dikshit, Asit Baran Puri, Atanu Maity

EMPIRICAL MODELLING OF DYNAMIC FORCES AND PARAMETER OPTIMIZATION USING TEACHING-LEARNING-BASED OPTIMIZATION ALGORITHM AND RSM IN HIGH SPEED BALL-END MILLING

Received: 28 January 2016 / Accepted: 09 March 2016

Abstract: *In the present paper, dynamic cutting force components have been modelled using response surface methodology based on design of experiments. Ball end milling tests have been performed according the experimental plan using central composite design. Analysis of variance (ANOVA) has been performed to test for adequacy on the experimental data and a full quadratic mathematical models have been established. ANOVA for the individual terms revealed that axial depth of cut is the most dominant cutting parameter for tangential and axial dynamic cutting forces, accounting for 49.27% and 45.10% contributions, respectively. Radial depth of cut is the most dominant parameter for radial force and contributes 64.21% for it. Composite desirability function and teaching learning based optimization (TLBO) algorithm have been used for determining optimal cutting process parameters like of feed per tooth, cutting speed, axial and radial depth of cut. Optimum values of cutting parameters have been obtained using composite desirability function (CD) and TLBO. The best optimum value of cutting process parameters has been obtained through TLBO and are feed per tooth (f_z) = 0.06 mm, axial depth of cut (a_p) = 0.79 mm, cutting speed (V) = 169 m/min, and radial depth of cut (a_e) = 0.42 mm. The optimum value of dynamic cutting force components have been validated by conformation experiments and are in good agreement with the predicted result.*
Key words: *Ball end milling, dynamic cutting force, optimization, response surface methodology, TLBO*

Empirijsko modelovanje dinamičkih sila i optimizacija parametara pomoću metode zasnovane na bazi algoritma poučavanja-učenja i metodom odzivnih površina kod visokobrzinskog glodanja loptastim glodalima. *U ovom radu, komponente dinamičke sile su modelovane pomoću metode odzivnih površina po planu eksperimenta. Testovi glodanja loptastim glodalima su sprovedeni saglasno planu eksperimenta korišćenjem centralnog kompozitnog plana. Analiza varijacije (ANOVA) je sprovedena da bi se odredila adekvatnost eksperimentalnih podataka a u završnoj fazi je generisan potpuno kvadratni matematički model. Za pojedine uticaje je ANOVA pružila podatke koji otkrivaju da je aksijalna dubina glodanja najuticajniji parametar pri tangencijalnim i aksijalnim dinamičkim silama procesa obrade. Brojčano izraženo imaju uticaj od 49,27% i 45,10%. Radijalna dubina glodanja je najuticajniji parametar kod radijalne sile sa udeom od 64,21%. Poželjna kompozitna funkcija (CD) i algoritam zasnovan na poučavanju-učenju (TLBO) su korišćeni pri određivanju parametara procesa glodanja, kao što su pomak po zubu, brzina rezanja i aksijalna i radijalna dubina rezanja. Optimalne vrednosti parametara obrade su određene pomoću CD i TLBO. Kao najpodobniji optimalni parametri procesa obrade, generisani sa TLBO, su pomak po zubu (f_z) = 0,06 mm, aksijalna dubina reza (a_p) = 0,79 mm, brzina rezanja (V) = 169 m/min, i radijalna dubina reza (a_e) = 0,42 mm. Optimalne vrednosti komponente dinamičke sile rezanja su potvrđene naknadnim eksperimentom i u dobrom su slaganju sa predviđenim vrednostima.*
***Ključne* reči:** *Glodanje loptastim glodalima, dinamička sila rezanja, optimizacija, metoda odzivnih površina, TLBO*

1. INTRODUCTION

High speed ball end milling is a machining process used extensively in automobile, aerospace and, die and mould making industries. This is a very efficient machining process for producing aerodynamic sculptured components like turbine blade and propellers with high dimensional accuracy and surface finish. Machinability, dimensional accuracy and tool deflection are highly influenced by cutting forces in high speed ball end milling. In addition, cutting forces play a major role in determining tool life, surface finish and machine tool vibration. Thus, a precise knowledge of cutting force is very much essential for an effective ball end milling process. In high speed machining process, high cutting speed results in highly localized temperature resulting in thermal softening of the workpiece material [1]. In addition, a high speed leads to decrease in chip thickness. This allows always a greater shear deformation and results in corresponding decrease in cutting force [2]. In ball end milling process, high cutting performance may be achieved by selecting appropriate cutting parameters. In industries, desired cutting parameters are usually determined based on the experience of the machining operators or by the use of handbook. Experience based cutting parameters do not ensure that the cutting performance is near optimal. Several mathematical models [3-9] have been proposed to select the appropriated cutting parameters to establish the relationship among cutting performances and cutting parameters based on statistical regression techniques like response surface

methodology (RSM), Taguchi method, and factorial methods or neural network. These mathematical model (models) has been further used as an objective function with constraints to solve for the optimal cutting parameters using optimization methods.

M. Alauddin et al. [3] attempted to model the cutting force for studying the effect of feed per tooth and axial depth of cut on average tangential cutting force in end milling of Inconel 718. It was found that both the feed and axial depth of cut affected the average cutting force. It increased with an increase in axial depth of cut or feed or both of them simultaneously. Ding et al. [4] also reported that cutting force components were mostly affected by axial depth of cut and feed in hard milling of AISI H13 steel. They had used maximum absolute value of cutting forces in one cutting period (i.e. one full rotation of the tool) for analysis using Taguchi method and concluded that a linear model could be fitted for all the three components of forces, namely axial force, feed force and normal force. Ozel et al. [5] employed four factor two level fractional factorial experiments to study the effect of cutting edge geometry, workpiece hardness, feed and cutting speed on surface roughness and cutting forces in hard turning of hardened AISI H13 steel. They found that all the above parameters were statistically significant. They reported that decrease in edge radius and workpiece hardness resulted in lesser tangential and radial forces. Dikshit et al. [6] carried out an experimental investigation to study the effect of feed per tooth, cutting speed, radial depth of cut and axial depth of cut in ball end milling of Al2014-T6 and reported that tangential, radial and axial cutting force components were mostly affected by axial depth of cut only.

C. K. Toh [7] studied the effect of cutter path strategies on tool life using the static and dynamic cutting forces. He concluded that, the cutting forces increased and tool life decreased with increase in axial depth of cut regardless of the milling path orientations. He also found that dynamic cutting forces were more sensitive to tool wear. Tangjitsitcharoen et al. [8] employed the dynamic cutting force ratio to predict in-process surface roughness using multiple regression analysis and found that increase in dynamic cutting force ratio increased surface roughness. Bhogal et al. [9] investigated the effect of process parameters on surface roughness and tool vibration in end milling using RSM. Dynamic cutting forces are very important in machining process because these are directly related to machine tool vibration, tool deflection and tool chattering, poor surface finish and premature tool failure. Dimla [10] established inter-relationship between vibration signals and the cutting forces to find out the dynamic nature of the cutting process. He reported that dynamic cutting forces have some impacts on the dynamic behavior of a cutting process. The developed model was further utilized for the development of tool condition monitoring systems (TCMSs).

In the present paper, mathematical models have been developed using RSM for dynamic cutting force components in high speed ball end milling to investigate the effect of process parameters viz. feed per tooth (f_z), cutting speed (V), radial depth of cut (a_e) and axial depth of cut (a_p). Machining experiments have been planned using design of experiments (DoE) based on response surface methodology. The analysis of variance (ANOVA) has been performed to investigate the effect of cutting process parameters on the dynamic forces in tangential (F_X), radial (F_Y) and axial (F_Z) directions. These mathematical models have been further used for optimization of dynamic cutting force components using meta heuristic optimization method called teaching learning based optimization (TLBO) and composite desirability function (CD). The optimal cutting parameters have been.

2. MATERIALS AND METHODS

2.1 Static and dynamic cutting forces

In ball end milling, time duration of tooth contact with the workpiece is a fraction of spindle period (time taken to complete one revolution of the tool or spindle) and the chip thickness varies over a revolution of the cutting tool. Force signals recorded by dynamometer are dynamic in nature due to the varying chip thickness and the nature of tool engagement with the workpiece. Post process of the collected force signals of each repeated test revealed that a section of force signal was constant and did not change with time as the cutting process progressed. This constant force signal was reported as static force signal [10] and was given by mean value of the sampled data as follows:

$$F_S = \frac{1}{N}\sum_{i=1}^{N} F_i\left(t_i\right) \qquad (1)$$

where F_S, N, Fi are static force components, number of sample points and force signal data at i^{th} position, respectively. The cyclic variation of the force components beyond the threshold may result in dimensional inaccuracy and machine tool chatter. It is difficult to eliminate this cyclic variation as well as to predict the cutting conditions under which this cyclic variation occurs. Therefore, to get an indication of the system fluctuations, the dynamic forces are required to be studied carefully. Dynamic force signal can be found by subtracting static force from the maximum recorded force. If F_D is dynamic force component and F_{max} is the maximum force, then the dynamic force component may be mathematically expressed as:

$$F_{D,XYZ} = F_{\max,\mathrm{XYZ}} - F_{S,XYZ} \qquad (2)$$

Dynamic cutting forces fluctuate with excursions to zero and then to higher magnitudes during cutting. The consequence of these excursions have been the onset of tool holder vibration whereby chattering often results at high magnitudes [11, 12]. For illustration, static and dynamic forces are shown in the Fig. 1. In the present paper, the dynamic cutting forces in F_X, F_Y and F_Z directions have been determined using Eqs. (1 and 2) using 20000 sample points. Analysis of variance (ANOVA) and regression analysis have been performed using response surface methodology [13].

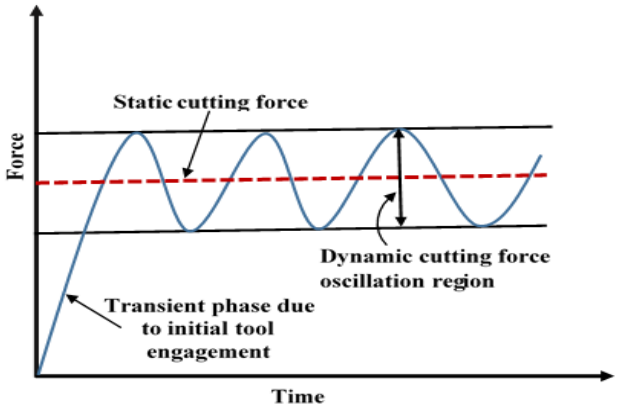

Fig. 1. Force (N) vs. time (s), showing static and dynamic forces (An illustrative figure)

2.2 Experimental plan

Response surface methodology (RSM) is a sequential procedure and is a collection of statistical techniques used for modelling and analysis of processes in which a response of interest is correlated with several input variables. The objective of RSM is to determine the optimum operating condition in terms of a region of factor space in which output requirement(s) are satisfied. In this methodology, a response variable Y is postulated to be a random variable and *k*'s number of input variables ($x_1, x_2, x_3 \ldots x_k$) are presumed to be continuous. On performing experiments, it is possible to represent the functional relationship between independent input factors and response variable in quantitative form by regression analysis. Thus, mathematically, it may be written as:

$$Y = f\left(x_1, x_2, x_3, \ldots, x_k\right) \pm \varepsilon \qquad (3)$$

If the system has curvature, then a polynomial of higher degree must be used. A second order polynomial in independent variables is given by:

$$Y = \beta_0 + \sum_{i=1}^{k} \beta_i x_i + \sum_{i=1}^{k} \beta_{ii} x_i^2 + \sum_{i=1}^{k} \sum_{j=1}^{k} \beta_{ij} x_i x_j \pm \varepsilon \qquad (4)$$

where, β_0 is constant, β_i, β_{ii}, β_{ij} are the constants of linear, square and interaction terms respectively. ε is the experimental error. A central composite design (CCD) is the most popular design of experiment used for fitting the second order models. In the present study, CCD is used to carry out the experiments. The response variables considered are dynamic cutting force components in F_X, F_Y, and F_Z directions. Four cutting parameters, i.e., f_z, a_p, a_e and V have been considered. The coded values along with actual values of these input variables are shown in the Table 1. The coded values of intermediate levels are obtained by:

$$X_i = \frac{\left[2X - \left(X_{\max} + X_{\min}\right)\right]}{X_{\max} - X_{\min}} \qquad (5)$$

where X_i is the required coded value of the variable X. X is any value of variable lies between X_{min} to X_{max} i.e. maximum and minimum values of cutting parameters.

No.	Factors	Coded level				
		-2	-1	0	1	2
1	f_z (X_1)	0.02	0.07	0.12	0.17	0.22
2	a_p (X_2)	0.2	0.6	1	1.4	1.8
3	a_e (X_3)	0.1	0.3	0.5	0.7	0.9
4	V (X_4)	75	100	125	150	175

Table 1. Experimental parameters and their levels

3. OPTIMIZATION METHODS

3.1 Teaching learning based optimization (TLBO)

TLBO is a meta-heuristic optimization algorithm based on teaching–learning process developed by Rao *et al.* [14]. This is a very efficient and accurate nature inspired optimization technique. Rao *et al.* [14] had applied TLBO on different mechanical design benchmark problems like design of pressure vessel, tension/compression spring, welded beam and gear train etc. The effectiveness of TLBO was compared with the research available on the above mentioned problems using different optimization techniques. They had also employed TLBO on constrained mechanical design problem available in literature and reported that the performance of TLBO is better than the other nature inspired optimization methods for the constrained mechanical design problems.

Rao *et al.* [15] employed TLBO on non-linear optimization problems. They had compared the TLBO and other optimization techniques like genetic algorithm (GA), particle swarm optimization (PSO), artificial bee colony (ABC) and harmony search (HS). The effectiveness of TLBO was checked on different performance criteria viz. mean solution, success rate, average function evaluations and convergence rate etc. It was reported that TLBO has better performance over other optimization techniques stated earlier. Rao and Kalyankar [16] successfully applied TLBO on the examples previously attempted by various researchers for parameter optimization of different modern machining processes like, ultrasonic machining, abrasive jet machining, wire electrical discharge machining, etc. They had also compared the results obtained by TLBO to other nature-inspired optimization techniques and reported that considerable improvement was observed in results and convergence using TLBO. Rao *et al.* [17] had also applied TLBO for parameter optimization of a few selected casting processes like, squeeze casting, continuous casting and die casting. They had observed that results obtained from TLBO was satisfactory and requires less computational efforts. Baghlani and Makiabadi [18] employed TLBO for shape and size optimization of truss structures with dynamic frequency constraints. Considering various benchmark problems they concluded that very satisfactory results were obtained using TLBO in comparison to those of PSO, HS and firefly algorithm (FA).

TLBO is a population based method and global optimum is obtained by using the population of solutions. TLBO is based on the effect of influence of a teacher on the output of learners in a class. The algorithm mimics teaching-learning ability of teacher and learners in a class room. In TLBO the population is

considered as a group of learners (students). Teacher and learners are the two vital components of the algorithm describing two basic modes of the learning, through teacher (known as teacher phase) and interacting with the other learners (known as learner phase). Thus, the algorithm is based on the teaching-learning ability of teacher and learners in a class room and is distinguished in two parts namely (1) teacher phase and (2) learner phase.

3.1.1 Teacher phase

In a class room the teacher tries to increase the level of the knowledge of the students up to their level. But in actual practice it is not possible (extremely difficult) to increase the knowledge level of the students to a desired level. Therefore, the teacher tries to move the mean result of the class up to some extent (close to desired level) in the specific subject taught by him or her depending on the capabilities of the class [14]. Let us suppose that number of subjects also called design parameters is represented by m, and n is the number of learners (students) i.e. population size. A teacher is treated as a highly knowledgeable who teaches learners for better results. Therefore, a teacher is considered as the best learner and hence tries to improve its mean results. At any particular iteration i, $M_{j,i}$ is the mean result of the learners in a particular subject j. The best overall result $X_{total\text{-}k\ \ teacher}$, obtained in the entire population of learners considering all the subjects together can be considered as the result of best learner k_{teacher}. The solution is updated according to the difference between the existing mean result of each subject and the corresponding result of the teacher for each subject and can be given by:

$$Difference\_Mean_{i,k,i} = r_i\left(X_{j,teacher} - T_F M_{j,i}\right) \quad (6)$$

where, $X_{j,teacher}$ is the result of the best learner (i.e., teacher) in subject j, T_F is the teaching factor and r_i is the random number varies over the range of [0, 1]. The value of T_F is decided randomly with equal probability as [15]:

$$T_F = round\left[1 + rand\left(0,1\right)\cdot\left\{2-1\right\}\right] \quad (7)$$

T_F is not a parameter but a heuristic step in the TLBO algorithm. The best optimal solution using TLBO can be obtained if the value of T_F is either 1 or 2 and decided randomly by the algorithm using equation (7), [16]. The existing solution is updated in the teacher phase using the difference mean according to the following expression shown in equation (8).

$$X'_{j,k,i} = X_{j,k,i} + Difference\_Mean_{j,k,i} \quad (8)$$

Where, $X'_{j,k,i}$ is the updated value of $X_{j,k,i}$. If $X'_{j,k,i}$ gives a better function value, then it has to be accepted. All the accepted function values at the end of the teacher phase are maintained and these values become the input to the learner phase.

3.1.2 Learner phase

The knowledge of the learners can be increased through input from the teacher and through interaction among themselves. A learner can learns new things and enhance his or her knowledge with interacting with another learner which has more knowledge [14]. For a population size of 'n', let us consider two learners P and Q. The learning procedure of P and Q can be obtained by the updated solution of P and Q i.e. $X'_{total\text{-}P,\ i}$ and $X'_{total\text{-}Q,I}$ at the end of teacher phase under the condition that $X'_{total\text{-}P,\ i} \neq X'_{total\text{-}Q,I}$.

$$X''_{j,p,i} = X'_{j,p,i} + r_i\left(X'_{j,p,i} - X'_{j,\mathrm{Q},i}\right) \ if\ X'_{total-p,i} < X'_{\mathrm{total}-Q,i} \quad (9)$$

$$X''_{j,p,i} = X'_{j,p,i} + r_i\left(X'_{j,p,i} - X'_{j,\mathrm{Q},i}\right) \ if\ X'_{total-p,i} > X'_{\mathrm{total}-Q,i} \quad (10)$$

$X''_{j,P,i}$ is accepted if it gives a better functional value. All the accepted functional values obtained at the end of the learner phase restored and these values become the input to the teacher phase of the next iteration. The random values (r_i) used in equations (6), (9), and (10) may be different. Equations (9) and (10) are used for a maximization problem. The reverse is also true for the minimization problem [16]. Pseudo code for TLBO for step by step demonstration is given below.

Set k=1;
Objective function $f(X_1, X_2, X_3, X_4)$
Generate initial population i.e. no of students
Calculate the objective function for all population
while (the termination conditions are not met)
{Teacher Phase}
Calculate the mean of each design variable $M_{j,i}$
Identify the best solution (teacher)
for 1:n
Calculate teaching factor $T_F = round\left[1 + rand\left(0,1\right)\left\{2-1\right\}\right]$
Modify solution based on best solution (teacher)
$X'_{j,k,i} = X_{j,k,i} + r_i\left(X_{j,teacher} - T_F M_{j,i}\right)$
Calculate objective function for new mapped learner $f(X'_{j,k,i})$
if $X'_{j,k,i}$ is better than $X_{j,k,i}$
$X'_{j,k,i} = X_{j,k,i}$
end if {End of Teacher Phase}
{Learner Phase}
Randomly select another learner X'_j, such that $X'_{total-P,i} \neq X'_{total-Q,i}$
if $X'_{total-p,i} < X'_{\mathrm{total}-Q,i}$
$X''_{j,p,i} = X'_{j,p,i} + r_i\left(X'_{j,p,i} - X'_{j,\mathrm{Q},i}\right)$
else
$X''_{j,p,i} = X'_{j,p,i} + r_i\left(X'_{j,Q,i} - X'_{j,P,i}\right)$
end if
if $X'_{total-P,i}$ is better than $X'_{total-Q,i}$
$X'_{total-P,i} = X'_{total-Q,i}$
end if {end of learner Phase}
end for
Set k=k+1
end while

3.2. Response surface optimization.

Response surface optimization is very useful to find out the cutting parameters (f_z, A_p, A_e, V) at which the response (F_X, F_Y, and F_Z) reach to the optimal value in high speed ball end milling process. Optimization using RSM may be divided into three groups, viz., (1) approach based on overlapping of contours, (2) composite desirability function and (3) dual response system methodology [19]. Composite desirability is one of the most widely used methods in industry which is based on weighted geometric mean of the individual desirability's for the responses on a range from zero to one. The common approach is to find out the individual desirability index of the responses by transforming the corresponding response y_i into the individual desirability function $d_i(y_i)$ varying over the range $0 \leq d_i(y_i) \leq 1$ using the suitable formulae as proposed by Derringer and Suich [20]. Ideal case is represented by 1 and 0 indicates the worst case, i.e., one or more responses are outside the desired limits. In this approach, the inputs are target value (T_i), upper value (y_{max}) and lower (y_{min}) value of the responses. There are three forms of desirability functions, viz., (1) the lower-is the-better, (2) the higher-is-the-better and (3) the target-is-the-best, depending on whether a particular response problem y_i is to be minimized, maximized or is assigned a target value. In the present study lower-is-the-better form is applied for minimizing F_X, F_Y, and F_Z which may be given as:

$$d_i(y_i) = \begin{cases} 1 & y_i \leq y_{\min} \\ \dfrac{y_i - y_{\min}}{T_i - y_{\min}} & y_{\min} \leq y_i \leq y_{\max},\ r \geq 0 \\ 0 & y_i \geq y_{\max} \end{cases} \quad (11)$$

Where, y_{min}, y_{max}, and T_i represents lower value, upper value and target value respectively of the response y_i. 'r' indicates the weight and its value is larger if the response is close to the target value, otherwise, it is set to the lower value. It is the most important parameter that determines the shape of the desirability function $d_i(y_i)$. Desirability function is linear if $r = 1$ and convex when $r > 1$. If the value of r lies between 0 and 1 the shape of $d_i(y_i)$ is concave. The individual desirability index of all the responses are then combined using the geometric mean to get the overall desirability or composite desirability D_c:

$$D_c = \left\{ d_1(y_1)^{w_1} * d_2(y_2)^{w_2} * d_3(y_3)^{w_3} * \ldots * d_m(y_m)^{w_m} \right\}^{\frac{1}{W}} \quad (12)$$

Where, d_i (i = 1, 2, 3… m) is the individual desirability of the response, m_i is the weight of d_i and W is the sum of the individual weights.

4. RESULTS AND DISCUSSION

4.1 Experimental details

The experiments have been conducted on a high speed three axis CNC vertical machining center (Model: MICRON VCP 710, Germany). All the test runs have been performed in dry environment. A 2-fluted solid carbide ball end milling cutter (Sandvik coromant, CoroMill Plura, R216.42-10030-Al10G 1620) with PVD monolayer coating of TiAlN has been used. The diameter, rake angle and helix angle of the cutter is 10 mm, 4^o and 30^o respectively. The experiments have been performed on aluminium alloy Al2014-T6 work piece block of size 160×100×100 mm^3. The cutting forces in F_X, F_Y and F_Z directions have been measured with Kistler 3-component piezoelectric dynamometer (Model: 9257B) along with multichannel charge amplifier (Type: 5011B) and a data acquisition system. The dynamometer was calibrated with static and dynamic loading before starting the experiments. Cutting force data have been collected at the sampling rate of 1200 Hz and the post processing of the cutting force data have been performed using Dynoware software in a computer with windows XP as operating system.

Dynamic cutting forces in F_X, F_Y and F_Z directions are obtained by slot milling tests performed according the experimental plan as shown in Table 2. Noises in the cutting force signals have been eliminated during the post processing and maximum cutting forces in F_X, F_Y and F_Z directions have been obtained. Thus, the cutting force signals in these three directions have been again post processed and subsequently, dynamic force components have been determined as mentioned earlier. A full quadratic model is considered and effect of each cutting parameters have been studied for each of the responses, i.e., F_X, F_Y and F_Z. MINITAB 16 has been used for the above purpose. Thus, the regression equations have been determined. The significance tests for the input parameters as well as for the models have been carried out and the model adequacy has been checked.

4.2. Analysis of variance (ANOVA) and mathematical model development

Significance tests for individual terms have been performed through ANOVA. Table 3 shows the ANOVA and fit summary for dynamic tangential cutting force component. The significant terms are characterized by the p-value less than 0.05 (i.e. α = 0.05 or 95% level of confidence). It may be observed that the linear terms of the model are significant, whereas some of the squared terms and interaction terms like, f_z*f_z, a_p*a_p, f_z*V, a_p*V and a_e*V are insignificant. The insignificant terms have been eliminated through backward elimination process one by one to reduce the model and in every step adequacy of the model has been checked. Thus, ANOVA and fit summary of the final model for F_X is shown in the Table 4. Table 4 also reveals that the second order regression model is highly significant and also the lack-of-fit is insignificant. An insignificant lack-of-fit is desirable. R^2 is one of the most important statistic which is a measure of the amount of reduction in the variability of response obtained by using the regressor variables in the model. As R^2 approaches to unity, the response model fits better with the actual data. However, a large value of R^2 does not necessarily imply that the regression model is good. Adding a variable to the model will always increase in R^2 as it always increases when terms are added to the model.

Run No.	Coded levels				Actual values				Responses		
	X_1	X_2	X_3	X_4	f_z (mm/tooth)	a_p (mm)	a_e (mm)	V (m/min)	F_X (N)	F_Y (N)	F_Z (N)
1	-1	-1	-1	-1	0.07	0.6	0.3	100	56.26	15.73	32.98
2	1	-1	-1	-1	0.17	0.6	0.3	100	76.42	19.72	43.88
3	-1	1	-1	-1	0.07	1.4	0.3	100	94.11	12.40	47.37
4	1	1	-1	-1	0.17	1.4	0.3	100	132.23	20.77	61.02
5	-1	-1	1	-1	0.07	0.6	0.7	100	66.22	33.90	40.11
6	1	-1	1	-1	0.17	0.6	0.7	100	103.19	48.59	52.05
7	-1	1	1	-1	0.07	1.4	0.7	100	117.65	42.19	62.28
8	1	1	1	-1	0.17	1.4	0.7	100	188.91	56.65	90.34
9	-1	-1	-1	1	0.07	0.6	0.3	150	40.48	9.43	25.10
10	1	-1	-1	1	0.17	0.6	0.3	150	59.23	13.09	28.97
11	-1	1	-1	1	0.07	1.4	0.3	150	80.49	10.90	37.07
12	1	1	-1	1	0.17	1.4	0.3	150	104.06	14.60	49.08
13	-1	-1	1	1	0.07	0.6	0.7	150	51.52	18.32	27.45
14	1	-1	1	1	0.17	0.6	0.7	150	82.48	26.96	35.70
15	-1	1	1	1	0.07	1.4	0.7	150	96.24	31.67	53.71
16	1	1	1	1	0.17	1.4	0.7	150	153.68	41.20	71.71
17	-2	0	0	0	0.02	1	0.5	125	48.71	12.84	26.70
18	2	0	0	0	0.22	1	0.5	125	134.53	29.05	64.24
19	0	-2	0	0	0.12	0.2	0.5	125	35.17	15.73	20.75
20	0	2	0	0	0.12	1.8	0.5	125	159.56	30.14	75.39
21	0	0	-2	0	0.12	1	0.1	125	43.05	5.66	25.49
22	0	0	2	0	0.12	1	0.9	125	102.15	46.31	55.77
23	0	0	0	-2	0.12	1	0.5	75	129.39	34.61	70.61
24	0	0	0	2	0.12	1	0.5	175	81.19	18.31	37.97
25	0	0	0	0	0.12	1	0.5	125	92.74	24.12	48.82
26	0	0	0	0	0.12	1	0.5	125	93.40	24.89	47.11
27	0	0	0	0	0.12	1	0.5	125	95.27	23.15	47.05
28	0	0	0	0	0.12	1	0.5	125	99.14	23.34	48.01
29	0	0	0	0	0.12	1	0.5	125	96.80	25.72	48.94
30	0	0	0	0	0.12	1	0.5	125	100.87	24.35	50.99
31	0	0	0	0	0.12	1	0.5	125	100.53	22.22	51.33

Table 2. Experimental design layout and results for cutting force component

Sources	DoF	Seq SS	F	p	S <0.05
Model	14	38759.0	116.64	0.000	Significant
f_z	1	9160.0	385.93	0.000	Significant
a_p	1	19286.5	812.57	0.000	Significant
a_e	1	4760.7	196.79	0.000	Significant
V	1	2886.6	121.62	0.000	Significant
f_z*f_z	1	15.2	1.12	0.305	Insignificant
a_p* a_p	1	18.0	0.27	0.612	Insignificant
a_e* a_e	1	1034.5	39.41	0.000	Significant
V*V	1	172.1	7.25	0.016	Significant
f_z* a_p	1	436.3	18.38	0.001	Significant
f_z* a_e	1	576.4	24.28	0.000	Significant
f_z*V	1	80.1	3.37	0.085	Insignificant
a_p*a_e	1	347.5	14.64	0.001	Significant
a_p*V	1	56.4	2.38	0.143	Insignificant
a_e*V	1	18.7	0.79	0.388	Insignificant
Resid. Error	16	379.8	-	-	-
Lack-of-Fit	10	313.6	2.84	0.107	Insignificant
Pure error	6	66.1	-	-	-
Total	30	39138.8	-	-	-

R^2 = 99.03% ; R^2-adj = 98.18%; F-table (lack of fit) = 4.06

Table 3. ANOVA and fit summary of tangential dynamic cutting force (F_X)

Therefore, adjusted R^2 (R^2-adj) is preferred. It often decreases if unnecessary terms are added [12]. When the difference between R^2 and R^2-adj is large, there would be a good chance that insignificant terms have been included in the model.

From Table 4, it is seen that the difference between R^2 and R^2-adj is very small (0.0062), which is desirable. The obtained R^2-adj value (0.9792) is very close to unity, which shows a very good correlation between experimental and predicted results. The adequacy of the model has been checked using the F-test also. The F-value for the lack of fit of developed model should not exceed the standard tabulated F-value. A very high F-value (157.58) and a very small p-value (negligibly small) for the model shows that the model is adequate. The F-value of lack-of fit of the developed quadratic model is 3.05, which is less than the standard tabulated F-value (4.06) at 95% confidence level. Thus, the model is sufficiently good to be acceptable.

Sources	Dof	Seq SS	F	p	PC (%)
Model	10	38567.7	157.58	0.000	98.56
f_z	1	9160.0	336.83	0.000	23.40
a_p	1	19286.5	709.21	0.000	49.27
a_e	1	4760.7	171.75	0.000	12.16
V	1	2886.6	106.15	0.000	7.3
a_e*a_e	1	1021.1	34.54	0.000	2.60
V*V	1	182.5	6.71	0.017	0.46
f_z*a_p	1	436.3	16.04	0.001	1.12
f_z*a_e	1	576.4	21.19	0.000	1.47
a_p*a_e	1	347.5	12.78	0.002	0.88
Residual Error	21	571.1	-	-	-
Lack-of-Fit	15	504.9	3.05	0.088	Insignificant
Pure error	6	66.1	-	-	-
Total	30	39138.8	-	-	-
		R^2 = 98.54%; R^2-adj = 97.92%			

Table 4. ANOVA and fit summary of tangential dynamic cutting force (F_X) for reduced model

Similar procedure has been employed for F_Y, F_Z dynamic cutting force components. ANOVA and fit summary for the reduced quadratic models are shown in the Table 5 and Table 6 respectively. Thus, the second order mathematical models for F_X, F_Y, F_Z in coded forms are determined as:

$$F_X = 96.50 + 19.53 f_z + 28.34 a_p + 13.95 a_e - 10.96 V - 5.67 a_e^2 + 2.50 V^2 + 5.22 f_z * a_p + 6.00 f_z * a_e + 4.66 a_p * a_e \quad (13)$$

$$F_Y = 23.62 + 4.14 f_z + 3.06 a_p + 11.00 a_e - 4.84 V + 0.86 a_e^2 + 0.97 V^2 + 1.72 f_z * a_e - 0.99 f_z * V + 2.70 a_p * a_e + 1.03 a_p * V - 2.66 a_e * V \quad (14)$$

$$F_Z = 48.00 + 7.57 f_z + 12.31 a_p + 7.01 a_e - 6.93 V - 1.92 a_e^2 + 1.490 V^2 + 2.29 f_z * a_p + 1.61 f_z * a_e + 3.69 a_p * a_e \quad (15)$$

Sources	Dof	Seq SS	F	p	PC (%)
Model	11	4464.87	123.24	0.000	98.61
f_z	1	412.18	125.14	0.000	9.10
a_p	1	224.85	68.27	0.000	4.96
a_e	1	2907.08	862.62	0.000	64.21
V	1	564.35	171.34	0.000	12.46
a_e*a_e	1	17.66	6.57	0.019	0.39
V*V	1	28.00	8.50	0.009	0.61
f_z*a_e	1	47.61	14.45	0.001	1.05
f_z*V	1	15.96	4.85	0.040	0.35
a_p*a_e	1	116.86	35.48	0.000	2.58
a_p*V	1	17.02	5.17	0.035	0.37
a_e*V	1	113.32	34.4	0.000	2.50
Residual Error	19	62.58	-	-	-
Lack-of-Fit	13	54.37	3.06	0.089	Insignificant
Pure error	6	8.21	-	-	-
Total	30	4527.45	-	-	-
		R^2 = 98.62%; R^2-adj = 97.82%			

Table 5. ANOVA and fit summary of radial dynamic cutting force (F_Y) for reduced model

Sources	DoF	Seq SS	F	p	PC (%)
Model	9	7889.00	100.36	0.000	97.72
f_z	1	1376.53	157.60	0.000	17.05
a_p	1	3641.30	416.90	0.000	45.10
A_e	1	1182.17	153.35	0.000	14.64
V	1	1155.37	132.28	0.000	14.31
a_e*a_e	1	123.97	12.34	0.002	1.53
V*V	1	65.09	7.45	0.013	0.80
f_z*a_p	1	84.46	9.67	0.005	1.04
f_z*a_e	1	41.67	4.77	0.040	0.51
a_p*a_e	1	218.45	25.01	0.000	2.70
Residual Error	21	183.42	-	-	-
Lack-of-Fit	15	165.72	3.75	0.056	Insignificant
Pure error	6	17.70	-	-	-
Total	30	8072.42	-	-	-
		R^2 = 97.73%; R^2-adj = 96.75%			

Table 6. ANOVA and fit summary of axial dynamic cutting force (F_Z) for reduced model

4.3. Analysis of the influences of cutting parameters on the responses

Percentage contribution (PC) of each term for F_X is shown in the Table 4. The main effect of a_p is most significant with a PC of 49.27% in linear part followed by f_z 23.40%, a_e 12% and V 7.3% respectively. The second order effect of radial depth of cut is more significant than cutting speed. The two level interaction of feed per tooth and radial depth of cut (f_z*a_e) is most significant. From the second order model, it is evident that dynamic cutting force in F_X increases with increase in a_p and f_z. It decreases with increase in V. From Table 5, it is revealed that F_Y is mostly affected by a_e with a PC of 64.21% followed by V and f_z. In two-level interaction a_e is also the most important factor. F_Z component of the dynamic force shows similar behavior like F_X. Axial depth of cut is most dominant factor among all the cutting parameters with the total effect of 45.10 % in linear terms followed by feed per tooth and cutting speed. It is interesting to note that the PC of cutting speed and radial depth of cut is almost same as shown in Table 6. Values of all the three components of the dynamic cutting force decrease with increase in cutting speed. F_X and F_Z are mostly affected by cutting speed whereas F_Y is affected very little by it. All the dynamic cutting forces (F_X, F_Y and F_Z) increase with increase in axial depth of cut. 3-D surface graphs for tangential, axial and radial components of the dynamic force are shown in Figs. 2-4 respectively. All the three components have curvilinear profile in accordance with the fitted quadratic model. From the Figs. 2-4, it is clear that the cutting force components increase with increase in axial depth of cut and feed per tooth.

Fig. 2 (a) reveals that an increase in a_p and a_e increases the tangential cutting force component. At lower value of a_p and a_e, the force value is minimum keeping other parameter fixed at zero level. Cutting speed has significant effect on cutting force component and decreases on increasing the cutting speed. From

Figs. 2 (b) and (d), we can observe that F_X decreases with the increase in V. In case of other parameters like f_z, a_p and a_e, Similar trend has been observed for F_Z as shown in the Figs. 3 (a-d).

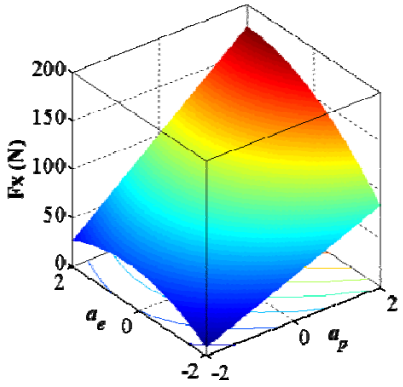

a) F_X as a function of axial and radial depth of cut

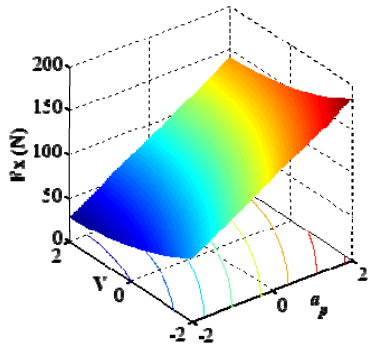

(b) F_X as a function of axial depth of cut and cutting speed

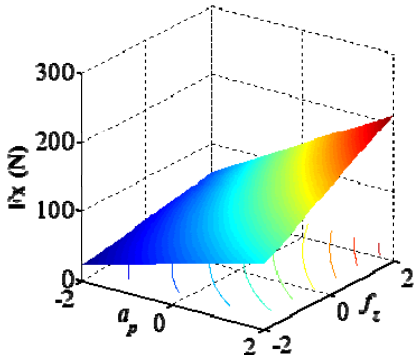

(c) F_X as a function of feed per tooth and axial depth of cut

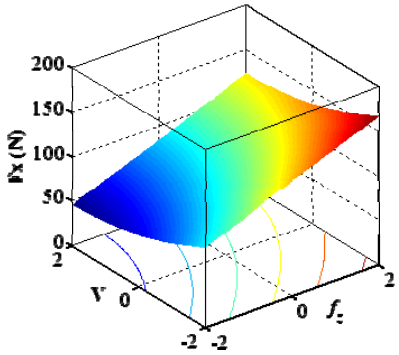

(d) F_X as a function of feed per tooth and cutting speed

Fig. 2. Response surface plots for tangential cutting force component (F_X)

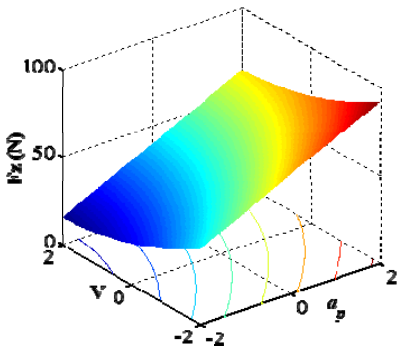

(a) F_Z as a function of axial depth of cut and cutting speed

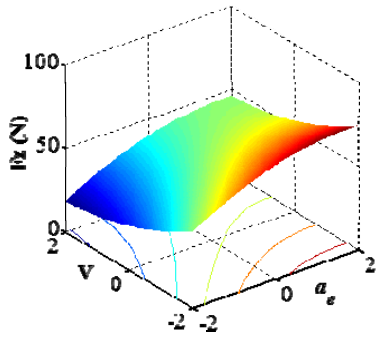

(c) F_Z as a function radial depth of cut and cutting speed

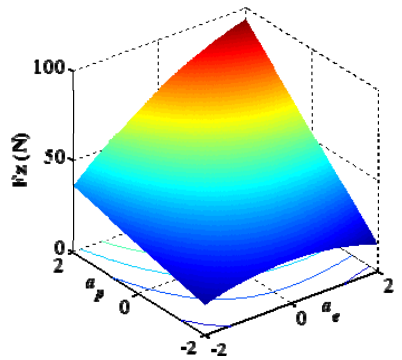

(b) F_Z as a function of axial and radial depth of cut

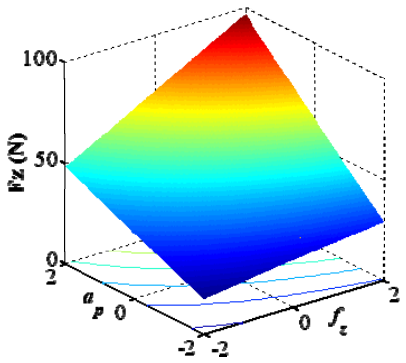

(d) F_Z as a function of feed per tooth and axial depth of cut

Fig. 3. Response surface plots for axial cutting force component (F_Z)

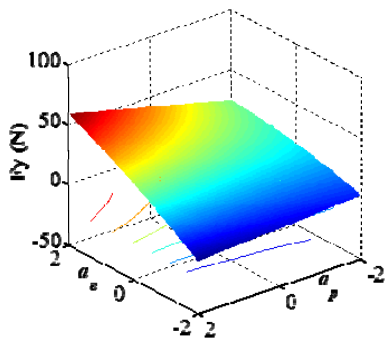

(a) F_Y as a function of axial and radial depth of cut

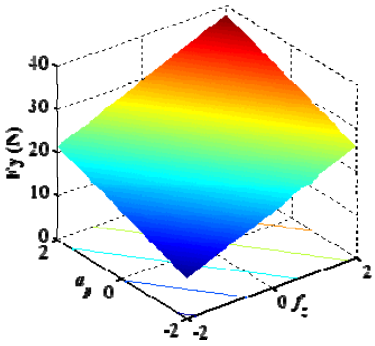

(b) F_Y as a function of feed per tooth and axial depth of cut

Fig. 4. Response surface plots for radial cutting force component (F_Y)

Contour and surface plots of F_Y is shown in Figs. 4 (a) and (b). From Fig. 4 (a), it is evident that the a_e is the most dominating cutting parameters. F_Y increases with increase in the value of a_e.

Predicted values of dynamic force components (F_X, F_Y and F_Z) obtained from the quadratic model (at 95% confidence level) are very close to the experimental values as shown in Fig. 5. The results show that there is a variations of 6.12%, -7.18% and 8.31% in tangential, radial and axial dynamic force components, respectively in the cutting speed range of 75-150 m/min and axial depth of cut range of 0.2-1.4 mm. The variation in predicted result is mostly observed at higher cutting speed of 150 m/min and axial and radial depth of cut ranging from 1-1.4 mm and 0.5-0.7 mm respectively. At lower depth of cut the variation is very small accounting 3.58%, -2.16% and 5.23% in tangential radial and axial components shown in Fig 5.

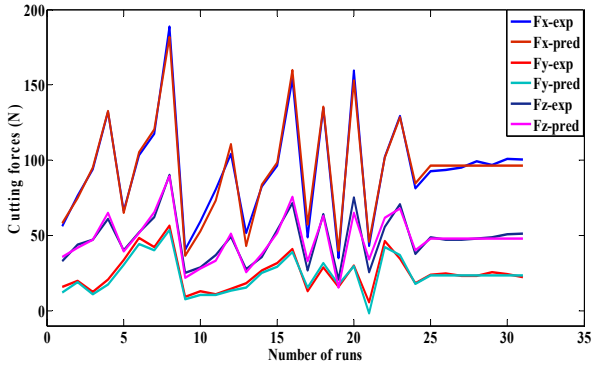

Fig. 5. Comparison between predicted and measured values of dynamic force components

4.4 Optimization results using CD

In the present study, the goal is to minimize the dynamic cutting forces components. Optimization result for dynamic cutting force components using composite desirability function (CD) is shown in Fig. 6. In Fig. 6, column represents cutting parameters while a row corresponds to responses. Variation of responses are indicated by each cell of the plot with change of a parameter keeping other parameters fixed. The current parameter settings are indicated at middle row of the top of the column and can change with the parameters settings interactively. The responses (dynamic cutting force components, F_X, F_Y and F_Z), goal for the response minimization, predicted values of responses at the current parameter settings with individual desirability score are indicated at each row in left column. The optimum results for F_X, F_Y and F_Z dynamic cutting force components using RSM optimization is shown in the Table 7. The optimum cutting parameters in coded unit are found to be feed per tooth of at level -1.01 (0.07 mm/tooth), axial depth of cut -0.45 (0.82 mm), radial depth of cut -0.67 (0.53 mm) and cutting speed at level of 1.56 (164 m/min). Corresponding optimized dynamic force components are F_X = 48.62 N, F_Y = 11.25 N and F_Z = 25.18 N respectively. Overall composite desirability is 0.93 shown in Fig. 6.

4.5 Optimization results using TLBO

The detailed procedures for implementation of TLBO are stated as follows:

(1) Defining the optimization problem as:

$$Minimize: \mathrm{R}_a\left(f_z, a_p, a_e, V\right)$$

Subjected to:

$$0.02\,mm/tooth \le f_z \le 0.22\,mm/tooth, \quad 0.2\,mm \le a_p \le 1.8\,mm$$

$$0.1\,mm \le a_e \le 0.9\,mm, \quad 75\,m/\min \le V \le 175\,m/\min$$

The developed mathematical model for dynamic cutting forces have been used as fitness function of TLBO for minimization. The constraints are f_z, V, a_p and a_e.

(2) Initialize the population.

In the second step, a random population is generated according to population size and number of cutting parameters. Learners represent population size and subjects represent the cutting process parameters in TLBO. The cutting process parameters are used to generate a random initial population.

(3) Teacher phase solution

(4) Learner phase solution

(5) Termination criterion.

The program will be terminated when the maximum generation number is achieved, otherwise it will again start from step 3 and will continue till the maximum generation number is achieved. In the present study, Deb's heuristic constraint handling method is adopted to handle the constraints in the problem. Initially various trails were carried out by running TLBO algorithm for different population size, numbers of generations and

teaching factor to get the consistent results. The optimum results have been obtained at 20 population size, 500 number of generations and in 100 iterations. Teaching factor was selected 1 after numerous trails. The obtained result is shown in the Table 7. From Table 7, it may be seen that the optimal cutting forces obtained by TLBO are better than those obtained from CD.

OM	R	Optimum combinations				PR (N)	D_c
		f_z	a_p	a_e	V		
CD	Fx	-1.01	-.45	-0.67	1.56	48.62	0.95
	Fy	-1.01	-.45	-0.67	1.56	11.25	0.91
	Fz	-1.01	-.45	-0.67	1.56	25.18	0.92
TLBO	Fx	-1.23	-0.52	-0.43	1.76	46.70	-
	Fy	1.23	-0.52	-0.43	1.76	11.26	-
	Fz	1.23	-0.52	-0.43	1.76	24.84	-

OM-Optimization methods; R-Responses;
PR-predicted responses; D_c- composite desirability
Table 7. Optimal value of process parameters (coded value)

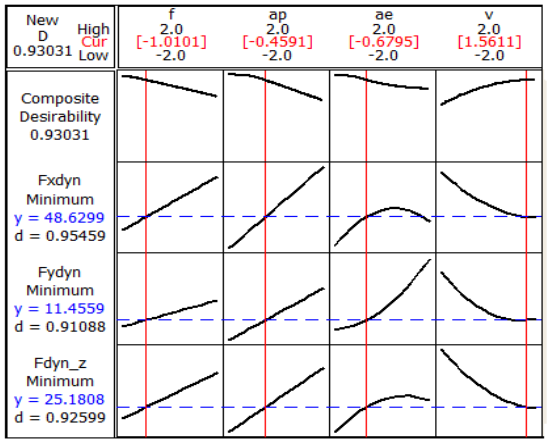

Fig. 6. Optimization results for cutting force components

4.6 Confirmation experiments

Confirmation experiments are carried out to with the set of cutting parameters obtained using CD and TLBO demonstrate the effectiveness of the multi-objective optimization approaches. Two test conditions are also selected from the previous experimental plan (from Table 2), one of the conformation test is performed by selecting random parametric value in the range of cutting parameters. That combination of cutting parameters are further used in the response equations of F_X, F, F_Y and F_Z to verify the developed mathematical models. Conformation experiment settings are shown in Tables 8. In Table, the number in parenthesis represents the coded level of the confirmation experiments. Predicted and experimental values dynamic cutting force components are shown in Table 9. It is found that the experimental values of the optimized cutting parameters are very close to predicted results.

Sl. No.	Exp. No.	f_z (mm/tooth)	a_p (mm)	a_e (mm)	V (m/min)
1	OC* (CD)	0.07 (-1.04)	0.82 (-.45)	0.53 (-0.67)	164 (1.56)
2	OC* (TLBO)	0.06 (-1.23)	0.79 (-0.52)	0.42 (-0.43)	169 (1.76)
3	IC#	0.07 (-1)	1.4 (1)	0.3 (-1)	100 (1)
4	Exp. No. 16	0.17 (1)	1.4 (1)	0.7 (1)	150 (1)
5	Exp. No. 22	0.12 (0)	1 (0)	0.9 (2)	125 (1)

*OC-optimal combination;
#IC-intermediate combination
Table 8. Parameter settings for confirmation experiments

Sl. No.	Predicted values (N)			Experimental values (N)		
	F_X	F_Y	F_Z	F_X	F_Y	F_Z
1	48.62	11.25	25.18	56.02	16.13	29.68
2	46.70	11.24	24.84	50.34	14.56	27.43
3	95.27	10.83	47.23	98.45	12.32	50.12
4	160.07	38.89	75.75	163.3	41.12	78.34
5	101.72	42.18	62.02	103.4	45.23	59.72

Table 9. Results of confirmation experiments

5. CONCLUSIONS

In the present work, an attempt has been made to determine the dynamic force components of the cutting forces obtained from the slot milling test in high speed ball end milling process of Al2014-T6. Dynamic cutting forces in F_X, F_Y and F_Z directions have been determined using Eqs. (1 and 2) using 20000 sample points. Machining experiments have been planned using central composite design. Analysis of variance (ANOVA) has been performed to investigate the effect of cutting process parameters on the dynamic forces and mathematical models have been developed. Developed mathematical models are further used as fitness function to get optimal combinations of cutting parameters using teaching learning based optimization and composite desirability function. Following conclusions have been drawn from the analysis of the results in the present study:

1) Tangential and axial cutting force components are influenced mainly by axial depth of cut with percentage contributions of 49.27% and 45.10%, respectively. Increase in axial depth of cut increases the dynamic cutting force components. Radial cutting force component is mostly affected by radial depth of cut with a percentage contribution of 64.21 %.

2) Cutting speed has significant effect on all the three dynamic cutting force components and increase in cutting speed decreases the magnitude of force component values.

3) Composite desirability function and a comparatively new optimization method TLBO have been applied for optimizing the cutting parameters for all the three

dynamic cutting force components. It is found that TLBO provides better results than composite desirability function approach.

4) The optimization using TLBO methodology took minimum effort and less computational time. The optimal parametric setting obtained by TLBO has been verified through experiments. Thus, the method is an efficient method and may further be employed for optimization of cutting forces and material removal rate in high speed ball end milling process.

5) Confirmation tests have been conducted with optimal cutting parameters to verify the optimization results and effectiveness of the multi-objective optimization approach. It is found that the experimental values at optimized cutting parameters are very close to the predicted results.

6. REFERENCES

[1] Abukhshim NA, Mativenga PT, Sheikh M.A. (2006), Heat generation and temperature prediction in metal cutting: A review and implication for high speed machining. International Journal of Machine Tools & Manufacture 46: 782-800. doi:10.1016/j.ijmachtools.2005.07.024

[2] Kitagwa T, Kubo A, Maekawa K (1997), Temperature and wear of cutting tools in high-speed machining of Inconel 718 and Ti-6A1-6V-2Sn., Wear 202: 142-148. doi:10.1016/S0043-1648(96)07255-9

[3] Alauddin M, El Baradie MA, Hashmi MSJ (1996), Modelling of cutting force in end milling Inconel 718. J. Mat. Proc. Tech 58(1): 100-108., doi:10.1016/0924-0136(95)02113-2

[4] Ding T, Zhang S, Wang Y, Zhu X (2010) Empirical model and optimal cutting parameters for cutting forces and surface roughness in hard milling of AISI H13 steel., Int J Adv Manuf Technol 51(1): 45-55. doi:10.1007/s00170-010-2598-2

[5] Ozel T, Hsu TK, Zeren E (2005) Effects of cutting edge geometry, workpiece hardness, feed rate and cutting speed on surface roughness and forces in finish turning of hardened AISI H13 steel., Int J Adv Manuf Technol 25(3): 262-269. doi:10.1007/s00170-003-1878-5

[6] Dikshit MK, Puri, AB, Maity A (2014) Experimental study of cutting forces in ball end milling of Al2014-T6 using response surface methodology. Procedia Materials Science 6: 612 -622. doi:10.1016/j.mspro.2014.07.076

[7] Toh CK (2004) Static and dynamic cutting force analysis when high speed rough milling hardened steel. Materials and Design 25(1): 41-50. doi:10.1016/S0261-3069(03)00160-2

[8] Tangjitsitcharoen S, Thesniyom P, Ratanakuakangwan S (2014) Prediction of surface roughness in ball-end milling process by utilizing dynamic cutting force ratio. J Intell Manuf, doi: 10.1007/s10845-014-0958-8.

[9] Bhogal SD, Sindhu C, Dhami SS, Pabla BS (2015), Minimization of surface roughness and tool vibration in CNC milling operation. Journal of Optimization. http://dx.doi.org/10.1155/2015/192030

[10] Dimla Snr DE (1998) Multivariate tool condition monitoring in a metal cutting operation using neural networks. Ph.D. Dissertation, The University of Wolver Hampton, UK

[11] Dimla Snr DE (2000) Sensor signals for tool-wear monitoring in metal cutting operations-a review of methods. International Journal of Machine Tools & Manufacture 40(8): 1073-1098. doi:10.1016/S0890-6955(99)00122-4

[12] Dan L, Mathew J (1990) Tool wear and failure monitoring techniques for turning-a review. International Journal of Machine Tools and Manufacture 30(4): 579-598. doi:10.1016/0890-6955(90)90009-8

[13] Montgomery DC (1997) Design and analysis of experiments. Wiley, New York

[14] Rao RV, Savsani VJ and Vakharia DP (2011), Teaching–learning-based optimization: a novel method for constrained mechanical design optimization problems. *Comput.-Aided Design.* 43: 303–315. doi:10.1016/j.cad.2010.12.015

[15] Rao RV, Savsani VJ and Vakharia DP (2012), Teaching–learning-based optimization: an optimization method for continuous non-linear large scale problem. *Information Sciences.* 183: 1-15. doi:10.1016/j.ins.2011.08.006

[16] Rao RV and Kalyankar VD (2013) Parameter optimization of modern machining processes using teaching–learning-based optimization algorithm., *Engineering application of artificial intelligence* 26:524-531. doi.org/10.1016/j.engappai.2012.06.007

[17] Rao RV and Patel V (2012) An elitist teaching-learning-based optimization algorithm for solving complex constrained optimization problems., *International Journal of Industrial Engineering Computations* 3 (4): 535-560. doi:10.5267/j.ijiec.2012.03.007

[18] Baghlani A and Makiabadi MH. Teaching-learning-based optimization algorithm for shape and size optimization of truss structures with dynamic frequency constraints. *IJST Transactions of Civil Engineering, No. C*$^{+}$ 2013; 37: 409-421.

[19] Puri AB, Banerjee S (2013) Multiple-response optimisation of electrochemical grinding characteristics through response surface methodology. IJAMT 64(5): 715-725. doi:10.1007/s00170-012-4065-8

[20] Derringer GC, Suich R (1980) Simultaneous optimization of several response variables. J Qual Technol 12: 214-219.

ACKNOWLEDGMENTS

The experimental work was carried out using Vertical Milling Center in Manufacturing Technology Laboratory, CSIR-CMERI Durgapur, India. The authors acknowledge the support extended by Mr. S. Y. Pujar for his assistance in conducting experiments.

Authors: Mithilesh K. Dikshit[1]*, Asit Baran Puri[2], Atanu Maity[3], [1,2]Department of Mechanical Engineering, National Institute of Technology Durgapur, Durgapur – 713209, India, [3]Advance Design & Optimization, CSIR-CMERI, Durgapur - 713209, India,

***Corresponding author:** Mithilesh Kumar Dikshit

E-mail: dixit.mithilesh@gmail.com, maity@cmeri.res.in,

Journal of Production Engineering
Vol.19 No.1
JPE (2016) Vol.19 (1) Original Scientific Paper
Vrabeľ, M., Maňková, I., Kovač, P., Beňo, J., Franková, M., Paľo, M.

ANALYSIS AND OPTIMIZATION OF HARD TURNING PROCESS USING Al_2O_3/TiCN CERAMIC TiN PVD COATED INSERT WITH REGARD TO SURFACE ROUGHNESS AND CUTTING FORCE COMPONENTS

Received: 01 December 2015 / Accepted: 20 March 2016

Abstract: *The present work focuses on an experimental research of hard turning of 100 Cr6 (62 HRC) material with coated mixed oxide ceramic inserts. The influence of cutting parameters (cutting speed and feed) on surface roughness as well as cutting force components has been analysed using Taguchi design of experiment and Response Surface Methodology (RSM). Graphs of the main effects and composite desirability are used as multi-objective optimization approaches to establish relationship between cutting conditions and investigated parameters. It has been found that the proposed experimental approach to optimize cutting parameters has proven its reliability and can be applied for different machining operations.*
Key words: *hard turning, RSM, optimization, mixed oxide ceramics*

Optimizacija procesa tvrdog struganja korišćenjem Al_2O_3/TiCN keramčkih PVD TiN presvučenih reznih pločica s obzirom na hrapavost obrađene površine i komponente sila rezanja. *Ovaj rad se fokusira na eksperimentalna istraživanja tvrdog struganja materijala 100 Cr6 (62 HRC) sa keramički presvučenim pločicama. Uticaj parametara rezanja (brzine rezanja i pomaka) na hrapavaost obrađene površine kao i na komponente sila rezanja je analiziran pomoću Tagučijevog plana eksperimenta i metode odaziva površina (RSM). Grafikoni zavisnosti je korišćeno kao multi-kriterijumska optimizacija da bi se formirala veza između uslova rezanja i posmatranih parametrima. Došlo se do zaključka da je predloženi eksperimentalni pristup optimizacije parametara rezanja prikladan i da može biti korišćen za razne operacije obrade.*
Ključne reči: *tvrdo struganje, RSM, optimizacija, oksidna keramika*

1. INTRODUCTION

Effective machining of hard to cut materials such as hardened steels represents a challenge of modern manufacturing. In recent years, hard machining (HM) of steel parts hardened to about 45–65 HRC performed by both mixed oxide ceramics and CBN tools became very popular and effective technology replacing successively grinding operations, traditionally used in many mass-production manufacturing processes. Unfortunately, extreme tribological conditions developing at dry severe friction and high tool–chip and work–flank interface temperatures tend towards the acceleration of tool wear, and as a consequence to relatively fast deterioration of surface finish and dimensional and shape accuracy. [1]. The traditional way of processing hard steel involves an established sequence of operations i.e. forming, annealing, rough cutting, heat treatment and grinding, all of which consume significant amounts of time and cost [2]. Cost reduction is due to the fact that in the process of turning several operations can be performed on one machine and fewer types of tools and short setup times are used. The energy necessary for the removal of some amount of material in a hard turning is 5-10% of the energy consumed in grinding [3]. Tonshoff et al. [4] published that the reduction of time in a hard turning is more than 60% compared to grinding. High heat resistance tools of cubic boron nitride (CBN) and ceramics allow the so-called dry machining (without coolant) without negative effects on tool life or on the subsurface properties of components [5]. According to Bouacha et al. [6], the surface roughness when hard turning of AISI 52100 bearing steel (63 HRC) is highly affected by cutting time and feed rate, whereas the depth ot cut presents a negligible influence. As well, it could be improved by increasing cutting speed as a result of less significant plastic behaviour at higher deformation velocity and workpiece material hardness. Horng et al. [7] have studied machinability evaluation of Hardfield steel in the hard turning with mixed oxide ceramic tool and concluded that the analysis of machining parameters using RSM technique has the advantage of investigating the influence of each machining parameter on the value of machinability evaluation.

2. EXPERIMENTAL PROCEDURE

In order to investigate the influence of machining parameters on surface roughness and cutting force component two cutting conditions, including cutting speed (v_c) and feed rate (f) were selected as a machining parameters while depth of cut was kept constant (ap = 0,5 mm).

Cutting conditions were chosen as an independant input variables. The desired responses were three compnonets of cutting force (Fp, Ff, Fc) and two parameters of surface roughness (Ra, Rz). Hard turning experiments were performed on conventional lathe machine tool (SUI 50). Experimental set-up for the test

is shown in Fig. 1. The sample material was 100Cr6 bearing steel with hardness of 62 HRC in the form of round bars with 118 mm diameter. The chcemical composition of 100 Cr6 steel is in mass % as follows: 1.121 C, 0.241 Si, 0.35 Mn, 0.022 P, 0.024 S, 0.092 Cu, 1.671 Cr, 0.053 Ni, 0.011 Nb.

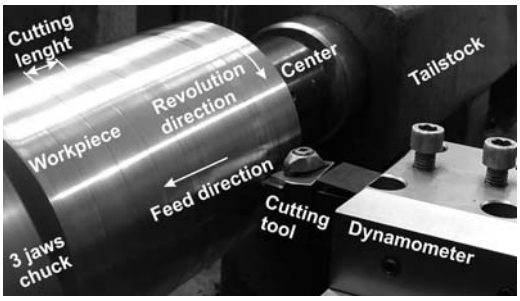

Fig. 1. Experimental setup on SUI 50 lathe

This material represents a chrome steel and is one of the non stainless steels especially recommende to the manufacture of the bearings, tools, drills and utensils. Mixed oxide ceramic (Al_20_3/TiCN) TiN PVD coated insert with designation SNGN 120408 manufactured by ISCAR with tool nose radius r_ε = 0,8 mm (Fig. 2) was used in experimental study. Type SNGN is square double sided ceramic insert with flat rake recommended for machining cast iron, hardened steel and superalloys. The insert was clamped onto tool holder, type CSRNR 2525 M12 020 with geometry as follows -6° rake angle (negative), 75° cutting edge angle, 11° clearance angle, -6° cutting edge inclination.

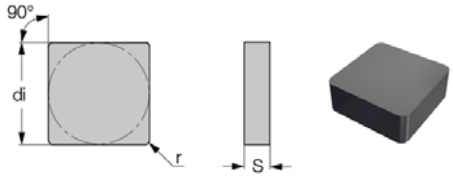

Fig. 2. Iscar SNGN 120408 coated ceramic insert

All turning experiments were carried out in dry cutting conditions. A Kistler 9441 force dynamometer was used to measure cutting forces in three mutually perpendicular directions. The roughness parameters measurement (Ra and Rz) for individual cutting conditions was obtained by a Surftest 301 Mitutoyo. The roughness measurement for one pass of the cutting tool was repeated three times acquire a more accurate results. The cutting parameters for tests were selected based on the cutting tool manufacturer´s recommendations and as well according to previours research carrierd out in a field of hard turning process [8].

Factors	**Levels**		
	1	2	3
Cutting speed v_c [m/min] – x_1	90	120	150
Feed f [mm/rev] – x_2	0,045	0,095	0,15

Table 1. Taguchi array design of two independent variables – factors with 3 levels

Table 1. shows the level of two machining parameters x_1 (cutting speed), x_2 (feed rate) and their range. In this research, an L9 Taguchi standard orthogonal array is adopted as the experimental design. Taguchi method is a systematic approach to find optimum values of design factors that lead to an economical design with low variablitlity [9]. This method can dramatically reduce the number of experiments required to gather necessarz data [10]. The 3 level L9 is shown in Table 2., where the numbers 1, 2 and 3 stand for the values of the independent variable level.

Experiment No.	**Independent variables level**	
	x_1	x_2
1.	1	1
2.	1	2
3.	1	3
4.	2	1
5.	2	2
6.	2	3
7.	3	1
8.	3	2
9.	3	3

Table 2. Taguchi array design of two independent variables – factors with 3 levels

Methodology for the optimization of the machining parameters for the hard turning operation based on Taguchi method and RSM with ceramic cutting tool is shown in Fig. 3. Many researchers have been used both optimization methods for various cutting operations like milling, drilling , turning etc., in machining various alloys [9-13].

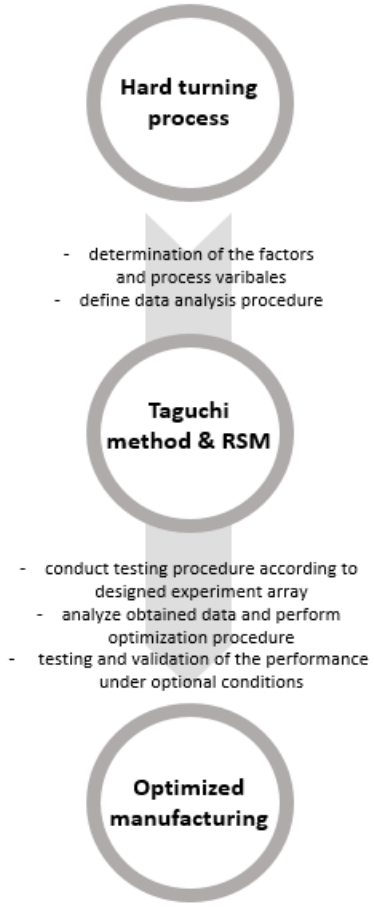

Fig. 3. Diagram of the hard turning optimization procedure

3. RESULTS AND DISCUSSION

The surface roughness parameters (Ra and Rz) and cutting force components (Fp, Ff, Fc) have been measured after the longitudinal turning operation. The experimental conditions and the results obtained are shown in Table. 3.

Experiment No.	Factors		Surface roughness parameters		Cutting force components		
	f [mm]	v_c [m/min]	Ra [um]	Rz [um]	Fc [N]	Ff [N]	Fp [N]
1	0,045	90	0,35	2,5	176	70	465
2	0,095	90	0,16	1,1	174	52	410
3	0,15	90	1,42	7,56	235	173	589
4	0,045	120	0,31	1,61	201	85	354
5	0,095	120	0,75	3,65	219	139	450
6	0,15	120	1,35	6,25	270	195	603
7	0,045	150	0,33	1,84	197	84	370
8	0,095	150	0,73	3,23	263	152	481
9	0,15	150	1,25	5,99	313	226	609

Table. 3 Experimental results for surface roughness parameters and cutting force components

2.1 Effect of cutting conditions on surface roughness parameters

The effect of investigated cutting conditions on surface roughness parameters is shown in Fig. 4. This figure displays that the value of Ra and Rz parameters increase with the increase of the feed rate (f). Both parameters (Ra, Rz) first appears to be increasing with increase of the cutting speed (v_c), but this increase diminished after v_c=120 m/min. The best surface roughness was achieved at the lowest feed rate as expected. In a case of roughness parameters the optimum level is the first one for both independent variales – factors x_1 and x_2.

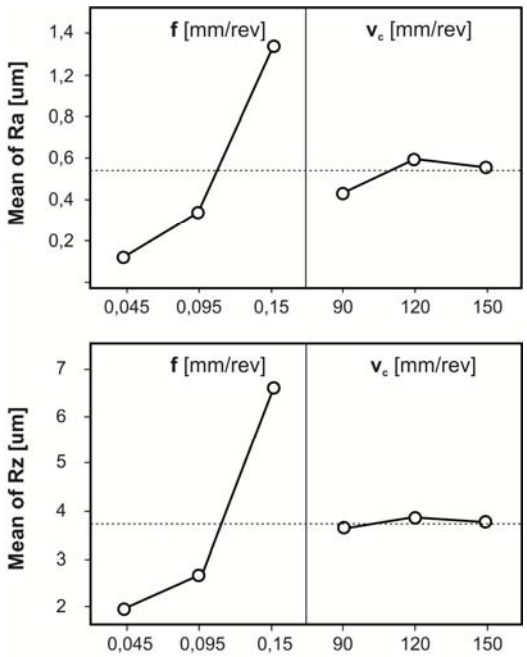

Fig. 4. Main effect plots for surface roughness

2.2 Effect of cutting parameters on cutting force components

The influence of cutting speed and feed rate on cutting force components is shown in Fig. 5. for three different factor levels. The cutting forces results show that the thrust force (Fp) is the largest, the tangencial cutting foce component (Fc) is the middle one and the feed force component (Ff) is the smallest. This is due to the yield strength of the workpiece material evolution after heat treatment and the use of a negative rake angle [14].

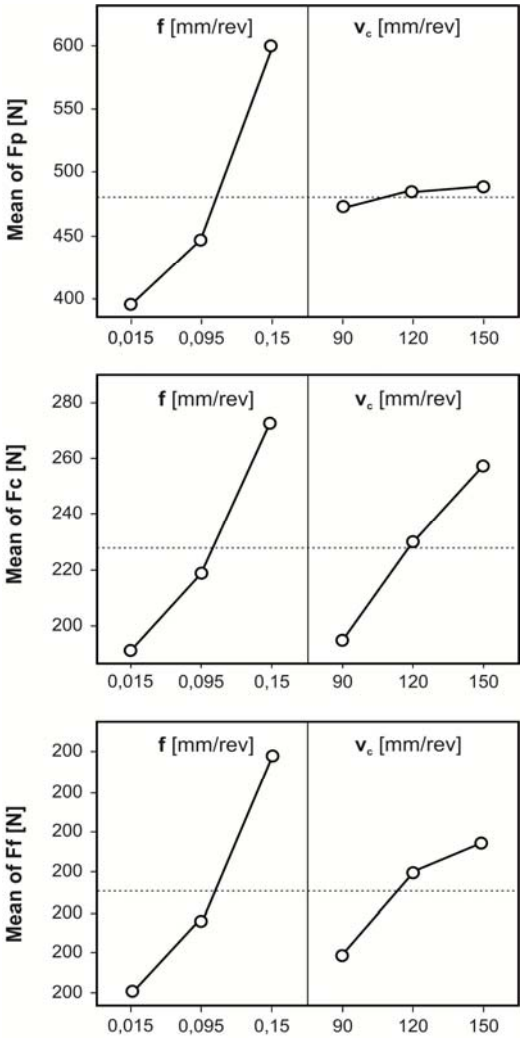

Fig. 5. Main effect plots for cutting foce components

2.3 Optimization using RSM method

Utilization of the response surface optimization method helps to identify the combination of machining conditions (v_c, f) that together optimize the surface roughness parameters and the cutting force components in the hard turning process. Joint optimization must satisfy the requirements for all the responses in the set. Optimization achievement is measured by the composite desirability which is weighted geometric mean of the individual desirability´s for the responses on a range from zero to one [14]. The value of one indicates that the response is in goal and the value of zero means that one or more responses are outside of the acceptable region [15]. Finally, the individual desirability functions are combined to provide a measure of the composite desirability of the multi-response system [16].

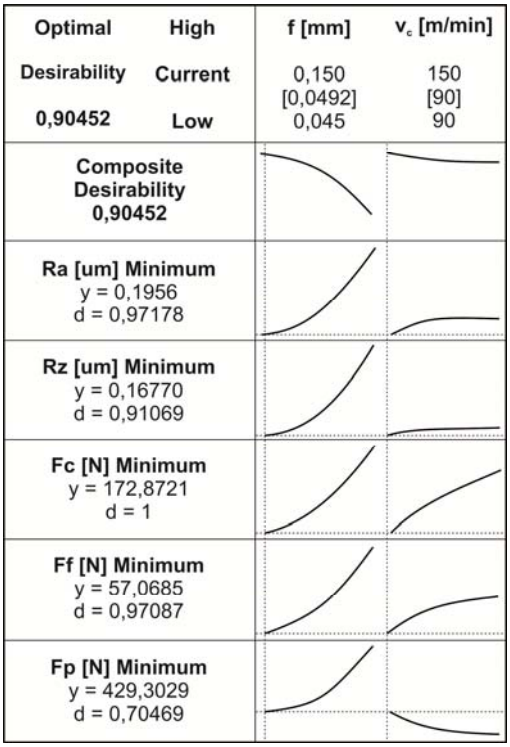

Fig. 6. Optimization plot for surface roughness parameters and cutting force components

RSM optimization results for the surface roughness parameters (Ra, Rz) and the cutting force components (Fc, Ff, Fp) are shown in Fig. 6. The optimum process parameters obtained are found to be cutting speed vc = 90 m/min and feed rate f = 0,049 mm/rev. The optimized cutting force components are as follows : Fc = 173 N, Ff = 57 N and Fp = 429 N. In addition, the optimzed surface roughness parameters Ra = 0,2 um and Rz = 1,7 um which also correspond with results in [17] and [18].

3. CONCLUSION

This study represents a combined application of the Taguchi method and RSM to optimize cutting parameters and investigate their influence on the surface roughness as well as cutting force components when hard turning of 100Cr6 (62 HRC) steel. Both machining parameters namely feed rate (f) and cutting speed (v_c) are optimized to meet minimal values of the study objectives. The results obtained from this research are given below:

- proposed appoach to optimize cutting parameters has proven its reliability and can be used in different machining operations as well
- according to the presented results, the surface roughness is highly affected by feed rate (f) more then by cutting speed (v_c)
- minimal value of the surface roughness parametes Ra and Rz was achieved at the lowest feed rate (f)
- feed rate (f) was also the most sighnificant factor for minimizing cutting force components Fc, Fp and Ff
- based on the response surface optimization and the composite desirability method of RSM, the optimal turning parameters are found to be as follows: f = 0,0492 mm/rev and v_c = 90 m/min

Further study could consider more factors such as insert microgeometry, different cutting materials or coatings when hard turning to investigate other machinability characteristics.

4. REFERENCES

[1] Grzesik, W.: *Wear development on wiper Al2O3–TiC mixed ceramic tools in hard machining of high strength steel*, Wear 266 (2009), pp. 1021–1028.

[2] Rashid, W. B., Goel, S., Luo, X., Ritchie, J. M.: *The development of a surface defect machining method for hard turning processes*, Wear 302 (2013), pp. 1124–1135.

[3] Winands, N.: *Hartdrehen aus der Umformwärme gehärteter Wälzlagerringe*, Dissertation, RWTH Aachen, 1996.

[4] Tonshoff, H. K., Wobker, H. G., Brandt, D.: *Hard turning–Influence on the workpiece properties*. Trans NAMRI/SME 1995;23:215–20.

[5] Ackerschott, G.: *Grundlagen der Zerspanung einsatzgehärteter Stähle mit geometrisch bestimmter Schneide*, Dissertation, RWTH Aachen, 1989.

[6] Bouacha, K., Yallese, M. A., Mabrouki, T., Rigal, J. F.: *Statistical analysis of surface roughness and cutting forces using response surface methodology in hard turning of AISI 52100 bearing steel with CBN tool*, Int. Journal of Refractory Metals & Hard Materials 28 (2010) 349–361

[7] Horng, J.T., Liu, N.M., Chiang, K.T.: *Investigating the machinability evaluation of Hard field steel in the hard turning with Al2O3/TiC mixed ceramic tool based on the response surface methodology*, J. Mater. Process. Technol. 208 (2008) 532–541.

[8] Grezesik, W.: *Influence of tool wear on surface roughness in HT using differently shaped ceramic tools*, Wear 265 (2008) 327–335.

[9] Debnath, S., Reddy, M. M., Yi, Q. S.: *Influence of cutting fluid conditions and cutting parameters on surface roughness and tool wear in turning*

process using Taguchi method, Measurement 78 (2016) 111–119

[10] Gupta, M., Kumar, S.: *Investigation of surface roughness and MRR for turning of UD-GFRP using PCA and Taguchi method*, Engineering Science and Technology, an International Journal 18 (2015) 70-81.

[11] Duchosal, A., Serra, R., Leroy R., Hamdi H.: *Numerical optimization of the Minimum Quantity Lubrication parameters by inner canalizations and cutting conditions for milling finishing process with Taguchi method*, Journal of Cleaner Production 108 (2015) 65-71

[12] Kıvak, T.: *Optimization of surface roughness and flank wear using the Taguchi method in milling of Hadfield steel with PVD and CVD coated inserts*, Measurement 50 (2014) 19–28.

[13] Pandey, R. K., Panda, S.S.: *Multi-performance optimization of bone drilling using Taguchi method based on membership function*, Measurement 59 (2015) 9–13.

[14] Bouacha, K., Yallese, M. A., Khamel, S., Belhadi, S.: *Analysis and optimization of hard turning operation using cubic boron nitride tool*, Int. Journal of Refractory Metals and Hard Materials 45 (2014) 160–178

[15] Derringer, G., Suich, R.: *Simultaneous optimization of several response variables*, J. Qual. Technol. 12 (1980) 214–219.

[16] Sarkar, S., Sekh, M., Mitra, S., Bhattacharyya, B.: *Modeling and optimization of wire electrical discharge machining of c-TiAl in trim cutting operation*, J. Mater. Process. Technol. 205 (2008) 376– 387.

[17] Szabo, G., Kundrák, J.: *Investigation of residual stresses in case of hard turning of case hardened 16MnCr5 Steel,* Key Engineering Materials. 581 (2014) 501 – 204.

[18] Čiliková, M., Mičieta, B., Neslušan, M.: *Prediction of the catastrophic tool failure in hard turning through acoustic emission*, Materiali i Tehnologije. 49 (2015) 355 – 363.

ACKNOWLEDGEMENT

This work was supported by the Slovak Research and Development Agency under the project APVV SK-SRB-2013-0037 "Implementation of the artificial intelligence into optimisation of the selected advanced removal processes" as well as by the project VEGA 1/0434/15 "Research on process dependent interface when milling with small diameter of end mill cutters"

Authors: **Dr. Marek Vrabeľ., Prof. Dr. Ildikó Maňková., Assist. Professor Dr. Jozef Beňo, Ing. Mária Franková., Ing. Miroslav Paľo.,** Technical University of Košice, Faculty of Mechanical Engineering, Deptartment of Manufacturing Technology and Materials, Mäsiarska 74, 040 01 Košice, **Prof. Dr. Pavel Kovac.,** University of Novi Sad, Faculty of Technical Sciences, Institute for Production Engineering, Trg Dositeja Obradovica 6, 21000 Novi Sad, Serbia, Phone.: +381 21 450-366, Fax: +381 21 454-495.

E-mail: marek.vrabel@tuke.sk
ildiko.mankova@tuke.sk
jozef.beno@tuke.sk
maria.frankova@tuke.sk
miroslav.palo@tuke.sk
pkovac@uns.ac.rs

Journal of Production Engineering
Vol.19 No.1
JPE (2016) Vol.19 (1) Original Scientific Paper
Himanshu Payal, Sachin Maheshwari, Pushpendra S. Bharti

EFFECT OF TOOL MATERIAL ON SURFACE ROUGHNESS IN ELECTRICAL DISCHARGE MACHINING

Received: 08 May 2016 / Accepted: 20 June 2016

Abstract: *H11 die steel is widely used in forging dies, aircraft landing gears and shafts. Electric discharge machining (EDM) is one of the most suitable processes to shape this material. This work demonstrates the effect of pulse-on-time (T_{on}) on surface roughness during EDM of H11 tool steel by taking three different tool electrode materials. Experiments have been conducted by varying T_{on} in four steps (10 µs, 20 µs, 30 µs, 40µs) while keeping the values of other variables fixed. On the basis of experimental results, it is concluded that tool properties of electrode play a vital role in machining characteristics of die-sinking EDM process. The results demonstrate that Copper-tungsten electrode offers the best surface finish followed by graphite and copper electrode in EDM of H11 too steel.*
Key words: *electrical discharge machining, surface roughness, pulse-on-time, H11*

Uticaj materijala alata na hrapavost obrađene površine kod elektro-erozivne obrade. *Alatni čelik H11 je široko primenjen kod alat za hladnu deformaciju, donjeg trapa aviona i vratila. Elektro erozivna obrada je jedan od najadekvatnijih postupaka obrade ovakvog tipa materijala. U ovom radu je demonstriran efekat vremena ciklusa pražnjenja na površinsku hrapavost obratka kod elektro erozivne obrade alatnog čelika H11 korišćenjem tri različita materijala elektrode. Eksperimenti su sprovedeni variranjem dužine vremena ciklusa pražnjenja na četiri nivoa (10 µs, 20 µs, 30 µs, 40µs) dok su ostali parametri konstantni. Na osnovu eksperimentalnih istraživanja zaključeno je da osobine materijala elektrode igraju ključnu ulogu u karakteristikama procesa elektro erozivne obrade punom elektrodom. Rezultati pokazuju da elektrode od legure bakar-volframa nude najbolju površinsku hrapavost a iza njih su grafitne i čisto bakarne elektrode kod elektro erozivne obrade alatnog čelika H11.*
Ključne reči: *elektro erozivna obrada, hrapavost površine, vreme ciklusa pražnjenja, H11*

1. INTRODUCTION

H-11, a hot die steel material, with distinctive properties like high hardenability, high strength, high toughness, resistance to thermal softening and high heat generation makes this steel suitable for the production of hot work dies, extrusion, forging, die casting etc.Its distinctive properties encompass the automotive and aerospace industries and find usage in gears, bearing, tool, aircraft landing gears, helicopter rotor blades and shafts [1].

The difficulties faced in the machining of H11 on conventional machines can be attributed to its mechanical and metallurgical properties. The addition of 1.5% Molybdenum imparts high hardenability to this steel and make difficult to machine by conventional process [2]. Non-traditional machining is found to be one of the alternatives for machining H11.EDM is a process in which material is eroded from the work piece by the use of electric sparks occurring between the tool and the work piece separated by a dielectric medium. The temperature which is created by the electrical spark is around 8000-12000^{0}C which is enough to melt and erode the work piece surface as well as tool electrode also. EDM is known for its thermal behaviour which can machine any electrically conductive material regardless of its strength and hardness [3]. Therefore, EDM is specialized in generating a complex structure with high precision in the range of several micrometres with remarkable surface finish [4].

EDM is a very complex process whose performance depends on the parameter chosen.Thus, certain input parameter which when varied in EDM process have a significant effect on performance measures such as material removal rate (MRR), tool wear rate(TWR),and surface roughness (SR) of the machined work piece. The efforts are constantly being made in the area of EDM to obtain high MRR and TWR along with low SR.A lot of work has been reported in the literature in respect of obtaining a high level of surface finish in the field of EDM.Payal et al. [5] investigated the machining characteristics of H11and H13 material by taking three electrode material i.e. aluminium, copper and graphite. They reported that copper electrode achieved the best surface finish among other electrodes. Singh et al. [6] conducted an experimental investigation on EDM for H11 tool steel. It was found from the experimental results that by selecting the negative polarity of the electrode and mixing of dielectric with suspension powder there will be an improvement in the SR. Singh et al. [7] explained the influence of electrode type and material on the EDM process by taking EN-31 tool steel as a work piece and copper, copper-tungsten, aluminium, and brass as an electrode material. They have taken discharge current as the input parameter which varies in steps. They reported that copper electrode showed better results related to MRR, diameter overcut, TWR and SR followed by the aluminium electrode. Jahan et al. [8] investigated the performance of micro-edm on Tungsten carbide (WC)

using copper tungsten (CuW), Tungsten (W) and silver-tungsten (AgW) as an electrode material. The performance measures selected were surface characteristics, average surface roughness and peak-to-valley. It was observed that AgW was the best electrode material in all performance measures. Muthuramalingam and Mohan [9] explained the importance of tool electrode materials (copper, brass, tungsten carbide) on the machining performance of AISI 2020 stainless steel in EDM process. They reported that copper electrode produces higher MRR and tungsten carbide electrode showed better surface finish. Dewangan et al.[10] studied the effects of EDM parameters as well as tool electrode materials (copper, brass and graphite) onAISIP20 tool steel .They have reported that graphite tool showed better results in regards towhite layer thickness,surface crack density and SR followed by brass, copper. Lee and Li[11] conducted an experimental investigation on EDM for Tungsten carbide material using copper, copper tungsten and graphite as tool electrode material. They have taken MRR, SR, TWR as the performance measures.It was observed from the results that graphite electrode offers higher MRR whereas copper electrode showed higher TWR but better surface finish.They also reported that with negative tool polarity maximum MRR, minimum TWR and SR could be achieved.

The present work investigates the EDM of AISI H11 tool steel material using three different electrode materials copper (Cu), copper-tungsten (CuW) and graphite (Gr). The pulse –on –time has been varied in four steps to study the SR.

2. EXPERIMENTATION

The experiments were conducted on Electronica PS50ZNC die sinking machine shown in figure 1with commercial grade EDM oil (density=0.784Kg/m^3, flash point=103^0 C, dielectric strength=45) was used a dielectric fluid. The work piece material was AISI H11 tool steel with the rectangular shape of 40mmx36mmx18mm dimension. Three different tool electrodes of cylindrically shaped namely Copper (Cu), Copper tungsten, Cu20%W80%) and Graphite (Gr) as shown in figure 2 were used in the present study. Typical mechanical properties and chemical composition of H11 are depicted in table 1and table 2. Table 3 represents the experimental conditions in which all the parameters were kept constant except pulse-on-time. The different properties of all the tool materials are depicted in table 4. The input parameter pulse-on-time has been varied in four steps. The other input parameters were kept fixed during experimentation. The SR is taken as the response variable.SR in measurement is defined in different ways like arithmetic average (R_a), average peak to valley height (R_z) and peak roughness (R_p), etc. In the present study arithmetic mean SR value (R_a) is found out. Arithmetic average roughness is defined as the deviation of the roughness profile from the central line along the measurement.The mathematical formula to calculate R_a isaverage deviation of profile *y(x)* from the mean line as shown in equation 1 and 2 [12].

$$R_a = \frac{Total\ shaded\ area}{L} \quad (1)$$

$$R_a = \frac{1}{L}\int_0^L |y(x)|dx \quad (2)$$

Where, y(x): Value of roughness profile L: Evaluation length. Figure 3 shows the photograph of Mitutoyo Surface Roughness Tester SJ2100 has been used in the evaluation of surface roughness value.

Property	Unit	Value
Density	g/cm^3	7.81
Melting Point	$^\circ$C	1427
Elastic modulus	GPa	207
Thermal expansion	(10-6/$^\circ$C)	11.9
Thermal conductivity	(W/m-K)	42.2
Hardness	HRC	57

Table 1. Mechanical properties of H11

Elements	C	Si	Mn	P	S
Wt. %age	0.648	0.603	0.262	0.0078	0.0145
Elements	Cr	Mo	V		
Wt. %age	5.17	1.23	0.756		

Table 2. Chemical composition (wt %) of H11 material

Pulse on Time	10µs,20µs,30µs,40µs
Sparking Voltage	60V
Current	8A
Dielectric used	Spark Erosion oil (SEO-250)
Polarity	Straight
Servo system	Electro Hydraulic
Electrode polarity	Negative
SEN/ ASEN	6/4

Table 3. Experimental Conditions

Material	Gr	Cu	CuW
Composition	-	99.9 % Cu	20%Cu +80%W
Density(g/cm^3)	1.811	8.904	15.2
Melting point(^{o}C)	3350	1083	3500
Electrical-resistivity(Ωmm^2/m)	10	9	5.5

Table 4. Electrode material properties

Fig.1. Physical set up of Electrical Discharge Machine

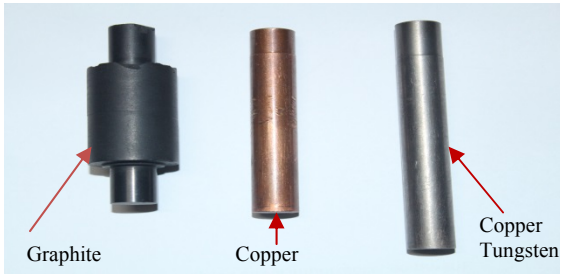

Fig. 2. Electrodes Gr, Cu and CuW


Fig.3. Mitutoyo Surface Roughness Tester SJ2100

The initial and final weights of the electrode and work piece are measured by the electronic weighing balance of make Shimadzu ATX224 having a resolution of 10mg. Figure 4 shows the H11 work piece machined by different electrode material i.e. copper tungsten, copper and graphite.

3. RESULTS AND DISCUSSION

On the basis of the experimental results, the effect of pulse-on-time on SR with different tool electrode materials has been shown in Figure 6. The surface profile of different electrode material for different value of pulse-on-time is given in figures 7-9. Figure 6 indicates that SR increases with increase in pulse-on-time for all the three electrode material. This may be attributed to the formation of deep craters with the increase in pulse-on-time resulting in rougher surface. SR is dependent on the value of the pulse-on-time, lower the value of pulse on time smoother will be the surface formed [13]. Hence, the surface finish of the work piece depreciates with an increase of pulse-on-time and gets better with low pulse-on-value. In the present study, the results depict that CuW exhibits best surface finish as compared to the other two electrodes because of the thermophysical property of the electrode. CuW has high density, high strength, high melting point as well as good thermal and electrical conductivity which contribute in obtaining high surface finish.

The melting point of electrode material can also be linked up with the surface quality of work piece. Higher pulse- on- time leads to more discharge energy resulting in more heat and temperature at the electrode part. At higher temperature, electrode melts and the debris of electrode material fall at the surface of work piece making the surface rougher. The melting points of Cu, CuW and Gr are 1083^0C, 3500^0C and 3350^0C respectively [14]. Therefore, CuW showed better surface finish than the other two electrodes.

Pulse on time (µs)	Ra by Cu (µm)	Ra by CuW (µm)	Ra by Gr (µm)
10	5.072	3.5385	3.563
20	5.4215	5.0855	4.322
30	5.5712	5.362	5.1155
40	5.6012	5.5585	6.202

Table 5. SR with Cu, CuW and Gr electrodes at different pulse-on-time.

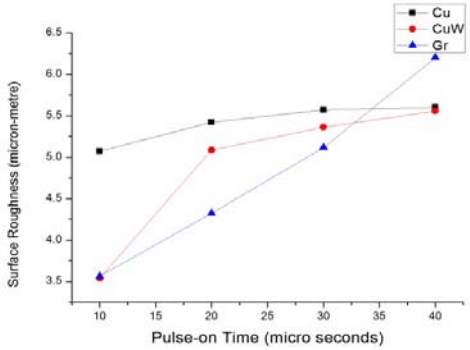

Fig.6. Pulse –on- Time vs SR

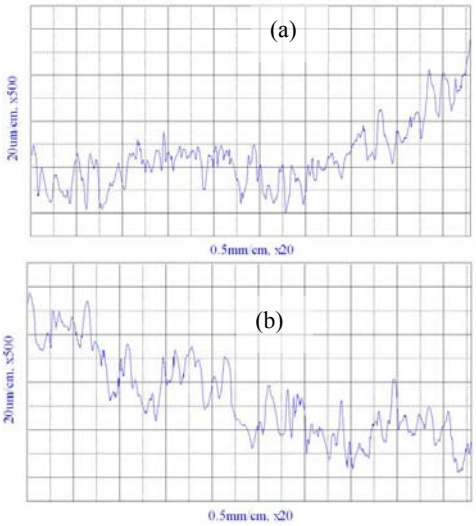

Fig. 7. SR profile of Cu at (a) 10 µs and (b) 40µs.

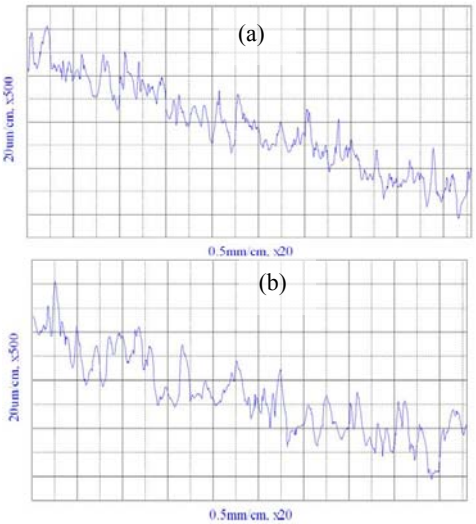

Fig .8. SR profile of CuW at (a) 10 µs and (b) 40µs.

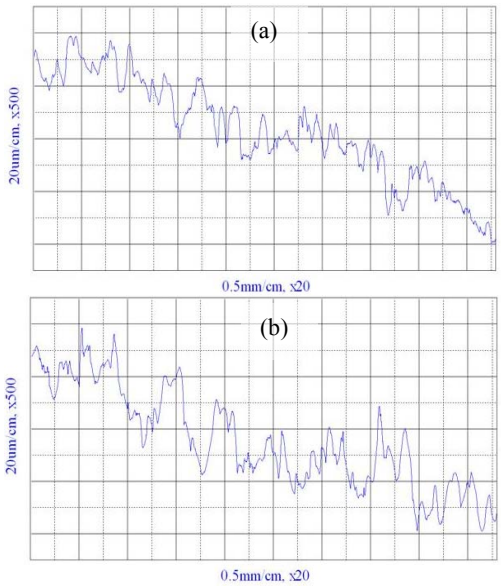

Fig. 9.SRprofile of Gr at(a) 10 µs and (b) 40µs.

4. CONCLUSION

The experimental study has been conducted to investigate the effect of pulse-on-time on SR during EDM of AISI H11 tool steel material by taking three different tool electrode materials. The value of SR with initially increases at a faster rate with increase in pulse-on-time and after a particular value that rate decreases. In the instant case, it is concluded that CuW offers the lowest SR followed by Gr and Cu.

5. REFERENCES

[1] Qamar,Z.S.: *Effect of heat treatment on mechanical properties of H11 tool steel,* Journal of Achievements in Material and Manufacturing Engineering**,** 35/2, pp.115–120, 2009.

[2] Mathew,N.,Kumar,D., Beri ,N., Kumar,A.:*Study Of Material Removal Rate Of Different Tool Materials During Edm Of H11 Steel At Reverse Polarity,* International Journal of Advance Engineering Technology,Vol.5(2), pp.25-30, 2014.

[3] Tsai,H.C,Yan,B.H.,Huang,F.Y.:*EDM performance of Cr/Cu based composite electrodes*, International Journal of Mechanical Tools Manufacture, 43, pp.245-252, 2003.

[4] Puertas, I., Luis, J.C., Villa, G.: *Spaceroughness parameter study on the EDM of silicon carbide*, Journal Material process technology 164-165, pp.1590-1596, 2005.

[5] Payal, Himanshu, Garg, K. R.,Sachdeva, A.: *Investigation of surface integrity of Hot die steel after EDM,* International conference on Advances in material and ManufacturingTechnologyChitkara University, 2011.

[6] Singh, Baljinder, Singh, Paramjit, Tejpal, Gaurav, Singh, G.: *An experimental study of surface roughnessof H11 steel in EDM process using copper tool Electrode*, International Journal of Advanced Engineering Technology,Vol.3, pp. 130-133, 2012.

[7] Singh, Shankar, Maheshwari,S., Pandey, C. P.: *Some investigations into the electric discharge machining of hardened tool steel using different electrode materials*, Journal of Materials Processing Technology, Vol.149, pp. 272–277, 2004.

[8] Jahan, P. M., Wong, S. Y.,Rahman,A.: M.*Study on the fine-finish die-sinking micro-EDM of tungsten carbide using different electrode materials*, Journal of materials processing technology, Vol.209, pp. 3956–3967. 2009.

[9] Muthuramalingam, .T., Mohan,.B.: *Influence of Tool Electrode Properties on Machinability in Spark Erosion Machining*, Materials and Manufacturing Processes, Vol.28,pp. 939–943, 2013.

[10] Dewangan, S.,Biswas, K.C.,Gangopadhyay, S.: *Influence of Different Tool Electrode Materials on EDMed Surface Integrity of AISI P20 Tool Steel,* Materials and Manufacturing Processes, Vol.29, pp.1387–1394, 2014.

[11] Lee. H.S., Li.P.X.: Study of the effect of machining parameters on the machining characteristics in electrical discharge machining of tungsten carbide, Journal of MaterialProcessing Technology, Vol.115, pp.344-358.

[12] Pradhan, K. M., Biswas, K. C.: *Modeling and analysis of process parameters on surface roughness in EDM of AISI D2 tool steel by RSM approach*., International Journal ofEng Applied Science, Vol.5(5), pp.346–351, 2009.

[13] Amorim L.F., WeingaertnerL.W.: *Thebehavior of graphite andcopper electrodes on the finish die-sinking electrical discharge machining (EDM) of AISI P20 tool steel,* Journal oftheBrazilian Society of Mechanical Sciences and Eng, Vol.29(4), pp. 367–371, 2007.

[14] Khan, Rahman Ashikur, Md., Rahman, M.M. Kadrirgama, K.: *An experimental investigation on surface finish in die-sinking EDM of Ti-5Al-2.5Sn*, International Journal of Advance Manufacturing Technology,Vol.77,pp. 1727–1740, 2015.

Authors: Himanshu Payal[1], Research Scholar., Prof. Dr. Sachin Maheshwari[1]., Dr.Pushpendra Singh Bharti[2]., Associate Prof.,[1]M.P.A.E. Division, NetajiSubhas Institute of Technology, New Delhi, India.,[2]U.S.I.C.T., Guru Gobind Singh Indraprastha University, New Delhi India.

E-mail: himanshupayal@rediffmail.com
ssaacchhiinn@gmail.com
psbharti@rediffmail.com

Journal of Production Engineering
Vol.19 No.1
JPE (2016) Vol.19 (1) Original Scientific Paper
Mitrovic, A., Kovac, P., Kulundzic, N., Savkovic, B.

3D FINITE ELEMENT SIMULATION OF MILLING

Received: 04 April 2016 / Accepted: 03 June 2016

Abstract: *The aim of this paper is the modeling and simulation of milling predictive temperature in the cutting zone by using the finite element method. Milling is one of the most common and complex conventional treatment processes and is influenced by a large number of output parameters. One of the most important parameters is temperature because it affects the wear and tool life. In order to predict the occurrence of thermal processing milling was used software package Third Wave AdvatEdge. 3D model of the workpiece and end mill was created in the software package SolidWorks. The results obtained from simulations and experimental work when compared was proved to be valid.*
Key words: *finite element analysis, milling, temperature, Third Wave AdvatEdge*

3D simulacija procesa obrade glodanjem metodom konačnih elemenata. *Cilj rada je modeliranje i simulacija procesa obrade glodanjem sa predviđanjem temperature u zoni rezanja pomoću metode konačnih elemenata. Obrada glodanjem je jedan od najčešćih i najsloženijih konvencionalnih postupaka obrade i pod uticajem je velikog broja izlaznih parametara. Jedan od najznačajnijih parametara je temperatura jer utiče na habanje odnosno postojanost alata. U radu je za predviđanje toplotnih pojava u obradi glodanjem korišćen programski paket Third Wave AdvatEdge. Kreiran je 3D model vretenastog glodala i obratka u softverskom paketu SolidWorks. Upoređivanjem vrednosti dobijenih simulacijama i eksperimentom dobijeni su validni rezultati .*
Ključne reči: *metoda konačnih elemenata, glodanje, temperatura, Third Wave AdvatEdge*

1. INTRODUCTION

Milling is one of the most conventional machining processes used in the industry. Also, it is one of the most complex processing of metals by cutting, because the milling cutter, as well as multi-cutter tool, presents a more complex operation compared to turning and drilling process, not only because of the large number of cutting edges, but also because of the variability of intersection of the chips while a tooth is processing. This process is influenced by many output parameters and one of the most important parameters is the temperature because it affects the tool wear and tool life. Cutting tools are expensive and have a duration that is measured in minutes and is therefore predicting temperature and tool wear during the machining process is of the great importance for the understanding and optimization of process parameters.

In addition, it is believed that after turning, milling process is the most common in removing material. The most common is face milling with milling heads and end milling. The end milling is one of the typical interruptible process. In the process, since the cutting tool repeats cutting material and air cutting, the temperature of cutting tool repeats heat up and cooling down. Cutting temperature is an important parameter because alternating heating and cooling of cutting tools affects the tool wear and surface quality.

To determine cutting temperature or temperature fields in end milling we can use different methods. Due to the complexity of milling processing main difficulties in measuring cutting temperature during the milling is because of the following: the tool rotates and teeth tools entering into engagement with the workpiece in and out of it; area covered with heat moves across the surface of the workpiece; chips can interfere with the measuring [1, 2].

Over the past decades large number of experimental methods has been developed to measure the temperature of milling. Thermocouples are often used in measuring temperature since they are easy to use, covering a wide range of temperatures and are relatively cheap, although there is possibility of errors in installation and in the interpretation of readings. Methods based on the radiation makes it possible to perform temperature measurement without contact with the object of measurement. These methods include measuring point temperature using infrared pyrometer and measurement of the temperature fields, or a certain area using an infrared thermal imaging camera. It turned out that the method of measuring temperature by using infrared thermal imaging camera the most appropriate method in terms of the recording of the temperature. High quality thermographic equipment offers the highest acceptable level of accuracy of the estimates, although this method can be inaccurate because of changes in the emission coefficient and the possibility that chips with its position shelters the area whose temperature is measured.

The experimental approach for studying treatment process is expensive and time-consuming especially when it includes a wide range of tool geometry, materials and processing parameters. Alternative approaches have been developed because of these difficulties such as mathematical simulations that use numerical methods. It turned out that the numerical

finite element methods most useful and widely used.

The proper selection of FEM software is very important for determining the scope and quality of analysis that will be performed. For the simulation processing is used software package Third Wave advantedge.

2. EXPERIMENTAL SETUP FOR END MILLING

The experiments were carried out on a vertical CNC machining centre in dry cutting conditions. Dimensions of workpiece were 50 × 20 × 10 millimeters of AISI 4340 steel with the material properties according to Table 1.

Density	785 (kg/m^3)
Melting point	1450 (^{O}C)
Young's modulus	208 (GPa)
Poission ratio	0,3
Specific heat	477 (J/kg^{o}C)
Thermal conductivity	44,5 (W/m^{o}C)

Table 1. AISI 4340 steel material properties

Tests used an uncoated tungsten carbide end mill model with 10 mm of diameter, length of 72 mm, depth of cut of 22 mm, and number of flutes of 4. The work pieces were painted black due to the emissivity. The machining operation is done for the cutting conditions shown in Table 2.

Cutting conditions	
Spindle speed, n	2200 (rev/min)
Feed per tooth, f	0,040 (mm/tooth)
Axial depth of cut, a_p	1 (mm)
Radial depth of cut, a_e	2 (mm)

Table 2. Selected machining parameters in experiment

Figure 1 shows the experiment's setup. The data acquisition of temperature was done using a FLIR InfraCAM Wester infrared camera, with an accuracy of 0.1°C. The assembly of the infrared camera was at 300 mm from the heat source.

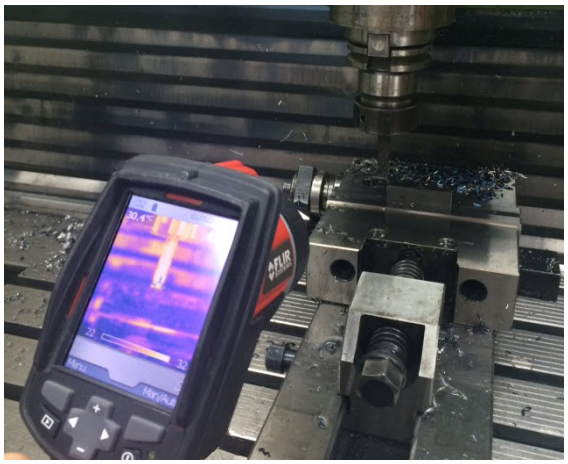

Fig. 1. Monitoring the temperature using infrared camera

Figure 2 shows temperature that was recorded on the end of work piece.

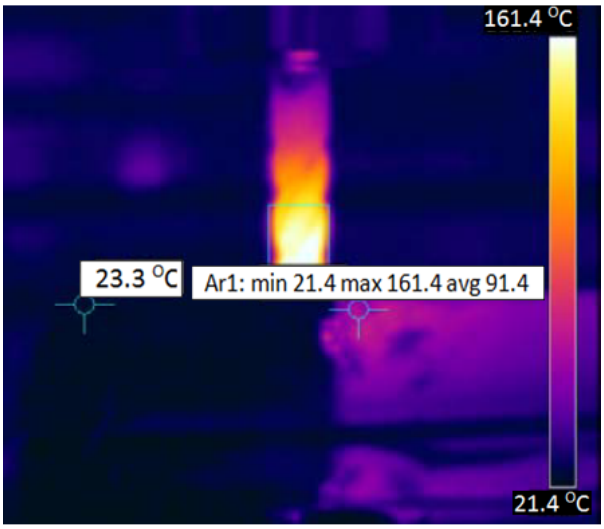

Fig. 2. Infrared imagery of end-mill process

3. FEM TOOL FOR CUTTING PROCESS

In the research field of cutting process, the finite element method is regarded as a very useful tool to study the cutting process of materials [3]. Finite Element Method (FEM) permits the prediction of cutting forces, stresses, tool wear, and temperatures of the cutting process so that the cutting tool can be designed. The right choice of finite element software is very important in determining the scope and quality of the analysis that will be performed [4]. One of The most important software package used for simulation of metal cutting is Third Wave AdvantEdge.

Third Wave AdvantEdge is a special program written for machining simulations. It is developed based on the dynamic explicit Lagrangian formulation. The model is built by selecting the type of machining operation (e.g. turning, broaching, sawing or milling) and defining the necessary process parameters [5]. AdvanEdge contains a user friendly interface and offers the possibility of creating new tool and workpiece geometries within the program and also to import complex geometries form other CAD files. Also allows users to import complex geometries and have extensive material library and allows specifying new materials uses adaptive meshing to increase the accuracy of solution. In AdvanEdge simulations can run in demonstration mode, decreases the simulation time but is less accurate and standard mode, requires longer simulation time but is more accurate [6].

AdvantEdge utilizes Tecplot software to display and assist in analyzing simulation results [7]. The Tecplot displays and assists in analyzing the simulation results. Among the displayed results there can be enumerated: chip formation, chip and tool temperature, cutting forces, steady state variables such as: strain, stress, strain von Misses, etc [6].

4. FEA SIMULATION OF END MILLING

According to the experiments presented in the previous section, a 10 mm diameter end mill have been

designed with SolidWorks. After that, one more simplified end mill model is created in the aim to gave a coarser mesh and based on that reduce the duration of the simulation. In both cases it is taken into account only cutting part of the mill participating in machining. Then end mill models were exported in STL files and imported into AdvantEdge. Figure 3 shows the end mills model imported in AdvantEdge.

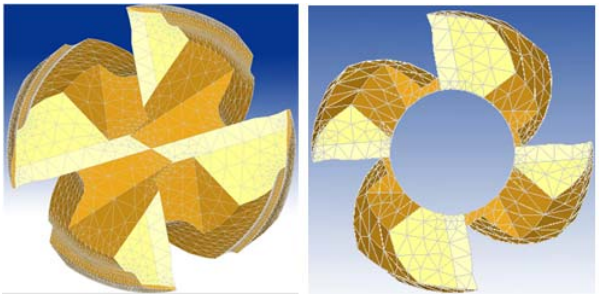

Fig. 3. End mills imported in AdvantEdge

Workpiece material AISI 4340 steel and tool material Carbide-General were selected from the library of 3D materials. Workpiece model was reduced regards to the workpiece from the experiment due to better mesh generation. Figure 4 shows model of complex end mill and the workpiece in Advantedge before starting the simulation.

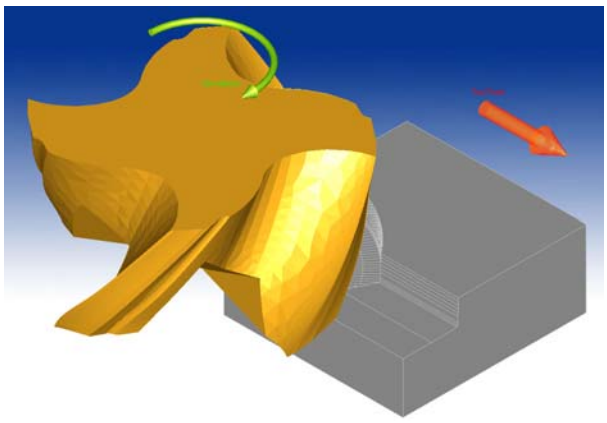

Fig. 4. End mill and workpiece in AdvantEdge

In AdvantEdge users have the option to alter the workpiece meshing parameters; however, these modifications may affect performance and accuracy. Meshing parameters selected within the Workpiece Meshing tab of the 3D Simulation Options window are important for successful 3D simulations. Minimum element edge length and the radius of regined region values are calculated differently depending on the process. In milling, these values are calculated using maximum chip load based on the feed per tooth and the radial depth of cut. For all of these processes, these meshing values will be recalculated every time the process parameters for these simulations are changed [6]. If a simulation crashes, for any reason, a new simulation can start where the previous stopped.

4.1 Simulation results

Two simulations were run in demonstration mode without changes in Workpiece Meshing. First simulation used simplified end mill. Second simulation used complex end mill in order to get more accurate simulation results. Cutting conditions used in the simulation correspond to the processing parameters in the experiment. The calculation time is approximately 3 days for simulation with simplified end mill and 7 days for simulation complex end mill. Simulation worked on a HP xw8600 workstation with 2 x CPU of 4 physical cores each, meaning a total of 8 physical cores and 16 GB RAM.

Figure 5 and 6 show the FEM model of milling operation and temperature distribution for cutting conditions from Tabele 2.

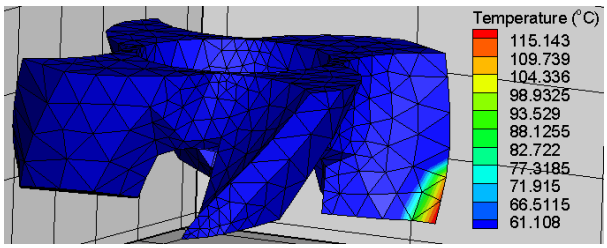

Fig. 5. Temperature distribution during simulation 1

The Contour tab of the AdvantEdge Quick Analysis window is used to select contour displays in Tecplot. The different colors on the tool represent different levels of temperature.

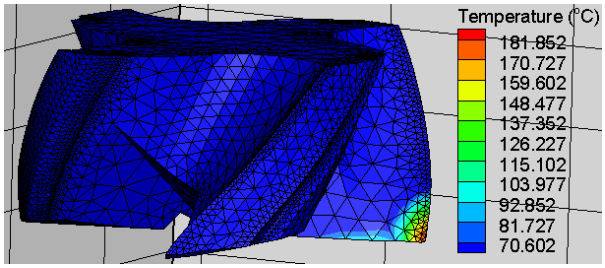

Fig. 6. Temperature distribution during simulation 2

Using Tecplot software it can be seen different steps during the simulation. It is possible to observe the chip formation during a tooth path. Figure 7 and 8 present the temperature contours on end mill, work piece and chips. A contour level is a value at which contour lines are drawn, or for banded contour flooding, the border between different colors of flooding [8].

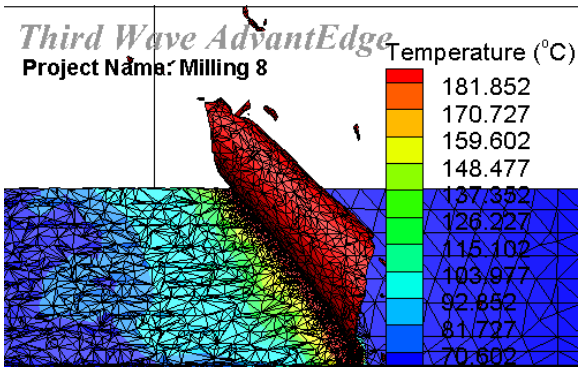

Fig. 6. Temperature contours on chips obtained through simulation results

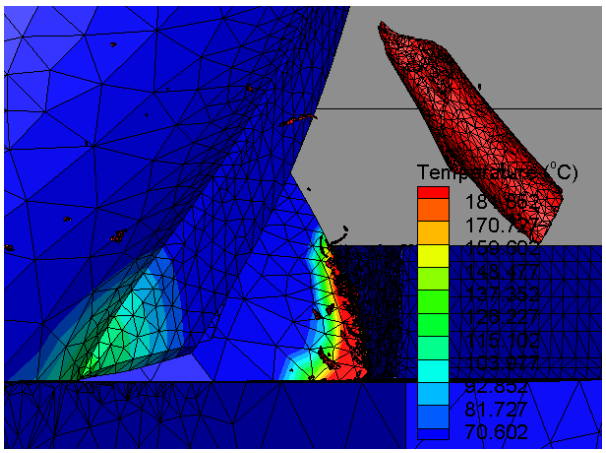

Fig. 7. Temperature contours on end mill and chips obtained through simulation results

4.2 Simulations vs. experiment

The variation of temperature distribution between FEA simulations and experimental work are shown in Table 3.

	Exp. Result	FEA Result	Error
Simulation No.1	161,4 ^{O}C	115,1 ^{O}C	-28,68%
Simulation No.2	161,4 ^{O}C	181,8 ^{O}C	12,64%

Table 3. Results comparation

By comparing the experiment and the simulations showed that the error for the first simulation of -28.68% and for the second simulation 12.64%.

5. CONCLUSION

Simulation of milling in AdvantEdge allows analyzing temperature in the cutting zone and permit obtaining reliable data for the experiment validation. The error between experimental work and simulation by FEA is in the range of ±30%. Accurate modeling of the end mill geometry should be used to improve the numerical prediction of cutting temperature even though it has a significant impact on increasing the duration of the simulation. The results of the work can be used for optimizing the parameters of milling operation of AISI 4340 steel.

6. REFERENCES

[1] G. Le Coz, M. Marinescu, A. Devillez, D. Dudzinski, L. Velnom: *Measuring temperature of rotating cutting tools: Application to MQL drilling and dry milling of aerospace alloys*, Applied Thermal Engineering 36, pp.434-441, 2012

[2] Savković B.; Modeliranje funkcija obradivosti pri procesu obrade glodanjem, Doctoral Thesis, University of Novi Sad, Faculty of Technical Sciences, 2015

[3] H. Wu, S. J. Zhang: *3D FEM simulation of milling process for titanium alloy Ti6Al4V*, International Journal of Advanced Manufacturing Technology Volume 71, pp.1319–1326, 2014.

[4] C. Constantin, S. Croitoru, G. Constantin, C. Bisu: *3D FEM Analysis of Cutting Processes, Advances in visualization*, Advances in visualization, imaging and simulation, ISSN 1792-6130, pp. 41-46, 2010.

[5] K. Kadirgama, M. Rahman, B. Mohamed, R. Abu bakar, A. Ismail: *Development of temperature statistical model when machining of aerospace alloy materials*, Thermal science, Vol. 18, Suppl. 1, pp.S269-S282, 2014.

[6] C. Constantin, S. Croitoru, G. Constantin E. Străjescu: *FEM tools for cutting process modelling and simulation,* U.P.B Scientific Bulletin, Series D, Vol. 74, Iss. 4, ISSN 1454-2358, 2012.

[7] Third Wave Sistems AdvantEdge 7.1, User's manual, 2015.

[8] Techplot 360, User's manual, 2011.

Authors: **MS.c Anđelija Mitrović,** College of Technical Vocational Studies Svetog Save 65, 32000 Cacak, Serbia, Phone +381 32 222-321, Fax: +381 32 222-321

Prof. Dr. Pavel Kovac, M.Sc Nenad Kulundzic, Dr. Borislav Savkovic, University of Novi Sad, Faculty of Technical Sciences, Department for Production Engineering, Trg Dositeja Obradovica 6, 21000 Novi Sad, Serbia, Phone.: +381 21 450-366, Fax: +381 21 454-495.

E-mail: andjelija.mitrovic@visokaskolacacak.edu.rs, pkovac@uns.ac.rs, kulundzic@uns.ac.rs savkovic@uns.ac.rs

Journal of Production Engineering
Vol.19 No.1
JPE (2016) Vol.19 (1) Original Scientific Paper
Odusote, J.K., Moshood, M.A.

PRODUCTION AND DETERMINATION OF THE EFFECT OF VEGETABLE OIL-BASED CUTTING FLUIDS ON AISI 1033 STEEL IN A TURNING OPERATION

Received: 02 December 2015 / Accepted: 22 March 2016

Abstract: *This work compares the performance of palm and shea butter oils based cutting fluids, mineral oil and dry machining during turning operation of AISI 1033 steel. The results revealed that the interface temperature increases with increased cutting speed during the turning operations. Thicker and more continuous chips were formed when cutting fluids were used as compared to dry machining. Based on these results, the use of vegetable oil based cutting fluids enhanced the cutting performance, and thus will increase the durability of the cutting edge of the tool and its service life.*
Key words: *vegetable oil-based cutting fluids, mineral oil, workpiece-tool interface, turning operation*

Proizvodnja i određivanje efekta tečnosti za hlađenje i podmazivanje na bazi biljnog ulja pri struganju AISI 1033 čelika. *U ovom radu je izvršeno upoređivanje efekta tečnosti za hlađenje i podmazivanje na bazi palminog i shea maslca pri struganju AISI 1033 čelika. Rezultati pokazuju povišenje temperature rezanja sa povećanjem brzine rezanja. Prilikom korišćenja pomenutih tečnosti za hlađenje i podmazivanje primećena je deblja i kontinualna strugotina u odnosu na suvu obradu. Shodno rezultatima se dolazi do zaključka da korišćenje tečnosti za hlađenje i podmazivanja na bazi biljnog ulja potpomaže poboljšanju reznih performansi i produžava postojanost alata.*
Ključne reči: *tečnost za hlađenje i podmazivanje na bazi biljnog ulja, mineralno ulje, obradak-alat, struganje*

1. INTRODUCTION

Cutting fluids are basically applied during machining processes based on their cooling and lubrication effects as well as their ability to take away formed chip from the cutting zones. The cooling effect of the fluids is very critical in order to reduce the effects of temperature on cutting tool and machined workpiece, while the lubrication effect will result into low friction coefficient between work piece cutting tool and cutting tool-chip interfaces and thereby cause easy chip flow on the rake face of cutting tool [1, 2, 3]. This friction usually resulted in heat generation at the interfaces, which in turn decreases the tool service life, increases surface roughness, decreases the machining productivity and quality of metal cutting [4]. Furthermore, the effect of the formed chip on the machined surface would be eliminated if the chips are quickly taken away from the cutting zone. This will result into better surface roughness and less built-up edge during machining operation [2, 3].

Various approaches have been adopted in order to protect the cutting tools either by reduction or elimination of friction at the different interfaces during machining operation [4]. However, one of the most commonly used methods to protect the cutting tools from generated heat during machining is the application of cutting fluids. The cutting fluids reduce the friction at the interfaces and thus improve the material removal rates. Mineral or petroleum oil based cutting fluids are commonly employed in practically all machining processes due to their high production levels in the world. According to Glenn and Antwerpen [6], in 1998 alone, approximately 2.3 x 109 liters of cutting fluids was used in the machining operations and its cost around \$ $2.75x10^9$. North America had a big ratio, followed by Asian continent and then European continent which was in the third order [7]. However, the adverse effect of these petroleum oil based cutting fluids on the environment and the safety of the users are some of the drawback for their continuous application in machining processes [5, 7-10].

Efforts to find suitable eco-friendly and hazard free alternatives to conventional mineral/petroleum oil based cutting fluids have led to the development of vegetable oil based cutting fluids for machining processes. Vegetable oils occur naturally and they have been identified as a reliable source of environmentally friendly cutting fluids. Previous studies have shown that vegetable oil based cutting fluids can extend the tool service life, improve surface finish and enhance the machining productivity [11, 12]. Other benefits of these oils include their good resistance to shear, low volatilities as manifested by their high flash points, high lubricity resulting in lower friction losses, high viscosity indices, which are about twice those of mineral oils [13].

Several authors have investigated the use of naturally occurring vegetable oils as cutting fluids during machining operations [14-17]. Obi et al., [13] investigated the use palm oil, groundnut oil, shear butter oil and cotton seed oil as cutting fluids in the turning operation of aluminum under varying spindle speeds, feed rates and depths of cut. They reported that these vegetable oils can replace the conventional soluble oil in the machining of aluminum as they exhibited good cooling behaviour at the work piece-tool interface. The use of the vegetable oils also

resulted into improved surface finish and reduction of chip thickness ratio. The work of Bhowmik et al., [15] focused on the comparison between the effects of the application of vegetable based cutting fluids including Groundnut oil, Neem Oil and Soya oil and conventional oil on the turning operation of mild steel on lathe machine. Their results revealed that samples machined with vegetable-oil based cutting fluid displayed fine surface morphology after machining, which indicates improved surface finish compared to conventional cutting fluids. Adekunle et al. [14] also investigated the use of groundnut and melon oils as cutting fluids during machining of mild steel on a conventional lathe machine. They reported that the cooling ability of melon oil was better than that of groundnut oil, while the mineral oil was found to extract heat most. The chips formed using vegetable oil coolants were observed to be more ductile and continuous than those obtained using mineral oil cutting fluid.

The assessment of suitability of vegetable oils (palm oil and groundnut oil) as base oil in cutting fluids with other additives was examined by Odusote and Kolawole [16]. The oil additives were emulsifier (9% Sodium Petroleum Sulphonate); anticorrosive (6% synthetic ester); bactericide (5% derivative of triazine, C3H3N3); and, antioxidant (2% lemon extract).The performance of these vegetable oil based cutting fluids compared with petroleum oil based fluid (supa oil) and dry machining under varying spindle speeds, feed rates and depths of cut was carried out during drilling operation of mild steel on Computer Numeric Controlled (CNC) milling machines using a 10 mm HSS drill bit. Their results showed that the vegetable-based oils performed similarly better due to their good lubricity, viscosity, cooling behaviour and wetting ability compared with the petroleum oil based fluid. In the present study, the possibility of improving the cutting tool performance during turning operation on mild steel through the use of shea butter and palm oils with additives as alternative cutting fluids to mineral oil was investigated. The temperature generated at the cutting interfaces and the effects of the vegetable oils fluids on the chip formation during machining were studied.

2. MATERIALS & METHODOLOGY

The materials used in this study include four (4) pieces of cylindrical steel samples of 25 mm diameter and 130 mm in length, lathe machine of maximum speed of 2000 rpm and 755 HP, stop watch, vernier caliper, MS6500 K-Type thermocouple, MBEB094816 Mastech digital multimeter, titration apparatus, digital weighing balance, oven, Ostwald viscometer, thermometer, CLEVELAND Open Cup flashpoint tester, cryostat, and LABTECH pH meter. This study focused on dry machining, and the use of vegetable oils (groundnut and shea butter) based as well as conventional mineral oil (supa oil) based cutting fluids.

Shea butter (trigyceride) and oil of palm nut (Elaeis guineensis) were purchased from a local market in Ilorin, Kwara State, Nigeria. These oils were melted and sieved to remove any foreign dirt. The oils were later placed in an oven at 120 °C to remove any moisture. Trans-esterification process was carried out on the shea butter to make it oily at all temperatures, while the Free Fatty Acids (FFA) of both the Shea butter and palm oils were then determined. The results are presented in Table 1.

2.1 Transesterification of the shea butter

150 ml of shea butter was measured into a clean conical flask, while 120 ml of methanol was added to it. The mixture was kept at 60 °C for about 30 minutes and thoroughly stirred until it becomes homogenous. 1.5 ml of H_2SO_4 was added to the mixture under continuous stirring at same temperature for 1 hour and left for another 30 minutes. The FFA content of the new oil was determined, and the above procedure was repeated until the FFA value becomes lower than 1%. Then, the shea butter was in its liquid state but could still solidify after some time due to interaction with the environment.

Parameters	Palm Oil	Shea butter
% Moisture content	2.77	1.23
Density (g/ml)	0.865	0.876
pH value	4.43	4.945
% FFA content	6.67	10.96

Table 1. Properties of Palm and shea butter oils

2.2 Preparation of the Vegetable Oil-Based Cutting Fluids

The additives, such as *Jatropha curcas* (JC) leaves extract to serve as corrosion inhibitor and the mixture of strawberry and lemon fruit to serve as antioxidant, were mixed with the oils in the proportion shown in Table 2 to produce a cutting fluid of 225 ml by volume. 0.5 g of emulsifier, sodium tripolyphosphate (STPP), was also added to prevent separation of the mixture. Some properties such as flash point, fire point, cloud point, pH value, saponification value of the prepared vegetable oil-based cutting fluids were carried out using CLEVELAND Open Cup flashpoint tester, Cryostat, LABTECH PH Meter, respectively for each test. The results obtained are presented in Table 3.

Cutting Fluids	**% Base Oil**	**% Anticorrosive***	**% antioxidant^{+}**	**Total %**
Palm oil	66.67	11.11	22.22	100
Shea butter	66.57	11.11	22.22	100

Table 2. Constituents of the cutting fluids

***Jatropha curcas* leaves extract, $^{+}$Strawberry and Lemon fruit mixture.

Parameters	Palm Oil-based	Shea butter Oil-based
Physical state at 30 °C	Liquid	Liquid
Colour	Red	Butter
Density at 30 °C (g/ml)	0.8745	0.8885
Kinematic viscosity at 30 °C (Pa s)	4.27	4.01
Flash point (°C)	210	210
Fire point (°C)	280	255
pH-value	4.43	4.95
Cloud point (°C)	21	26
Saponification Value	140.25	280.5

Table 3. Physical properties of vegetable oil-based cutting fluids

2.3 Machining of the work piece samples

Prior to machining, the chemical composition of the work piece is obtained using optical emission spectrometer and the result is given in Table 4. Turning of the steel samples was carried out on a conventional lathe machine using a 10 x 200 mm HSS cutting tool at an ambient environment of 29 °C. High speed steel (HSS) cutting tool is used because of its suitability for use with all types of cutting fluids [4]. Four test specimens were machined using dry machining and three different cutting fluids on each sample. The cutting fluids, which were applied through flooding, were shea butter-based, palm oil-based and mineral oil-based (supa oil).

Each of the test specimens was mounted on the machine and turned through depth of 0.5 mm, 1.0 mm and then 1.5 mm. The temperature of the work pieces were first measured on the machine at a constant cutting speed of 108 rev/min and feed rate of 0.25 mm/rev at varied depth of cut for each specimen. Later, the cutting speeds were varied as the feed rate also varies for each constant depth of cut. For chip thickness determination, machine speeds of 108 rev/min, 140 rev/min, 350 rev/min and 470 rev/min were used at feed rate of 0.25 mm/rev on each of the test specimens.

Elements	**Sample (wt %)**	**Elements**	**Sample (wt %)**
C	0.3320	Ca	0.0001
Si	0.2070	As	0.0005
P	0.0510	Sn	0.0022
Mn	0.7580	Cr	0.1181
S	0.0451	Al	0.0013
Ni	0.1067	Pb	0.0005
Cu	0.3002	W	0.0065
Co	0.0126	Zn	0.0013
V	0.0193	Fe	98.039

Table 4. Chemical Composition of the AISI 1033 steel sample (wt. %)

2.4 Interface Temperature Measurement

The thermocouple was attached to the rake side of the tool location on the workpiece to take measurement of the change in temperature on the position during the turning operation from the multimeter readings as illustrated in Fig. 1.

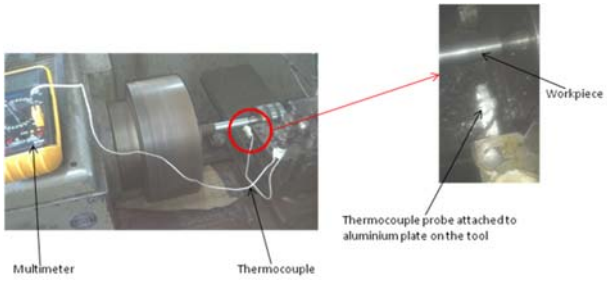

Fig. 1. Interface Temperature setup.

3. RESULTS AND DISCUSSION

3.1 Chemical composition of the samples

The chemical composition of the steel sample used for the current study is given in Table 4. The result showed that the carbon and manganese content of the sample are 0.33 wt% and 0.76 wt%, respectively. This indicates that the sample belongs to the class of plain carbon steel, that is, mild steel [17]. Mild steel find application in automobile components such as crankshafts, gears, connecting rods and valves [18]. In most of these applications, machining of the components is very critical.

3.2 Variation of Interface temperature with cutting speed

Figure 2 shows the variation of temperature of the cutting tool-workpiece interface with spindle speed using different cutting fluids. The ambient temperature was 29 °C. The results revealed that the interface temperature increases with increased cutting speed during dry machining and with the use of all the cutting fluids except shea- butter based fluid. This may be due to increased friction between the tool and workpiece during increased spindle speed. The figure also revealed that the trend of all the curves is such that low cutting speeds lead to minimal heat generation as shown by low interface temperature reading. It can therefore be inferred that to minimize energy consumption, low cutting speed and feed rates must be used. In addition, all cutting parameters must be selected at their low levels to obtain optimum machining and maximum tool life. Ojolo et al. [17] and Odusote and Kolawole [16] have also shown that using lowest machining parameters in conjunction with appropriate cutting fluids will improve the tool service.

The figure also revealed that highest interface temperature was constantly obtained during dry machining due to low adhesion between the workpiece and cutting tool. Hassan et al. [18] reported that the adhesion of two surfaces loaded together over some part of their contact is one form of surface interaction causing frictions, wearing and generation of excessive heat without protector. Palm oil gave highest interface temperature compared with other cutting fluids at all cutting speed indicating that it may not be suitable to use as lubricant during machining. However, the conventional cutting fluid tends to have the lowest interface temperature at low spindle speed while shea butter oil-based cutting fluid gave the lowest interface temperature during high spindle speed machining. This

may be due to better wettability of shea butter oil. Odusote and Kolawole [16] after relating the phenomenon to wettability in their groundnut oil study, stated that it can be conveniently said that shea butter oil-based and the conventional oil may have had almost the same wettability at lower cutting speeds, but there is better perceived thermal stability of shea butter oil-based due to its higher viscosity index which makes it more fluidic at high temperature using higher cutting speed. Shea butter oil-based competitive performances with the conventional oil may be due to its good viscosity even at higher temperatures. This performance may also be related to the presence of surface active agents such as *stearic* acid and halogens, such as chlorine which help to reduce surface energy of a liquid and increase its wetting ability or oiliness [15].

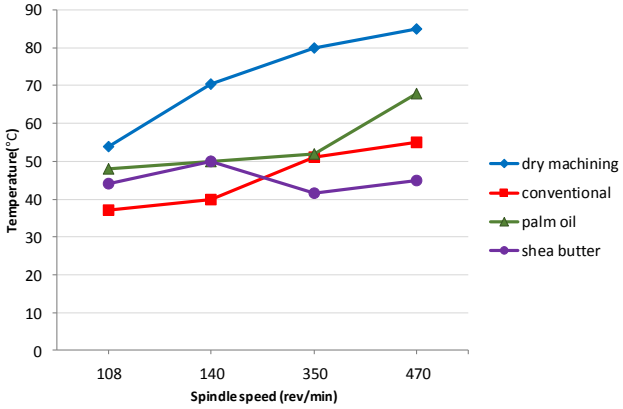

Fig. 2. Varying spindle speed at constant depth of cut of 1.0 mm and feed rate of 0.25rev/mm.

3.2 Variation of Interface temperature with depth of cut

The variation of interface temperature of the cutting tool-workpiece with depths of cut at constant low spindle speed and feed rate using different cutting fluids is given in Fig. 3. The figure shows that the interface temperatures were higher during dry machining.

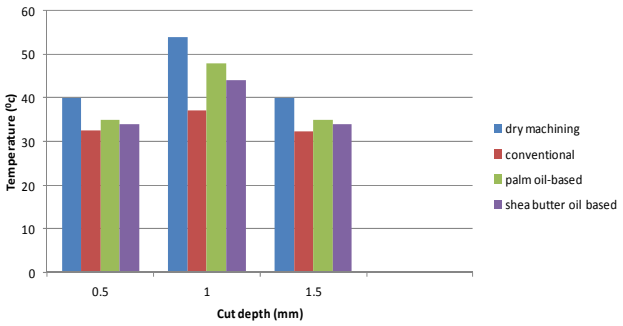

Fig. 3. Varying cut depth at constant spindle speed 108 rev/min and feed rate 0.25rev/mm

The figure also shows that among other fluids, palm oil produces the highest temperature variation while conventional coolant temperature variation is lowest. However, due to the damaging influence of conventional cutting fluid on the environment such as surface water and groundwater contamination, air pollution, soil contamination and consequently, agricultural product and food contamination, its poor biodegradability and the need for safe of users, the competiting shea butter oil-based cutting fluid of closer range would be highly recommended.

Fig. 4. presents the variation of interface temperature of the cutting tool-workpiece with depths of cut at constant high spindle speed and feed rate using different cutting fluids. The figure shows that nature of the interface temperature varies higher in dry machining. Shea butter is seen to have the lowest temperature variation due to its viscosity which enables it to have capability of spreading more readily than other fluids at high temperature.

Cutting fluids are essentially applied to reduce heat generated by the tool and workpiece in order to improve the service life of the tool and also not to alter the microstructure of the workpiece. Hence shea butter oil-based has a potential to replace the soluble oil in metalworking processes.

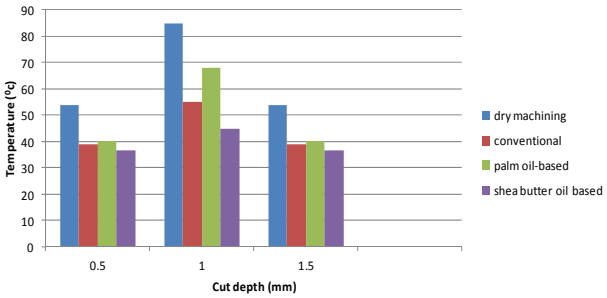

Fig. 4. Varying cut depth at constant spindle speed 470 rev/min and feed rate 0.25 rev/mm

3.4 Chip Formation

Figs. 5-8 represent the pictorial view of the chips formed using each cutting fluids during machining of the workpiece. All the cutting fluids formed continuous chips during high speed machining of workpiece as shown in Figs. 5-7, while the chips obtained during dry machining were discontinuous (Fig. 8) as a result of high heat generation in the cutting zone which also makes the chip brittle [14]. The chips formed during machining using shea butter oil-based cutting fluid was more continuous compared with those from dry machining and other cutting fluids indicating better lubrication effect. Cutting fluid with better lubrication effect usually resulted in low friction and allows easy chip flow on the rake face of cutting tool [4]. The chips formed using shea butter oil-based cutting fluid was not only continuous but ductile as shown in Fig. 6. The chip formation results, as shown in Figs. 5-8, indicate that the vegetable oil based cutting fluids have better lubrication effect on the workpiece than the mineral oil and dry machining. Adekunle et al. [14] investigated chip formation of machining mild steel using groundnut oil and melon oil as the cutting fluid and reported cutting fluids that produces more of continuous and more ductile chips produces less wear on cutting tool.

Fig. 5. Chip formed with the use of conventional cutting fluid

Fig. 6. Chip formed with the use of shea butter-based cutting fluid

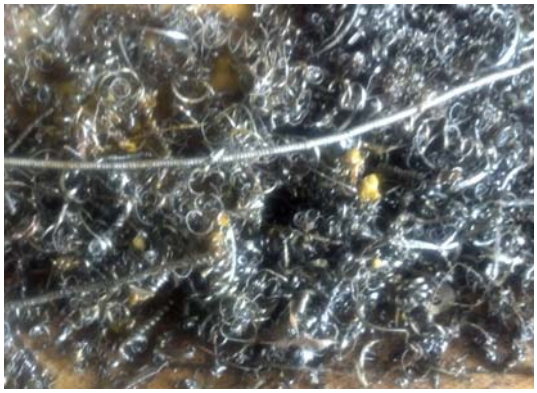

Fig. 7. Chip formed with the use of palm oil-based cutting fluid.

Fig. 8. Chip formed during dry machining.

3.5 Chip thickness

Table 5 shows the chip thickness of the machine workpieces using different cutting fluid at a low spindle speed and a high spindle speed. On the overall, the values obtained when palm oil-based was used as cutting fluid was the highest indicating high lubricating ability. The thick chips were most likely formed as a result of the better relative ease of slide between tool and workpiece with palm oil-based that has higher oiliness. In addition, it is noted that average thickness values of chips formed at a relative low cutting speed 108 rev/min are consistently higher than those obtained at 350 rev/min except during dry machining. High values of chip thickness means better rate of metal removal and this is desirable to complete machining at a lesser time [4]. Lowest chip thickness was obtained in dry machining due to high friction. Thus, cutting fluids greatly influence the size of chips that are formed during any metal working process. The low thickness of dry machined samples may be due to ease of fracturing as a result of striking of the chips with the workpiece. Although, this may be advantageous if the target is to obtain chips that would not tangle with cutting tool. However, balance has to be made to choose between quick machining and operator safety [5, 7-10]. These results therefore revealed that the level of cutting speed has a significant effect on the workpiece temperature. In addition, an increase in cutting speed is always accompanied by a reduction in chip thickness as shown in Table 5.

Cutting Fluids	Chip thickness (mm) at 108 rev/min, 0.25mm/rev, 1.5 mm depth	Chip thickness (mm) at 350 rev/min, 0.25 mm/rev, 1.5 mm depth
Dry machining	0.54	0.72
Conventional oil	0.83	0.60
Palm oil-based	1.10	0.80
Shea butter oil-based	0.94	0.86

Table 5. Variation in chip thickness using different cutting fluids and parameters

4. CONCLUSIONS

The results from this study have shown potentialities of locally sourced, ecology-friendly vegetable oil-based cutting fluids to replace the non-biodegradable and toxic petroleum based cutting fluids as machining fluids for mild steel. Even with slight modifications and deliberate but careful alterations in some of the components of such oils, better performing cutting fluids could be obtained. The study was able to reveal the following:

- The ability of vegetable oil-based cutting fluids to reduce the interface temperature offers a competitive performance with that of conventional soluble oil, as shown by the narrow temperature difference between the values obtained using shea butter based-oil and that of conventional soluble oil.

- The continuous and ductile chips formed using shea butter oil-based cutting fluid indicate that vegetable oil-based cutting fluids produce less wear on cutting tool thereby possible maximizing of tool life during machining process.
- The chips thickness produced using palm oil-based and shea butter oil-based as cutting fluid was highest at low and high spindle speed respectively, probably due to their better lubricating ability, especially at elevated temperature. This allows easier and deeper penetration of cutting tool into workpiece and better metal removal rate.
- Vegetable oil based cutting fluid is an environmental and user friendly fluid which can serve a suitable replacement for the non-biodegradable and toxic petroleum based cutting fluids as machining fluids for mild steel. Dry machining consumes more time than machining using any form of cutting fluids probably due reduced tool performance in the absence of cutting fluids.

5. REFERENCES

[1] M. A. El Baradie, Cutting Fluids, Part I: Characterisation, Journal of Materials Processing Technology 56 (1996) 786-797.

[2] Md. Mizanur Rahman, Mahamudul Hassan, Md Abdullah-Al Bari, An optimize system of using cutting fluid in machining operation for light work machine shop, International Journal of Engineering & Applied Sciences (IJEAS), Vol.4, Issue 1(2012)1-8.

[3] M.B. Da Silva, J. Wallbank (1998), Lubrication and application method in machining, Lubrication and Tribology 50, pp.149-152.

[4] O. Çakīr, A. Yardimeden, T. Ozben, E. Kilickap, Selection of cutting fluids in machining processes, Journal of Achievements in Materials and Manufacturing Engineering, volume 5, issue 2, 2007.

[5] T.F. Glenn, F. van Antwerpen (1998), Opportunities and market trends in metalworking fluids, Lubrication Engineering 54, pp.31-37.

[6] E. Brinksmeier, A. Walter, R. Janssen, P. Diersen (1999), Aspects of cooling lubrication reduction in machining advanced materials, Proceedings of the Institution of Mechanical Engineers, Journal of Engineering Manufacture, pp.769-778.

[7] M. Sokovic, K. Mijanovic (2001), Ecological aspects of the cutting fluids and its influence on quantifiable parameters of the cutting processes, Journal of Materials Processing Technology 109, pp.181-189.

[8] W.J. Bartz (2001), Ecological and environmental aspects of cutting fluids, Lubrication Engineering 57, pp.13-16.

[9] M.A. El Baradie (1996), Cutting Fluids, Part II: Recycling and clean machining, Journal of Materials Processing Technology 56, pp.798-806.

[10] C. A. Sluhan, "Considerations in the selection of coolants used in flexible machining cells," Society of Manufacturing Engineers Technical Paper MS86-124, Dearborn, Michigan: SME, 1986, p.1-5.

[11] P. Waurzyniak, 2012, Society of manufacturing engineers, pp. 66-70.

[12] Honary, L.A.T.: Biodegradable / Biobased Lubricants and Greases, Machinery Lubrication Magazine Issue Number 200109 Noria Corporation, 2004. www.oilmaintenance.com.

[13] A. I. Obi, A. A. Alabi, R. B. O. Suleiman, and F. O. Anafi, Verification of some vegetable oils as cutting fluids for aluminum, Nigerian journal of technological development, vol. 10, no 1, 2013, pp. 7-12.

[14] Adekunle A.S., Adebiyi K.A., Durowoju M.O. (2015), "Performance Evaluation of Groundnut Oil and Melon Oil as Cutting Fluids in Machining Operation", ACTA TEHNICA CORVINIENSIS – Bulletin of Engineering ISSN:2067-3809 VIII (1), pp.97-100.

[15] Papiya Bhowmik, Gaurav Arora, Nitesh Pal, Nitin Bhardwaj, Improving the Surface Texture of Mild Steel using Vegetable Oil as Cutting Fluid, International Journal of Applied Engineering Research, volume 9, Number 8 (2014) pp. 883-888.

[16] Odusote, J.K. and Kolawole (2015): Assessment of Suitability of Vegetable-Based Oils as Cutting Fluids in Drilling Operation. Annals of Faculty Engineering Hunedoara-International Journal of Engineering, XIII; 169-174.

[17] Ojolo, S.J., Amuda, M.O.H., Ogunmola, O.Y. and Ononiwu, C.U. (2008), 'Experimental Determination of the effect of some straight biological oils on cutting force during cylindrical turning', Revista Materia 13(4): pp.650-663.

[18] Hassan, A.B., Abolarin, M.S., Nasir, A. and Ratchel, U. (2006). 'Investigation on the use of palm olein as lubrication oil', Leonardo Electronic Journal of Practices and Technologies 5(8): pp.1-8.

ACKNOWLEDGEMENTS

The authors would like to gratefully acknowledge the support of Engr. Ibrahim Lateef and other technical staff of the Department of Mechanical Engineering, Federal Polytechnic, Offa, Kwara State, Nigeria for help rendered during samples' machining on the lathe machine.

Authors: **Senior Lecturer, Dr. Jamiu Kolawole Odusote,** Department of Materials and Metallurgical Engineering, **B.Sc. Moshood, Mueez A.** Department of Mechanical Engineering, University of Ilorin, P.M.B. 1515, Ilorin, Nigeria, Phone.: +2347038848812

E-mail: *jamiukolawole@gmail.com/*
odusote.jk@unilorin.edu.ng
mueezmoshood@yahoo.com

Journal of Production Engineering
Vol.19 No.1
JPE (2016) Vol.19 (1) Original Scientific Paper
Suresh, R.K., Krishnaiah, G., Venkataramaiah, P.

A STRATEGIC EXPERIMENTATION TOWARDS OPTIMALITY DURING TURNING OF AISI D3 STEEL USING CASTOR OIL AS CUTTING FLUID USING GREY TAGUCHI APPROACH

Received: 01 December 2015 / Accepted: 18 March 2016

***Abstract**: To combat environmental pollution caused because of using conventional cutting fluid used in metal cutting industry, a novel approach is the development of minimum quantity lubrication. Turning is widely used in material removal process in manufacturing industry which involves the generation of high cutting forces and high tool-work interface temperature which reduces life of the cutting tool. Lubrication plays a major role in minimizing the above said factors but flooded lubrication is also hazardous both with regard to human as well as environment. To overcome these problems minimum quantity lubrication with castor oil as lubricant has been used in this work. Experimentation is designed as per Taguchi design of orthogonal array is carried out on a TURNMASTER 35 Conventional lathe in combination with DNMG styled CVD tool. The input parameters considered are cutting speed, feed and depth of cut and quality targets are surface roughness, material removal rate, interface temperature, cutting force and power consumed. The optimality conditions were obtained by Grey relational analysis. Finally, confirmation test was performed to make comparison between the experimental results and developed model and concluded that the results are in specified limits.*
***Key words:** Turn master conventional lathe, DNMG, CVD tool, castor oil and Grey relational analysis*

Strateški eksperiment u cilju optimizacije pomoću Grej-Tagiuči metode pri struganju AISI D3 čelika korišćenjem ricinusovog ulja kao sredstva za hlađenje i podmazivanje. *Za borbu protiv zagađenja životne sredine izazvano zbog korišćenja konvencionalnih sredstva za hlađenje i podmazivanje koja se obično koristi u industriji rezanja metala, novina je razvoj metode minimalne količine reznog fluida. Struganje je široko korišćena tehnologija obrade u proizvodnji pri kojoj se generišu visoke rezne sile i visoka temperatura u zoni obrade što dovodi do smanjenja postojanosti reznog alata. Podmazivanje igra značajnu ulogu pri smanjenju uticaja gore navedenih faktora ali preterano podmazivanje takođe predstavlja opasnost kako po operatera tako i po životnu sredinu. Da bi se izbegli ovi problemi vršeno je ispitivanje minimalne količine sredstva za hlađenje i podmazivanje sa ricinusovim uljem. Plan eksperimenta je izvršen po klasičnom Tagučijevom planu ortogonalnih redova a realizovan je na Turnmaster 35 konvencionalnom strugu sa DNMG CVD reznim pločicama. Ulazni podaci su brzina rezanja, pomak i dubina da bi izlazni podaci procesa činili hrapavost obrađene površine, proizvodnost, temperatura u zoni obrade, kao i potrošena električna energija. Optimalni parametri obrade su dobijeni Grejovom relacionom analizom. Na kraju su izvršeni eksperimenti provere dobijenih rezultata i došlo se do zaključka da postavljeni model daje rezultate u zadovoljavajućim granicama.*
***Ključne reči:** konvencionalnis strug, DNMG, CVD alat, ricinusovo ulje i Grejeva relaciona analiza*

1. INTRODUCTION

(The important goal in the modern industries is to manufacture the product with lower cost and with high quality in short span of time. There are two main practical problems that engineers face in a manufacturing process, the first is to determine the product quality (meet technical specifications) and the second is to maximize manufacturing system performance using the available resources. The challenge of modern machining industry is mainly focused on achievement of high quality ,in terms of work piece dimensional accuracy, surface finish ,high production rate, less wear on the cutting tools ,economy of machining in terms of cost saving and increase the performance of the product with reduced environmental impact. During the recent years, the use of lubricants in Metal cutting will gain popularity. By the mid 19th century mineral oil has been med extensively used in machining operation. In the year 1883, Taylor used water as lubricant in machining and observed that the cutting speed has been increased by 30-40%. The main objective of machining operation is to improve quality and productivity without sacrificing machining cost.

The same can be achieved by machining of highest cutting speed with appropriate feed and depth of cut. Machining can be done in dry conditions with proper selection of cutting fluid ensures improved productivity and tool life, quality but prevent the cutting tool and machine from overheating as well. The proper application of cutting fluid provides higher cutting speeds and higher feed rates possible. The selection of cutting fluid not only improves cutting performance but also fulfils a number of requirements which are non-harmful to health for operators, not a fire hazard, no smoke (or) for and cost is less. Cutting fluids are applied to the cutting zone to improve cutting performance. The primary function of cutting fluid is to reduce interface temperature between tool and work

thus tool lip will be extended. Secondary cutting fluid acts as good lubricant by which heat generated due to friction will be reduced. To conclude with high lubricant capacity are suitable in low speed machining such as screw cutting, broaching, gear cutting and difficult to cut materials whereas cutting fluids with high cooling ability are generally employed in high speed machining. In the present work, AISI D3 steel was selected as work material which finds applications in the manufacture of Blanking & Forming dies, press tools, punches, bushes, forming rolls and many more. For the purpose of experimentation, factorial design experiments are considered as per Taguchi DOE. By advocating Taguchi design, a clear understanding of the nature of variation and economical consequences of quality engineering in the world of manufacturing can be clearly got through. In the present study, Grey relational analysis were performed to combine the multiple performance characteristics in to one numerical score which is an indicative of the optimal process parameter setting. Analysis of variance (ANOVA) is also performed to investigate the most influencing parameters on the surface roughness, material removal rate, interface temperature, cutting force and power consumed.

2. LITERATURE REVIEW

Chorng-Jyh Tzeng etal [1] investigated the optimization of CNC turning operation parameters for SKD11 (JIS) using the Grey relational analysis method. Nine experimental runs based on an orthogonal array of Taguchi method were performed. The surface properties of roughness average and roughness maximum as well as the roundness were selected as the quality targets. An optimal parameter combination of the turning operation was obtained via Grey relational analysis. By analyzing the Grey relational grade matrix, the degree of influence for eachcontrollable process factor onto individual quality targets can be found. The depth of cut was identified to be the most influence on the roughness average and the cutting speed is the most influential factor to the roughness maximum and the roundness. Additionally, the analysis of variance (ANOVA) is also applied to identify the most significant factor; the depth of cut is the most significant controlled factors for the turning operations according to the weighted sum grade of the roughness average, roughness maximum and roundness.

Bala Murugan Gopalsamy etal [2] dealt with experimental investigations carried out for machinability study of hardened steel and to obtain optimum process parameters by grey relational analysis. An orthogonal array, grey relations, grey relational coefficients and analysis of variance (ANOVA) are applied to study the performance characteristics of machining process parameters such as cutting speed, feed, depth of cut and width of cut with consideration of multiple responses, i.e. volume of material removed, surface finish, tool wear and tool life The optimum process parameters are calculated for rough machining and finish machining using grey theory and results are compared with ANOVA.

Mohamed Handawi Elmunafi etal [3] envisaged the use of cutting fluids in machining processes can reduce the cutting temperature and provides lubrication to tool and workpiece. These translate to longer tool life and improved surface quality. Due to the issues of using fluids in machining related to environment, health, and manufacturing cost that need to be solved, options to reduce their use. A technique called minimal quantity lubrication (MQL), which sprays small amount of cutting fluid (in the range of approximately 10 – 100 ml/h) to the cutting zone area with the aid of compressed air, was developed to merge the advantages of both dry cutting and flood cooling. For the type of cutting fluids, vegetable oils are common cutting fluids used in MQL because of its superior lubrication and high-pressure performance. This study evaluates the performance of MQL using castor oil as cutting fluid. The workpiece is hardened stainless steel 48 HRC. Results are compared with dry cutting. It was found that using small amount of lubricant of 50 ml/h during the particular turning process produces better results compared to dry cutting, in terms of longer tool life. Surface roughness and cutting forces were also enhanced albeit slightly. From the results, MQL can be a good technique for turning hardened stainless steel using coated carbide cutting tools for cutting parameters of up to 170 m/min cutting speed and 0.24 mm/rev feed.

Papiya Bhowmik etal [4] focused on an experimental investigation into the role of green machining on surface Roughness (Ra), in the machining of aluminium AA1050. A comparative study of turning experiments, between VBCFs and MBCFs under various cutting conditions, using neat or straight Sunflower oil and Coconut oil, was conducted using the same machining parameter set-up. Vegetable oils used on the principle of Minimum Quantity Lubrication (MQL) that is oil dropped between the cutting tool and workpiece interface directly. The results show that vegetable oil performance is comparable to that of mineral oil machining. The results show that Vegetable oils have potential to replace the mineral oils.

Ujjwal Kumar etalc [5] focuses on an experimental investigation into the role of green machining on surface Roughness (Ra), in the machining of aluminium AA1050. A comparative study of turning experiments, between VBCFs and MBCFs under various cutting conditions, using neat or straight Coconut oil and Castor oil, was conducted using the same machining parameter set-up. Vegetable oils used on the principle of Minimum Quantity Lubrication (MQL) that is oil dropped between the cutting tool and workpiece interface directly. The that vegetable oil performance is comparable to that of mineral oil machining. The results show that Vegetable oils have potential to replace the Mineral oils.

Reddy Sreenivasulu etal [6] studied the effects of drilling parameters on surface roughness and roundness error were investigated in drilling of AI6061 alloy with HSS twist drills. In addition, optimal control factors for the hole quality were determined by using Taguchi - Gray relational analysis. Cutting speed, feed rate, drill

diameter, point angle and cutting fluid mixture ratio were considered as control factors, and L18 (3*5) orthogonal array was determined for experimental trials. Gray relational analysis was employed to minimize the surface roughness and roundness error achieved via experimental design. Confirmation experiments showed that Gray relational analysis precisely optimized the drilling parameters in drilling of Al6061 alloy.

A. H. A. Shah etal [7] studued the multi objective optimization in CNC turning of S45C carbon steel by using Taguchi and Grey Relational Analysis (GRA) method is reported in this paper. Based on grey relational analysis, a grey relational grade (GRG) is computed to optimize the CNC turning process with multiple performance characteristics which are surface roughness, material removal rate (MRR) and tool wear. In this study,two important parameters were selected, namely spindle speed and feed rate while the depth of cut was fixed. The experimental results show that machining parameter in CNC turning can be improved by using this approach. Kirby et al. [8] presented an application of the Taguchi parameter design method to optimize the surface finish in a turning operation. The control parameters for this operation included: spindle speed, feed rate, depth of cut and tool nose radius. A confirmation run was used to verify the results, which indicated that this method was both efficient and effective in determining the best turning parameters for the optimal surface roughness.

M.Y Wang & T.S. Lan [9] presents Orthogonal array of Taguchi experiment where in four parameters like cutting speed, feed rate, tool nose run off with three levels in optimizing the multi-objective such as surface roughness, tool wear and material removal rate in precision turning on CNC lathe. For the purpose of multi response optimization, Grey relational analysis was employed.

From the literature survey, it is evident that little work has been reported on AISI D3 steel work with combination of DNMG styled CVD coated cemented carbide tool.. Hence the experimentation is done on above said combination of work piece and tool and optimization method- Grey relational analysis is put forth.

3. EXPERIMENTATION

In the present study, three turning parameters were selected with three levels as shown in Table.1. The experimentation was carried out using L9 orthogonal array based on Taguchi design of experiments. The work material selected for this experiment is AISI D3 steel of 40 mm diameter, length 100 mm. The chemical composition of AISI D3 steel has been done by chemical Analyser and is reported as below in table1.

Element	C	Si	Mn	P	S	Cr	V	W
Specified values	2.00-2.35	0.10-0.60	0.10-0.60	0.03 max	0.03 max	11.00-13.50	1.00 max	1.00 max
Observed values	2.07	0.406	0.457	0.02	0.029	11.28	0.037	<0.003

Table1. Chemical Analysis report

Turning parameters	Level 1	Level 2	Level 3
Cutting speed, V(m/min)	100	150	200
Feed, F(mm/rev)	0.05	0.07	0.09
Depth of cut, d(mm)	1.0	1.5	2.0

Table 2. Turning parameters and their levels

Machine used	Turn master 35 conventional lathe, power: 5 HP
Work material	AISI D3 steel
Size of work piece	Diameter 40 mm x 70 mm
Cutting tool holder	PCLNR2525M12
Cutting insert	DNMG 150608 EN-TMR CTC2135
MQL supply	Castor oil (300 ml/ hour)
Cutting parameters	Cutting speed, Feed and Depth of cut
Cutting velocity	100-200 mm/min
Feed	0.05-0.09 mm/rev
Depth of cut	1.0-2.0 mm
Response variables measured	Surface roughness, SR (μm), Material removal rate MRR (mm^3/sec), Interface temperature, Temp (^{0}C), Cutting force, CF (kgf) and Power consumed (watts).

Table 3 Experimental condition

The turning tests were carried out on Kirloskar model centre lathe machine to determine the responses characterstics for various runs of experiment.

Surface roughness is measured using “SJ 201-P” surface roughness measuring instrument.

The material removal rate (mm^3/sec) is calculated using formula:

$$MRR = [\pi/4(D_1^2-D_2^2)L]/t \ mm^3/sec \quad (1)$$

Where

D_1 = Diameter of the work piece before turning.mm

D_2 = Diameter of the work piece after turning.mm

L = Length of turning, mm

t = Machining time, sec

The cutting zone temperature is measure using Model IRT-4 make infrared thermometer with the laser targeting the specifications of IR temperature range of -50^0C to 550^0C with response time 500 ms & (8-14) μm. Power consumed is measured by using Watt meter.

4. METHODS USED

4.1 Grey relational analysis

In the procedure of GRA, the experimental result of surface roughness, material removal rate, interface temperature and flank wears are normalized at first in the range between zeros to one due to different measurement units. This data pre-processing step is termed as 'grey relational generating'. Based on the normalized experimental data, grey relational coefficient is calculated to correlate the desired and actual experimental data using equation (4). The overall Grey Relational Grade (GRG) is determined by averaging the grey relational coefficient corresponding to selected responses using equation (5). This approach converts a multiple response process optimization problem into a single response optimization by calculating overall grey relational grade. The normalized experimental results can be expressed as follows.

For larger is better,

$$xi(k) = \frac{yi(k) - \min yi(k)}{\max yi(k) - \min yi(k)} \qquad (2)$$

For smaller is better,

$$xi(k) = \frac{\max yi(k) - yi(k)}{\max yi(k) - \min yi(k)} \qquad (3)$$

Where

$\max yi(k)$ and $\min yi(k)$ are the largest and smallest values of $yi(k)$ respectively

The Grey relational coefficient ξ(k) for $\gamma_i(k)$ is calculated as

$$\xi(k) = \frac{\Delta\min + \psi\Delta\max}{\Delta oi(k) + \psi\Delta\max} \qquad (4)$$

where $\Delta oi(k)$is

reference sequence deviation which is equal to mod $(\max yi(k) - yi(k))$

ψ is a distinguishing coefficient which varies from 0 to 1, the value of ψ is set as 0.5 to maintain equal weightage of surface roughness and material removal rate.

Grey relational grade ,

$$\gamma_i = \frac{1}{n}\sum_{i=1}^{n}\xi_i(k) \qquad (5)$$

4.2 Taguchi method

Taguchi method has been extensively adopted in manufacturing to design a product or a process robustly with a single response characteristics. The response characteristic may be to maximize or minimize the response as per the requirement. The unique calculation in Taguchi method is to calculate S/N/ratios which aims at achieving the target value by minimizing the noise or error variation. The application of Taguchi in machining industry has been extremely successful.

4.3 Analysis of Variance

Analysis of variance(ANOVA) is a method of oprtioning variability into identifiable sources of variation and the associated degree of freedom in an experiment. The frequency test(F-test) is used in statistics to analyze the significant effects of the parameters which form the response characteristics. The analysis is carried out for a level of significance of 5% ie. 95% o level of confidence. The last column in the ANOVA table signifies the "percent" contribution of each factor as the total variation, indicating its influence on the result.

5. RESULTS

A series of turning tests were conducted to assess the effect of turning parameters on surface roughness and material removal rate and the results of experimentation are shown in table 3.

S No	Speed	Feed	Doc	SR	MRR	Temp	CF	Power
1	100	0.05	1.0	0.534	38.517	35	119.906	1902.21
2	100	0.07	1.5	0.506	141.300	38	165.475	2597.24
3	100	0.09	2.0	0.472	135.406	37.8	172.023	2304.60
4	150	0.05	1.5	0.268	86.587	38.6	99.614	2414.34
5	150	0.07	2.0	0.890	171.374	46	111.780	2725.28
6	150	0.09	1.0	0.404	98.938	37.5	94.558	2377.76
7	200	0.05	2.0	0.708	203.071	38.6	76.348	2999.63
8	200	0.07	1.0	0.384	143.078	38	71.987	2853.31
9	200	0.09	1.5	0.478	280.821	45.2	73.840	2963.05

Table 3. Experimental data and results for 3 parameters, corresponding Ra, MRR, Interface temperature, Cutting force and power consumed for CVD tool

S No	Speed	Feed	Doc	SR	MRR	Temp	CF	Power
1	100	0.05	1.0	0.5723	0.0000	1.000	0.5209	1.0000
2	100	0.07	1.5	0.6174	0.4242	0.7272	0.0654	0.3666
3	100	0.09	2.0	0.6720	0.3998	0.7455	0.0000	0.6333
4	150	0.05	1.5	1.0000	0.1984	0.6727	0.7238	0.5333
5	150	0.07	2.0	0.0000	0.5483	0.0000	0.6022	0.2499
6	150	0.09	1.0	0.7814	0.2494	0.7727	0.7744	0.5667
7	200	0.05	2.0	0.2926	0.6791	0.6727	0.9564	0.0000
8	200	0.07	1.0	0.8134	0.4315	0.7272	1.0000	0.1336
9	200	0.09	1.5	0.6624	1.0000	0.0727	0.9815	0.0333

Table 4. Normalized values

S No	Speed	Feed	Doc	SR	MRR	Temp	CF	Power
1	100	0.05	1.0	0.4277	1.0000	0.0000	0.4791	0.0000
2	100	0.07	1.5	0.3826	0.5728	0.2728	0.9346	0.6334
3	100	0.09	2.0	0.3280	0.6002	0.2525	1.0000	0.3667
4	150	0.05	1.5	0.0000	0.8016	0.3273	0.2762	0.4667
5	150	0.07	2.0	1.0000	0.4517	1.0000	0.3978	0.7501
6	150	0.09	1.0	0.2186	0.7506	0.2273	0.2256	0.4333
7	200	0.05	2.0	0.7074	0.3209	0.3273	0.0436	1.0000
8	200	0.07	1.0	0.1866	0.5685	0.2728	0.0000	0.8664
9	200	0.09	1.5	0.3376	0.0000	0.9273	0.0185	0.9667

Table 5. Evaluation of Reference sequence deviation

S No	Speed	Feed	Doc	SR	MRR	Temp	CF	Power
1	100	0.05	1.0	0.5389	0.3333	1.0000	0.5107	1.0000
2	100	0.07	1.5	0.5621	0.4661	0.6469	0.3485	0.4412
3	100	0.09	2.0	0.6038	0.4545	0.6645	0.3333	0.5769
4	150	0.05	1.5	1.0000	0.3841	0.6044	0.6442	0.5172
5	150	0.07	2.0	0.3333	0.5254	0.3333	0.5569	0.3999
6	150	0.09	1.0	0.6958	0.3998	0.6875	0.6891	0.5357
7	200	0.05	2.0	0.4141	0.6091	0.6044	0.9198	0.3333
8	200	0.07	1.0	0.7282	0.4679	0.6470	1.0000	0.3659
9	200	0.09	1.5	0.5969	1.0000	0.3503	0.9643	0.3409

Table 6. Evaluation of Grey relational coefficient

S No	Speed	Feed	Doc	GRC	GRG	S/N Ratos
1	100	0.05	1.0	3.3829	0.6766	-3.393
2	100	0.07	1.5	2.4648	0.4929	-6.145
3	100	0.09	2.0	2.633	0.5266	-5.570
4	150	0.05	1.5	3.1499	0.6299	-4.402
5	150	0.07	2.0	2.1488	0.4298	-7.335
6	150	0.09	1.0	3.0079	0.6016	-4.414
7	200	0.05	2.0	2.8807	0.5761	-4.790
8	200	0.07	1.0	3.209	0.6418	-3.852
9	200	0.09	1.5	3.2524	0.4576	-6.790

Table 7. Evaluation of Grey relational grade & corresponding S/N ratios

Process parameters	Average relational grade				
	Level 1	Level2	Level3	Max-Min	Rank
Spindle speed(V)	0.5654*	0.5537*	0.5585*	0.0117	3
Feed (F)	0.6275*	0.5215	0.5286	0.1060	2
Depth of cut(d)	0.6400*	0.5268	0.5108	0.1292	1
Total mean value of the Grey relational grade = 0.5592 *Optimum levels					

Table 8. Response table for Grey relational grade

Process parameters	Average relational grade				
	Level 1	Level2	Level3	Max-Min	Rank
Spindle speed(V)	-5.036*	-5.384	-5.144	0.108	3
Feed (F)	-4.195*	-5.777	-5.779	1.582	2
Depth of cut(d)	-3.886*	-5.779	-5.898	2.012	1
Total mean value of S/N ratios of Grey relational grade = -5.188 *Optimum levels					

Table 9. S/N ratios table for Grey relational grade

Source of variation	Degrees of freedom	Sum of squares	Mean sum of squares	F-ratio	Percent contribution
Spindle speed	2	0.000204	0.0000102	0.0022	0.338
Feed	2	0.21081	0.01054	2.2980	35.011
Depth of cut	2	0.02975	0.01487	3.2430	49.413
Error	2	0.00917	0.00458		15.235
`	2				100.000

Table 10. ANOVA based on Grey relational grade

5.1 Prediction at optimum levels

The objective of the prediction at optimum levels is to validate the conclusions drawn during the analysis phase. Once the optimal level of process parameters is selected, the next step is to verify the improvement in response characteristics using optimum level of parameters. A conformity test is conducted using the following equation.

$$\gamma = \gamma_m + \sum_{i=1}^{n} \gamma_i - \gamma_m \quad (6)$$

where, γm is total mean of the required responses
γj is the mean of the required responses at optimum level
n is the number of process parameters that significantly affects the multiple performance characteristics

	Optimum process parameters		
	Initial process parameters	Predicted values	Experimental values
Level of parameters setting	V1-F1-d3	V1-F1-d1	V1-F1-d1
Surface roughness (μm)	0.708	0.4159	0.534
MRR (mm^3/sec)	203.071	19.291	38.517
Temperature(^{0}c)	38.60	32.344	35
Cutting force	76.348	127.789	119.906
Power consumed	2999.63	1934.854	1902.21
Grey relational grade	0.5761	0.7155	0.6766

Table 11. Comparison of predicted and Experimental results using GRA

6. CONCLUSIONS

1. The optimal parameters setting with Grey relational analysis lies at 100 m/min cutting speed, 0.05 mm/rev feed and 1.0 mm depth of cut. The optimum predicted value for surface roughness is 0.4159 μm, MRR 19.291 mm^3/sec, interface temperature 32.344^{0}C, cutting force is 127.789 kgf, power consumed is 1934.854 watts and grey relational grade is 0.7155. Also the experimental value for surface roughness is 0.534 μm, MRR is 38.517 mm^3/sec, interface temperature 35^{0}C, cutting force is 119.906 kgf, power consumed 1902.21 watts and grey relational grade is 0.6766
2. Iit is found that both predicted and experimental response characteristics are significantly better as compared to initial machining parameters. To be specific predicted surface roughness(0.4159μm) and experimental surface roughness (0.534μm) are significantly lower than surface roughness at initial setting level which is highly commendable. Also predicted MRR and experimental MRR are reasonably close to each other. Also predicted interface temperature(32.344^{0}C) and experimental interface temperature(35^{0}C) are much lower than initial setting which is highly expected and by which life of tool will be increased. Also predicted MRR and experimental MRR are reasonably close to each other. As Also predicted power consumed(1934.854 watts) and experimental power consumed(1902.21 watts) are much substantially lower than initial setting(2999.63 watts) It may be noted that there is a good agreement between the predicted GRG (0.7155) and experimental GRG(0.6766) and therefore the condition **V1-F1-D1** of process parameters combination was tested as optimal. Further significant improvement in machinability is observed and measured that there is 32.39%

improvement in surface roughness (Experimental value), 10.28% improvement in interface temperature(Experimental value), 57.69% improvement in power consumed as compared with initial machining parameters. This encourages applying Grey relational analysis for optimizing multi response problems.

3. Further, from Analysis of variance (ANOVA) depicts that depth of cut is the most significant parameter followed by feed affecting multi response characteristics with depth of cut 49.41%, feed 35.011% and cutting speed almost negligible.

7. REFERENCES

[1] Chorng-Jyh Tzeng , Yu-Hsin Lin, Yung-Kuang Yang , Ming-Chang Jeng, *Optimization of turning operations with multiple performance characteristics using the Taguchi method and Grey relational analysis*, journal of materials processing technology 209, 2753–2759, (2009).

[2] Bala Murugan Gopalsamy, Biswanath Mondal , *Optimisation of machining parameters for hard machining: grey relational theory approach and ANOVA*, Int J Adv Manuf Technol, 45:1068–1086, (2009).

[3] Mohamed Handawi Saad Elmunafi, D. Kurniawan, M.Y. Noordin, *Use of Castor Oil as Cutting Fluid in Machining of Hardened Stainless Steel with Minimum Quantity of Lubricant*, 12th Global Conference on Sustainable Manufacturing, Procedia CIRP 26, 408 – 411, (2015).

[4] Papiya Bhowmik, , Ujjwal Kumar, and Gaurav Arora, *Vegetable Oil Based Cutting Fluids–Green and Sustainable Machining – I*, Journal of Material Science and Mechanical Engineering (JMSME), Volume 2, Number 9, pp. 1-5, April-June, 2015.

[5] Ujjwal Kumar, , Atif Jamal, , Aftab A. Ahmed, *Performance Evaluation of Neat Vegetable Oils as Cutting Fluid during CNC Turning of Aluminium (AA1050)*, Journal of Material Science and Mechanical Engineering (JMSME), Volume 2, Number 7, pp. 70-75, ; April-June, 2015.

[6] Reddy Sreenivasulu, Dr.Ch.SrinivasaRao, *Application Of Gray Relational Analysis For Surface Roughness And Roundness Error In Drilling Of Al 6061 Alloy*, International Journal of Lean Thinking Volume 3, Issue 2 (December 2012).

[7] A. H. A. Shah,1,a, A. I. Azmi and A. N. M. Khalil, *Multi-Objective Optimization in CNC Turning of S45C Carbon Steel using Taguchi and Grey Relational Analysis Method*, Journal of Advanced Research in | Vol. 11, No. 1. Pages 8-15, 2015.

[8] Daniel Kirby, E., Zhang, Z., Chen, J. C., & Chen, J. (2006). *Optimizing surface finish in a turning operation using the Taguchi parameter design method*, International Journal of Advanced Manufacturing Technology, 30, 1021-1029.

[9] M.Y. Wang and T.S. Lan, *Parametric optimization on multi-objective precision turning using Grey relational analysis*, Information Technology Journal 7(7), pp.1072-1076, 2008.

Authors: **Assist. Professor (Sr) R.K Suresh, Professor Dr. G.Krishnaiah, Assosiate Professor Dr. P. Venkataramaiah**

Sri Kalahastheeswara institute of Technology, Faculty of Mechanical Department, S.V.University college of Engineering, Faculty of Mechanical Department, S.V.University college of Engineering, Faculty of Mechanical Department.

E-mail: rayakuntapalli@gmail.com

Journal of Production Engineering
Vol.19 No.1
JPE (2016) Vol.19 (1) Original Scientific Paper
Wang, Y., Guo, Z., Liu, B.,Luo, H., Zhu, Y.

INVESTIGATION OF BALL SCREW'S ASSEMBLY ERROR BASED ON DYNAMIC MODELING AND MAGNITUDE ANALYSIS OF WORKTABLE SENSED VIBRATION SIGNALS

Received: 20 December 2015 / Accepted: 29 March 2016

Abstract: *Considering the effect of the installation error of ball screw on the working precision of machine tools, a method of detecting ball screw's assembly error via monitoring the average vibration magnitude induced by ball screws (VMBS) is proposed. In this study, the ball screw was simplified to a freely supported beam. Ball screw's assembly error (BSPE) can be reduced by means of the fine adjustment of bearing seat's position. A mathematical model of the effect of BSPE on the contact angle of the ball and ball raceway was established. The change of contact angle has influence on the deformation and contact stiffness, the change of contact force can be calculated according to the Hertz contact theory. Thus, a method of detecting BSPE by the detection of VMBS is proposed. Aiming at improving the accuracy of experimental results, the sample data was mean process and curve fitting. The experimental results show that the average VMBS raises with the increase of assembly error under the speed 1000rpm and 1500rpm and the assembly error from 0 to 0.2mm. This study provides an approach to monitor the BSAE, which is valuable for improving the assembly accuracy and working precision of ball screws.*
Key words: *Assembly error, Ball screw, Vibration characteristic, Contact angle, Machine tools*

Istraživanje greške sklopa zavojnog kugličnog vretena na osnovu dinamičkog modelovanja i analize signala vibracija na pomičnom stolu. *Uzimajući u obzir uticaj greške motaže zavojnog kugličnog vretena na preciznost mašine alatke, predložena je metoda određivanja greške sklopa kugličnog vretena preko praćenja srednje vrednosti vibracija generisanih kugličnim zavojnim vretenom (VMBS). U ovom radu je zavojno kuglično vreteno pojednostavljeno i predstavljeno kao prosta greda. Greška montaže kugličnog zavojnog vretena (BSPE) može da se redukuje finim podešavanjem pozicije sedla kugličnog ležaja. Matematički model uticaja greške montaže kugličnog zavojnog vretena na ugao kontakta između kuglica i vretena, je predložen. Promena ugla kontakta utiče na deformaciju i krutost kontakta a promena sile kontakta se može izračunati po Hercovoj teoriji kontakta. Stroga je predložena metoda detekcije BSPE na osnovu VMBS. U cilju poboljšanja tačnosti eksperimentalnih rezultata, srednje vrednosti prikupljenih podataka su predstavljene pomoću funkcije pripadnosti. Rezultati eksperimenta pokazuju da prosečne VMBS rastu sa povećanjem greške montaže ispod brzine 1000 obrt/min i 1500 obrt/min kao i greška montaže od 0 do 0,2 mm. Ova studija pruža pristup praćenja BSPE, što je važno za poboljšanje greške montaže kao i radne preciznosti zavojnih kugličnih vretena.*
Ključne reči: *Greška montaže, zavojno kuglično vreteno, karakteristike vibracija, kontaktni ugao, mašine alatke.*

1. INTRODUCTION

Over the past few decades, developing more precise and high-speed feed drive system has become a noticeable trend for engineers due to the necessity of higher component quality and productivity boosts [1]. The feed drive system is widely applied to machine tools and automation equipments for its high transmission efficiency and working precision. In a considerable amount of research on modern feed drive systems, ball screws play a significant role in converting rotary motion into linear motion to carry medium/high loads [2].

Kinematic analysis of the ball screw mechanism, which considers variable contact angles, preload and elastic deformations, were done in the study of Wei et al. [3] The contact angles formed at the position of each ball in ball screws is conventionally assumed to be a constant value in determination of contact stiffness, the variable contact angles and normal forces of the ball screw are predicted by Chen et al.[4] A preload is always applied in the ball–screw to avoid vibration and backlash during all linear transmission periods. theories for the kinematics of a single-nut double-cycle ball screw are developed in a dry contact condition by Wei et al. [5]; The sliding wear is the main reason why the applied preload decreases or vanishes, a new two body abrasion model combining the kinematic theory describes the variations in the axial wear depths with the operating strokes [6]. For the diagnosis of the ball screw preload during its operation. Feng et al. [7] construct a preload-adjustable feed drive system, and also verify that the preload variation of a ball screw can be diagnosed by the vibration signals sensed at the ball nuts. In the case of monitoring the ball screw preload, a technique of determining the onset of preload loss in a ball screw feed drive system via monitoring the change of ball pass frequency is proposed [8]. Elastic deformations occur in ball screw drives typically due to inertial forces, guideway friction, and cutting forces. Amin et al. [9] present a new strategy for mitigating the detrimental effect of elastic deformations, in order to

improve the translational accuracy of ball screw drives when only rotational feedback is available. Concluding from the studies mentioned above, we can find that the effect of preload and elastic deformations on ball screws cannot be ignored. Meanwhile, the method of vibration detection is feasible. In order to meet the requirement of machine tools' assembly accuracy, reduce the temperature-rise and deformation of ball screws, reduce the transmission torque of the servo motor and improve the reliability of the machine tools, the installation accuracy of ball screws should be improved.

The parallelism error between ball screws and linear guides exists during the installation. However, there is a lack of literature discussing about diagnosis of the BSPE during its installation. Therefore, this paper studies the effect of BSPE on the VMWBS to realize the detection of BSPE. The remainder of the paper is organized as follows : Firstly, a mathematical modeling of the effect of BSPE on the contact angle between the ball and ball raceway has been established, Saccording to Hertz contact theory, in which the relation between contact force and contact deformation is expounded, the method of studying the effect of the BSPE on the VMBS is proposed. And a data processing mathematical modeling is built up for the accuracy of results. Finally, the method we proposed is verified by experiments.

2. EFFECT OF BSPE ON VMBS

2.1. Effect of BSPE on the contact angle

Both ends of ball screw are connected with bearing seats for supporting and locating. Therefore, BSPE δ can be reduced by means of the fine adjustment of bearing seat's position shown in Figure 10. With the increase of BSPE, a deflection angle will appear. Thus, the original system can be simplified to a freely supported beam system in which one side is fixed and another is free, as shown in Figure 1.

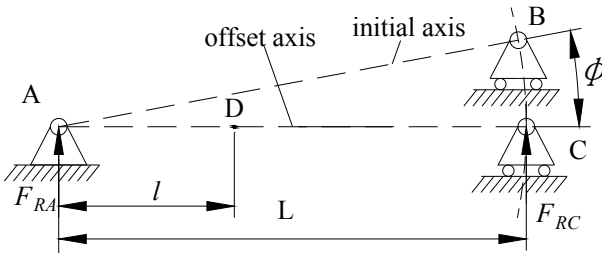

Figure 1. Effect of assembly error on ball screw

The deflection will lead to the change of contact angle and even the elastic deformation or contact stiffness. When $\delta \le C_b+C_g+C_s+\varepsilon$, it is equivalent to diminishing the clearance between the ball and ball raceway. When $\delta > C_b+C_g+C_s+\varepsilon$, it will cause the change of contact angle and even elastic deformation or contact stiffness. C_b represents bearing clearance, C_g denotes the clearance between the rail and the carriage, C_s denotes the clearance between the ball screw and the nut, ε is other clearance.

If the effect of clearance is ignored and a assembly error is added to bearing seat, an inflection angle φ is generated between the initial axis and the offset axis. Given the length of screw is L, we can regard it as a right-angled triangle ΔACB as for φ is small. φ can be calculated according to the law of cosines.

$$\varphi = \arctan\frac{\delta}{L} \qquad (1)$$

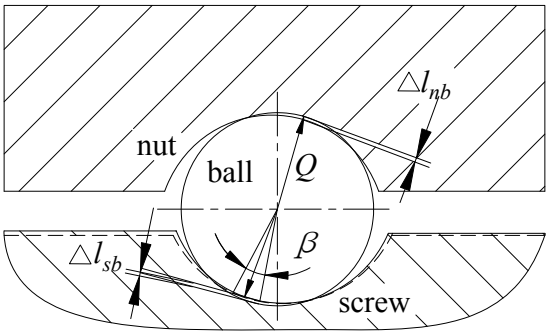

Figure 2. The change of contact angle

After the offset of ball screw, the radial displacement of different positions on the ball screw is varied. Therefore, the contact angles variation of the ball and ball raceway is also disparity. The trajectory of random point D denotes equivalent to the rolling arc on the ball for the tiny error. It can be seen from Figure 2.

$$\beta r_b = \varphi l \qquad (2)$$

Where r_b denotes the ball radius. l denotes the random length of the ball screw, β denotes the variation of contact angle.

Combining equations (1) and (2), β can be calculated as follows:

$$\beta = \frac{l}{r_b}\arctan\frac{\delta}{L} \qquad (3)$$

Figure 3 is the three dimensional variation when the effective length of the ball screw is 800 millimeter, the diameter of the ball changes from 3.75 to 9.75mm and the assembly error varies from 0 to 0.2 mm.

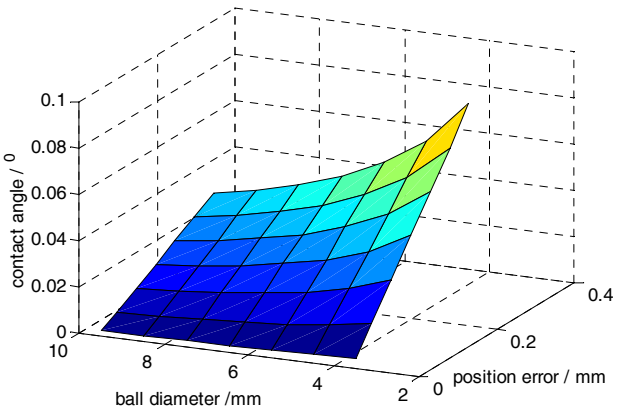

Figure 3. The effect of ball diameter and assembly error on contact angle

2.2. The change of contact force

BSPE not only increases the preload between the ball and ball raceway, but also results in the change of contact angle. Integrating with the bending deformation of ball screw, assembly error leads to the contact deformation between the ball and ball raceway. Figure 2 shows a normal section in the ball and ball raceway area. The contact deflection Δl in the ball and ball raceway area is defined by the following formula [10]

$$\Delta l=\delta^* \sqrt{\frac{1}{8}(1.5E)^2 Q_1^2 \sum \rho} \qquad (4)$$

Where Q_1 denotes the normal force , $\sum\rho$ denotes the sum of principle curvature, $\Delta l = \Delta l_{sb} + \Delta l_{nb}$, Δl_{sb} denotes the deformation between ball and screw, Δl_{nb} denotes the deformation between ball and nut ; the value of δ^* can be found in table [11]. The principle curvature ρ is given by [12]

$$\rho = \frac{2\cos\beta\cos\lambda}{d_0 \pm d\cos\beta} \qquad (5)$$

Where λ denotes helix angle, d denotes the ball diameter, d_0 denotes the ball screw diameter. The substitution of ρ expression into Eq.(4) gives

$$\Delta l = 2.794\times10^{-4}\delta^*\sqrt[3]{Q_1^2\sum\rho} \qquad (6)$$

Where k^* denotes the contact surface stiffness coefficient among ball, ball screw and nut. Details are available in the literatures [14, 15] and k^* can be given

$$k^* = 2.14075\times10^5\left(\sum\rho\right)^{-0.5}\left(\delta^*\right)^{-1.5} \qquad (7)$$

As ball screw's bending deformation, the actual contact force Q is given [13]

$$Q = k^*\Delta l^{3/2} + kw \qquad (8)$$

Where the total stiffness among ball screw, nut and ball is k. ω denotes the deflection

As the assembly error of the ball screw, the ball screw has unbalance in the working process, the method of VMBS is adopted.

3. THE PROCESSING METHOD OF VIBRATION DATA

The change of contact force will hinder the rotation of ball screw, which results in the increase of VMBS. VMBS can be detected by acceleration sensor. As the feed drive system composed by the rolling functional components is instable during operation, so the VMBS is fluctuant. Thus, multiple measurements on the ball screw's rotational frequency are needed to ensure that the data values obtained can reflect the actual situation accurately.

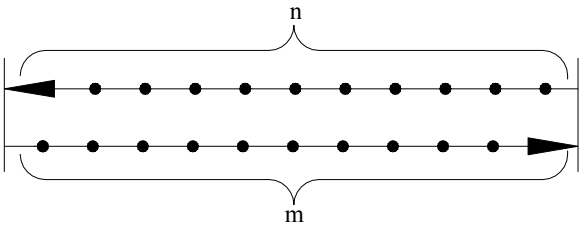

Figure 4. Vibration measurement point

In the process of vibration measurement, when the sampling interval time is the same and the rotation speeds are different, the number of sampling points is varied in the axis of ball screw. That is to say, the higher rotation speed, the fewer number of points is collected. n and m are the numbers of sampling back and forth shown in Figure 4. Because of the shock at both ends of the ball screw have effect on VMBS, so the data at both ends of the ball screw is excluded.

Under each certain rotation speed and BSPE, we make the average of different VMBS gathered from multiple measurements. Then the optimal value can be selected where the minimum contact force can be got. The average of VMBS in different BSPE is Z_δ.

$$Z_\delta = \frac{\sum_{k=1}^{P}\left(\frac{\sum_{i=1}^{n}x_i + \sum_{j=1}^{m}y_j}{n+m}\right)}{P} \qquad (9)$$

Where P is the times of feed drive system runs back and forth, P≥1 ; When the feed drive system runs back, the VMBS of point i is x_i, while runs forth, the VMBS of point j is y_i. The final fixed position is determined by comparing the average value of Z_δ under the different δ. For accurately reflects the relationship between the error and amplitude, the method of the minimum two polynomial curve is adopted.

4. EXPERIMENTAL VERIFICATION

4.1 Experiments setup

According to the experimental requirements, a test bed is set up shown in Figure 5. The ball screw pair's type is HWIN R16-5T4-FSI of which effective length is 800mm. The linear guide's type is THK AP-C of which length is 800mm. The driving motor is ECMA-C20604 of Delta and the server is ASDA-B2 series. The bearing seats at both ends are standard. The fixed end is BK12, while the supported end is BF12. An initial location area is designed in the bearing seat and different BSPE can be achieved by using the feeler gauge of DL9502 series shown in Figure 8.

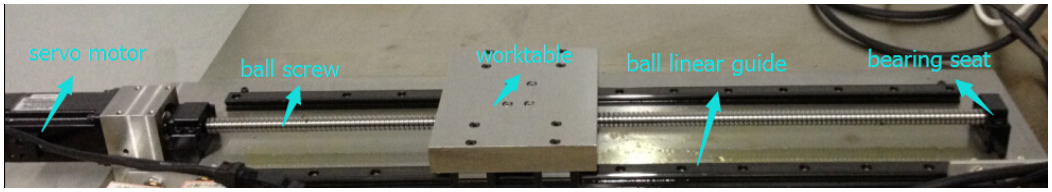

Figure 5. Feed drive system setup

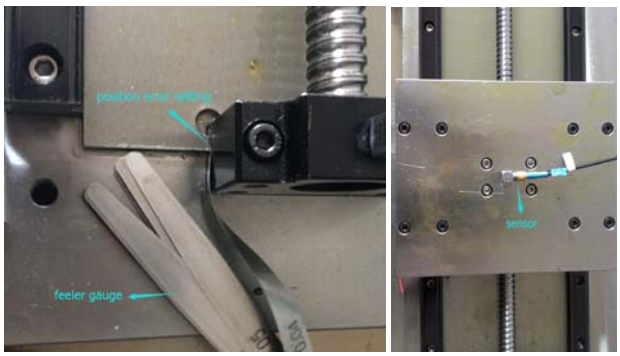

Figure 6. Error setting and data collection

4.2. Data collection

The sensor which is the three-dimensional acceleration sensor of Dytran is fixed on the worktable as shown in Figure 6. Vibration signal is collected and analyzed by using ECON MI-7008 in different rotation frequency of ball screw.

After setting the sample frequency and sampling number respectively as 10240Hz and 8192, we can collect the vibration signal when the value of speed is 1000 rounds per minute (rpm) and 1500rpm. The vibration signals perpendicular to the plane of worktable are collected. As the useful frequency is dozens of Hertz, so the low pass filter is added, the frequency and time domain signals are shown in Figure 7-8.

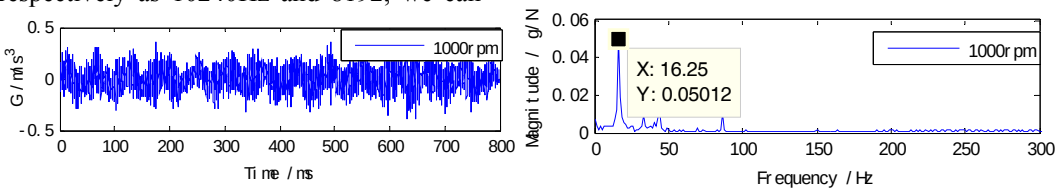

Figure 7. Time domain signal and frequency, when the rotation speed is 1000rpm

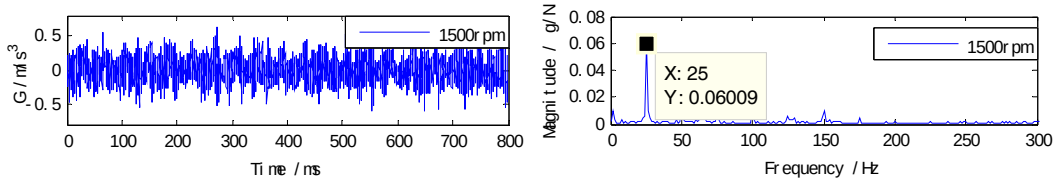

Figure 8. Time domain signal and frequency, when the rotation speed is 1500rpm

4.3. Data processing and analysis

The VMBS will be extracted in different assembly error with special rotation speed. When the rotation speed is 1500rpm, 1000rpm, the data of the VMBS is shown in Figure 9-10. As shown in Figure 9-10, the change of VMBS is fluctuant, which gradually similar to sine curve as the speed diminishes. This is because the higher speed, the less sampling number is collected, under the same sample interval. During the actual installation, the bending deflection of ball screws is reduced by applying the pre-stretch force. Then the bending deflection degree can be detected by the proposed method.

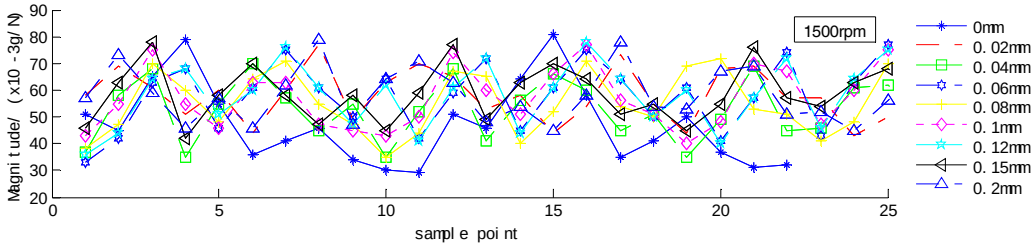

Figure 9. The collected VMBS curve, when the rotation speed is 1500rpm

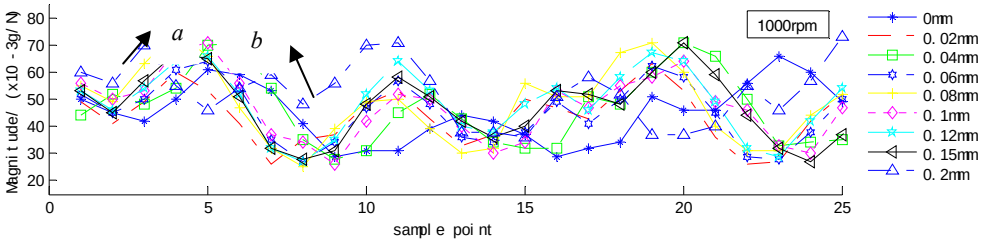

Figure 10. The collected VMBS curve, when the rotation speed is 1000rpm

Averaging the extracted magnitude and data fitting according to equation (9), the change of average VMBS with different BSPE is got under the varied speeds, shown in Figure 11.

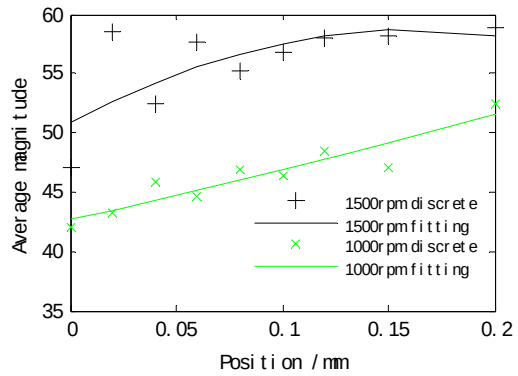

Figure 11. Effect of assembly error on frequency magnitude

From Figure 11, we can find that the average VMBS increases with the increase of BSPE. Under the speed of 1000rpm, the average VMBS rises steadily. In order to improve the installation accuracy and efficiency, we can find out the speed at which the average VMBS of the special drive feed system rises steadily with the adjustment of BSPE.

5. CONCLUSIONS

In order to improve the assembly accuracy and efficiency of machine tools, reduce the effect of ball screw's temperature rise on working precision, reduce the transmission torque of the servo motor and improve the reliability of the machine tools, this paper researches the effect of BSPE on the VMWBS by experiment. The results are as follows:

(1) The average VMBS increases with the adjustment of BSPE. It provides theoretical basis for the study of assembly error. The result data also verifies the feasibility of detecting the parallelism error between ball screw and rolling linear guide by vibration test.

(2) This study provides an approach to monitor the ball screw's bending deflection and the BSPE, which is valuable for improving the working precision and assembly accuracy of machine tools.

6. REFERENCES

[1] S. Frey, M. Walther, A. Verl. Periodic variation of preloading in ball screws. Production Engineering 4 (2010) 261–267.

[2] H. Nurhadi, Y S. Tarng, Experimental approached optimisation of a linear motion performance with grey hazy set and Taguchi analysis methods (GHST) for ball-screw table type. The International Journal of Advanced Manufacturing Technology 44 (2009) 149–160.

[3] C C Wei, J F Lin. Kinematic analysis of the ball screw mechanism considering variable contact angles and elastic deformations. ASME Journal of Mechanical Design 125 (2003) 717–33.

[4] Y J Chen, W C Tang. Determination of contact stiffness in ball screws considering variable contact angles. Proceeding of The Institution of Mechanical Engineers Part C: Journal of Mechanical Engineering Science 228(12) (2014) 2193-2203.

[5] C C Wei, J F Lin, J H Horng. Analysis of ball screw with a preload and lubrication. Tribology International 42 (2009) 1816-1831.

[6] C C Wei, W L Liu, R S Lai. Wear analysis of the offset type preload ball-screw operating at high speed. Wear 292-293(2012) 111-123.

[7] G H Feng, Y L Pan. Investigation of ball screw preload variation based on dynamic modeling of a preload adjustable feed-drive system and spectrum analysis of ball-nuts sensed vibration signals. International Journal of Machine Tools & Manufacture, 52(2012) 85-96.

[8] P.C Tsai, C.C. Cheng, Y.C. Hwang. Ball screw preload loss detection using ball pass frequency. Mechanical system and signal processing 48(2014) 77-91.

[9] Amin Kamalzadeh, Daniel J. Gordon, Kaan Erkorkmaz. Robust compensation of elastic deformations in ball screw drives. International Journal of Machine Tools & Manufacture 50(2010) 559-574.

[10] Harris T A, Kotzalas M N. Rolling bearing analysis [M].5th ed. London: Taylor & Francis, 2006.

[11] Hertz H. On the contact of elastic solids. J. Reine Angew Math 92(1882) 156-171.

[12] G Liu, X C Zhang, S J Ma, et.al..Studies on dynamic contact characteristics of ball screws. Journal of Chongqing University 36(3) (2013) 42-47.

[13] Jery Z. Sobolewski. Vibration of the ball screw drive. Engineering Failure Analysis 24(2012) 1-8.

[14] D.E. Brewe, B.J. Hamrock. Simplified solution for elliptical-contact deformation between two elastic solid. Transactions of the ASME, Journal of Lubrication Technology 99(1997) 485–487.

[15] J.A. Greenwood. Analysis of elliptical Herztian contacts. Tribology International 30(1997) 235–23.

Acknowledgments This research is supported by state key science and technology special projects for advanced CNC machine tools and basal manufacturing equipments (2012ZX04011021)

Authors: **Yiqiang Wang[a*], Zhengcai Guo[b*], Botao Liu[c], Haibo Luo[c], Yanfei Zhu[d],** [a]College of Mechanical and Energy Engineering, Institute of Technology, Zhejiang University, Ningbo, 315100,China; [b]School of Mechanical Engineering, Taiyuan University of Science and Technology, Taiyuan, 030000,China, [c]School of Mechanical Engineering, Zhejiang University, Hangzhou, 310000,China, [d]School of Mechanical Engineering, Shandong University of Technology, Zibo,255000, China

*Corrosponding author. Tel: +8615058030369; +8618368497811; fax: 057488229586. E-mail addressl:jluwang@gmail.com,gzc_9007@163.com

Journal of Production Engineering
Vol.19 No.1
JPE (2016) Vol.19 (1) Original Scientific Paper
Knežev, M., Živković, A., Mlađenović, C.

ANALYSIS STATIC AND DYNAMIC BEHAVIOR OF HYDRODYNAMIC SPINDLE

Received: 04 January 2016 / Accepted: 20 March 2016

Abstract: *Becoming more stringent demands with regard to quality of ball bearings, as well as complexity of physical and chemical process that occur inside of them, which cannot be explained based on theoretical knowledge, caused intensive development of experimental methods and devices for testing and diagnostic of rolling bearings. Experimental tests are carried out on special for this purpose intended devices. The most important element of device is hydrodynamic spindle from who depend the accuracy of device. The objective of this work is to study the static and dynamic behavior of spindle supported by hydrodynamic bearings, using the FEM method.*
Key words: hydrodynamic spindle, hydrodynamic bearings, static analysis, dynamic analysis, CAE

Analiza statičkog i dinamičkog ponašanja hidrodinamičkog vretena. *Strogi zahtevi u pogledu kvaliteta kugličnih ležaja, kao i složenost fizičkih i hemijskih procesa koji se dešavaju unutar njih, koja se ne mogu objasniti na osnovu teorijskog znanja, dovelo je do intenzivog razvoja eksperimentalnih metoda i uređaja za ispitivanje i dijagnostika kotrljajnih ležaja. Eksperimentalna ispitivanja se izvode na specijalno za tu svrhu namenjena uređajima. Najvažniji element uređaja za ispitivanje vibracija kotrljajnih ležaja su hidrodinamička vretena od kojih zavisi tačnost uređaja. Cilj ovog rada je da se metodom konačnih elemenata ispita statičko i dinamičko ponašanje vretena uležišteno hidrodinamičkim ležajima.*
Ključne reči: *hidrodinamička vretena, hidrodinamički ležaji, statička analize, dinamička analiza, CAE*

1. INTRODUCTION

Experimental results have a major impact both on the resolving existing problems and the development of new designs and technologies throughout the life of the roller bearings, therefore is very important that results are accuracy [1]. The hydrodynamic spindle system is the most important element of a measuring device since its properties are closely related to the accuracy of the device, because during the test roller bearing is placed on spindle and every imperfection of spindle will reflect on results. The dimension of the spindle as well as the location, the stiffness of the hydrodynamic bearings, loads of tourniquet and driving system affect the spindle behavior. For the hydrodynamic bearings, the journal and the bearing surface are separated by the sliding action with a wedge pressure-generating mechanism to develop a pressure within the bearing [2]. So that stiffness depends on the pressure and thickness of the lubrication film [3-4]. Spindle used in precision devices must have low error motion over a range of operation speeds, small temperature rise and minimum wear. The above requirements can be achieved by appropriate choice material and construction of the spindle and its bearings [5]. Hydrodynamic bearings are characterized by very high accuracy of work, running smoothness with high vibrations dumping, simply technology and low cost of making, economically maintenance and so on.

The purpose of static analysis is validation that the spindle deformations are in allowed limits and finding the force in bearings. On the other hand dynamic analysis is made with aim to analyze the dynamic behavior, for what is used modal analysis to determinate natural frequencies and mode shapes as well as harmonic analysis to determine the response of certain nodes at the effect of the load. Both analyzes are carried out using the finite element method.

2. STATIC AND DYNAMIC ANALYZES

The spindle is mounted in a housing of device via two radial and one axial hydrodynamic bearing for satisfying the high precision rotating of spindle. The Fig 1 shows the 3D model of hydrodynamic spindle system with marked characteristic parts.

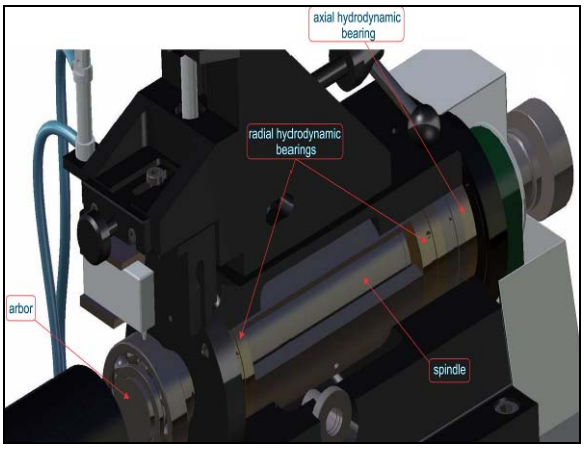

Fig. 1. 3D CAD model of hydrodynamic spindle system [6]

Due to simple Axial-symmetric nature of the spindle system, the spindle is represented by one dimensional element type with two nodes BEAM188, which is six degree element, based in Timoshenko beam theory, with circular annular cross-section, which

is suitable for representing the stepped nature of spindle. Stiffness of hydrodynamic bearings is defined by equivalent spring-dumper element type COMBIN14 whereby value of initial stiffness both hydrodynamic bearings are Cr=70 N/μm [7]. The front conical surface of the spindle which is used to accept and positioning the arbor is replaced with cylindrical surface with the dimension of middle diameter of cone. The Fig. 2a shows model described with 16 nodes and 15 elements type BEAM 188 and 2 elements type COMBIN14 (Fig. 2b).

In reality, the spindle has a total length of 324 mm and its outside diameter is variable, on place where is spindle connected with bearings diameter is 60 mm. The spindle is connected with front and rear bearing with the isotropic bearing stiffness designated as nodes 15 and node 16 respectively.

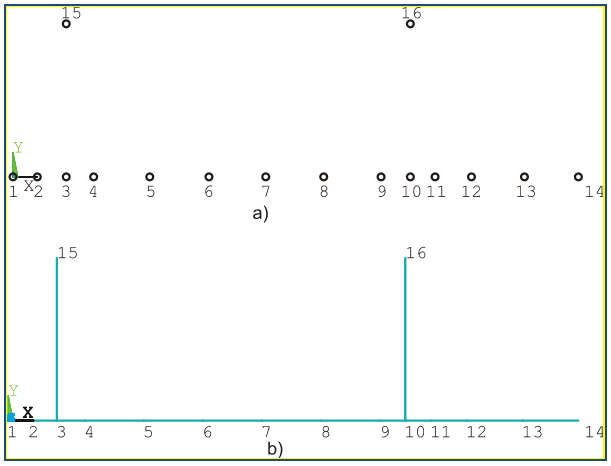

Fig. 2. Spindle described by; a) the nodes, b) BEAM188 elements

Using ANSYS APDL, a static model was built, consisting of a solid shaft rigidly connected to arbor and belt pulley and supported by the bearings hydrodynamic bearings.

The Fig. 3 shows model for analysis, the same model will be used for static and dynamic analysis, only the constraints will be changed.

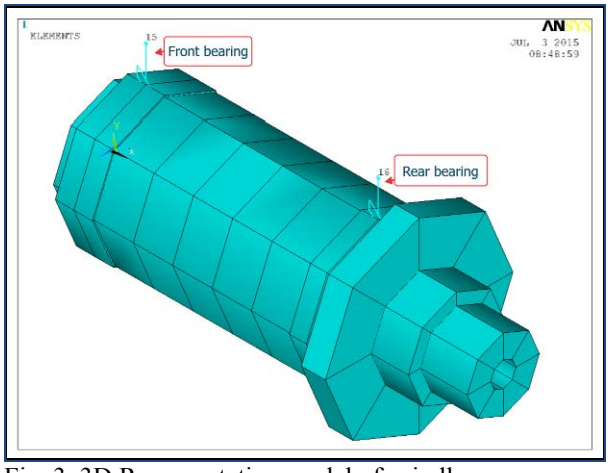

Fig. 3. 3D Representation model of spindle

Material of spindle is 20MnCr5, and his data are specified in Table 1.

Material	20MnCr5
Modulus of elasticity	2.1E+05 MPa
Density	7.8E-06 kg/mm^3
Tensile strength	800 MPa
Poisson Ratio	0.3

Table 1. Spindle material data

2.1 Static analysis

The static analysis is carried out with radial load on node of finite element mesh where is spindle in contact with belt pulley (node 14), and axial load on spindle nose (node 1). Applied forces are the result of the maximal axial force (Fa=200 N), which acting on the test bearing and the radial force (Fr=430 N) by the belt transmissions.

The Fig. 4 shows deformations in Y direction, the biggest value of deformations is on the end of spindle, showed by blue color, what was expected because that is the place of radial force. The maximum of radial displacement occurs at the end of the spindle and is 16.9 μm, while the minimum radial displacement occurs at the spindle nose and is 0.5 μm (Fig. 4). On the place where is spindle connected with a front hydrodynamic bearing deformation is 5.0 μm, and on the rear bearing place is 12.0 μm. Hydrodynamic bearings are designed with clearance of 20 μm, so then mentioned displacements on front and rear bearing will not disturb proper work. Force reactions in bearings are: front and rear bearing F_{fb}=203N, and F_{rb}=633N respectively.

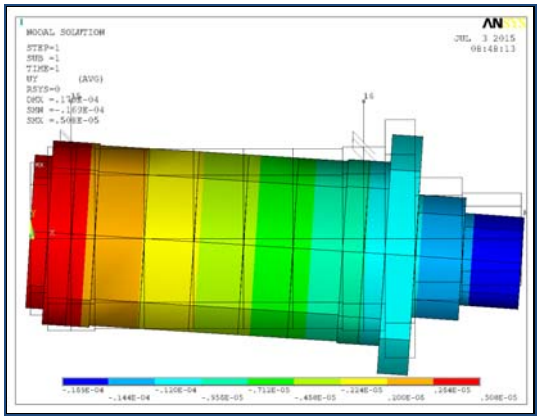

Fig. 4 Structural displacement due to loads

The spindle stiffness includes the axial and bending stiffness. In this operating condition, the axial stiffness is more important than bending stiffness. The axial stiffness (C_a) of the spindle unit is defined as follows: if the front part of the spindle generates unit axial displacement δ_a, the force required to be imposed on the direction of the displacement is F_a. [8] The static axial stiffness of the spindle nose can be calculated as:

$$Ca = \frac{Fa}{\delta_a}; N/\mu m$$
$$C_a = \frac{200}{1.8} \cong 111; N/\mu m \quad (1)$$

On the basis of displacement from Figure 4, radial stiffness of the front ($C_{r,f}$) and rear bearing ($C_{r,r}$), under applied the radial load are:

$$C_{r,f} = \frac{203}{5} = 40.6; \text{N}/\mu\text{m}$$
$$C_{r,r} = \frac{633}{12} = 52.7; \text{N}/\mu\text{m} \quad (2)$$

Similar stiffness values for the given displacements are shown in the paper [1].

2.2 Dynamic analysis

For dynamic analysis spindle is freely supported, because mode frequencies as well as the natural frequencies are depend on the system parameters. In order to find the spindle natural frequencies domain of the spindle was used finite element model represented in Fig. 5. Two nodes 15 and 16 are taken all degrees of freedom, to node 3 where is spindle connected with front bearing is taken rotational degree around X axis, and translation in Z direction, while to node 10 are taken translations in X and Z directions, and rotation around X axis.

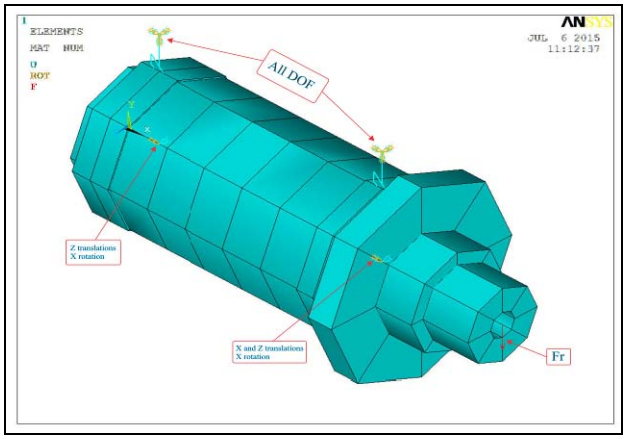

Fig. 5. Finite element model for dynamic analysis with constraints

Reason for that kind of limitations is radial on front and radial with axial bearings on rear side of spindle.

Accordingly numerical models were obtained the results for the first five natural frequencies of model (represented in Fig. 5.) values are given in Table 2.

Mode	Frequency [Hz]
f_{01}	355
f_{02}	504
f_{03}	5088
f_{04}	5580
f_{05}	9000

Table 2. Natural frequencies of the spindle

Based on the calculated values, plotted are the mode shapes for corresponding natural frequencies. Vibration modes according third and fifth natural frequencies are represented, Fig 6 shows third, and Fig. 7 shows fifth mode shapes. We can observe that the first spindle natural frequency of the spindle is about 355 Hz corresponding to 21300 rpm, and it is much higher than maximum spindle speed which is 1800 rpm.

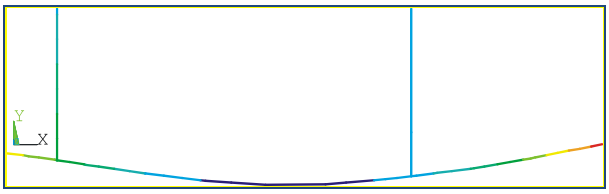

Fig. 6 Third natural frequencies of the test spindle

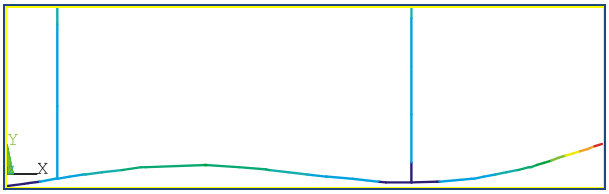

Fig. 7 Fifth natural frequencies of the test spindle

The spindle is modeled as a stationary reference frame where the general dynamic equation includes the rotational effects as follows:

$$[M]\{\ddot{u}\} + [G]\{\dot{u}\} + [K]\{u\} = \{F\} \quad (3)$$

Where:

$[M]$ = Structural mass matrix

$[G]$ = Gyroscopic effect originated from the rotational angular velocity applied to the structure

$[K]$ = Stiffness matrix

[F] = External force vector

In this paper, damping is not considered.

In the considered frequency interval 0 ÷ 10000 Hz, given by modal analysis, was performed harmonic response analysis spindle at the effect of loads. The Fig. 8 shows the displacement of characteristic nodes of spindle.

The Fig. 8 shows harmonic response of the characteristic nodes, and can be seen that maximum responses are different for each node. All the maximum values are taking place above operational frequency of 30 Hz what corresponding to 1800 rpm. So in the normal conditions, the deformations will be with the limits.

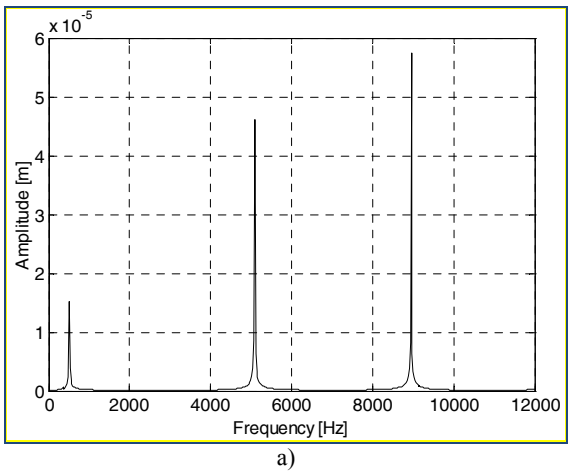

a)

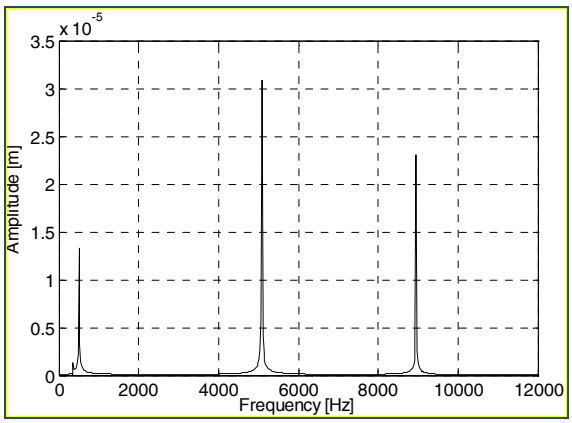

Fig. 8. Harmonic responses of characteristic nodes on: a) spindle nose (node 1), b) the front bearing (node 3), c) the rear bearing (node 10), d) the end of spindle (node 14)

3. CONCLUSION

The spindle made of multiple steps is modeled and analyzed for different boundary conditions for static and dynamic analysis. The analysis summary is as follows.

Initial static analysis shows minimum, maximum and deformations of significant parts of spindle, as well as the forces in both hydrodynamic radial bearings. The value of spindle stiffness is validated through theoretical calculations.

Modal analysis carried out with bearing supports under flexible conditions shows that natural frequencies of spindle are a much bigger than the operational frequency, so than they can not endanger measuring process.

Harmonic response analysis of characteristic nodes represented along with natural frequencies, shows that the maximum values of displacement are different for each node, because they are depended of vibration bending mode.

All the results shows that device can operate safe and accurately with the given bearing values and spindle dimensions.

Acknowledgments: In this paper some results of the project: *Contemporary approaches to the development of special solutions related to bearing supports in mechanical engineering and medical prosthetics* – TR 35025, carried out by the Faculty of Technical Sciences, University of Novi Sad, Serbia, are presented. The project is supported by the Ministry of Science and Technological Development of the Republic of Serbia.

4. REFERENCES

[1] Tomović, R.: *Research of rolling bearings construction parameters impact to the condition of their labouring correctness*, Doctoral dissertation, Faculty of Mechanical Engineering, Niš 2009.

[2] Chen, Y., S., Cheng, Y., D., Chiou, C., C.: *The critical speeds of a machine tool spindle bearing system with the high stiffness hydrostatic journal bearings*, Yuan-Ze Univerity Chungli, Taoyuan, Taiwan, 2014.

[3] Badrway, S.: *Dynamic modeling and analysis of motorized milling spindles for optimizing the spindle cutting performance,* Technical papers Moore Nanotechnology Systems, LLC, 2015.

[4] Delgado, A., S., Ozturk, E., Sims, N.: *Analysis of Non-Linear Machine Tool Dynamic Behavior*, The Manufacturing Engineering Society International Conference, MESIC, ELSEVIER, Zaragosa, 26th-27th, June 2013

[5] Borovkov, A., Artamanov, I.: *3D Finite Element Modeling and Vibration Analysis of Gas Turbine Structural Elements*, St.Petersburg State Polytechnical University, Russia, 2015.

[6] Knežev, M.: *Design of virtual device for measuring and control vibrations of rolling bearings*, Master thesis, Faculty of Technical Science, Novi Sad, July 2015.

[7] Bellakhdhar,B. Dogui, A. , Ligier, J.L.: *Main Bearing Stiffness Investigation,* World Academy of Science, Engineering and Technology, Vol. 5, pp.1492-1496, 2001

[8] Damodar, A., Kondayya, D., Prasad, B.: *Static and dynamic analysis of spindle of a CNC machining centre,* International Academy of Science, Engineering and Technology, Volume 2, 165-170, 5, Nov 2013.

Authors: **M.Sc. Miloš Knežev, Assistant Professor, Aleksandar Zivković**, **M.Sc. Cvijetin Mlađenović,** University of Novi Sad, Faculty of Technical Sciences, Department for Production Engineering, Trg Dositeja Obradovica 6, 21000 Novi Sad, Serbia, Phone.: +381 21 485 2330, Fax: +381 21 454-495.

E-mail: milosknezev@gmail.com, acoz@uns.ac.rs , mladja@uns.ac.rs;

Journal of Production Engineering
Vol.19 No.1
JPE (2016) Vol.19 (1) Original Scientific Paper
Cica, Dj., Zeljkovic, M., Sredanovic, B., Borojevic, S.

IDENTIFICATION OF DYNAMICAL CONTACT PARAMETERS FOR SPINDLE-HOLDER-TOOL ASSEMBLY

Received: 03 January 2016 / Accepted: 19 March 2016

Abstract: *With the fast advances in computing technology accurate identification of contact dynamics in spindle–holder-tool assemblies is of great importance for predicting tool point frequency response function and evaluating the cutting process stability. This paper describes the mathematical formulation of the Levenberg-Marquardt method which was applied to identify the unknown parameters at spindle-holder and holder-tool interfaces. In order to verify the proposed mathematical model numerical and experimental analysis of the spindle-holder-tool assembly was carried out.*
Key words: *parameter identification, contact dynamics*

Identifikacija parametara veza sistema glavno vreteno – držač alata – alat. *Pouzdana identifikacija parametara veza sistema glavno vreteno – držača alata – alat je od izuzetnog značaja za predikciju funkcije frekventnog odziva i obezbjeđenja procesa obrade bez pojave samopobudnih vibracija. U radu je prezentovana matematička formulacija Levenberg-Marquardt-ovog metoda za identifikaciju nepoznatih parametara veza između glavnog vretna i držača alata, te između držača alata i alata. U cilju verifikacije predloženog matematičkog modela izvršena je numerička i eksperimentalna analiza sistema glavno vreteno – držač alata – alat.*
Ključne reči: *identifikacija parametra, predikcija funkcije odziva*

1. INTRODUCTION

Spindle-holder-tool assembly is one of the most important machine tool components because its static and dynamic behavior, strength, speed, among many others, have a significant impact on machine tools overall performance. Regenerative chatter is a well-known machining problem caused by cutting tool-workpiece dynamic interaction that could result in process instability, reduced material removal rate and poor surface quality. In order to identify the stable and unstable cutting zone in the machining process stability lobe diagrams of spindle-holder-tool assemblies have been used for decades. For generation of these diagrams frequency response function (FRF) of the assembly should be achieved firstly. The tool point FRF is typically obtained by experimental modal analysis. However, due to the large number of holder and tool combinations, in order to minimize time-consuming modal testing many researchers have developed semi-analytically approaches for obtain tool point FRF. The accuracy of these models strongly depends on the accurate identification of dynamical contact parameters at the spindle-holder and holder-tool interfaces. Therefore, the identification dynamical contact parameters of spindle assemblies is of great importance for obtaining the accurate tool point FRF. Erturk et al. [1] proposed and experimentally verified analytical model for predicting tool point FRF by combining the receptance coupling and structural modification techniques where all components of the spindle-holder-tool assembly were modeled analytically with Timoshenko beam theory. Schmitz et al. [2] introduced off-diagonal elements to the diagonal joint stiffness matrix to account for the translations imposed by moments and rotations caused by forces.

In this paper Levenberg-Marquardt method was applied to identify the unknown parameters of a spindle-holder-tool assembly. Proposed mathematical model is first used in a case study for analytical demonstration. Then, it is verified experimentally for a spindle-holder-tool assembly.

2. MATHEMATICAL MODEL

Analysis of complex dynamical systems such are spindle assemblies can be simplified by breaking a global system down to a set of interconnected subsystems. Therefore, in this paper the problem referring to dynamic properties of the spindle-holder-tool assembly can be simplified so that instead of viewing it as single, the specified system is regarded as the one composed of three separate subsystems, namely: a spindle, holder and tool. Components of these assembly should be coupled elastically due to flexibility and damping introduced by contact parameters at spindle-holder and holder-tool interfaces. In this paper, we applied the approach [1], where part of the holder inside the spindle is considered rigidly joined to the spindle (Fig. 1a) and the part of the tool inside the holder is considered rigidly joined to the holder (Fig. 1b).

Complex stiffness matrix, representing the spindle-holder interface dynamics, has the following form:

$$ {}_{SH}\mathbf{K} = \begin{bmatrix} {}_{SH}k_t + i\cdot\omega\cdot {}_{SH}c_t & 0 \\ 0 & {}_{SH}k_r + i\cdot\omega\cdot {}_{SH}c_r \end{bmatrix} \quad (1) $$

Here, ${}_{SH}k_t$ is the translational stiffness, ${}_{SH}c_t$ is the

translational damping, $_{SH}k_r$ is the rotational stiffness and $_{SH}c_r$ is the rotational damping at the spindle-holder interface.

Assuming that response matrices of the subsystem *S* (spindle with bearings) and subsystem *H* (holder) are known, then it is possible by using a method of receptive coupling, to obtain the global system response matrix *SH* (spindle-holder) at the holder tip:

$$\mathbf{SH}_{ii} = \mathbf{H}_{ii} - \mathbf{H}_{ic} \cdot \left(\mathbf{H}_{cc} + \mathbf{S}_{cc} + {}_{SH}\mathbf{K}^{-1} \right)^{-1} \cdot \mathbf{H}_{ci} \quad (2)$$

The interface dynamics between the holder and the tool can be expressed in Eq. (3):

$$ {}_{HT}\mathbf{K} = \begin{bmatrix} {}_{HT}k_t + i \cdot \omega \cdot {}_{HT}c_t & 0 \\ 0 & {}_{HT}k_r + i \cdot \omega \cdot {}_{HT}c_r \end{bmatrix} \quad (3)$$

Here, $_{HT}k_t$ and $_{HT}c_t$ are the translational stiffness and damping at the holder-tool interface, respectively. And $_{HT}k_r$ and $_{HT}c_r$ are the rotational stiffness and damping at the holder-tool interface, respectively.

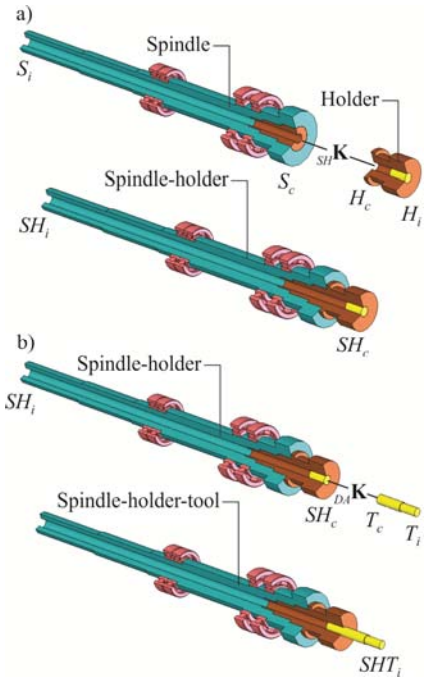

Fig. 1. Elastic coupling of spindle, holder and tool

Receptance matrix of the global system SHT (spindle-holder-tool) at the tool tip is obtained by Eq. (4):

$$\mathbf{SHT}_{ii} = \mathbf{T}_{ii} - \mathbf{T}_{ic} \cdot \left(\mathbf{T}_{cc} + \mathbf{SH}_{cc} + {}_{HT}\mathbf{K}^{-1} \right)^{-1} \cdot \mathbf{T}_{ci} \quad (4)$$

In order to be able to use equations (2) and (4) to predict the frequency response function at the holder and at the tool tip, respectively, it is necessary to recognize all unknowns, namely, the translational stiffness, the translational damping, the rotational stiffness and the rotational damping at the spindle-holder and holder-tool interface. The following section presents methodology for identification these parameters.

3. PARAMETER IDENTIFICATION OF THE SPINDLE-HOLDER-TOOL ASSEMBLY

3.1 Mathematical background

Fig. 2 shows the general approach to the problem of parameters identification, from problem definition to achieving optimal solutions. A system that is optimized should be presented by appropriate mathematical model (e.g. a system of differential equations), after which should be defined analysis objectives. In order to optimize the system, it is necessary to enable the changes of its form and structure.

The assumption is that the mathematical model can be described by a system of differential equations:

$$\mathbf{D}\dot{\mathbf{y}} = \mathbf{f}\left(t, \mathbf{y}, \boldsymbol{\theta}\right), \quad y\left(t_0, \boldsymbol{\theta}\right) = \mathbf{y}_0\left(\boldsymbol{\theta}\right) \quad (5)$$

Here, $\boldsymbol{\theta}$ is vector of unknown parameters, $\mathbf{y}$ is dependent state vector of t and $\boldsymbol{\theta}$, $\mathbf{f}$ is generally, nonlinear function, $\mathbf{D}$ is nxn constant diagonal matrix.

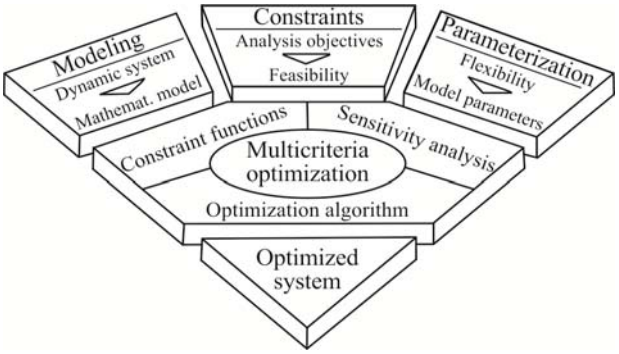

Fig. 2. Process of parameter identification

Each measurement can be defined by following parameters:

$$\left(c_i, t_i, \tilde{y}_i\right), \qquad i = 1, 2, ..., m \quad (6)$$

Here, c_i is component vector $\mathbf{y}$ which is measured, t_i is time of measurement, $\tilde{y}_i$ is measured value and m is total number of measurements. The solution of Eq. (5) for *ci* component at a time t_i, which corresponds to the *i*-th measurement, is marked with $y_{c_i}\left(t_i, \boldsymbol{\theta}\right)$. The general approach to the problem of parameter identification is to minimize the differences between the results obtained by measuring and by the mathematical model, i.e.:

$$r_i\left(\boldsymbol{\theta}\right) = y_{c_i}\left(t_i, \boldsymbol{\theta}\right) - \tilde{y}_i \quad (7)$$

One of the most widely used method of parameter identification is the least squares method, where the estimates of the constants of the models are chosen such that the sum of the squared residuals is minimized. Differences between the results experimentally obtained and using the mathematical model can be represented as a vector $\mathbf{r}$:

$$\mathbf{r}\left(\boldsymbol{\theta}\right) = \left[r_1\left(\boldsymbol{\theta}\right) \quad r_2\left(\boldsymbol{\theta}\right) \quad \cdots \quad r_m\left(\boldsymbol{\theta}\right) \right]^T \quad (8)$$

which is a basis to obtain an expression for the objective function:

$$f\left(\boldsymbol{\theta}\right) = \frac{1}{2}\left\| \mathbf{r}\left(\boldsymbol{\theta}\right) \right\|^2 = \frac{1}{2}\mathbf{r}\left(\boldsymbol{\theta}\right)^T \mathbf{r}\left(\boldsymbol{\theta}\right) \quad (9)$$

Identification of the parameters can be formulated as follows:

$$\boldsymbol{\theta}^* = \arg\min_{\theta} f\left(\boldsymbol{\theta}\right) \quad (10)$$

Here, θ is vector of parameters and $\boldsymbol{\theta}^*$ is vector that minimizes the objective function. If objective function is twice continuously differentiable, then the following Taylor expansion for *f* applies:

$$f(\boldsymbol{\theta}+\mathbf{h}) = f(\boldsymbol{\theta}) + \nabla f^T(\boldsymbol{\theta})\mathbf{h} + \frac{1}{2}\mathbf{h}^T\nabla^2 f(\boldsymbol{\theta})\mathbf{h} + O\left\|\mathbf{h}^3\right\| \quad (11)$$

Gradient **g** and Hessian matrix **H** are defined as follows:

$$\mathbf{g} = \nabla f(\boldsymbol{\theta}) = \left[\frac{\partial f}{\partial \theta_1} \quad \frac{\partial f}{\partial \theta_2} \quad \cdots \quad \frac{\partial f}{\partial \theta_{n_p}}\right]^T \quad (12)$$

$$\mathbf{H} = \nabla^2 f(\boldsymbol{\theta}) = \begin{bmatrix} \frac{\partial^2 f(\boldsymbol{\theta})}{\partial^2 \theta_1} & \frac{\partial^2 f(\boldsymbol{\theta})}{\partial \theta_1 \partial \theta_2} & \cdots & \frac{\partial^2 f(\boldsymbol{\theta})}{\partial \theta_1 \partial \theta_{n_p}} \\ \frac{\partial^2 f(\boldsymbol{\theta})}{\partial \theta_2 \partial \theta_1} & \frac{\partial^2 f(\boldsymbol{\theta})}{\partial^2 \theta_2} & \cdots & \frac{\partial^2 f(\boldsymbol{\theta})}{\partial \theta_2 \partial \theta_{n_p}} \\ \vdots & \vdots & \ddots & \vdots \\ \frac{\partial^2 f(\boldsymbol{\theta})}{\partial \theta_{n_p} \partial \theta_1} & \frac{\partial^2 f(\boldsymbol{\theta})}{\partial \theta_{n_p} \partial \theta_2} & \cdots & \frac{\partial^2 f(\boldsymbol{\theta})}{\partial^2 \theta_{n_p}} \end{bmatrix} \quad (13)$$

For the objective function the gradient and Hessian matrix are:

$$\mathbf{g} = \nabla f(\boldsymbol{\theta}) = \sum_{i=1}^{m} r_i(\boldsymbol{\theta}) \nabla r_i(\boldsymbol{\theta}) = \mathbf{J}(\boldsymbol{\theta})^T \mathbf{r}(\boldsymbol{\theta}) \quad (14)$$

$$\mathbf{H} = \mathbf{J}(\boldsymbol{\theta})^T \mathbf{J}(\boldsymbol{\theta}) + \sum_{i=1}^{m} r_i(\boldsymbol{\theta}) \nabla^2 r_i(\boldsymbol{\theta}) \quad (15)$$

Here, **J(θ)** denotes the Jacobian matrix.

Levenberg-Marquardt algorithm is based on the assumption that the error **r(θ)** around the point $\boldsymbol{\theta}^{(k)}$ may approximate by the first two members of Taylor's series:

$$\mathbf{r}^*(\boldsymbol{\theta}) \cong \tilde{\mathbf{r}}^*(\boldsymbol{\theta}) = \mathbf{r}^*\left(\boldsymbol{\theta}^{(k)}\right) + \nabla \mathbf{r}^*\left(\boldsymbol{\theta}^{(k)}\right) \cdot \left(\boldsymbol{\theta} - \boldsymbol{\theta}^{(k)}\right) \quad (16)$$

Then, instead of minimizing the objective function, its approximation is minimized:

$$\tilde{f}(\boldsymbol{\theta}) = \frac{1}{2}\tilde{\mathbf{r}}^{*T}(\boldsymbol{\theta}) \cdot \tilde{\mathbf{r}}^*(\boldsymbol{\theta}) \quad (17)$$

Equating the previous equation to zero, the following expression which minimizes the function (17) is obtained:

$$\mathbf{J}^T\left(\boldsymbol{\theta}^{(k)}\right) \cdot \mathbf{J}\left(\boldsymbol{\theta}^{(k)}\right) \cdot \left(\boldsymbol{\theta} - \boldsymbol{\theta}^{(k)}\right) + \mathbf{J}^T\left(\boldsymbol{\theta}^{(k)}\right) \cdot \mathbf{r}^*\left(\boldsymbol{\theta}^k\right) = \mathbf{0} \quad (18)$$

Adding the learning coefficient $\alpha^{(k)}$, with $\boldsymbol{\theta} = \boldsymbol{\theta}^{(k+1)}$, it is possible to obtain the following equation:

$$\boldsymbol{\theta}^{(k+1)} = \boldsymbol{\theta}^{(k)} - \alpha^{(k)}\left[\mathbf{J}^T\left(\boldsymbol{\theta}^{(k)}\right) \cdot \mathbf{J}\left(\boldsymbol{\theta}^{(k)}\right)\right]^{-1} \mathbf{J}^T\left(\boldsymbol{\theta}^{(k)}\right) \cdot \cdot \mathbf{r}^*\left(\boldsymbol{\theta}^{(k)}\right) \quad (19)$$

In literature these equation represent Gauss-Newton algorithm for $\alpha^{(k)} = 1$, that is, Gauss-Newton damped algorithm for variable $\alpha^{(k)} < 1$, where the Hessian matrix is replaced by a matrix:

$$\tilde{\mathbf{H}}\left(\boldsymbol{\theta}^{(k)}\right) = \mathbf{J}^T\left(\boldsymbol{\theta}^{(k)}\right)\mathbf{J}\left(\boldsymbol{\theta}^{(k)}\right) \quad (20)$$

Levenberg introduced the approximate matrix of the Hessian matrix:

$$\breve{\mathbf{H}}\left(\boldsymbol{\theta}^{(k)}\right) = \mathbf{J}^T\left(\boldsymbol{\theta}^{(k)}\right) \cdot \mathbf{J}\left(\boldsymbol{\theta}^{(k)}\right) + \mu\mathbf{I} \quad (21)$$

By replacing the Hessian matrix with Levenberg matrix, the final expression for calculation of the parameters is obtained:

$$\boldsymbol{\theta}^{(k+1)} = \boldsymbol{\theta}^{(k)} - \breve{\mathbf{H}}^{-1}\left(\boldsymbol{\theta}^{(k)}\right) \cdot \mathbf{J}^T\left(\boldsymbol{\theta}^{(k)}\right) \cdot \mathbf{r}^*\left(\boldsymbol{\theta}^{(k)}\right) \quad (22)$$

Based on the presented mathematical model, a program for identification of unknown parameters was written in the MATLAB software package.

3.2 Numerical case study

In this section, an numerical case study for the identification approach described is provided. Geometry of the spindle-holder-tool assembly used for numerical simulation, bearings and interface dynamics properties and all other information related to FEM model are given in [3]. Values of identified parameters are shown in Table 1, together with errors of identification. Fig. 3a and 3b shows the comparison of FRF at the tip of the tool holder and at the tip of the tool with the identified and real values, respectively. As shown in Fig. 3, the accuracy of the identified parameters is more than satisfactory. Somewhat larger errors are encountered in the identification of the rotational stiffness, because this parameter has no significant impact in the synthesis of dynamic subsystems. The most dominant factor in the synthesis of dynamic subsystems is translational stiffness, and this values are most accurately identified.

	Exact value	Identified value	Relative error [%]
$_{SH}k_t$ [N/m]	$6.5\cdot10^7$	$6.47984\cdot10^7$	0.31
$_{SH}k_r$ [Nm/rad]	$3.5\cdot10^6$	$3.7393\cdot10^6$	6.84
$_{SH}c_t$ [Ns/m]	50	44.8	10.24
$_{SH}c_r$ [Nms/rad]	7	3.8	45.71
$_{HT}k_t$ [N/m]	$2.1\cdot10^7$	$2.10254\cdot10^7$	0.12
$_{HT}k_r$ [Nm/rad]	$1.4\cdot10^6$	$1.26983\cdot10^6$	9.3
$_{HT}c_t$ [Ns/m]	15	12.24	18.4
$_{HT}c_r$ [Nms/rad]	3	2.11	29.67

Table 1. Identified contact parameters of the spindle-holder-tool system

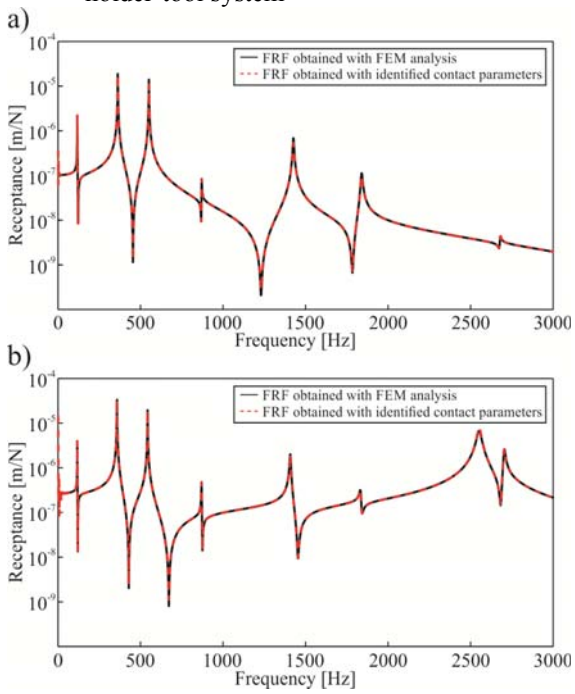

Fig. 3. FRF of the spindle-holder (a) and spindle-holder-tool (b) system with identified contact parameters

3.3 Experimental case study

In this section in addition to the analytical case study, an experimental case study for the parameter identification approach is described, combining experimental and FEM data. The spindle-holder-tool

assembly shown in Fig. 4 is suspended to obtain free–free end conditions for performing an impact tests. Experiments were performed with ISO 30 type holder, in which carbide tools with different combination of tool diameters (D = 9-30 mm) and different tool overhang lengths (L = 16-83 mm). These two parameters have the strongest influence on their values.

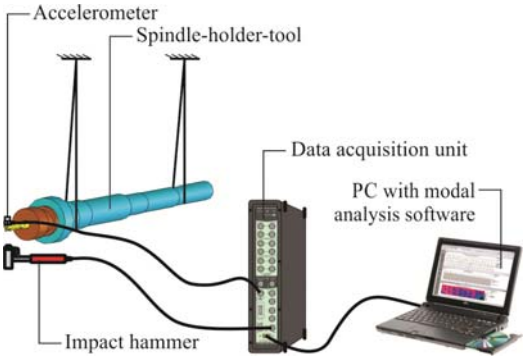

Fig. 4. Schematic layout of experimental setup

In order to provide sufficient data for analysis of the connection parameters at the holder-tool interface 178 measurements was made with different combinations of spindle–holder–tool assembly. Fig. 5 and Fig. 6 shows the result identified translational stiffness and damping at the holder-tool interface, respectively. From these figures it can be concluded that with increasing diameter and tool overhang length occur increase size of translational stiffness at holder-tool interface. On the other hand, it is not possible to derive general conclusions on the impact of these parameters on translational damping.

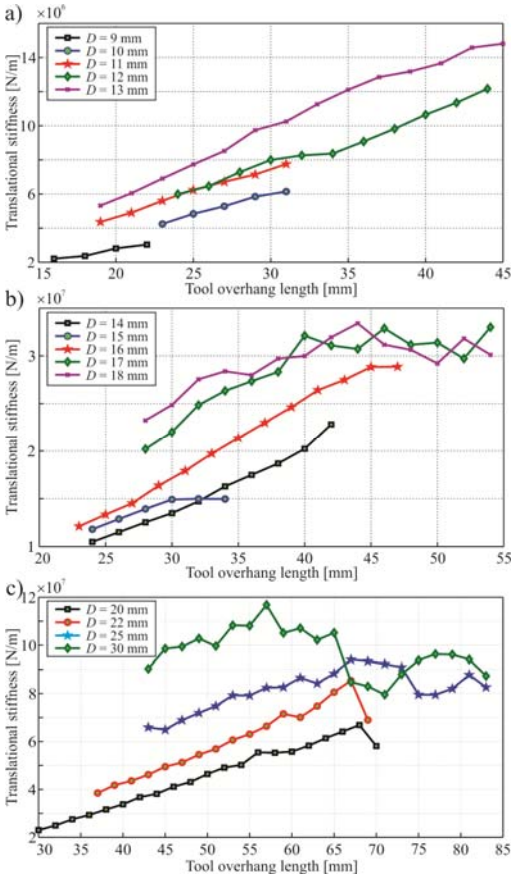

Fig. 5. Identified translational stiffness

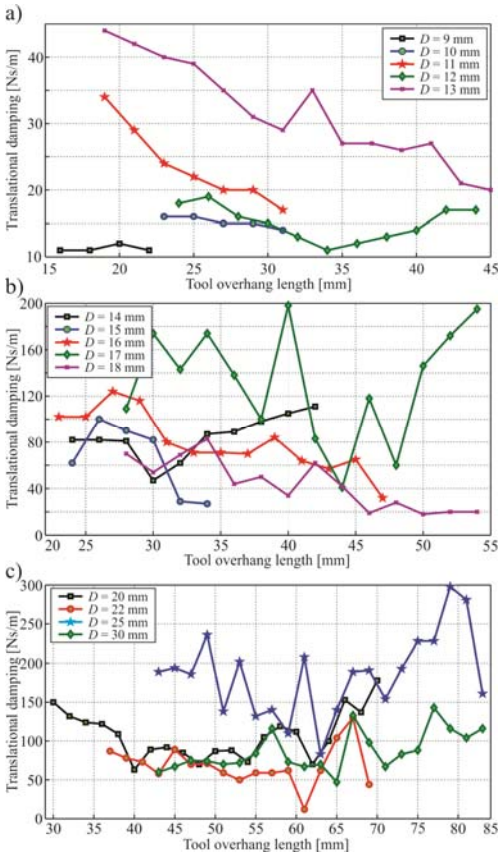

Fig. 6. Identified translational damping

4. CONCLUSIONS

One of the most important requirements in exploitation of the spindle assembly is its dynamic behavior, so the main aim of this study was to develop a mathematical model for identification of the contact parameters at spindle-holder and holder-tool interfaces. The proposed model was analytically and experimentally verified and satisfactory accuracy of the identified parameters was concluded.

5. REFERENCES

[1] Erturk, A, Ozguven, H., Budak, E.: *Analytical modeling of spindle-tool dynamics on machine tools using Timoshenko beam model and receptance coupling for the prediction of tool point FRF,* International Journal of Machine Tools & Manufacture, 46(15), p.p. 1901-1912, 2006.

[2] Schmitz, T.; Donaldson, R.: *Predicting high-speed machining dynamics by substructure analysis*, Annals of the CIRP, 49(1), p.p. 303-308, 2000.

[3] Čiča, Đ.: *Modeling dynamic behavior spindle - tool holder – tool assembly*, PhD thesis, Faculty of Mechanical Engineering, Banja Luka, 2010, (in Serbian).

Authors: **Djordje Cica, Assistant Professor, Prof. dr Milan Zeljkovic, M.Sc. Branislav Sredanovic, M.Sc. Stevo Borojevic**, University of Banja Luka, Faculty of Mechanical Engineering, Stepe Stepanovica 75, 78000 Banja Luka, BiH, Phone.: +381 21 450-366,
E-mail: djordjecica@gmail.com; milanz@uns.ac.rs;

Journal of Production Engineering
Vol.19 No.1
JPE (2016) Vol.19 (1) Original Scientific Paper
Grujić, J., Romček, A., Tabaković, N.

CONTROL OF PROCESS OF MACHINING OF AN ARTIFICIAL FEMORAL HEAD

Received: 05 January 2016 / Accepted: 22 March 2016

Abstract: *The hip joint is one of the most important joints of the musculoskeletal system of man, which facilitates the movement of walking upright. The hip joint is a naturally conceived as a spherical joint. At the proximal part of the femur is the head of the femur, balls, placed at right angles to the vertical axis of the body. Acetabular cup placed in the pelvis and is specially oriented to the vertical axis of the body. Femoral head has a spherical form and allows mobility and rotation in all directions, sufficient to perform the functions of the movement of the locomotive system. This document presents a method for determining the machining parameters and the machining allowance for roughing turning and milling, grinding, sanding and super finishing a function of processing time per operation, and satisfactory dimensional control, surface roughness Ra, micro roughness, centricity and the error forms.*
Key words: *Hip joint, acetabular cup, femoral head, endoprosthesis*

Upravljanje procesom obrade veštačke femoralne glave. *Zglob kuka predstavlja jedan od najvažnijih zglobova lokomotornog sistema čoveka, koji omogućuje kretanje uspravan hod. Zglob kuka je prirodno koncipiran kao sferni zglob. Na proksimalnom delu butne kosti nalazi se glava femura, kuglica, postavljena pod odgovarajućim uglom u odnosu na vertikalnu osovinu tela. Čašica zgloba, acetabularna kapa, postavljena u karlici i specijalno je orijentisana u odnosu na vertikalnu osu tela. Glava femura ima oblik kugle i omogućuje pokretljivost, rotaciju u svim pravcima, dovoljnu za obavljanje funkcije kretanje lokomotornog sistema. U radu je prikazan postupak određivanja režima obrade i dodatka za obradu za grubu obradu struganjem ili glodanjem, grubo i fino brušenje kao i superfiniš u funkciji vremena obrade po operacijama, a za zadovoljavajuću dimenzionu kontrolu, hrapavost Ra i mikrohrapavost, centričnost, greška oblika.*
Ključne reči: *Zglob kuka, proksimalni deo, glava femura, endoproteza*

1. INTRODUCTION

The hip joint is one of the most important joints of the musculoskeletal system of man, whose operation allows moving and walking upright. The hip joint is a naturally conceived as a spherical hinge consists of a spherical part and the socket. At the proximal part of the femur is the head of the femur, the ball, which is set at the appropriate angle to the vertical axis of the body. Acetabular cup that is placed in the pelvis is specially oriented to the vertical axis of the body. Femoral head has a spherical form and provides mobility and rotation in all directions, sufficient to perform the functions of the movement of the musculoskeletal system, and occasional acrobatics.

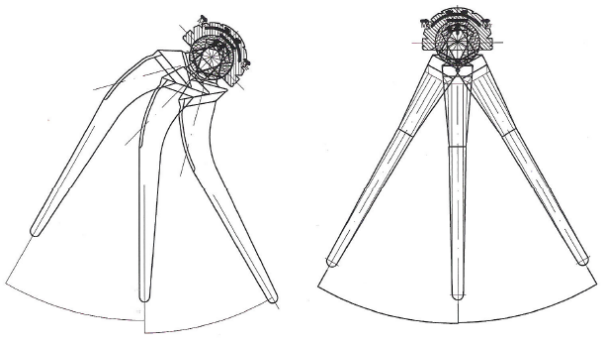

Fig. 1. The possibility of rotation in the hip joint.

Looking kinematic, in the hip joint during movement comes to a mutual sliding between the femoral head and acetabular cups.

The occurrence of degenerative changes in the hip joint, arthritis, necrosis, benign or malignant diseases or mechanical complications, fracture of the proximal part of the femur or pelvis, leading to difficulty or impossibility of displacement in the area of the hip joint, and therefore the displacement of the entire musculoskeletal system is difficult or impossible.

Fig. 2. Degenerative changes and fracture in the hip joint and incorporated endoprosthesis

Fig. 3. Malignant changes in the hip joint and incorporated prosthesis

Restoration of these complications in hip joint is solved successfully by surgical method of removing damaged or diseased parts and installation of endoprosthesis of the hip joint.

Head endoprosthesis and acetabular cup are in constant contact and make tribo-mechanical system in the presence of synovial fluid as lubricants [1,2].

The main task of acetabular cup and head endoprosthesis is to load, which comes from the mass of the body, upper extremities and additional cargo, transfer with acetabular cup on the head of prosthesis, and then across the body endoprosthesis transfer to the lower extremity and to thereby provide a painless mobility in the hip joint [3].

Tribological processes in the areas of contact of acetabular cup and head prosthesis are in function of the technological process and the machining parameters used in forming the contact surfaces. Wear between the contact surfaces due to friction depends on the micro roughness, R_a, macro roughness, the error forms, conditions of lubrication, load size due to body weight, BMI and way of sterilization polyethylene acetabular cups.

The main objective of the research described in this document is the determination of cutting data and supplements for roughing scraping and milling, grinding, sanding and super finishing in the function of processing time per operation, and for dimensional control, surface roughness R_a micro roughness, centricity and error forms.

2. MATERIAL AND METHODS

The study observed making head prosthesis Ø32k6 and Ø28k6 of materials suitable for making implants, C316 LVM where the raw materials bar Ø35 and Ø30. In doing so, they analyzed all processing operations. The main cut-off time on a lathe is constant. Production of conical holes Ø16 / Ø14 or Ø14 / Ø12 is also constant. The main time for this operation cannot be radically shortened regime change processing.

Operation roughing ball turning and milling operations with the presentation of the main time and additional material for the next operation is shown in Table 1.

For the operation of processing coarse grinding with rubble with Bakelite bond 22A46M6JB. The main time and the addition of further operation are shown in Table 2.

Femoral head	Ø32	Ø32	Ø32	Ø32	Ø32	Ø30	Ø30	Ø30	Ø30	Ø30
Milling	28	26	22	29	28	24	27	28	27	25
addition material	+0,2	+0,18	+0,2	+0,17	+0,2	+0,17	+0,18	+0,2	+0,19	+0,18
Turning	18	17	20	21	17	17	16	18	17	20
addition material	+0,17	+0,12	+0,18	+0,17	+0,15	0,18	+0,15	+0,15	0,2	0,17

Table 1. Coarse mashining of the Femoral head

Femoral head	Ø32	Ø32	Ø32	Ø32	Ø32	Ø28	Ø28	Ø28	Ø28	Ø28
Grinding	28	30	29	30	29	30	32	31	30	28
addition material	+0,08	+0,08	+0,09	+0,07	+0,09	+0,06	+0,09	+0,08	+0,09	+0,09

Table 2. Coarse grinding of the Femoral head

For finishing grinding with rubble 22A320M.

Femoral head	Ø32	Ø32	Ø32	Ø32	Ø32	Ø28	Ø28	Ø28	Ø28	Ø28
Grinding	11	11	12	10	10	12	12	10	18	17
addition material	+0,05	+0,04	+0,03	+0,05	+0,04	+0,03	+0,03	+0,04	+0,03	+0,03

Table 3. Finishing grinding of the Femoral head

For finishing super finishing with rubble with rubber binder TYROLIT C320-75VB3.

Femoral head	Ø32	Ø32	Ø32	Ø32	Ø32	Ø28	Ø28	Ø28	Ø28	Ø28
Main time	12	15	10	13	15	13	15	12	12	15
final dimensions	32,00	31,99	32,01	32,00	31,98	28,00	28,00	28,01	27,98	27,98

Table 4. Finishing by super finishing of the femoral head

Figure 3 presents distribution of time in process of mashining of a ariphical femoral head.

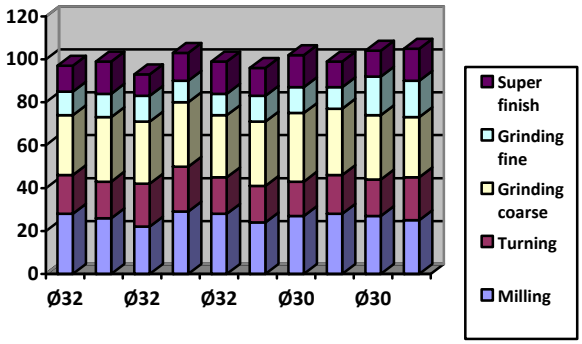

Fig. 3 Distribution of mashining time

Figure 4 shows used grinding wheels.

Fig. 4. The used grinding wheels

Control shape, macro roughness and roughness is made on the device Form Talysuff Taylor Hobson. This device is equipped with a computer system that provides management, measurement, processing of measured data as well as a visual display on the screen and the ability to print or archiving.

Fig. 5. Machine control macro roughness

Fig. 6. Machine control micro roughness

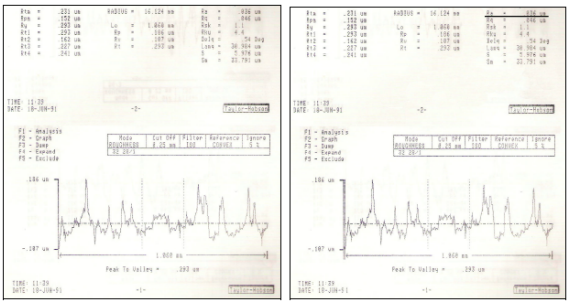

Fig. 7. Numerical and graphical display micro roughness

3. DISCUSSION

By observing the results of the measurements it can be concluded that it is possible to influence the main time of making the choice of equipment, control equipment, treatment regime (for rough scraping or milling). By reducing the addition of a sending is possible to influence the time of rough sending. The main time of the final sanding and super finishing can be considered constant. Appendix for these operations must provide the ability to achieve the required dimensions and surface quality. If the supplement for super finish is bigger, the time of processing is longer. For demanding surface quality, micro roughness (R_a<0,05), the error forms, macro roughness will be increased. Final control of roundness, macro roughness has established three forms: circle, ellipse, triangular closed fault lines.

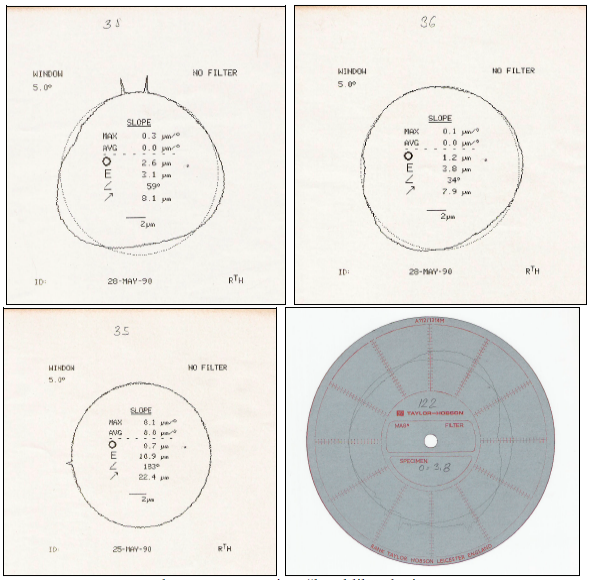

Fig. 8. Graphic errors shape, macro roughness

Spherical head endoprosthesis in the production provides relative rolling between the tool and the work piece. It is necessary to choose the mode of processing, speed tools, shift speed of the work piece, the radius of the blade, grain size and binder binder wheels for milling, turning, grinding or super finishing, so that roughness peaks do not exceed the tolerance zone for the intended operation.

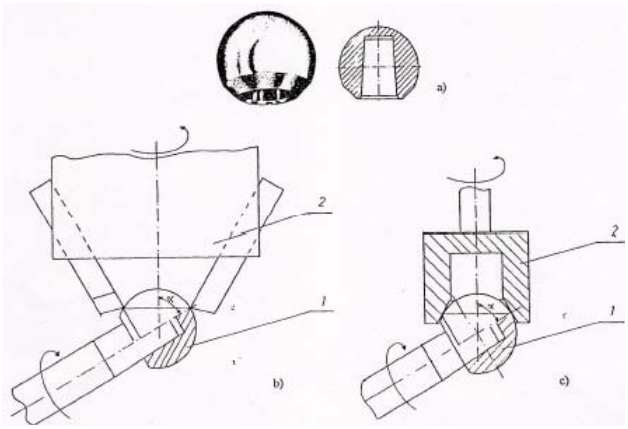

Fig. 9. Scheme of processing sphere (a); milling (b); by grinding (c)

4. CONCLUSION

Looking at the total processing time head prosthesis can decrease the main time for rough machining or milling. The shortening of the running time for fine grinding, especially super finish is insignificant. Supplement for super finish must be sufficient to achieve the required quality processing R_a<0,05. Greater additional material for super finish increases main processing time. The result is greater macro roughness, the error forms.

5. REFERENCES

[1] Grujić, J.: Računarsko modeliranje i eksperimentalno ispitivanje proteze zgloba kuka, *Magistarska teza*, Novi Sad, 2008.

[2] Grujić, J., Sovilj, B., Krklec, V., Vukelić, B.: Analiza triboloških procesa veštačkog zgloba kuka, Savetovanje tribologije, Kragujevac, 1992.

[3] Zlatić, M., Radojević, B.: Degenerativna oboljenja kuka i hirurško lečenje, Beograd, 1989.

Authors:

Mr Jovan Grujić, Grujić & Грујић, Novi Sad, Bul. Vojvode Stepe 6 +381 21 518 381,

E-mail: grujicigrujicns@gmail.com

Mr Andrija Romček, FTL Temerin, Factory of rolling bearings and cardan shafts, Industrijska zona bb, +381 21 6841 100

Natalija Tabakovic, Technical school Novi Sad,: Bulevar kralja Petra I 38, Novi Sad 21000, +381 21 444 606

E-mail: natalija.tabakovic@gmail.com;

Journal of Production Engineering
Vol.19 No.1
JPE (2016) Vol.19 (1) Original Scientific Paper
Jakovljevic, Z., Markovic, V., Zivanovic, S.

RECOGNITION OF QUADRICS FROM 3D POINT CLOUDS GENERATED BY SCANNING OF ROTATIONAL PARTS

Received: 10 January 2016 / Accepted: 29 March 2016

Abstract: *This paper presents a method for recognition of second order surfaces (quadrics) from point clouds containing information about scanned rotational parts. The method is region growing method that exploits the scatter of data during least squares fitting of quadrics as a region growing criterion. The presented procedure is convenient for segmentation of regions with high (G1 or higher) continuity. Besides, the region seed point is automatically selected which is its comparative advantage to a number of existing methods. The applicability of the proposed method is evaluated using two case studies; the first case study refers to a synthesized signal, and the second presents the applicability of the method on a real world example.*
Key words: *3D point cloud, surface recognition, quadrics segmentation, reverse engineering*

Prepoznavanje kvadrika iz 3D oblaka tacaka dobijenih skeniranjem rotacionih delova. *U ovom radu je predstavljen metod za prepoznavanje površi drugog reda (kvadrika) iz oblaka tacaka koji sadrže informaciju o skeniranim rotacionim delovima. Metod spada u klasu metoda zasnovanih na rastu regiona, a kao kriterijum za rast regiona koriste se svojstva informacione matrice koja se izracunava tokom regresije kvadrika. Predložen metod je pogodan za segmentaciju kontinualnih regiona (G1 ili viša kontinualnost). Pored toga, pocetna tacka za rast regiona bira se automatski što predstavlja komparativnu prednost ovog metoda u odnosu na dosada razvijene metode segmentacije kvadrika. Primenljivost razvijenog metoda je ilustrovana na dva primera; prvi primer se odnosi na sintetizovani, a drugi na oblak tacaka dobijen skeniranjem realnog objekta.*
Ključne reči: *3D oblak tacaka, prepoznavanje površi, segmentacija kvadrika, reverzno inženjerstvo*

1. INTRODUCTION

Research efforts and practical applications in the field of implementation of 3D scanning devices in on-line manufacturing process control are expanding over the years. Typical examples are assembly automation and robots navigation. The hardware of contemporary 3D scanning devices, and especially optical ones, is characterized by high resolution, speed, and accuracy, and it is suitable for on-line applications. The same holds for algorithms for raw data preprocessing (3D data registration, integration and meshing). However, there is a lack of efficient real-time applicable algorithms for automatic recognition (segmentation and fitting) of geometric primitives from point cloud. During reverse engineering in CAD systems, geometric primitives from point clouds are recognized interactively by user [1], where user recognizes geometric primitives and then annotates a number of points on them. Afterwards, software is capable of fitting the best surfaces through selected points. On the other hand, implementation of 3D scanning devices in control applications requires fully automatic recognition of geometric primitives from point cloud.

Motivated by applications in a number of fields, such as mobile robots navigation [2] and seam pose detection in robotized welding [3], automatic recognition of planes has attracted many research efforts [4, 5]. Besides planar surfaces, in mechanical engineering rotational surfaces are most frequently met. These surfaces usually consist of second order surfaces (quadrics), planes, and general tori. In the focus of this paper is recognition of quadrics from scanned rotational surfaces.

There are a number of algorithms for detection of quadrics from point cloud, and a survey of these methods can be found in [6]. Generally, the methods belong to one of the two classes: 1) edge based, and 2) region based methods. Edge based techniques can be employed for G0 continuous surfaces where there exists an abrupt change between adjacent regions. Region based methods employ split and/or merge or region growing approach. Region growing approaches start from a seed point and grow region around it using different criteria such as local surface normal [7], average curvature [8], or principle curvature [9].

Recent methods combine edge based approaches for initial segmentation and region based approaches for surface fitting and segmentation of regions with higher continuity. For example, procedure proposed in [10] detects feature edges using dihedral angle; afterwards variational shape approximation is employed for region partition and general shape quadrics are fitted through obtained regions; finally, over-segmented adjacent regions are merged using combination of Euclidean distance and normal deviation as metrics. Another approach from [11] employs tensor voting based method for edges detection and combination of RANSAC, slipping motion analysis, Gauss map and principle curvature for recognition of shapes. An interesting research in the field of recognition of planes, spheres, cones and cylinders from sparse 3D meshes obtained from CAD is presented in [1]. The presented method recognizes feature edges using

dihedral angle, and employs region growing based on principal curvature for primitives' extraction.

In this paper we propose a method for automatic recognition of quadrics from point cloud obtained by scanning of rotational parts. The proposed method is in its essence region growing method based on scatter of data during direct least squares fitting of second order surfaces. The presented method is applicable for recognition of G1 (or higher) continuous surfaces.

The remainder of the paper is structured as follows. In Section 2 we provide some theoretical background and present the proposed recognition method and corresponding algorithm. Section 3 presents the implementation of the algorithm on a synthesized point cloud, as well as on a real-world example. Finally, in Section 4 we give some concluding remarks.

2. METHOD FOR RECOGNITION OF QUADRICS FROM SCANNED ROTATIONAL PARTS

The method for recognition of quadrics from scanned rotational parts that is presented in this paper is based on the properties of scatter matrix during least squares fitting of second order surfaces (quadrics). General quadric can be represented by the following equation:

$$a_1x^2 + a_2y^2 + a_3z^2 + a_4xy + a_5yz + a_6xz + a_7x + a_8y + a_9z + a_{10} = 0 \quad (1)$$

where a_i represent surface parameters and $[x\ y\ z]$ are the coordinates of a point on quadric. Equation (1) can be represented in matrix form:

$$\mathbf{x} \cdot \mathbf{a} = 0 \quad (2)$$

where $\mathbf{x}=[x^2\ y^2\ z^2\ xy\ yz\ xz\ x\ y\ z\ 1]$, and $\mathbf{a}=[a_1\ a_2 \ldots\ a_{10}]^T$ represents the vector of surface parameters.

Coefficients **a** can be estimated by solving the following minimization problem [12, 13]:

$$\min \|\mathbf{Da}\|^2 \quad \text{subject to } \mathbf{a}^T\mathbf{Ca} = 1 \quad (3)$$

where **C** is 10×10 matrix with all elements equal zero except **C**(10,10) =1, and **D** is design matrix in the form:

$$\mathbf{D} = \begin{bmatrix} x_1^2 & x_2^2 & x_3^2 & \ldots & x_N^2 \\ y_1^2 & y_2^2 & y_3^2 & \ldots & y_N^2 \\ z_1^2 & z_2^2 & z_3^2 & \ldots & z_N^2 \\ x_1y_1 & x_2y_2 & x_3y_3 & \ldots & x_Ny_N \\ y_1z_1 & y_2z_2 & y_3z_3 & \ldots & y_Nz_N \\ x_1z_1 & x_2z_2 & x_3z_3 & \ldots & x_Nz_N \\ x_1 & x_2 & x_3 & \ldots & x_N \\ y_1 & y_2 & y_3 & \ldots & y_N \\ z_1 & z_2 & z_3 & \ldots & z_N \\ 1 & 1 & 1 & \ldots & 1 \end{bmatrix}^T \quad (4)$$

Solution of minimization problem (3) is positive eigen value of

$$\mathbf{Sa} = \lambda\mathbf{Ca} \quad (5)$$

where

$$\mathbf{S} = \mathbf{D}^T\mathbf{D} \quad (6)$$

represents scatter matrix, and λ is Lagrange multiplier.

When all data in design matrix are sampled from one exact quadric, scatter matrix will be singular [12]. On the other hand, when data are sampled from approximate quadric, such as scanned quadric surface, the scatter matrix will be close to singular. As data that do not belong to the particular quadric enter design matrix, matrix S will be farther from singular matrix. We have exploited this property of scatter matrix to create the method for segmentation of quadrics from considered class of point clouds.

The proposed method is in its essence region growing method. Region growing procedure starts from the first point in the point cloud and adds point by point to the region using reciprocal condition number of scatter matrix as region growing criterion. When reciprocal condition number of **S** passes predefined threshold, a point that does not belong to quadric is detected. In this situation region growing is stopped and the coefficients **a** of recognized quadric are estimated. The region is considered a quadric if it contains more than 30 points from the cloud. Otherwise, it is assumed that points do not belong to quadric, but to another type of surface.

```
INPUT: x, y, z – points from the cloud
       thres1, thres2 – segmentation thresholds
put axis of rotation along z axis
cloud=[x, y, z];
sortrows(cloud,-3);
m=0; trials=0;
while trials<30
 m=m+1;
 surfaces(m).surf(1,:)=cloud(1,:)
 for i=1:length(cloud)
  surf_aux= [surfaces(m).surf; cloud(i,:)];
  calculate rcond(S) using surf_aux
  if rcond(S)<thres1
   add cloud(i,:) to surfaces(m).surf; end
 end
 if length(surfaces(m).surf)>30
  l1=0; l2=1000;
  while l1<l2
   l1=length(surfaces(m).surf)
   calculate A
   for i=1:length(cloud)
    if distance<thres2
     add cloud(i,:) to surfaces(m).surf
    else add cloud(i, :) to new_cloud; end
   end
   l2=length(surfaces(m).surf)
  end
 cloud=new_cloud;
 else trials=trials+1; end
 if length(cloud)<2 trials=31; end
end
OUTPUT: surfaces – structure containing segmented quadrics
```

Fig. 1. Pseudo-code of the algorithm for implementation of the method for recognition of quadrics from scanned rotational parts

When region growing procedure stops, all points that belong to recognized quadric within predefined threshold are excluded from point cloud; for detection of distance between points from the cloud and surface we exploit estimated surface parameters. The

parameters estimation and point exclusion procedure is iteratively repeated until no more points are recognized to belong to given quadric. The pseudo-code of the algorithm for implementation of the procedure is presented in Fig. 1.

Since we are dealing with rotational parts, to accelerate and facilitate computational efforts, the algorithm starts with alignment of scanned part's rotation axis with z axis of point cloud, and with sorting of points from point cloud in descending order along z axis. The alignment of rotation axis along z direction is carried out using moments of inertia for all three axes of coordinate system, center of mass, and elementary computer graphics transforms.

3. IMPLEMENTATION OF THE PROPOSED METHOD

To illustrate and experimentally verify the proposed procedure, we have implemented it in recognition of second order surfaces in two case studies. The first case study refers to a synthesized point cloud, while the second considers a real world example.

3.1 Case study 1: synthesized point cloud

The point cloud that we use in this case study consists of four second order surfaces, i.e. of one sphere, two ellipsoids (spheroids in particular), and one cylinder. Sphere and cylinder are G0 continuous with adjacent surfaces, while between ellipsoids G1 continuity is achieved. The CAD model of synthesized part is presented in Fig. 2.a, and parameters of synthesized surfaces in Table 1. Synthesized point cloud is noised by white noise with signal to noise ratio of 90dB.

After application of the proposed method, all four surfaces were adequately recognized. Segmentation results are graphically presented in Fig. 2.b, and estimated parameters in Table 1.

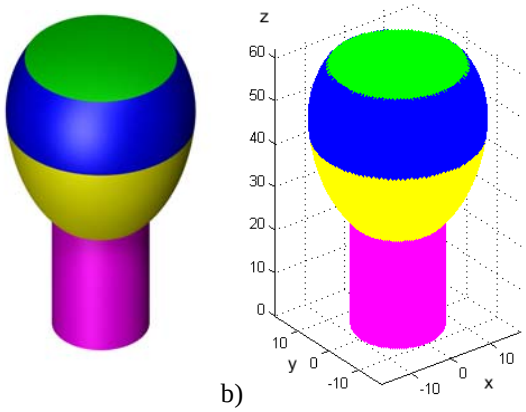

a) b)

Fig. 2. Case study 1: a) synthesized part; b) segmentation results

From Table 1 it can be observed that the algorithm was able to adequately recognize surfaces. The discrepancy between estimated surface parameters and generated surface parameters is less than 0.3%. It should be noted that the parameters of ellipsoids are close and that accurate distinction between these surfaces is a challenging task.

	Seg. no	Parameters of quadric[$a_1 \times 10^2$], i=1,…10
genertaed	1	[0.04 0.04 0.04 0 0 0 0 0 -0.96 -94.24]
	2	[0.33 0.33 0.25 0 0 0 0 0 -24 476]
	3	[0.32 0.32 0.11 0 0 0 0 0 -11.29 186.76]
	4	[1.23 1.23 0 0 0 0 0 0 -100]
estimated	1	[0.04 0.04 0.04 0.0 -0.0 -0.0 0.0 -0.0 -0.96 -94.28]
	2	[0.33 0.33 0.25 -0.0 -0.0 -0.0 0.0 0.0 -23.98 474.61]
	3	[0.32 0.32 0.11 -0.0 0.0 -0.0 0.0 -0.0 -11.29 186.76]
	4	[1.23 1.23 -0.0 0.0 -0.0 -0.0 0.0 0.0 0.0 -100.0]

Table 1. Generated and estimated surface parameters in case study 1

3.1 Case study 2: real-world example

In second case study we consider the part presented in Fig. 3. The part consists of ellipsoid, hyperboloid, cone and cylinder. The parameters of the designed part are presented in Table 2. The part was made on CNC lathe TCN410 – echoENG. The point cloud (Fig. 3.c) is obtained by 3D digitization of the part using ZScanner® 700 [13, 14] handheld laser scanner with resolution of 0.1mm.

As presented in pseudo-code from Fig. 1, the recognition procedure starts by alignment of part's rotation axis with z axis of the coordinate system (Fig. 4). After applying the whole procedure, four quadric surfaces were adequately recognized. Segmentation results are presented in Fig. 5, and estimated parameters in Table 2.

From estimated parameters it can be observed that for all four surfaces adequate surface types (ellipsoid, hyperboloid, cone and cylinder) were recognized. The discrepancy between designed and estimated parameters for all coefficients except for a_3 in cone segment is less than 6%. This discrepancy includes all errors introduced during machining and scanning process, such as interpolation error (ellipse and hyperbola are approximated by circular and linear segments), machining error, scanner accuracy and resolution. It should be noted that the scanner has shown poor performance as presented in Fig. 3c. It has very low accuracy in vicinity of sharp edges and cone segment is located between two sharp edges.

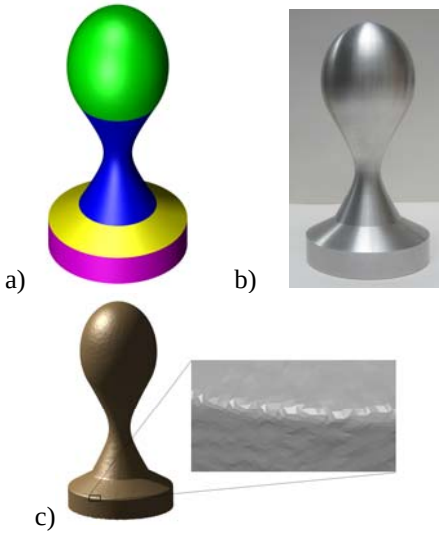

a) b)

c)

Fig. 3. Part from case study 2: a) designed part; b) photo of real-world part; c) scanned part

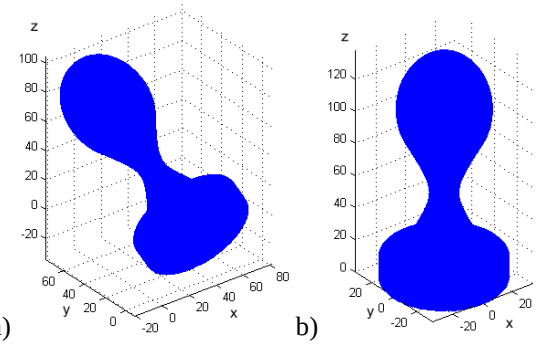

a) b)

Fig. 4. Point cloud from case study 2: a) before graphic transforms; b) after alignment

	Seg no	Parameters of quadric[$a_i \times 10^2$], i=1,…10
designed	1	[0.16 0.16 0.09 0 0 0 0 0 -19.78 933.87]
	2	[2.04 2.04 -0.68 0 0 0 0 0 71.46 -1976.42]
	3	[0.33 0.33 1.0 0 0 0 0 0 0 66.64 1.11e+3]*100
	4	[0.086 0.086 0 0 0 0 0 0 0 -100]
estimated	1	[0.17 0.17 0.09 -0.0 0.0 -0.0 0.04 -0.02 -19.81 930.61]
	2	[2.04 2.04 -0.68 -0.0 0.01 -0.0 0.34 -1.11 72.68 -2033.5]
	3	[0.34 0.34 -0.89 -0.0 0.0 0.0 0.04 -0.29 64.4 -1.13e+3]*100
	4	[0.086 0.086 0.0 0.0 0.0 0.0 0.01 -0.04 0.0 -99.91]

Table 2. Designed and estimated surface parameters in case study 2

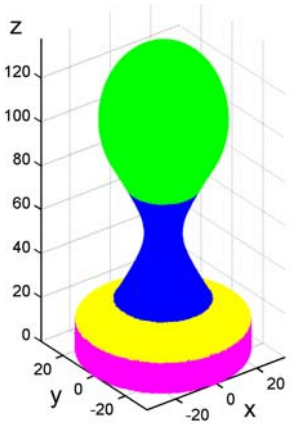

Fig. 5. Segmentation results in case study 2

4. CONCLUSION

In this paper we have presented a method for recognition of quadrics from point clouds generated by scanning of rotational parts. It is a region growing method based on properties of scatter matrix calculated during least squares fitting of second order surfaces. The method is convenient for segmentation of adjacent segments with G1 or higher continuity, and this is its comparative advantage to edge based procedures. Another important property of this method is that seed point is automatically selected as the highest point (point with maximum z coordinate) on the part.

The performances of the method were presented using a synthesized and a real-world point cloud, and the method has shown good recognition results.

To increase the robustness of the method to poor scanner performances, the future work will address the combination of the presented region growing method with edge based segmentation during preprocessing. In addition, recognition of tori, which are also frequently met in rotational parts, will be a part of future research efforts.

5. REFERENCES

[1] Bénière, R., Subsol, G., Gesquière, G., Le Breton, F., Puech, W.: *A comprehensive process of reverse engineering from 3D meshes to CAD models*, Computer-Aided Design, Vol. 45, p.p. 1382–1393, 2013.

[2] Fu, G., Corradi, P., Menciassi, A., Dario, P.: *An Integrated Triangulation Laser Scanner for Obstacle Detection of Miniature Mobile Robots in Indoor Environment*, IEEE/ASME Transactions on Mechatronics, Vol.16, No.4, p.p.778 – 783, 2011.

[3] Fang, Z., Xu, D., Tan, M.: *A Vision-Based Self-Tuning Fuzzy Controller for Fillet Weld Seam Tracking*, IEEE/ASME Transactions on Mechatronics, Vol.16, No.3, p.p.540 – 550, 2011.

[4] Wang, L., Cao, J, Han, C.: *Multidimensional particle swarm optimization-based unsupervised planar segmentation algorithm of unorganized point clouds*, Pattern Recognition, Vol.45, No.11, p.p. 4034–4043, 2012

[5] Jakovljevic, Z., Puzovic, R., Pajic, M.: *Recognition of Planar Segments in Point Cloud based on Wavelet Transform*, IEEE Trans. on Industrial Informatics, Vol. 11, No. 2 , p.p. 342-352, 2015.

[6] Petitjean, S.: *A Survey of Methods for Recovering Quadrics in Triangle Meshes*, ACM Computing Surveys, Vol.2, No.34, p.p.1-61, 2002.

[7] Rabbani, T., Van den Heuvel, F.A., Vosselman, G.: *Segmentation of point clouds using smoothness constraint*, International Archives of Photogrammetry, Remote Sensing and Spatial Information Sciences, Vol.36, No.5, p.p.248-253, 2006.

[8] Lai, H.C., Chang, Y.H., Lai, J.Y., *Development of feature segmentation algorithms for quadratic surfaces*, Advances in Engineering Software, Vol.40, No.10, p.p.1011–1022, 2009.

[9] Lavoue, G., Dupont F., Baskurt A.: *Curvature Tensor Based Triangle Mesh Segmentation with Boundary Rectification*, Proceedings of the Computer Graphics International, p.p. 10-17, IEEE, 2004.

[10] Yan, D., M., Wang, W., Liu, Y., Yang, Z.: *Variational mesh segmentation via quadric surface fitting*, Computer-Aided Design Vol. 44, pp. 1072–1082, 2012.

[11] Yi, B., Liu, Z., Tan, J., Cheng, F., Duan, G., Liu, L.: *Shape recognition of CAD models via iterative slippage analysis*, Computer-Aided Design Vol. 55, pp. 13–25, 2014.

[12] Fitzgibbon, A., Pilu, M., Fisher R.B.: *Direct Least Square Fitting of Ellipses*, IEEE Transactions on Pattern Analysis, Vol.21, No.5, pp.476-480, 1999.

[13] Rosin, P., L.: *A note on the least squares fitting of ellipses*, Pattern Recognition Letters, Vol. 14, No. 10, p.p. 799–808, 1993.

[14] http://www.zcorp.com/documents/380_ZScanner700_PX_SpecSheet_HiRes.pdf

Authors: **Dr. Zivana Jakovljevic, Assistant Professor, M.Sc. Veljko Markovic, Dr. Sasa Zivanovic, Assistant Professor,** University of Belgrade, Faculty of Mechanical Engineering, Kraljice Marije 16, 11000 Belgrade, Serbia
E-mail: zjakovljevic@mas.bg.ac.rs; vmarkovic@mas.bg.ac.rs; szivanovic@mas.bg.ac.rs;
Acknowledgements. This research was partially supported by Serbian Ministry of Education, Science and Technological Development under research grants TR35007 and TR35020.
om

Journal of Production Engineering
Vol.19 No.1

Tadic, B., Matejic, M., Kocovic, V., Novkinic, B., Brzakovic, L., Simunovic, G., Vukelic, D.

DEVELOPMENT A GROUP FIXTURE SYSTEMS FOR MACHINING CENTERS

Received: 12 January 2016 / Accepted: 05 April 2016

Abstract: *A special problem in the construction of the fixture is a limited workspace of machines and large overall dimensions of the workpiece. This problem is especiall pronounced during machining in more work plane at machining centers. In these cases, recognize fixture systems can not be applied. The dedicated fixture systems, in parinciple, could satisfay the basic function but have a number of disadvantages in terms of high costs and low flexibility, especially when it comes to machining process of geometrical and technological similar workpiece. This paper presents a model of group fixture system that allows cutting process with different cutting tools in four work plane. Construction of group fixture system has been optimized from the aspect the minimum required workspace of machines. This very complex problem of design was solving through optimization phase of a large number of conceptual solutions, phases of numerical analysis of structures and phase of calculate making errors.*
Key words: *group fixture, finite element analysis, stiffness.*

Razvoj sistema grupnih pribora za obradne centre. *Poseban problem prilikom konstruisanja pribora je ograničen radni prostor mašine alatke i velike gabaritne dimenzije radnog predmeta. Ovaj problem je posebno izražen u procesu obrade u više ravni rezanja na obradnim centrima. U ovim slučajevima, postojeći sistemi pribora se ne mogu primeniti. Specijalni sistemi pribora, u principu, ispunjavaju osnovne funkcije, ali imaju brojne nedostatke u pogledu visokih troškova i niske fleksibilnost, posebno kada je reč o procesu obrade geometrijski i tehnološki sličnih radnih predmeta. U radu je prikazan model grupnog sistema pribora koji obezbeđuje proces rezanja sa različitim reznim alatima u četiri ravni obrade. Konstrukcija grupnog sistema pribora je optimizovana sa aspekta minimuma potrebnog radnog prostora. Izuzetno kompleksan problem projektovanja je rešen kroz optimizaciju faze velikog broja konceptualnih rešenja, fazu numeričke analize konstrukcija i fazu proračuna grešaka izrade.*
Ključne reči: *grupni pribori, metod konačnih elemenata, krutost.*

1. INTRODUCTION

Design of fixture systems in conditions of limited workspace of machines is a very complex problem. Especially when cutting processing is performed on the thin-walled workpieces in more work plane, which is more often case in cutting process on horizontal milling machine centers [1]. Small dimensions of workbenches machining center, in the processing of parts of larger dimensions, disabling the formation of stable structures of the fixture systems [2].

In the theory of fixture, systems have been developed many techniques related to the fixture layout optimization to achieve optimal effects. Developed techniques finite element analysis (FEA), artificial neural networks (ANN), genetic algorithms (GA) and many other combined techniques allow solve many problems. Chen et al. [3] presented the results related to the fixture layout design and clamping force optimization procedure based on the GA and FEA. Deng et al. [4] presented a model-based framework for determining the minimum required clamping force, which ensures the dynamic stability of a fixture workpiece during machining. Xiuwen et al. [5] reported a model for improving workpiece location accuracy by optimizing the clamping force. Ishikawa and Aoyama [6] used the GA to determine the optimal clamping condition for an elastic workpiece. Kaya [7] presented a GA-based continuous fixture layout optimization method. Krishnakumar and Melkote [8] presented a GA-based discrete fixture layout optimization method to minimize the deformation of the workpiece under static conditions. Liu et al. [9] is proposed a method to optimize the fixture layout in the peripheral milling of a low-rigidity workpiece. Liao [10] used the GA to find the optimal numbers of locators and clamps as well as their optimal positions in sheet metal assembly such that the workpiece deformation and variation are minimized. Mittal et al. [11] presented a dynamic model of the fixture-workpiece system to analyze the fixturing stability of the system. Meyer and Liou [12] presented a methodology to generate the configuration of fixture, which was under dynamic machining. Padmanaban et al. [13] used an ant colony algorithm-based discrete optimization method and optimized the fixture layout under dynamic conditions. Tan et al. [14] described the modeling, analysis, and verification of optimal fixturing configurations by the methods of force closure, optimization and finite element modeling. Zuperl et al. [15] developed an intelligent fixturing system, which adaptively adjusts variable clamping forces to achieve minimum elastic deformation of the workpiece according to the cutter position and the dynamic cutting forces. Tian et al. [16] presented an approach for optimally selecting the locating positions of workpieces and identifying

feasible clamping regions that meet the requirements of the form-closure principle for fixture layout. Xiong et al. [17] proposed two quantitative indices, sum of all normal contact forces and the maximum normal contact force, to assess form-closure fixtures. Vishnupriyan et al. [18] proposed a method of using an ANN for the prediction of dynamic workpiece motion. They optimized parameters of the ANN using a GA to achieve better prediction capability of the ANN. Dai et al. [19] described a method for application of a rule-based reasoning on the modular element database, which can be used effectively for integrating with a CAD system and for modeling fixture subassemblies. Vukelic et al. [20] presented a system for computer-aided fixture design. The structure of this system is based on modular principle, and uses data base and knowledge base. Lin and Huang [21] presented modular fixture planning system, which combines the pattern recognition capability of the neural networks and the concept of group technology to group the workpieces with different patterns but identical fixture modes into the same group. Gologlu [22] presented a rule-based reasoning methodology for setup planning and datum selection incorporating machining and fixturing constraints. Hu et al [23] proposed a method of selecting type for checking fixtures that harnesses advantages of neural networks. This method is attempted to capture relevant domain knowledge and is used to produce acceptable solutions. Vukelic et al. [24] used a combination of feature-based, knowledge-based and geometry-based methodology for development complex system for fixture selection, modification and design.

The majority of these studies refers to defining the optimum location of certain elements of the fixturing systems. In addition, discussed the issue of locating and clamping the workpiece of simple form, i.e. processing one surface with one cutting tool, which in most cases belong to the conventional treatment of universal machine tools. Considered the fixture systems have not universal character, already highly specialized and intended for processing workpieces simple geometry. Modern production conditions imposed by the need for fixtures that should provide a reliable locating and clamping of workpiece very complex shapes, when in a single clamping processing is performed with a large number of different cutting tools to cut in different planes. Modern cutting tools provide best production and economic effects when working in cutting regimes that are on the verge of endurance tool [25]. In such conditions processing, fixturing, due to the complex requests (high load levels, the required accuracy of processing and other requirements) are a serious problem in theoretical and in engineering terms.

The paper presents the conceptual design of the support structure of group fixtures intended for processing workpieces of complex shape on machining centers. Calculations of fixtures construction derived by the method of FEA. This paper is an example of computation of displacement in the cutting process of the transmission housing and provides examples of projected and realized construction of fixture for three similar technological workpieces in performance of treatment processes in four planes of cutting.

2. THEORETICAL BACKGROUND - FEM ANALYSIS

The stability of the workpiece in the fixture was analyzed in detail the method of finite elements. To perform the analysis used program FEMAP. Calculations were performed with 37617 tetrahedral finite element shapes and 66047 nodes. Workpiece was made of ductile iron NL 500-7, modulus of elasticity 160000 N/mm^2. Material of fixture is a steel alloy hardening with modulus of elasticity 220000 N/mm^2. Special attention was given to defining the boundary conditions. The boundary conditions can be viewed on the basis of a simplified 3D model shown in Fig. 1. Red color shows restrain achieved by clamping screws and pins for locating, and green color shows the workpiece contact with the base surface.

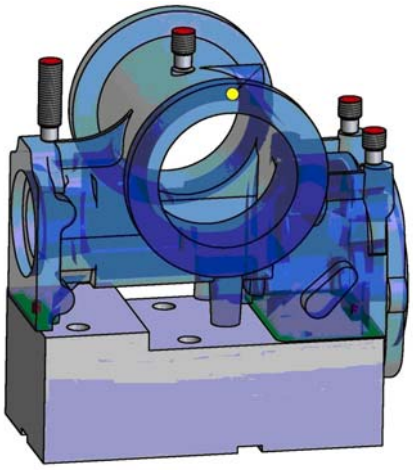

Fig. 1. The boundary conditions.

Loads workpiece and fixtures are also simulated to determine the maximum value of the machining load in areas that will not cause a displacement greater than 0.03 mm. Permitted displacements are determined based on the allowable machining errors of the workpiece and certain values of safety, which should be introduced with regard to the impacts that are not taken into account. On the other hand, simulated load values represent the maximum value of the cutting force with which allowed to operate on the workpiece. The values of cutting forces are input to the calculation of the maximum value of cutting (cutting depth and feed), the geometry of the cutting tools and the optimization technology of the finished product. On this way, in terms of fixtures set border conditions related to the choice of cutting tools (selection cutting tool geometry), which will allow the maximum production given the available stability of the workpiece in the fixture, optimization processing technology (for example, a combination of rough and finish milling or milling "wiper" plates) and a choice of cutting that will, for a limited displacement of the workpiece in certain zones to ensure maximum production.

The calculation was performed by the FEA in the

critical cutting zone. Varied the intensity and direction of cutting forces (Fig. 2) in the areas of processing and specific and sensitive directions (directions of greatest compliance), direction and intensity of the load, which is very important from the aspect of applied ways of basing the clamping of the workpiece.

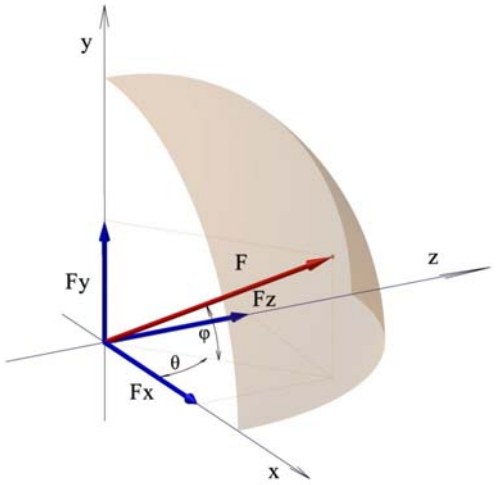

Fig. 2. The direction of the resulting cutting forces.

The results of FEA are intended to assist in the selection of the machining and geometry of cutting tools, in order to ensure the required maximum productivity with regard to the stability of the workpiece in the fixture with regard to the displacement of the workpiece, which to a certain extent constitute making mistakes of workpiece.

The 3D diagram (Fig. 3) represents the total displacement of the workpiece in the function of the direction of the cutting force (in the function of the angles φ and θ). From the diagrams can be clearly seen that the deformation of the workpiece dependent on the direction of the force and the position of the cutting zone. Just based on the quantification of these differences was optimized cutting tool selection and optimization of cutting parameters of choice in certain zones cutting.

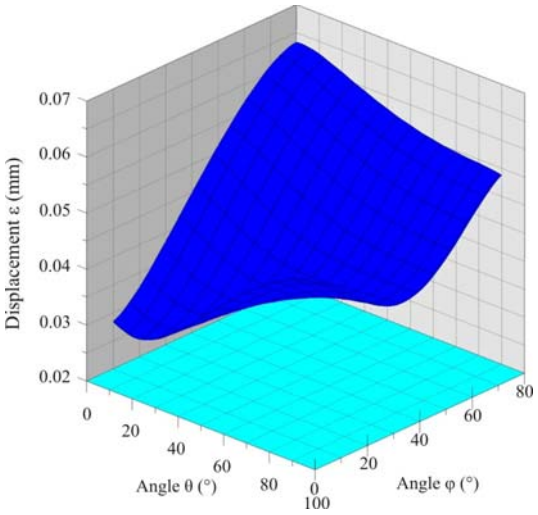

Fig. 3. Total displacement of the workpiece in the fixture depending on the direction of the cutting force.

In Fig. 4 shows the 3D model of the workpiece with a network of finite elements and deformations in the direction of the X axis during machining in a designated zone. From the Fig. 4 can be observed that the maximum deformation localized in a narrow cutting zone as a result of concentrated forces (F=1000N; φ=30, and θ=20) and a thin wall in the zone.

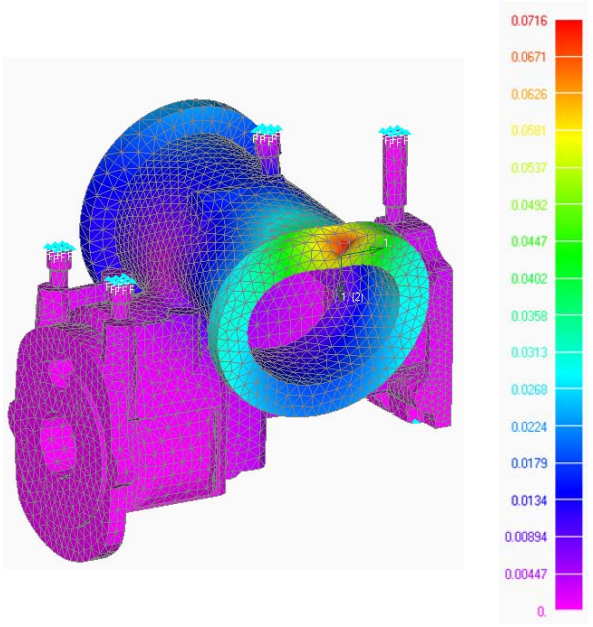

Fig. 4. 3D model of the workpiece with a network of finite elements and scale of displacement when φ =70 and θ =10.

Dependence of the size of the deformation of the angles φ and θ for a given zone is shown in Fig. 5. and 6.

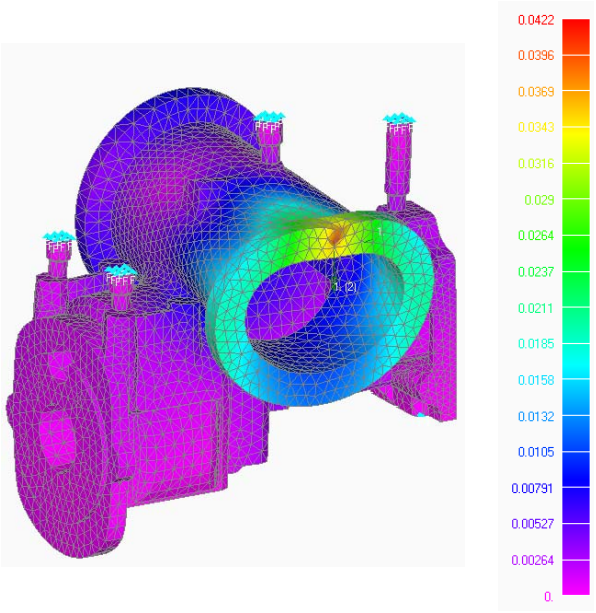

Fig. 5. 3D model of the workpiece with a network of finite elements and scale of displacement when φ=70 and θ=30.

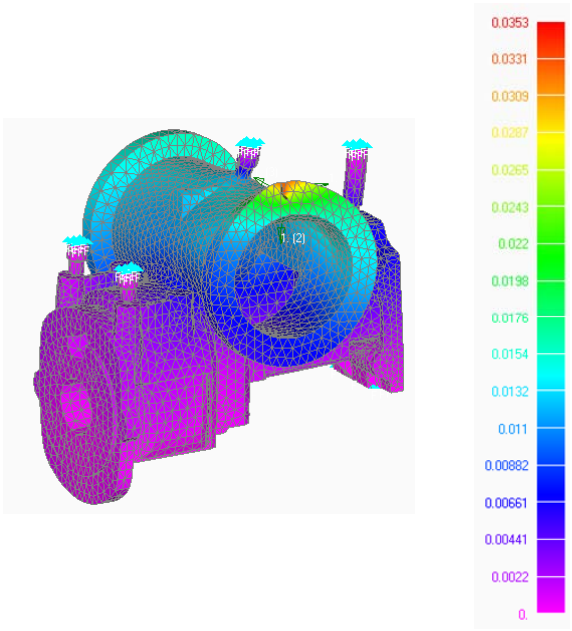

Fig. 6. 3D model of the workpiece with a network of finite elements and scale of displacement when φ=60 and θ=60.

In Fig. 7 is shown the workpiece (transmission housing) and the chosen cutting tools based on conducted budget provides the minimum displacement at maximum productivity.

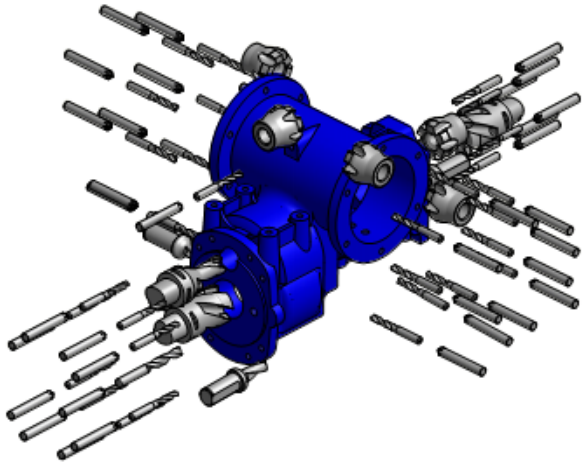

Fig. 7. Cutting tools used for machining.

3. DESIGNED SOLUTIONS OF FIXTURES

Based on the results of theoretical considerations adopted the concept of a group supporting structure of fixtures intended to locating and clamping of given workpieces. The supporting structure is a form of a closed frame.

This concept of structure has been optimized in terms of dimensions of a machining centers and dimensions of the technology of family housing agricultural machines.

Optimization of the structure is covered FEA of structures of varying the dimensions of the supporting elements and real loads, as well as, calculation parts making mistakes. The result of optimization is designed and implemented the construction of high performance in terms of stability and processing performance with multiple cutting tools at four levels. In Fig. 8 show only some of the possible applications of this type of construction.

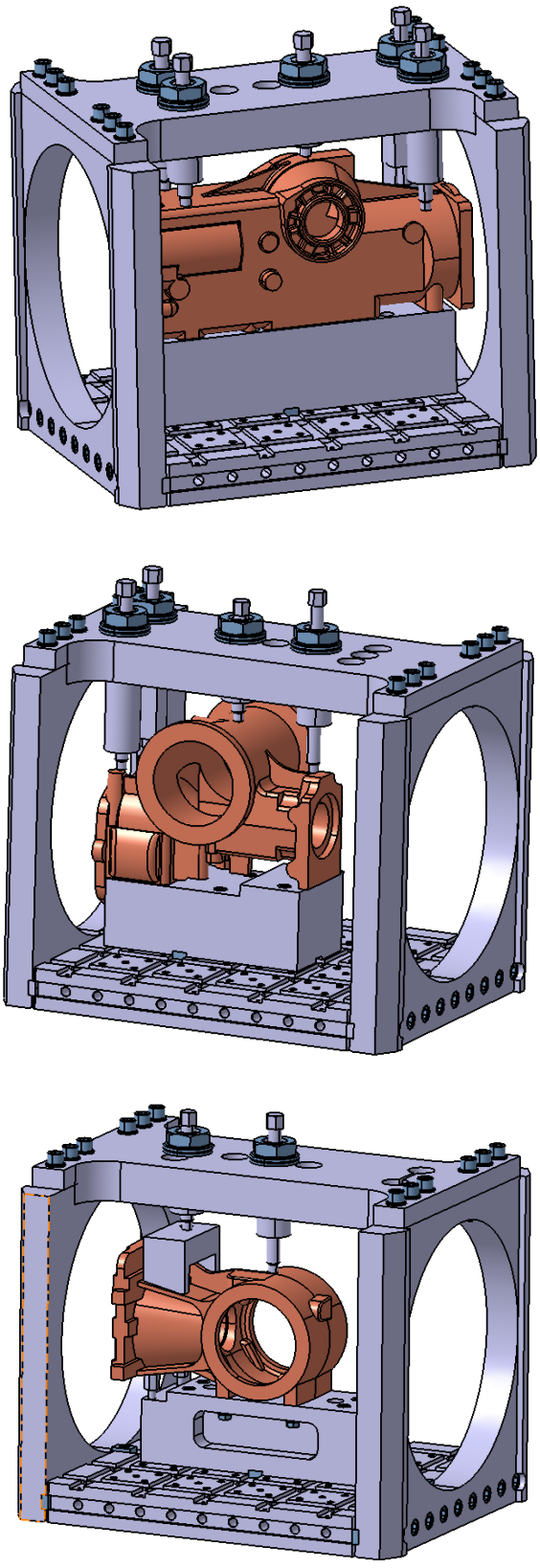

Fig. 8. 3D models of group fixture systems for machining centers.

4. DISCUSION

Based on the review and analysis of literature sources can be said that a small number of research deals with the problem group fixtures intended for the processing on machining centers. Fixtures of this type should provide a reliable and basing clamping workpiece when in a one locating and clamping processing performed with a number of cutting tools that cut in different cutting planes. Problem fixture design is particularly acute when the dimensions of the parts to be processed very close overall dimensions of working table (pallet machining center).

Adopted preliminary design support structure group fixtures intended for the production of housings of different shapes and sizes has, compared to other types of fixtures, a number of advantages in terms of:

- flexibility,
- structure stiffness, and
- open structure suitable for access and processing of various types of cutting tools.

The flexibility of the structure is reflected in the fact that by changing only a small number of elements to locating and clamping screw design can be adapted for different purposes (basing housing and contraction of various shapes and sizes). The base plate to supporting and the upper bearing plate (bracket clamping elements) are made as modular construction elements as shown construction expands the possible application area.

Calculations supporting structure of fixtures group derived method of FEM analysis indicate high stiffness, i.e. small deformations that occur in the real values of simulated load. Based on the results of calculation support structure can be concluded that the simulated load of 1000 N, according to X, Y and Z axis, causing the maximum displacement of structural elements less than 0.007 mm. Adopted regimes finishing processes, according to calculations which are not presented in this paper, do not produce cutting forces greater than 1000 N, and that just means that simulated real load. Connections of structural elements were achieved through the channels and wedges for alignment and a large number of high load capacity bolts. Compiliance connections generated in this way can be neglected if one takes into account a number of elements for the connection load capacity elements and high precision manufacturing of all elements of fixture.

Showed construction of group fixtures is open and enables access and processing of various types of cutting tools. It being possible to use cutting tools with very small overhangs. Small overhangs cutting tools, as it is known a very positive effect on reducing vibration, increasing tool life and improve surface quality. During the processing of the holes some cutting tools perform planetary motion with the spindle turning center undisturbed enters the inside of the the supporting frame. Basing workpiece is realized via centering pins. The construction of this type is very suitable for this type of supporting of the workpiece although the much wider field of application. In fact, changing elements to supporting this type of of fixtures can also be applied to the processing of parts that are based over a long plug and processing workpieces that are based on the principle supporting prismatic element or disc elements. It should be noted that they are exposed to physical solutions implemented and the treatment processes fully meet function.

5. CONCLUSION

According to obtained results it can be concluded that the proposed conceptual design group fixtures intended for processing of family housing on machining centers fulfill the conditions required of stiffness, flexibility as well as the condition of an open type of construction.

Calculations carried out by the method FEM analysis shows that expected levels of load of supporting structure of fixtures displacement is very small. Small displacement of elements of supporting structure fixtures provide the required angle of the exercise tolerance and quality of the surfaces in terms of processing a large number of cutting tools that cut in different planes cutting.

Open type of construction of fixtures provides great flexibility in terms of the possibility locating and clamping of various elements, in particular parts form the casing. It should be noted that in the present case, the adopted concept of supporting structure of fixtures allow it to be on a workbench of the machining center processing parts of large dimensions of which could not be provided fixtures of a different type. The authors believe that it exposed the construction of fixtures can build on additional elements and significantly expand the area of its application.

6. REFERENCES

[1] Tadic, B., Todorovic, P., Novkinic, B., Buchmeister, B., Radenkovic, M., Budak, I., Vukelic, D.: Fixture layout design based on a single-surface clamping with local deformation, International Journal of Simulation Modelling, Vol. 14, No 3, pp. 379-391, 2015.

[2] Tadic, B., Bogdanovic, B., Jeremic, B., Todorovic, P., Luzanin, O., Budak, I., Vukelic, D.: Locating and clamping of complex geometry workpieces with skewed holes in multiple-constraint conditions, Assembly Automation, Vol. 33, No 4, pp. 386-400, 2013.

[3] Chen, W., Ni L., Xue J.: Deformation control through fixture layout design and clamping force optimization, International Journal of Advanced Manufacturing Technology, Vol. 38, No. 9-10, pp. 860-867, 2008.

[4] Deng, H.Y., Melkote, S.N.: Determination of minimum clamping forces for dynamically stable fixturing, International Journal of Machine Tools and Manufacture, Vol. 46, No. 7-8, pp. 847-857, 2006.

[5] Xiuwen, G., Fuh, J.Y.H., Nee, A.Y.C.: Modeling of frictional elastic fixture–workpiece system for improving location accuracy, IIE Transactions, Vol. 28, pp. 821-827, 1996.

[6] Ishikawa, Y., Aoyama, T.: Optimization of fixturing condition by means of the genetic algorithm, Japan Society of Mechanical Engineers, Vol. 62, No. 598, pp. 2409-2416, 1996.
[7] Kaya, N.: Machining fixture locating and clamping position optimization using genetic algorithms, Computers in Industry, Vol. 57, No. 2, pp. 112-120, 2006.
[8] Krishnakumar, K., Melkote, S.N.: Machining fixture layout optimization using the genetic algorithm, International Journal of Machine Tools and Manufacture, Vol. 40, No. 4, pp. 579-598, 2000.
[9] Liu, S.G., Zheng, L., Zhang, Z.H., Li, Z.Z., Liu, D.C.: Optimization of the number and positions of fixture locators in the peripheral milling of a low-rigidity workpiece, International Journal of Advanced Manufacturing Technology, Vol. 33, No. 7-8, pp. 668-676, 2007.
[10] Liao, Y.G.: A generic algorithm-based fixture locating positions and clamping schemes optimization, Proceedings of the Institution of Mechanical Engineers, Part B - Journal of Engineering Manufacture, Vol. 217, No. 8, pp. 1075-1083, 2003.
[11] Mittal, R.O., Cohen, P.H., Gilmore, B.J.: Dynamic modeling of the fixture-workpiece system, Robotics and Computer-Integrated Manufacturing, Vol. 8, No 4, pp. 201-217, 1991.
[12] Meyer, R.T., Liou, F.W.: Fixture analysis under dynamic machining, International Journal of Production Research, Vol. 35, No. 5, pp. 1471-1489, 1997.
[13] Padmanaban, K.P., Prabhaharan, G.: Dynamic analysis on optimal placement of fixturing elements using evolutionary techniques, International Journal of Production Research, Vol. 46, No. 15, pp. 4177-4214, 2008.
[14] Tan, E.Y.T., Kumar, A.S., Fuh, J.Y.H., Nee, A.Y.C.: Modeling, analysis and verification of optimal fixturing design, IEEE Transactions on Automation Science and Engineering, Vol. 1, No. 2, pp. 121-132, 2004.
[15] Zuperl, U., Cus, F., Vukelic, D.: Variable clamping force control for an intelligent fixturing, Journal of Production Engineering, Vol. 14, No. 1, pp. 19-22, 2011.
[16] Tian, S., Huang, Z., Chen, L., Wang, Q.: A feature-based approach for optimal workpiece localization and determination of feasible clamping regions, International Journal of Advanced Manufacturing Technology, Vol. 30, No. 1-2, pp. 76-86, 2006.
[17] Xiong, C.H., Li, Y.F., Rong, Y.K., Xiong, Y.L.: Qualitative analysis and quantitative evaluation of fixturing, Robotics and Computer Integrated Manufacturing, Vol. 18, No. 5-6, pp. 335-342, 2002.
[18] Vishnupriyan, S.: Effect of system compliance and workpiece dynamics on machining error, Assembly Automation, Vol. 32, No. 2, pp. 175-184, 2012.
[19] Dai, J.R.; Nee, A.Y.C.; Fuh, J.Y.H.; Kumar, S.A.: An approach to automating modular fixture design and assembly, Proceedings of the Institution of Mechanical Engineers - Part B: Journal of Engineering Manufacture, Vol. 211, No. 7, pp. 509-521, 1997.
[20] Vukelic, D., Tadic, B., Luzanin, O., Budak, I., Krizan, P., Hodolic, J.: A rule-based system for fixture design, Scientific Research and Essays, Vol. 6, No. 27, pp. 5787-5802, 2011
[21] Lin, Z.C.; Huang, J.C.: The application of neural networks in fixture planning by pattern classification, Journal of Intelligent Manufacturing, Vol.8, No. 4, pp. 307-322, 1997.
[22] Gologlu, C.: Machine capability and fixturing constraints-imposed automatic machining set-ups generation, Journal of Materials Processing Technology, Vol. 148, No. 1, pp. 83-92, 2004
[23] Hu, C.Q.; Lin, Z.Q.; Lai, X.M.: Concept design of checking fixture for auto-body parts based on neural networks, International Journal of Advanced Manufacturing Technology, Vol. 30, No. 5-6, pp. 574-577, 2006.
[24] Vukelic, D.; Zuperl, U.; Hodolic, J.: Complex system for fixture selection, modification, and design, International Journal of Advanced Manufacturing Technology, Vol. 45, No. 7-8, pp. 731-748, 2009.
[25] Smith, G.T.: Cutting Tool Technology, Springer, 2008.

Authors

Branko Tadic, **Marija Matejic**, **Vladimir Kocovic**, University of Kragujevac, Faculty of Engineering, Kragujevac, Serbia.
Bekir Novkinic, Ministry of Defence, Banja Luka, Bosnia and Herzegovina.
Ljiljana Brzakovic, Higher Technical School of Mechanical Engineering, Trstenik, Serbia.
Goran Simunovic, Josip Juraj Strossmayer University of Osijek, Mechanical Engineering Faculty, Slavonski Brod, Croatia.
Djordje Vukelic, University of Novi Sad, Faculty of Technical Sciences, Novi Sad, Serbia.
E-mail: vukelic@uns.ac.rs

Journal of Production Engineering
Vol.19 No.1
JPE (2016) Vol.19 (1) Original Scientific Paper
Subba Rao, E., Ramanaiah, N.

MICROSTRUCTURE AND MECHANICAL PROPERTIES OF Al-Mg-Si BASED METAL MATRIX COMPOSITES REINFORCED WITH B_4C PARTICLES PRODUCED THROUGH STIR CASTING PROCESSES

Received: 11 December 2015 / Accepted: 11 March 2016

Abstract: *The present study is aimed to evaluating the mechanical properties of aluminium metal matrix composite (AMMC). An effort is made to enhance the mechanical properties like hardness, tensile strength, yield strength, % of elongation of AMMCs by reinforcing AA6061 matrix with Boron carbide (B_4C) particles. AMMCs were made, AA6061 as matrix material and B_4C as reinforcement material, through stir casting method. AMMCs with varying percentage by different wt. %, 1%,2 %, 3%, 4%,5% B_4C were fabricated. A systematic study of the matrix metal and AMMCs were done to evaluate the mechanical properties (hardness, yield strength and tensile strength) in as cast and heat treated condition. It was observed that in comparison to the matrix metal, the precipitation kinetic was accelerated by adding the B_4C particles. It was noticed that, mechanical properties are increase with the increase in wt. % of the reinforcement up to 4% B_4C further addition there is a diminution in both the conditions (as cast and heat treatment condition). It was also thought-out that 4% B_4C composite shows better mechanical (hardness, yield strength and tensile strength) properties and low % of elongation than all other compositions in both the conditions. Optical microscopy and Scanning electron micrographs were carried out to authenticate the mechanical properties of the matrix metal and AMMCs.*
Keywords: AA6061, AMMC, B_4C particles, as cast,heat treatment, microstructure and SEM.

Mikrostruktura i mehaničke osobine Al-Mg-Si kompozita sa metalnom matricom ojačanih B_4C česticama proizvedenih STIR procesom livenja. *Ovo istraživanje ima za cilj da oceni mehaničke osobine kompozita aluminijuma sa metalnom matricom (AMMC). Cilj je bio dobiti poboljšanje mehaničkih osobina kao što su tvrdoća, čvrstoća, napon tečenja, % izduženje AMMC ojačavanjem aluminijumske matrice AA6061 sa česticama karbida bora (B_4C). Izrađeni su pripremci AMMC, sa AA6061 kao matričnim materijalom i B_4C kao ojačavajućim materijalom, metodom STIR livenja. Ovi AMMC poseduju različite procentualne udele B_4C - 1%, 2%, 3%, 4% i 5%. Sprovedena je sistematska studija matričnog materijala i AMMC radi određivanja mehaničkih osobina (čvrstoće, napona tečenja i zatezne čvrstoće) u livenom stanju i posle tretmana termičke obrade. Primećeno je, da je u poređenju sa metalnom matricom, ubrzan proces taloženja dodavanjem B_4C čestica. Uočeno je poboljšanje mehaničkih osobina povećanjem procentualnog udela B_4C, do 4% kada počinje umanjenje osobina kod oba primerka (livenog i termički obrađenog). Zaključak je da kompozit od 4% B_4C pokazuje bolje mehaničke osobine (tvrdoća, napon tečenja i zatezna čvrstoća) i nisko % izduženje, nego bilo koji od ostalih posmatranih kompozita u oba stanja (liveni i termički obrađeni). Mikrografije putem optičkog i skening elektron mikroskopa su sprovedene radi potvrde mehaničkih osobina metalnih matrica i AMMC.*
Ključne reči: *AA6061, AMMC, B_4C čestice, liveno, termičke obrade, mikrostruktura i SEM.*

1. INTRODUCTION

Composites are engineered or naturally occurring materials made from two or more constituent materials with significantly different physical or chemical properties that remain separate and distinct within the finished structure. The bulk material forms the continuous phase that is the matrix (e.g.,metals, polymers)and the other acts as the discontinuous phase that is the reinforcement (e.g. ,ceramics, fibers, whiskers, particulates).While the reinforcing material as usually carries the major amount of load &the matrix enables the load transfer by holding them together [1]. Composite materials are gaining wide spread acceptance due to their characteristics of behavior with their high strength to weight ratio [2]. The interest in material matrix composites (MMCs) is due to the relation of structure to properties such as specific stiffness or specific strength. Material matrix composites are being increasingly used in aerospace and automobile industries owing to their enhanced properties such as elastic modulus, hardness, tensile strength at room and elevated temperatures, wear resistance combined with significant weight savings over and reinforced alloys [3, 4]. The material matrix composite can be reinforced with particles and fibers. However, the biggest interest in composite materials is observed for those reinforced with hard ceramic particles due to the possibility of controlling their mechanical properties.

Increasing demands for lightweight metals as structural components in the automotive and aerospace industries have led to the extensive use of Al-Si-Mg–based foundry alloys. One advantage of using lightweight materials is to increase the payload capacity. Al-Si-Mg alloys are candidate materials for such applications due to their good castability characteristics [5]. Heat treatable wrought aluminiu-

Magnesium-Silicon alloys (AA6xxx) are of medium strength and extensively employed in aircraft, automobiles and marine applications. AA6061 aluminum alloy is often used for its light weight, good mechanical properties obtained through Mg_2Si precipitate at the micrometer scale [6].

Mechanical properties were affected by selection of the volume fractions, size, and distribution of the reinforcing particles in the matrix [7]. They are used more often, compared with the composite materials of other metals, due to the broad range of their properties and also due to the possibility of replacing the costly and heavy elements made from the traditionally used materials [8,9]. Metal matrix composites reinforced with particles tend to offer enhancement of properties processed by conventional routes [10].

AMMC are the competent material in the industrial world. Due to its excellent mechanical properties it is widely used in aerospace, automobiles, marine etc. [11]. The aluminium matrix is getting strengthened when it is reinforced with the hard ceramic particles like B_4C, SiC, TiC and Al_2O_3 etc. Aluminium alloys are still the subjects of intense studies, as their low density gives additional advantages in several applications. These alloys have started to replace cost iron and bronze to manufacturewear resistance parts. The alloys primarily utilized today in construction of aircraft structures, such as wings and fuselages, more commonly in homebuilt aircraft than commercial or military aircrafts.

Aluminum hybride metal matrix composites shows better improvement in hardness with the increasing in percentage of reinforcement where as decrease in density [12]. Mechanical properties (hardness, tensile strength and yield strength) of hybrid composites were increased with increasing Wt. % addition of reinforcements [13]. Aluminium alloy AA6061 is available in a wide range of structural shapes, as well as sheet and plate products. This alloy has good weldable characteristics [14]. Aluminium is also ubiquitous element and one of the trace elements with moderate toxic effect on living organisms[15].Hence the desire in the engineering community to develop a new material with greater mechanical properties, without much compromising on the strength to weight ratio led to the development of the metal matrix composites [16, 17]. Grain refiners (Sc, Tibor and Zr) containing AA4043 and AA5356 fillers added to AA6061 alloy was attributed to lower silicon/ magnesium segregation at grain boundaries [18]. The intermetallic particles are distributed uniformly in the composites and thus produced are fully dense with improved strength, which increases with the reinforcement content [19].

A limited research work has been reported on AMMCs reinforced with B_4C due to higher raw material cost and poor wetting. B_4C is a robust material having excellent chemical and thermal stability, high hardness (HV=30 Gpa) and low density(2.52g/cm3) and it is used for manufacturing bulletproof vests, armor tank etc. Hence, B_4C reinforced aluminium matrix composite has gained more attraction with low costing route [20].

2. MATERIALS and METHODS

2.1 Materials

AA6061 is used as matrix metal and Boron carbide(B_4C) powder of size 3-5 mesh as reinforcement material. The chemical composition of AA6061 and B_4C powder are shown in table.1 and table.2 respectively.

Ele	Cu	Mg	Si	Fe	Cr	Al
%	0.19	0.82	0.67	0.19	0.08	Rem

Table 1: composition of AA6061 matrix metal

Ele	B+C	B min	C max	B_2O_3	Fe	Si
%	96.5	75.3	21.2	0.72	o.35	0.21

Table 2: composition of B_4C

2.2 EXPERIMENTAL WORK

The simplest and the most cost effective method of liquid state fabrication is stir casting [21]. In this work stir casting technique is employed to fabricate, which is a liquid state metal in which a dispersed phase (reinforcement particulates) is mixed with a molten metal by means of stirring. The matrix AA6061 was melted at 700^0C in an electric furnace. At this high temperature magnesium ribbons were added into the molten alloy to increase the wetability. An appropriate amount(1% of the wet. Of base metal) of B_4C powder was preheated (350^0C) and then added slowly to the molten aluminium alloy. Simultaneously, the molten metal was stirred thoroughly at a constant speed of 300rpm with a stirrer for a period of 15 min. for evenly dispersing B4C particles in the molten aluminium alloy. The high temperature AMMC was poured into the preheated (400^0C) cost iron mould (having inside mold dimensions 300mmx300mmx6mm). The same procedure was followed to get the AMMC 's of different wt. %,1%, 2%, 3%, 4% and 5% B_4C powder. the experimental setup is shown in Fig:1.

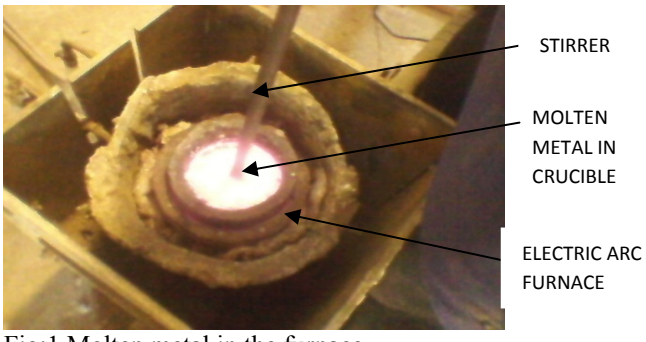

Fig:1 Molten metal in the furnace

2.3 TREATMENT OF AMMC

Fabricated composite was divided into equal parts of size 150x150x 6mm by mechanical cutting and are used for studying the mechanical properties in both the conditions (as cast and heat treatment).

2.3.1As Cast

The fabricated specimens (150x150x6) were proposed to test for mechanical properties without any treatment.

2.3.2 Heat Treatment (HT)

AMMC plates were solutionized at 520^0C for 1Hr and water quenched then the specimen are artificially aged at 180^0C for a period of 12Hrs followed by air cooling.

2.4 TESTING OF AMMC

The fabricated specimens were proposed to test for mechanical properties like hardness, tensile strength, yield strength and % of elongation.

2.4.1 Hardness test

Hardness measurements were carried out on the matrix metal and composite samples by using standard Vickers hardness test machine. Vickers hardness measurements were carried out in order to investigate the influence of particulate weight fraction on the matrix hardness.

2.4.2. Tensile Testing

The specimens were machined to get dog boned structure as per ASTM E-8 standards. Test was carried out on a computerized UTM (TUE-C-600 Model Machine). The tensile test specimens are as per ASTME-8 as shown in Fig: 2

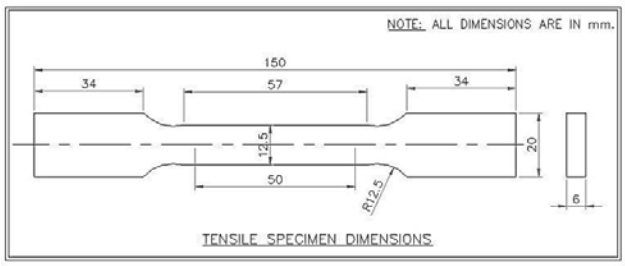

Fig. 2 Tensile Test Specimen as per ASTM –E8

2.5 MICROSTRUCTURE OF AMMC

Microscopic analysis of the matrix metal and composite samples were performed by optical microscopy and Scanning electron microscopy. An Image analyzer was used to examine the distribution of the reinforcement particles within the aluminum matrix. The mechanical properties of any particle reinforced metal matrix composites depend on the particle distribution, particle size, particle flaws, surface irregularities and particle matrix bonding. It is therefore, necessary to conduct a microscopic analysis on the new material in order to gain better understanding of its micro structural characteristics. The polished specimens were cleaned with acetone and etched with (Methanol (25ml) + Hydrochloric acid (25ml) + Nitric Acid (25ml) + Hydrofluoric acid 1 drop) solution.

3. RESULTS & DISCUSSIONS

3.1 Hardness

The tests revealed that, the hardness of the composite specimen is increased gradually with increase in the wt. % of B_4C powder incorporated in the metal matrix. The same thing was observed in hybrid composites [10, 11]. Table 3 shows hardness (VHN) of the composite at various percentage of reinforcement (B_4C) in both the conditions (as cast and Heat treatment). Fig: 3 show the hardness all composites (1%, 2%, 3%, 4% & 5% of B_4C) in both the conditions. Heat treatment condition composite shows better hardness values than as cast conditionandin heat treatment out of all compositions, 4% of B_4C composite shows better hardness.

Condition / %B_4C	As cast	Heat treated
1%	80	92.72
2%	83	99.20
3%	90	109.30
4%	103	113.20
5%	82	109.00

Table 3. Hardness (VHN) of the composite at various percentage of reinforcement (B_4C) in both the conditions (as cast and heat treatment)

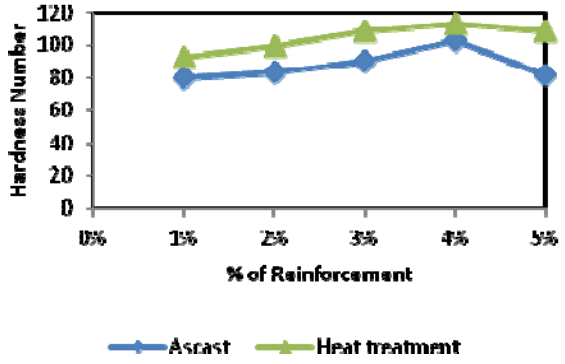

Fig. 3. Hardness (VHN) of the composite at various percentage of reinforcement(B_4C) in both the conditions (as cast and Heat treatment)

3.2 Mechanical Properties (Tensile Strength, Yield strength & % of Elongation)

The tests revealed that, the tensile strength of the composite specimen is increased gradually with increase in the wt. % of B_4C powder incorporated in the metal matrix. The same thing was observed in hybrid composites [11]. Fig:4 shows the tensile strength of all composites (1%, 2%, 3%, 4% & 5% of B_4C) in as cast, and heat treatment condition. The heat treated composite shows better tensile strength values than all cast condition. Out of all, 4% of B_4C composite made with heat treatment shows better mechanical properties than all other compositions. Similar trend was observed for yield strength (Fig:5).

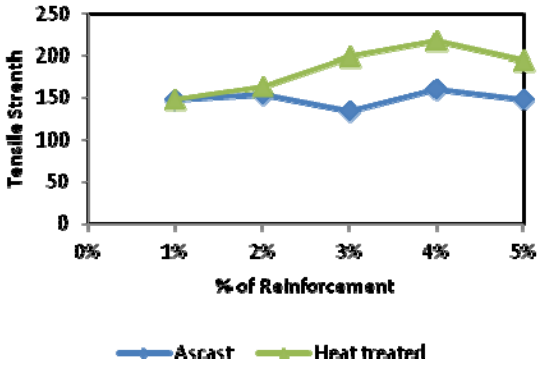

Fig. 4. Tensile strength of composites (1%, 2%, 3%, 4% & 5% of B_4C) in as cast and heat treatment condition.

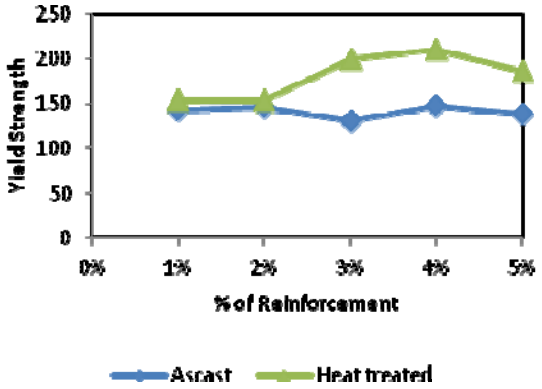

Fig. 5. Yield strength of composites (1%, 2%, 3%, 4% & 5% of B_4C) in as cast and heat treatment condition

Whereasthe percentage of elongation of the composites are decreased gradually with increase in the wt. % of B_4C powder incorporated in the metal matrix. Fig: 6 shows the percentage of elongation of all composites (1%, 2%, 3%, 4% & 5% of B_4C) in both the conditions. Composites made with as cast and heat treatment shows the lower percentage of elongation values than as cast condition. Out of all 4% of B_4C Composite shows lowest % elongation than all other composites.

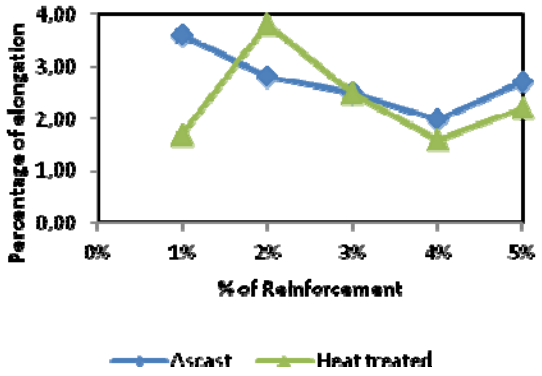

Fig. 6. The percentage of elongation of as casted and heat treatment of AMMCs

4. MICRO STRUCTURE

The morphology, density, type of reinforcing particles and its distribution have a major influence on the properties of particulate composites [1]. The specimens were prepared for microstructure analysis by thoroughly polishing and etching. Then the specimens were observed under an optical microscope and SEM for studying the microstructure.

Micrograph of the matrix metal (AA6061) in T6 temper is shown in the Fig. 7a. It shows number of Mg_2Si particles are present in artificially aged (T6) alloy and shows columnar without reinforcement where as significant grain refinement was noticed when reinforced material (B_4C) were added to the matrix metal (Fig. 7b-d) in as cast condition.

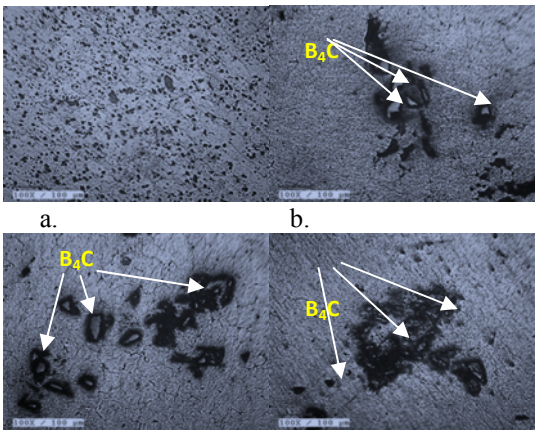

a. b. c. d.

Fig. 7. Micrographs of (a) Matrix metal-T6 (b) 3% B_4C cast composite, (c) 4% B_4C cast composite and (d). 5% B_4C cast composite

Micrograph of the heat treatment composite is shown in the Fig. 8a-c. It shows number of Mg_2Si and B_4C particles present and significant grain refinement was noticed when reinforced material (B_4C) were added to the matrix metal.

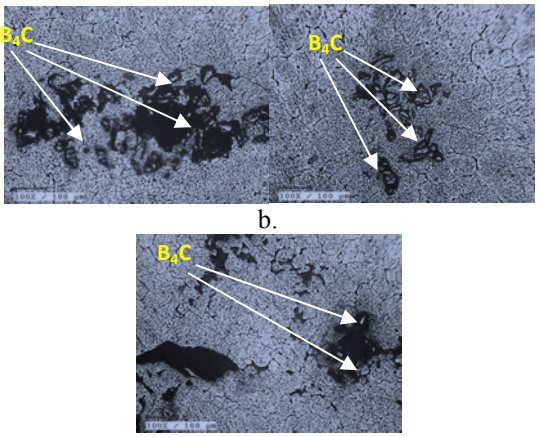

a. b. c.

Fig. 8. Micrographs of (a)3% B_4C heat treatment composite, (b) 4% B_4C heat treatment composite and (c) 5% B_4C heat treatment composite

In Fig: 9 b and c, small B_4C particles are clearly visible, while almost no fine B_4C particles are visible in the cast composite (the particles appear white in the SE images due to charging of the nonconductive B_4C). Comparing the grain structure of the composite there is some grain refinement over the matrix material (Fig:9.a). While complete quantitative data were difficult to obtain from the matrix material, columner grains are clearly visible.

Conversely, the microstructure of the composite has much smaller grains. Fig: 9.c. shows a fine with many smaller grains predominantly near B_4C particles. . With the observed dispersion of fine B_4C particles throughout the matrix in the heat treated composite, it is possible that the high number of potential heterogeneous nucleation sites could give rise to a further refined grain structure [18]. However, in the as cast composite (Fig:9.b), there are large grains are observed.

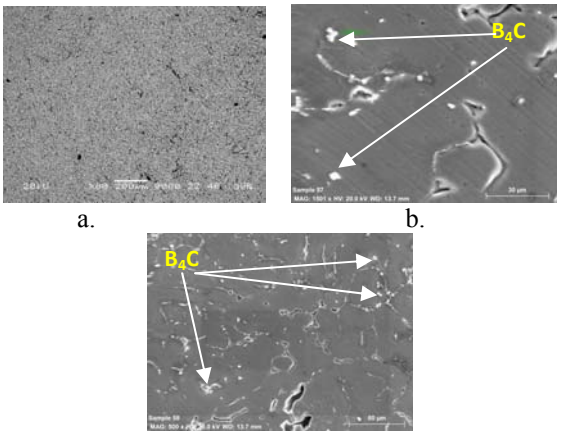

a. b.

c.

Fig. 9 SEM micrographs of (a) Matrix metal (b) As cast (AA6061+B_4C)composite and (c) heat treatment (AA6061+B_4C)composite

5. EFFECT OF HEAT TREATMENT

Aluminum–Magnesium- Silicon alloys are a typical example of a heat-treatable and precipitation-hardening materials. Four sequential structures can be identified during the artificial aging of Al–Mg-Si alloys

Al–Mg–Si e.g., 6061: SS → GP → β'Mg_2Si → βMg_2Si

where SS denotes the supersaturated solid solution. It should be pointed out, however, that coherency strains are not observed in the GP (Guinier–Preston) zones or β'transition stages of precipitation in Al–Mg–Si alloys such as 6061. Therefore, it has been suggested that precipitation hardening in such aluminum alloys is due to the increased energy required for the dislocations to break the Mg–Si bonds as they pass through the precipitate, rather than due to coherency strains. the precipitation range for the most effective strengthening phase β is 160–240°C and that for the less effective strengthening phase β' is 240–380°C [22, 23] and proposed that the losses of hardness and strength is a result of over aging due to β coarsening and β' formation. The lattice strains are much more severe around a coherent precipitate than around an incoherent one. The severe lattice strains associated with the coherent precipitate make the movement of dislocations more difficult and, therefore, strengthen the material to a greater extent.

5. CONCLUSIONS:

The AA6061-B_4C composites of combinations 1%, 2%, 3%, 4% & 5% were produced through stir casting method. The mechanical properties of the composite of as cast and heat treatment were evaluated and compared matrix material and observed the distribution of reinforcements (precipitates) are homogenously distributed.The following conclusions are made from the study.

1. AA6061- B_4C composites AMMCs (AA6061/B_4C) were successfully fabricated by stir casting method.
2. The mechanical properties (yield and tensile strength) of heat treated 4% B_4CAMMC shows better value than all other composites.
3. Out of all the conditions, heat treated 4% B_4C AMMC shows lower % of elongation.
4. Optical micrographs and SEM micrographs revealed that the B_4C particles were well distributed in the Aluminium matrix in heat treatment condition.

6. REFERENCES

[1] Prashant Sharma, Determination of Mechanical Properties of Aluminium Based Composites International JournalonEmerging Technologies3(1):157-159(2012), ISSN No. (Print): 0975-8364

[2] Pai, B.C.,T.P.D. Rajan and R.M. Pillai, 2004. Aluminium matrix composite castings for automotive applications. Ind. Foundry J., 50: 30-39.

[3] A. Chennakesava Reddy and EssaZitounIndian Journal of Science and Technology Vol. 3 No. 12 (Dec 2010) ISSN: 0974- 68 46.

[4] B. Neitzel, M. Barth, M. Matic, "Weight Reduction of Discs Brake Systems with the Utilization of New Aluminum Material", SAE Technical Paper Series, 940335, Warrendale, PA, USA.

[5] D. Apelian, S. Shivkumar, and G. Sigworth: *AFS Trans*., 1989, vol. 89–138, p. 727.

[6] Shen Y, Garnier J, Allais L, Crepin J, Ancelet O, Hiver JM. ProcEng 2011;10:3429

[7] R. Dwivedi,"Development of Advanced Reinforced Aluminum Brake Rotors", SAE Technical Paper Series, 950264, Warrendale, PA, USA, 1995, 8 p.

[8] G. Mrówka-Nowotnik, J.Sieniawski, M. Wierzbika Analysis of intermetallic particles in AlSi1MgMn aluminium alloy, Journal of Achievements in Materials and Manufacturing Engineering 20 (2007) 155-158.

[9] A. Wodarczyk-Fligier, L.A. Dobrzaski, M. Adamiak Influence of heattreatment on properties and corrosion resistance of Al-composite, Journal of Achievements in Materials and Manufacturing Engineering 21/1 (2007) 55-58.

[10] L.A. Dobrzaski, A. Wodarczyk, M. Adamiak, Composite materiale based on EN AW-Al Cu4Mg1(A) aluminium alloy reinforced with the Ti(C,N) ceramic particles, Materials Science Forum 530-531 (2006) 243-248].

[11] Mohanty RM, Balasubramanian K, Seshadri SK. Boron carbide-reinforced alumnium 1100 matrix composites: fabrication and properties. Material Science Eng. A 2008; 498:42–52]

[12] Ch. Shoba, N. Ramanaiah, D. NageswaraRao, Aging behavior of aluminium hybride metal matrix composites, Materials Science an Indian journal, Vol.10 issue11, 2014 484-489

[13] BhargaviRebba and N. Ramanaiah, Investigations on Mechanical Behaviour of B_4C and MoS_2 Reinforced AA2024 Hybrid Composites, Journal of Manufacturing Science and Production, Oct, 2015, DE GRUYTER

[14] Feng YC, Geng L, Zheng PQ, Zheng ZZ, Wang GS. Fabrication and characteristic of Al-based hybrid composite reinforced with tungsten oxide particle and aluminum borate whisker by squeeze casting. Materials& Design 2008; 29: 2023–6.

[15] Ibrahim, I.A., F.A. Mohamed, E.J. Lavernia, 1991. Metal matrix composites-a review. J. Mater. Sci., 26: 1137-1157. DOI: 10.1007/BF00544448.

[16] Buraimoh, A.A., S.A. Ojo, J.O. Hambolu and S.S. Adebisi, 2012. Aluminium chloride exposure had no effects on the epididymis of wistar rats. Am. Med.J., 3: 210-219. DOI: 10.3844/amjsp.2012.210.219.

[17] Sinclair, I. and P.J. Gregson, 1997. Structural performance of discontinuous metal matrix composites.Mater. Sci. Technol., 3: 709-726. DOI: 10.1179/026708397790290254.

[18] K. Prasad Rao , N. Ramanaiah , N. Viswanathan, Partially melted zone cracking in AA6061 welds, Materials and Design, Vol: 29, 2008, 179–186

[19] C.J. Hsu, P.W. Kao , N.J. Ho, Intermetallic-reinforced aluminum matrix compositeproduced in situ by friction stir processing, Materials Letters 61,2007, 1315-1318.

[20] Sannino, A.P. and H.J. Rack, 1995. Dry sliding wear of discontinuouslyreinforced aluminum composites: Review and discussion. Wear, 189: 1-19. DOI: 10.1016/0043-1648(95)06657-8.

[21] Kerti I, Toptan F. Microstructural variations in cast MOS2-reinforced aluminium matrix composites (AMCs). Mater.Lett.2008; 62:1215–8.

[22]. Panseri, C., and Federighi, T., *J. Inst. Metals*, **94:** 94, 1966.

[23]. Miyauchi, T., Fujikawa, S., and Hirano, K., *J. Jpn. Inst. Light Metals*, **21:** 595, 1971.

Authors:

E. Subba Rao[1], N. Ramanaiah[2], [1.]*Associate Professor,* Department of Mechanical Engineering, Loyala, Institute of Technology and Management, sattenapalli, Guntur, Andhra Pradesh, India, [2.]*Professor*, Department of Mechanical Engineering, A. U. College of Engineering (A), Andhra University , Visakhapatnam-530 003, Andhra Pradesh, India

E-mail: n.rchetty1@gmail.com

Journal of Production Engineering
Vol.19 No.1
JPE (2016) Vol.19 (1) Original Scientific Paper
Pujari Srinivasa Rao, P. Raju, Ch. Kodanda Rama Rao, S. P. Priyangeli

EFFECT OF HALIDE FLUXES AND WELDING PARAMETERS ON PENETRATION AND HAZ OF TITANIUM ALLOY

Received: 08 May 2016 / Accepted: 20 June 2016

Abstract: *The present work was an investigation of effect of both halide fluxes (NaCl and CaCl2) and major welding parameters on welding of Ti-6Al-4V. S/N ratio analysis was conducted using Taguchi method to find optimal setting of parameters for weld penetration and heat affected zone (HAZ). ANOVA was performed to find significance of parameters and their interactions on the above responses. The highest penetration and lowest HAZ values of 4.982mm and 81.765µm respectively were obtained at optimum conditions. All the parameters, one 2-way and 3-way interaction on penetration whereas all parameters and interactions on HAZ were found to have significant effect.*
Key words: *A-TIG Welding, Penetration, HAZ, Ti6Al4V alloy*

Uticaj halidnih flukseva i parametra zavarivanja na penetraciju i ZUT kod legura titanijuma. *U ovom radu je sprovedeno istraživanje halidnih flukseva (NaCl i $CaCl_2$) i većine parametara zavarivanja titanijuma Ti-6Al-4V. S/N odnos analiza je sprovedena pomoću Taguči metode radi pronalaženja optimalnih parametara za penetraciju zavara i zone uticaje toplote. ANOVA je sprovedena da se pronađe značaj parametara i njihova interakcija gornjih odaziva. Najviša penetracija i najniža zona uticaje toplote sa vrednostima od 4,982 mm odnosno 81,765µm su postignuti sa optimalnim parametrima. Svi parametri, jedna dvosmerna i trosmerna interakcija provara i svi parametri i interakcija zone uticaja toplote su otkriveni da imaju značajan uticaj.*
Ključne reči: *A-TIG zavarivanje, penetracija, ZUT, Ti6Al4V legura*

1. INTRODUCTION

Welding of titanium and its alloys is difficult because of the affinity titanium and its alloys for oxygen, nitrogen and hydrogen and the subsequent embrittlement. So the welding of titanium was restricted to gas shielded and solid state welding processes. Despite this reactivity welding of titanium alloys was a cost effective manufacturing method for the components used in chemical processing, offshore, aerospace, ordinance and defence applications. The tungsten inert gas welding (TIG) is ideally suitable for welding of titanium alloys with precise and high quality weld. High depth of penetration and low heat affected zone (HAZ) plays an important role in improving the mechanical properties of the weld [1]. However, the relatively shallow penetration capability and low productivity are the main disadvantages in the TIG welding process. Achieving full penetration of welds with superior mechanical properties in single pass weld the notable technique was to use activating flux with TIG (A-TIG) welding process [2].

In view of that many researchers investigated the effect of activated fluxes on various performance measures in welding, in which Nayee and Badheka [3] studied the effect of oxide based fluxes on mechanical and metallurgical properties of weldments prepared by carbon steel and 304 SS materials. Vasantharaja and Vasudevan [4] attempted to develop a flux material for ferritic –martensitic steels. The effect of flux material was studied by considering micro hardness and micro-structural properties. Ramkumar et al., [5] prepared a compound flux using 50% SiO_2 and 50% MoO_3 for A-TIG welding of Inconel X750 and they identified that post weld heat treated components attained better tensile properties than as weld components. Cai et al., [6] investigated the effect of cerium oxide activated flux on penetration, microstructure and mechanical properties of BS700MC super steel weld. They obtained the optimum content (15%) of cerium oxide for improving the above performance measures. Xie et al., [7] used the mixer of TiO_2 and nano-SiC particles in welding of AZ31 magnesium alloy in TIG welding. They evaluated the micro-structural and mechanical behavior of weldments and found that addition of nano materials improved the above responses. Zhang and Liu [8] investigated the effect A-TIG welding of magnesium alloy AZ31B with three oxide flux materials under alternating current mode. The effects of welding speed, weld current and electrode gap were studied and they found that there is an increase in the weld penetration of AC A-TIG welding. Huang et al., [9] investigated the weld morphology, arc voltage and mechanical properties using oxide flux powders of Al_2O_3 Cr_2O_3, TiO_2, SiO_2 and CaO during welding of SS 304. The greatest improvement in performance was observed with the use of SiO_2. The effect of activated flux composition was optimized by Maduraimuthu and vasudevan [10] to achieve 6mm depth of penetration in single-pass A-TIG welding and the results were compared with mulipass conventional TIG welding. Kumar [11] made an attempt to study the effect of pulsed TIG welding process parameters on mechanical properties. Taguchi method was used to optimize the

pulsed TIG welding process parameters of heat-treatable (Al-Mg-Si) aluminum alloy weldments.

The available literature was mostly restricted to welding of various types of steels, Inconel, aluminum and magnesium alloys. In addition to the above, most of the investigations on activated -TIG welding were performed by using oxide fluxes only. The use of oxide flux is problematic in welding of titanium alloys as it produces the surface oxide layer. Hence, there is a dearth of information in finding the effect of activated TIG welding in welding of titanium alloys. So in this work an attempt has been made to find effect of halides (NaCl and CaCl2) and major welding parameters viz., welding current and welding speed on penetration and HAZ of titanium alloy.

2. EXPERMENTAL STRATEGY AND SETUP

The TIG welding operations were performed on the Miller syncrowave 300 with shielding gas as argon. For uniformity ERTi-5 filler rod was selected, as its composition was same as the composition of workpiece material as shown in Table 1. The type of edge preparation made was bevel weld, where one of the joining pair will have a straight edge and other part of the pair with angle cut. The angle that was considered is 60° for the edge with a root opening of 2mm as shown in Fig. 1.

Titannium Alloy	**Filler Rod**
Aluminum(Al) - 6.38	Aluminum(Al) - 5.5-6.7
Vanadium(V) – 4.07	Vanadium (V) – 3.5-4.5
Ferrous(Fe) – 0.19	Ferrous (Fe) – 0.25 Max
Oxygen(o) – 0.17	Oxygen (o) – 0.15
Nitrogen(N) – 0.008	Nitrogen(N) – 0.020 Max
Carbon(C) – 0.012	Carbon(C) – 0.05 Max
	Hydrogen(H) – 0.008 Max
Titanium - Balance	Titanium - Balance

Table 1. Composition of Ti-6Al-4V Titanium alloy and Filler rod

Fig. 1. Edge preparation for Ti6Al4V workpiece

Plates of 5mm thickness which were cut into strips of 50x50mm were polished with 400 grit (silicon carbide) flexible abrasive paper to remove surface impurities and then cleaned with acetone. Activating flux was prepared using the two kinds of halides (NaCl and CaCl2) by mixing them with acetone and a layer less than 0.2mm thick was applied to the surface using brush before TIG welding. The flux coated Ti6Al4V alloy is shown in Fig. 2.

The parameters considered for investigation was flux coatings, welding current and welding speed with 2 levels each as shown in Table 2. The weldments were cut at the centre as 10x10mm size with wire EDM for analysis of the cross-section. The cut pieces were etched with Keller's etchant and the composition of the etchant in 200ml solution was hydrofluoric acid, 2ml, nitric acid, 5ml, hydrochloric acid, 3ml, and the remaining is 190ml of distilled water. The test specimens were immersed in this etchant for a period of 15-30 seconds. The penetration and HAZ values were measured using XJP-6A metallurgical microscope.

Fig. 2. Flux coated Ti6Al4V workpiece

Parameters	Symbol	Level 1	Level 2
Flux coating	FC	NaCl	CaCl2
Welding current (Amp)	WC	50	60
Welding speed (mm/s)	WS	0.96	1.67

Table 2. Welding parameters and their levels

3. DESIGN OF EXPERIMETNS (DOE) FOR PENETRATION AND HAZ

The S/N ratio (η) analysis was conducted to find optimal setting of optimum parameters in which signals were predominant and eventually leads to a situation in which the system is least sensitive to noise [12]. The above three parameters with two levels were selected for penetration and HAZ experiments. The parametric optimization was performed by Taguchi method using MINITAB 16 software and the experiments were planned using L8 orthogonal array (OA). The experimental strategy used here was full factorial design of high resolution, which facilitates evaluation of main effects, 2-way and 3-way interaction effects on penetration and HAZ. The significance of individual parameters and their interactions on penetration were obtained by ANOVA. A confidence level of 95% (α = 0.05) was used throughout the analysis.

3.1. Taguchi's Signal to Noise (S/N) ratio for penetration.

The measured penetration values are given in Table 3. The penetration should be as high as possible so the characteristic selected in Taguchi method for penetration was "Larger is better" and the equation is as given in (1). Where 'y' is the individual measured response value and 'n' is the number of measurements.

$$\eta = -10\log\frac{1}{n}\sum_{i=1}^{n}\left(\frac{1}{y^2}\right) \quad (1)$$

Trial No	FC	WC	WS	Penetration
1	NaCl	50	0.96	3.663
2	NaCl	50	1.67	3.585
3	NaCl	60	0.96	3.951
4	NaCl	60	1.67	3.617
5	CaCl2	50	0.96	4.589
6	CaCl2	50	1.67	4.175
7	CaCl2	60	0.96	4.982
8	CaCl2	60	1.67	4.709

Table 3. Experimental results for penetration.

The main control factors (FC, WC and WS) have significant effect on the penetration values since the S/N ratio changes significantly with the change in the levels of these factors as shown in Table 4. It shows the minimum and maximum S/N ratios for each factor and the difference between the ratios was known as delta. The higher the delta, the effect of the factor was most significant on performance measure and the corresponding factor was awarded with highest rank. So among the main control factors flux coating had shown most significant effect followed by weld current and weld speed. The effect of main control factors on penetration is given in Fig. 3 indicates that the factor at level 2 for FC, level 2 for WC and level 1 for WS gives maximum penetration value and hence an optimal combination was obtained at $A_2B_2C_1$; as it was known that irrespective of the characteristic largest value of S/N ratio indicates the optimal condition for the corresponding factor.

Level	FC	WC	WS
1	11.37	12.02	12.60
2	13.26	12.61	12.03
Delta	1.90	0.58	0.57
Rank	1	2	3

Table 4. Signal to Noise ratio values for penetration.

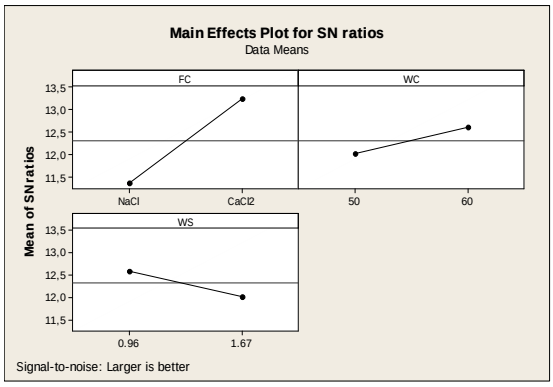

Fig. 3. Effect of main control factors on penetration

If the effect of one factor depends on the other factor, then the interaction plot was useful to visualize the possible interactions. The greater the difference in slope between lines, then higher the degree of interaction. However, the interaction plot does not give whether the interaction was statistically significant or not [13]. Fig. 4 shows the interaction effect of among the parameters for penetration.

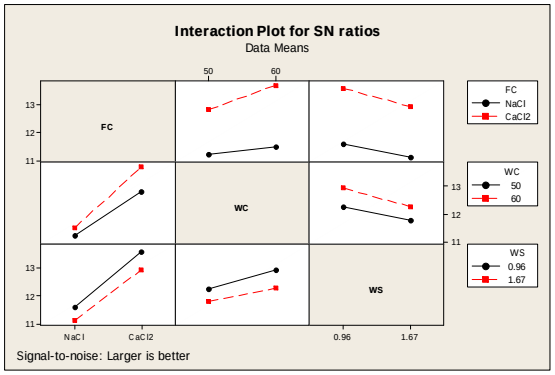

Fig. 4. Interaction effect between FC,WC and WS on penetration.

3.2. Analysis of variance for penetration.

The results of ANOVA for penetration are given in Table 5. P-value determines the appropriateness of rejecting the null hypothesis in a hypothesis test. So, the P-values which were less than 0.05 (95% confidence level) indicate that null hypothesis should be rejected and thus the effect of respective factor was significant. The absolute value of source terms for penetration is displayed in a Pareto chart as shown in Fig. 5. It consists of a reference line on the chart corresponding to a 'α' value of 0.05. The effects that past this reference line was potentially important. Normal plot of the standardized effects for penetration is shown in Fig. 6. The sources which were away from the line had significant effect and the sources near to zero were insignificant. From the two figures it was observed that FC, WC, WS, FC*WC and FC*WC*WS were potentially important and its relative effect on penetration is in decreasing order. Whereas the interaction between FC*WS and WC*WS were found to be insignificant on penetration.

Source	DF	Seq SS	Adj SS	Adj MS	F	P
FC	1	3.313	3.313	3.313	606.8	0.00
WC	1	0.348	0.348	0.348	63.9	0.00
WS	1	0.301	0.301	0.301	55.1	0.00
FC*WC	1	0.112	0.112	0.112	20.6	0.00
FC*WS	1	0.018	0.018	0.018	3.48	0.09
WC*WS	1	0.007	0.007	0.007	1.43	0.26
FC*WC *WS	1	0.053	0.053	0.053	9.75	0.01
Pure Error	8	0.043	0.043	0.043		
Total	15	4.199				

DF = Degrees of freedom; Seq.SS= Seqential sums of squares; Adj.SS=Adjusted sums of squares; Adj.MS=Adjusted means squares; F=F-value; P=P-value

Table 5. Analysis of variance for penetration

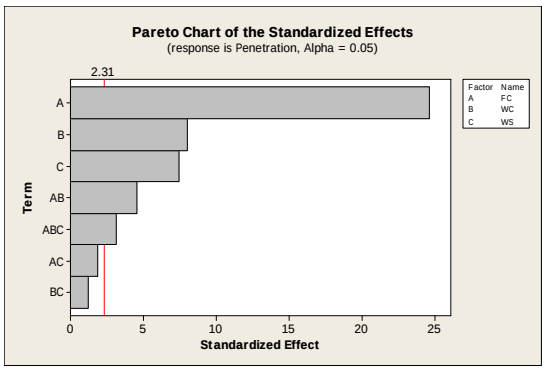

Fig. 5. Pareto chart of the standardized effects for penetration.

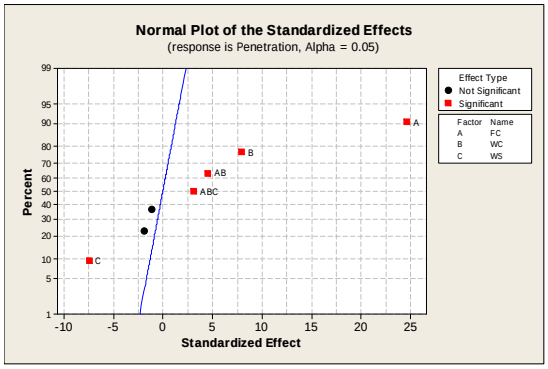

Fig. 6. Normal chart of the standardized effects for penetration.

3.3. Results and Discussion for penetration.

At the combination of CaCl2 as flux material, weld current at 60A and weld speed at 0.96mm/s the highest penetration value of 4.982 mm is observed as shown in Fig. 7(a). Conversely the lowest penetration value of 3.585mm was observed at conditions of NaCl as a flux material, weld current at 50A and weld speed 1.6mm/s as shown in Fig. 7(b).

The deep penetration was achieved with activated TIG welding is due to arc constriction and surface tension. In A-TIG welding activating flux constricts the welding arc and tends to increases the penetration. In addition, temperature coefficient of surface tension on the molten pool changes from a negative to a positive value. Therefore, the surface tension at the pool center is higher than at the pool edge resulting in change of direction of fluid flow in the molten pool; hence a relatively deeper and narrower weld is produced. Both the activating fluxes helped to increase the penetration because of the above reasons. The obtained results are in line with previous literature [14].

In the present investigation higher penetration values were obtained when the welding was carried using CaCl2 as a flux material and the reason may be the thermal properties of base and flux materials. The thermal conductivity of titanium Ti6Al4V alloy is 6W/mK. The higher conductivity of the base metal makes the weld penetration too shallow. By applying the activated flux materials like NaCl and CaCl2 it helps to reduce the conductivity in the welding area. As the conductivity values for CaCl2 and NaCl at room temperature is 0.60 and 0.55 W/mK respectively. So the lower values of thermal conductivity may be helped to obtain the deeper penetration values. As the current increases the heat input increases which increases the depth of penetration. Increase in torch speed decreases the heat received by the base metal therefore depth of penetration decreases.

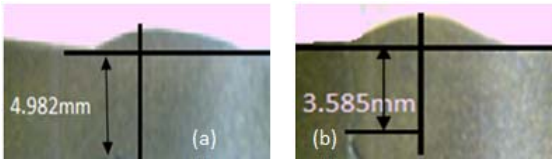

Fig. 7. (a) Penetration at $A_2B_2C_1$ condition, and (b) Penetration at $A_1B_1C_2$ condition.

3.4. Taguchi's Signal to Noise (S/N) ratio for HAZ.

The heat affected zone is an area of a base metal, which is not melted but causes the changes in its strength, induced stresses, resistance to corrosion, hardness and microstructure. The size of the HAZ is dependent on number of factors, including base material, thickness of the material being cut, flux material, heat input and weld speed. Suitable selection of welding parameters reduces the size of the HAZ. The heat affected zone should be as small as possible, so the type of characteristics selected for HAZ was "Smaller is better" and the equation is as given in (2). The measured HAZ values and the results of the S/N ratio for the HAZ are given in Tables 6 & 7 respectively.

$$\eta = -10 \log \frac{1}{n} \sum_{i=1}^{n} y^2 \qquad (2)$$

Trial No	FC	WC	WS	HAZ
1	NaCl	50	0.96	138.365
2	NaCl	50	1.67	127.14
3	NaCl	60	0.96	276.55
4	NaCl	60	1.67	204.245
5	CaCl2	50	0.96	161.675
6	CaCl2	50	1.67	81.765
7	CaCl2	60	0.96	211.445
8	CaCl2	60	1.67	119.575

Table 6. Experimental results for Heat affected zone.

Level	FC	WC	WS
1	-44.99	-41.83	-45.58
2	-42.62	-45.77	-45.02
Delta	2.37	3.94	3.56
Rank	3	1	2

Table 7. Signal to Noise ratio values for HAZ.

Among the main control factors welding current had shown most significant effect followed by weld speed and flux coating. The effect of main control factors and their interactions on HAZ is shown in Figs. 8 & 9 respectively. The factor at level 2 for FC, level 1 for WC and level 2 for WS gives minimum HAZ value and hence an optimal combination was obtained at $A_2B_1C_2$. All the interactions among the parameters were found to be significant.

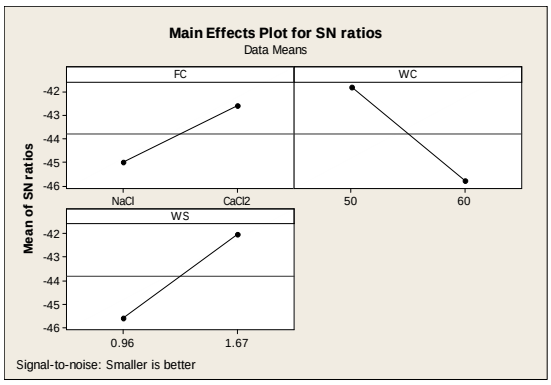

Fig. 8. Effect of main control factors on HAZ.

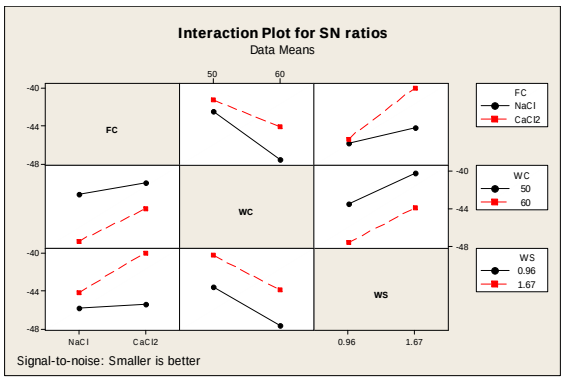

Fig. 9. Interaction effect between FC,WC and WS on HAZ.

Source	DF	Seq SS	Adj SS	Adj MS	F	P
FC	1	7382	7382	7382	11932	0.0
WC	1	22932	22932	22932	37066	0.0
WS	1	16295	16295	16295	26339	0.0
FC*WC	1	4077	4077	4077	6590	0.0
FC*WS	1	1947	1947	1947	3147	0.0
WC*WS	1	1333	1333	1333	2155	0.0
FC*WC*WS	1	603	603	603	974	0.0
Pure Error	8	4.9	4.9	0.6		
Total	15	54576.9				

Table 8. Analysis of variance for heat affected zone.

3.5. Analysis of variance for Heat affected zone.

Analysis of variance was performed for HAZ and the results are given in Table 8. Pareto chart and Normal plot of the standardized effects for HAZ are shown in Figs. 10 & 11 respectively.

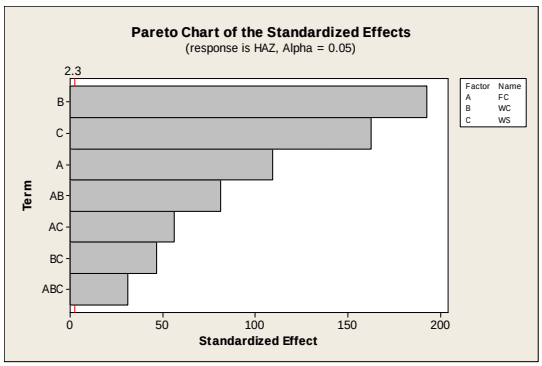

Fig. 10. Pareto chart of the standardized effects for HAZ.

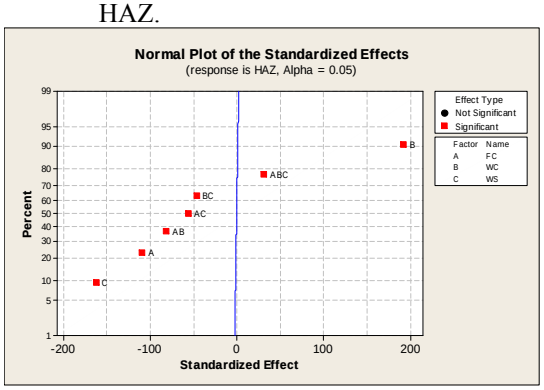

Fig. 11. Normal chart of the standardized effects for HAZ.

From the two figures it was observed that all the effects past the reference including all main control factors, 2-way and 3-way factors viz., WC, WS, FC, FC*WC, FC*WS, WC*WS and FC*WC*WS were significant and its relative effect on HAZ is in decreasing order.

3.3 Results and Discussion for penetration.

The combination of CaCl2 as flux material, weld current at 50A and weld speed at 1.67mm/s the lowest HAZ value was observed as shown in Fig. 12(b). Conversely the highest HAZ value was observed at conditions of NaCl as flux material, weld current at 60A and weld speed 0.96mm/s as shown in Fig. 12(a). The penetration values obtained in the present investigation was an effect on the HAZ. The arc constriction and surface tension of the molten metal changes the direction of fluid flow and makes the welds with deeper penetration resulting in smaller HAZ. The thermal conductivity of the CaCl2 flux powder helped in obtaining the better penetration values hence relatively lower values of HAZ was observed.

Welding current has significant effect on the HAZ. Increase in welding current increases the heat input and temperature resulting in increase of both HAZ and penetration. Thermal gradients which were generated due to heating and cooling over a larger volume of metal due to increased heat input increases HAZ. As the torch speed increases heat input to the base metal decreases hence the depth of penetration and HAZ decreases. The obtained result matches with the other literature [15-16].

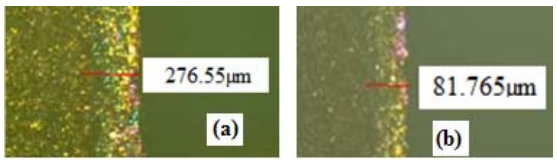

Fig. 12 (a). HAZ at $A_1B_2C_1$ condition and (b) HAZ at $A_2B_1C_2$ condition.

4. CONCLUSIONS

The main aim of the work was fulfilled with the welding of Ti6Al4V titanium alloy using halides as activating fluxes.

- The use of halide fluxes in this investigation successfully prevented the formation of oxide layer and proved that the activated TIG welding can be performed for titanium alloys.
- The main control factors of flux coating, welding current and welding speed were found to be significant on both the performance measures of penetration and HAZ.
- Thermal properties of the halides were an effect in obtaining the better penetration and HAZ values in A-TIG welding when compared to conventional welding method i.e., without using activating fluxes.
- An optimal combination of parameters was obtained at $A_2B_2C_1$ for highest penetration and it was measured to be 4.982mm. Whereas the optimal combination for lowest HAZ was $A_2B_1C_2$ and the value was as small as 81.765µm.
- One 2-way interaction (FC*WC) and 3-way interaction (FC*WC*WS) was found to be significant on penetration. Whereas all the 2-way and 3-way interactions were found to be significant for HAZ.

5. REFERENCES

[1] Pal, S., Pal, S.K., Samantaray, A.K., *Determination of optimal pulse metal inert gas welding parameters with a Neuro-GA technique*, Materials and Manufacturing Processes, 25, 606-615, 2010.

[2] Tseng, K.H., Hsu, C.Y., *Performance of activated TIG process in austenitic stainless steel welds,* Journal of Materials Processing Technology, 211, 503–512, 2011.

[3] Nayee, S.G., Badheka, B.J., *Effect of oxide-based fluxes on mechanical and metallurgical properties of Dissimilar Activating Flux Assisted-Tungsten Inert Gas Welds*, Journal of Manufacturing Processes, 16, 137-143, 2014.

[4] Vasantharaja, P., Vasudevan M., *Studies on A-TIG welding of Low Activation Ferritic/Martensitic (LAFM) steel*, Journal of Nuclear Materials, 421, 117–123, 2012.

[5] Ramkumar, K.D., Ramanand, R., Ameer, A., Simon, K.A., Arivazhagan, N., *Effect of post weld heat treatment on the microstructure and tensile properties of activated flux TIG welds of Inconel X750*, Materials Science and Engineering: A, 658, 326-338, 2016.

[6] Cai, Y., Luo, Z., Huang, Z., Zeng, Y., *Effect of cerium oxide flux on active flux TIG welding of 800 Mpa super steel*, Journal of Materials Processing Technology, 230, 80-87, 2016.

[7] Xie, X., Shen, J., Cheng, L., Li, Y., Pu, Y., Effects of nano-particles strengthing activating flux on the microstructures and mechanical properties of TIG welded AZ31 magnesium alloy joints, Materials & Design, 81, 31-38, 2015.

[8] Zhang, Z., Liu, L., AC TIG welding with single-component oxide activating fluxfor AZ31B magnesium alloys, Journal of Materials Science, 43, 1382-1388, 2008.

[9] Huang, H.Y., Shyu, S., Tseng, K., Chou, C.P., *Effects of the Process Parameters on Austenitic Stainless Steel by TIG-flux Welding*, Journal of Materials Science & Technology, 22, 367–374, 2006.

[10] Maduraimuthu, V., Vasudevan., Hot Effect of Activated Flux on the Microstructure, Mechanical Properties, and Residual Stresses of Modified 9Cr-1Mo Steel Weld Joints, Metallurgical and Materials Transactions B, 61, 82–93, 2011.

[11] Kumar D.S., Effect of welding parameters on mechanical properties and optimization of pulsed TIG welding of Al-Mg-Si alloy, International journal of advanced manufacturing technology, 42, 118-125, 2009.

[12] Rao, P.S., Ramji, K., Satyanarayana, B., *Prediction of Material removal rate forAluminum BIS-24345 Alloyin wire-cut EDM*, International Journal of Engineering Science and Technology, 2, 7729-7739, 2010.

[13] Rao, P.S., Ramji, K., Satyanarayana, B., *Effect of wire EDM conditions on generation of residual stresses in machining of aluminum 2014 T6 alloy,* Alexandria Engineering Journal, 2016. doi:10.1016/j.aej.2016.03.014.

[14] Shyu, S.W., Huang, H.Y., Tseng, K.H., Chou C.P., *Study of the Performance of Stainless Steel A-TIG Welds*, Journal of Materials Engineering and Performance 17, 193–201, 2008.

[15] Zuber, M., Chaudhri, V., Suri, V. K., Patil, S. B., *Effect of Flux Coated Gas Tungsten Arc Welding on 304L,* International Journal of Engineering and Technology, 6, 177-181, 2014.

[16] Dongjie Li, Shanping Lu, Wenchao Dong, Dianzhong Li, Yiyi Li., *Study of the law between the weld pool shape variations with the welding parameters under two TIG processes*, Journal of Materials Processing Technology 212, 128-136, 2012.

Authors: **Dr. Pujari Srinivasa Rao,** Asst. Professor, Corresponding author, Tel.: +91 99895 90407, **Mr. P. Raju,** Asst. Professor, **Mr. Ch. Kodanda Rama Rao,** Asst. Professor, **S. P. Priyangeli,** B.Tech Student; Department of Mechanical Engineering, GITAM Institute of Technology, GITAM University, Visakhapatnam, India Fax: +08912790399.
E-mail: pujari.vizag@gmail.com;
raju_prathipati@yahoo.co.in**;**
kodandaram.nitw@gmail.com**;**

Journal of Production Engineering
Vol.19 No.1
JPE (2016) Vol.19 (1) Original Scientific Paper
Manapparai, M., Elango, A.

TAGUCHY BASED OPTIMISATION OF TIG WELDING PARAMETERS ON AISI 310 AND 321 GRADE AUSTENITIC STAINLESS STEEL

Received: 01 April 2016 / Accepted: 05 June 2016

Abstract: *Tungsten inert gas welding is an important welding process used to weld stainless steel material in power plant, chemical industries, and refineries. The aim of the work is to weld the dissimilar grades of Austenitic stainless steel (AISI 310 and 321) which are aimed to use at high temperature and high pressure application. A corrosion resistant filler material AISI 347 is used to join these materials. The weldment strength is based upon input parameters of welding and hence a design of experiments is conducted to find the influence of process parameters for optimal setting using Taguchy's concept. A series of experiments are conducted to find the tensile strength and hardness of the material. From the experimental results the effect of process parameters are studied and the optimized level of process parameters are predicted. A confirmation experiment is conducted to validate the optimal level of process parameters prediction.*
Key words: *TIG Welding, Austenitic Stainless Steel, dissimilar Grades, Optimization, Taguchy's methodology*

Optimizacija parametara TIG procesa zavarivanja pomoću Taguči metode kod austenitnih nerđajućih čelika AISI 310 i 321. *Zavarivanje metodom volfram inertnog gasa (TIG) je važan proces zavarivanja koji se koristi pri zavarivanju nerđajućeg čelika u raznim elektranama, hemijskoj industriji i rafinerijama. Cilj ovog rada je zavarivanje različitih vrsta austenitnih nerđajućih čelika (AISI 310 i 321) koji su namenjeni korišćenju pri uslovima povišene temperature i pritiska. Kao dodatni nerđajući materijal je iskorišćen AISI 347 radi spajanja dva osnovna materijala. Čvrstoća zavara je praćena shodno promenama parametara zavarivanja i plan eksperimenta je sproveden kako bi se utvrdilo uticaj parametara procesa i optimalnog podešavanja parametara pomoću Tagučijeve metode. Serija eksperimenta je sprovedena radi određivanja zatezne čvrstoće i tvrdoće materijala. Na osnovu eksperimentalnih istraživanja je praćena promena usled variranja parametara procesa i određeni su optimalni nivoi parametara procesa. Sproveden je eksperiment radi potvrđivanja predviđanja optimalnih vrednosti parametara procesa.*
Ključne reči: *TIG zavarivanje, austenitni nerđajući čelik, različite vrste čelika, optimizacija, Tagučijeva metodologija*

1. INTRODUCTION

The gas tungsten arc welding (GTAW) process is based on the electric arc established between a non-consumable electrode of tungsten and the work-pieces to be joined. Part of the heat generated by the electric arc is added to the work- pieces, promoting the formation of a weld pool. The weld pool is protected from air contamination by a stream of an inert gas (Ar or He) or a mixture of gases. This process is extensively used for welding thin components of stainless steel, aluminum, magnesium or titanium alloys as well pieces of carbon and low alloy steels.

Heat input in GTAW does not depend on the filler material rate. Consequently, the process allows a precise control of heat addition and the production of superior quality welds, with low distortion and free of spatter. Material information that may be required to evaluate a steel structure includes chemical composition, tensile strength, bend ductility, fillet weld shear strength, hardness, and fracture toughness. Tensile tests provide information on the strength and ductility of materials under uniaxial tensile stress. The base metal and weld metal tests are performed on a tensile testing machine in accordance with the requirements of ASTM E8.

Hardness tests are used to provide generic information on the material properties (toughness and strength).Hardness measurements provide indications of metallurgical changes caused by welding. Vickers hardness test makes small indentations and is suited for hardness measurements in base metal, weldment, and heat affected zone in accordance with the requirements of ASTM E140.

2. LITERATURE REVIEW

R.Sathish et.al [1] carried out an experiment on Process Parameter Optimization of dissimilar carbon steel and stainless steel pipes welding by GTAW. Non-destructive test of the welded specimens was carried out using Radiography test method and susceptibility to inter granular corrosion of the welded specimens is studied for varying heat inputs .The percentage contribution of each parameter and prediction of tensile strength is found by analysis of variance (ANOVA) technique.

Mr.Pasupathy et.al [2] carried out an experiment to find the influence of welding parameters like welding

current, welding speed on strength of low carbon steel on AA1050 material during welding. A plan of experiments based on Taguchi technique has been used to acquire the data. An Orthogonal array, signal to noise (S/N) ratio and analysis of variance (ANOVA) are employed to investigate the welding characteristics of dissimilar joint and optimize the welding parameters.

Mr.L.Suresh et.al [3] carried out an experiment on AISI 304 AND 316 by Taguchi technique .In this paper they discuss about the mechanical properties of austenitic stainless steel for the process of TIG and MIG welding.

Sreejith S Nair et.al [4]. Carried out an experiment by multipass TIG welding using Response surface methodology In this work Central composite Design Methodology of Response surface methodology is used to conduct the experiments. Analysis of variance is used to analyze the influence of parameters during machining.

Raghuvir et.al [5] carried out an experiment to find optimized parameter on 304L Stainless Steel using Response surface methodology. From the results of the experiments, mathematical models have been developed to study the effect of process parameters on penetration and width.

A.Raveendra et.al [6] carried out a study on pulsed and non pulsed current TIG Welding of Stainless Steel (304). In this experimental work were conducted on the weldments of SS304 using GTAW with pulsed current and non-pulsed current at different frequencies of 5Hz &10Hz on 3mm thick sheets.

P. Sathiya et.al [7] carried out an experiment on friction welding of austenitic stainless steel optimization on weld quality**.** The objectives of this study are optimizing the friction welding parameters in order to establish the weld- quality. Acoustic emission emanated by the joints during tensile testing was acquired to assess the quality of the joints. Also a method to decide near optimal settings of the process parameters using Genetic Algorithm is proposed.

Benjamin Joseph et.al [8] conducted an experiment to study Weld metal characterization of 316L (N) austenitic stainless steel by electron beam welding process by varying the welding parameters such as beam power and welding speed. He analyzed the mechanical and metallurgical properties of the welded material through optical microscopy.

3. EXPERIMENTAL WORK

3.1. Problem identification

In steam power plant of about 800 MW capacity or above the equipments such as boilers and allied pipelines are subjected to high temperature and high pressure. For the high temperature application suitable materials are required. Searching of new materials and its capability of fabrication and evaluating its strength is a challenging work. Thus High temperature application materials are selected from literature and work is carried out to study the behavior of this material.

3.1.1 Methodology

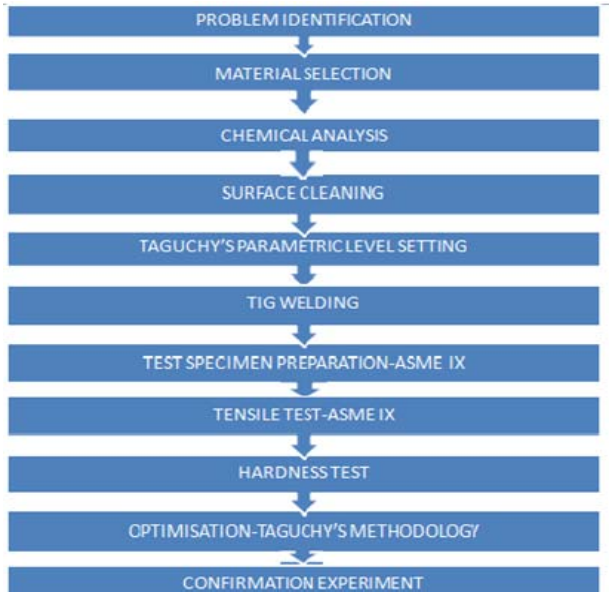

Fig. 1. Flow chart of the Experimenal Work

3.2 Selection of Materials

For high temperature application such as boiler, steam pipe line the austenitic grade stainless steel materials AISI 310 and AISI 321 are selected due to the following aspect of that materials.

3.2.1 Property of 310 Grade

310 family of Austenitic grade have excellent toughness. The increased chromium content increases its high temperature properties. It has excellent corrosion resistance. In high temperature application they exhibit good resistance to oxidation and carburizing atmospheres. They are good resistance to thermal fatigue and cyclic heating in continuous service. Typical applications of these grades include furnace parts, oil burner parts, carburizing boxes, heat treatment baskets and heat exchangers.

3.2.2 Property of 321 Grade

321 is the basic 18/8 austenitic steel (Grade 304) stabilized with Titanium. This grade is not sensitive to intergranular corrosion after heating within the range of 425-850°C. 321 is the grade of choice for applications in the temperature range of up to about 900°C, combining high strength, resistance to scaling and phase stability with resistance to subsequent aqueous corrosion. Like other austenitic grades, 321 has excellent forming and welding characteristics, is readily brake or roll formed and has outstanding welding characteristics. Post-weld annealing is not required. Grade 321 also has excellent toughness, even down to cryogenic temperatures.

Grade 321H is a modification of 321 with a controlled higher carbon content, to provide improved high temperature strength. A limitation with 321 is that titanium does not transfer well across a welding arc, so is not usable as a welding consumable. 321 has higher hot strength than 304L and is the best choice if the requirement is resistance to an operating environment over about 500°C.

3.2.3 Selection of filler wire.

Grade 347 contains niobium which performs the same carbide stabilization task but can be transferred across a welding arc. Grade 347 is therefore the standard consumable for welding 321 and 310 grades.

3.3 Chemical Analysis.

When the chemical composition of an existing structural (steel) material is not available, it may be necessary to perform a chemical analysis. This is an important initial task in the overall material and weld testing program. From this analysis, the information will provide a basis for characterizing the properties of the unknown materials. This information can be used for assessing corrosion problems, conducting fracture analyses, and material weld ability. A chemical analysis should be in conformance with ASTM E30, E350, and E1086. The chemical analysis report as per ASTM E1086 is shown in Table 1 [9].

Type	310
%C	0.023
%Mn	1.46
%Si	1.19
%S	0.009
%P	0.027
%Ni	19.07
%Cr	24.1

Type	321
%C	0.020
%Mn	1.52
%Si	0.53
%S	0.014
%P	0.025
%Ni	9.20
%Cr	17.15
%Ti	0.41

Table 1. Chemical Analysis, Report of AISI 310 and 321 Stainless Steel

3.4. Welding of Stainless Steel

Materials Size: Length = 150mm, Breath = 50mm, Thickness = 6mm are chosen as a standard specimen (ASME Section IX) for welding [10]. The influence of current, Argon flow rate, Bevel angle and Root gap on weld strength is to be studied. For this purpose edge preparation at various angles 30º, 45º and 60° is carried out using a grinding machine. After edge preparation the surface of the material is polished using emery sheet (Abrasive E 14) to remove impurities and then cleaned with acetone.

3.4.1. Taguchy's Design of Experiment.

Taguchy's L9 Orthogonal Array is used for the experiment work [11]. The welding parameters and their levels are shown in table 2.

Factors / Notations		-1	0	+1
Current	A	125A	150A	175A
Argon flow rate	B	4LPM	5LPM	6LPM
Bevel angle	C	30º	45º	60º
Root gap	D	1mm	1.5mm	2mm

Table 2. Welding Parameters used for Welding AISI 310 And 321 Grades of Stainless Steel.

Fig. 2. Welded specimen

Tensile test [ASME SEC IX] is carried out to evaluate tensile strength of the weldment and the results are shown in table 3.

Fig. 3. Tensile tested specimen

Exp. No.	Current (A)	Argon flow rate (B)	Bevel angle (C)	Root gap (D)	Tensile strength (MPa)
1	1	1	1	1	494.70
2	1	2	2	2	573.68
3	1	3	3	3	571.13
4	2	1	2	3	560.60
5	2	2	3	1	595.13
6	2	3	1	2	356.04
7	3	1	3	2	586.36
8	3	2	1	3	575.62
9	3	3	2	1	588.96

Table. 3. L9 Orthogonal Array for tensile test and Experimental Results

Vickers hardness test is conducted to evaluate hardness of the weldment and the results are shown in table 4.

Exp. No.	Current (A)	Argon flow rate (B)	Bevel angle (C)	Root gap (D)	Vickers hardness no. at weldment		
					Y1	Y2	Y3
1	1	1	1	1	216	198	203
2	1	2	2	2	243	251	259
3	1	3	3	3	247	235	251
4	2	1	2	3	228	231	229
5	2	2	3	1	233	241	216
6	2	3	1	2	221	212	209
7	3	1	3	2	235	246	242
8	3	2	1	3	214	203	216
9	3	3	2	1	247	235	251

Table 4. L9 Orthogonal Array for hardness test and Experimental Results

3.5.Taguchy's Methodology:

In recent years, the Taguchi method is widely used as a powerful tool for designing high-quality system during research and development so that high quality products can be produced in a minimum time and minimum cost. Taguchi parameter design is an important tool for robust design. This method uses a special design of orthogonal arrays to study the entire parameter space with a minimum number of experiments. Taguchy's methodology is used to find the factor influence on tensile strength and hardness. The ANOM table is shown in table 5 and table 6. The factor Bevel angle (C) has higher influence on both tensile strength and hardness. The factor Root gap (D) has least influence on both tensile strength and hardness.

Factor	A	B	C	D
Level-1	1639.51	1641.66	1426.36	1678.79
Level-2	1511.77	1744.45	1723.24	1516.08
Level-3	1750.94	1516.13	1752.62	1707.35
Range	239.17	228.32	326.23	191.27
Rank	2	3	1	4

Table 5. ANOM for Factor Influence on tensile strength

Factor	A	B	C	D
Level-1	2103	2028	1892	2040
Level-2	2020	2076	2174	2118
Level-3	2089	2108	2146	2054
Range	83	80	282	78
Rank	2	3	1	4

Table 6. ANOM for Factor Influence on hardness

The optimized parameter A3B2C3D3 is used to conduct a confirmation experiment for tensile strength.From the Confirmation experiment, tensile strength = 603.10 MPa is obtained.

4. CONCLUSION

TIG welding of AISI 310 & 321 grades of austenitic stainless steel is done successfully using 347 filler wire by varying current, argon gas flow rate, bevel angle and root gap by Taguchy's DOE techniques. Taguchy's methodology is used to find the optimized parameter level. The optimized parameter A3 B2 C3 D3 is used to conduct a confirmation experiment. From the confirmation experiment it was found that the maximum value of tensile strength was predicted as 603.10 MPa.

5. REFERENCING

[1] R.Sathish, B. Navwin, P.Nijanthan, K.Arun Vasantha Geethan, Vaddi Seshagiri Rao*: International Journal of Engineering Research and Applications*. Vol.2 (2012), p.2525

[2] J.Pasupathy, V.Ravisankar: International Journal of Scientific and Engineering Research. Vol. 4(2014)

[3] Mr.L.Suresh Kumar Dr.S.M.Verma, P.Radhakrishnaprasad, P.Kiran Kumar Dr.T.Siva Shanker: *International journal of Engineering Trends and Technology*- Vol. 2 (2011)

[4] Sreejith S Nair: International Journal of Mechanical Engineering and Robotics Research, Vol.2 (2013)

[5] Raghuvir Dr. N.M Suri, Prof. Jagjit Randhawa: *International Conference on Mechanical and Industrial Engineering*, 26th May-2013, New Delhi, India

[6] A.Raveendra, Dr.B.V.R.Ravi Kumar: International Journal of Innovative Research in Science, Engineering and Technology Vol. 2 (2013)

[7] P. Sathiya, S. Aravindanand A. Noorulhaq T: *International Symposium of Research Students on Materials Science and Engineering*, December 20-22, 2004, Chennai, India

[8] Benjamin Joesph, D. Katherasan P. Sathiya and C.V. Srinivasa Murthy: *International Journal of Engineering, Science and Technology* Vol. 4 (2012) pp. 169-176

[9] ASTM Hand Book

[10] ASME Hand Book

[11] Rajesh Kumar, M. K. Pradhan, Rishi kumar, "Modeling and optimization of end milling parameters on aluminum 6061 alloy using GRA based Taguchi method coupled with PCA" 5th International & 26th All India Manufacturing Technology, Design and Research Conference (AIMTDR 2014) December 12th–14th, 2014 *IIT Guwahati, Assam.*

Authors: **Prof.Manapparai.M, Assist.Professor** ARM College of Engineering and Technology Chennai, Tamil Nadu,India.Phone.: +91 766 75 90 522. E-mail: manaps69@gmail.com

Prof.Dr.Elango.A, Professor Alagappa Chettiar College of Engineering and Technology, Karaikudi, Tamil Nadu,India.Phone.: +91 96 29 70 30 96.
E-mail: elango.arum69@gmail.com

Journal of Production Engineering
Vol.19 No.1
JPE (2016) Vol.19 (1) Original Scientific Paper
Babič, M.

NEW METHOD FOR DETERMINATION MARTENSITE OF MICROSTRUCTURE OF HEAT TREATMENT MATERIALS

Received: 16 January 2016 / Accepted: 28 March 2016

Abstract: *In this article we present new method for determination martensite of microstructure of heat treatment materials. The martensite of a material is an important property that affects of materials. The martensite reaction in steels is the best known of a large group of transformations in alloys in which the transformation occurs by shear without change in chemical composition. The generic name of martensitic transformation describes all such reactions. Fractal characterization of surface topography is applied to the study of contact mechanics and heat treatment processes. The structure function method is used to find the fractal dimension D and the topothesy L. We develop a fractal geometry model, which predicts the wear rate in terms of these two fractal parameters for martensite structure of robot laser hardening process prediction.*
Key words: *hardening, fractal structure, martensite, intelligent system,*

Nova metoda određivanja martenzitne mikrostrukture posle termičke obrade materijala. *U ovom radu će biti predstavljena nova metoda za određivanje martenzitne strukture materijala posle termičke obrade. Martenzitna struktura materijala je važna osobina koja utiče na materijal. Martenzitna reakcija kod čelika je najviše poznata od velike grupe transformacija kod legura pri kojoj se transformacija odigrava mešanjem bez promene u hemijskom sastavu. Opšti naziv martenzitne transformacije karakteriše sve takve reakcije. Fraktalna karakterizacija topografije površine je primenjena pri studiji mehanizma kontakta i procesa termičke obrade. Metoda funkcije strukture je korišćena radi određivanja fraktalne dimenzije D i topotezije L. Razvijen je model fraktalne geometrije koji predviđa brzinu habanja u smislu ova dva fraktalna parametra pri martezitnoj strukturi kaljenjem robotskim laserom.*
Ključne reči: *kaljenje, fraktal struktura, martenzit, inteligentni sistem,*

1. INTRODUCTION

The robot laser surface-hardening [1] heat treatment is complementary to the conventional flame or inductive hardening. By laser remelting the surface of the materials, we can significantly improve their wear properties better like inductive hardening. Robot laser surface remelting is one of the most promising techniques for surface modification of the microstructure of a material to improve wear and corrosion resistance. A hard martensitic microstructure provides improved surface properties, such as wear resistance and high strength. Rapid quenching of austenite to room temperature often results in the formation of martensite [2], a very hard structure in which the carbon, formerly in solid solution in the austenite, remains in solution in the new phase. Unlike ferrite or pearlite, martensite forms by a sudden shear process in the austenite lattice which is not normally accompanied by atomic diffusion. The martensite reaction in steels is the best known of a large group of transformations in alloys in which the transformation occurs by shear without change in chemical composition. It should however be mentioned that there is a large number of transformations which possess the geometric and crystallographic features of martensitic transformations, but which also involve diffusion. Consequently, the broader term of shear transformation is perhaps best used to describe the whole range of possible transformations.

Many objects observed in nature are typically complex, irregular in shape and thus, cannot be described completely by Euclidean geometry. Fractal geometry [3] is becoming increasingly popular in material science to describe complex irregular objects. Fractal geometry is a workable geometric middle ground between the excessive geometric order of Euclid and the geometric chaos of general mathematics. It is based on a form of symmetry that had previously been underused, namely invariance under contraction or dilation. Fractal geometry is conveniently viewed as a language that has proven its value by its uses. Fractal geometry, in which infinite numbers of fractional dimensions are permitted in contradistinction to the three integer dimensions in Euclidean geometry, has been applied to the study of martensite structure of robot laser hardening process.

Machine learning [4] represents a key evolution in the fields of computer science, data analysis, software engineering, and artificial intelligence. It has quickly become industry's preferred way to make sense of the staggering volume of data our modern world produces. Machine learning engineers build programs that dynamically perform the analyses that data scientists used to perform manually. These programs can "learn" based on millions of experiences, all rigorously and numerically defined. Machine learning is impacting so many critical industries, including healthcare,

education, finance, robotics, artificial intelligence, astronomy, and more. The ability to develop machines and systems that automatically improve, puts machine learning at the absolute forefront of virtually any field that relies on data. Machine learning is at the forefront of incredible new innovations in several fields. Healthcare, education, astronomy, finance, robotics, and more are all being influenced by new developments in machine learning.

The aim of the contribution is to outline possibilities of applying intelligent system [5] namely; multyple regression [6] for the prediction of martensite structure in materials after robot laser heat treatment and to judge their perspective use in this field.

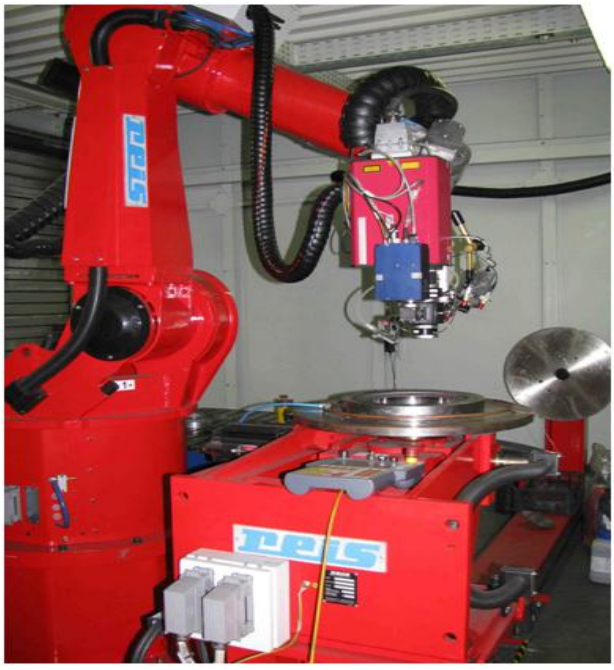

Fig. 1. Robor laser cell for hardening

2. MATERIAL PREPARATION AND METHOD

The study was undertaken using tool steel standard label 1.7225 tool steel. We change parameter of speed v∈[2, 5] mm/s in steps of 1 mm/s, and temperatureT∈ [0, 2000] °C. On Fig. 2 we label with *F* (blue cicle) ferit and with *M* (red cicle) martensite structure.

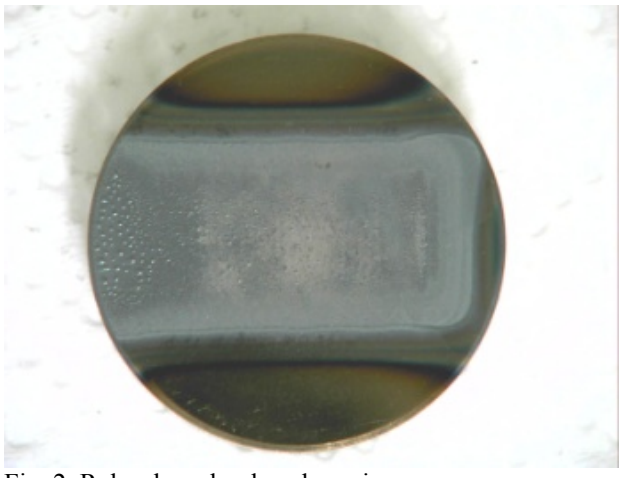

Fig. 2. Robor laser hardened specimens

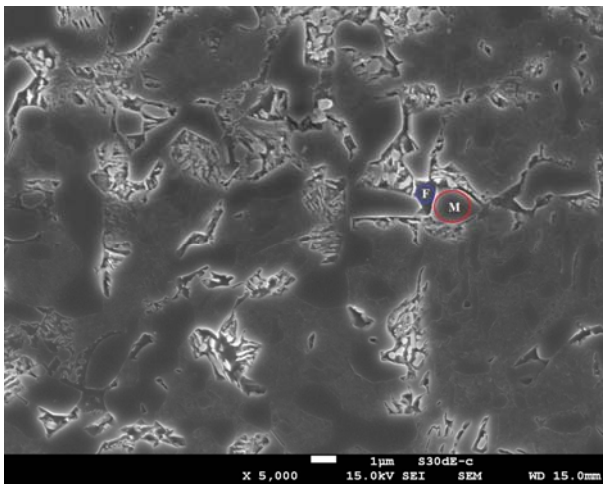

Fig. 3. Microstructure of robot laser hardening specimes

Martensite structure of microstructure of hardened specimens present area label with M (Fig. 3). We calculate area of SEM pictures of all this structures. Microstructure of robot laser hardened specimens have not self similar fractal structure but statistical self-affinity fractal structure. On Fig. 4 is presented statistical self-affinity fractal structure of robot laser hardened specimens.

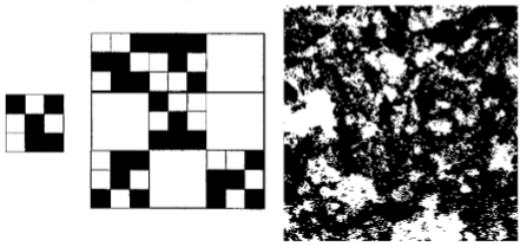

Fig. 4. Statistical self-affinity fractal structure of robot laser hardened specimens

Firstly, we use program ImageJ to convert SEM images to *3D* images of *SEM* images. Then, we find all point of *3D* images od *SEM* images. We find coodinates *(x,y,z)* of graphs of *3D* images od *SEM* images. We use new method [7] for estimating Hurst exponent *H* and calculating fractal dimension for *3D* object with equation *D=3-H*.

For analysis of the results, we used an intelligent system method [8], namely multiple regression [9-11]. The area of Intelligent Systems (ISs) has expanded phenomenally over the years since the 1940s; both in terms of the range of techniques and also in terms of the number of applications wherein they have often provided a competitive edge when compared with others approaches. IS includes a range of techniques that work synergistically and provides, in one form or another, flexible data/information processing capabilities for handling real life situations. IS, unlike conventional techniques, can exploit the tolerance for imprecision, uncertainty/ambiguities, approximate reasoning and partial truth in order to achieve tractability, robustness, and low cost solutions. The Multiple Regression operation studies the relationship between several predictor variables and a response

variable. Multiple regression designs are to continuous predictor variables as main effect ANOVA designs are to categorical predictor variables, that is, multiple regression designs contain the separate simple regression designs for 2 or more continuous predictor variables. The regression equation for a multiple regression design for the first-order effects of 3 continuous predictor variables *P*, *Q*, and *R* would be

$$Y = b_0 + b_1P + b_2Q + b_3R$$

On Fig. 5 is presented example od multiple regression.

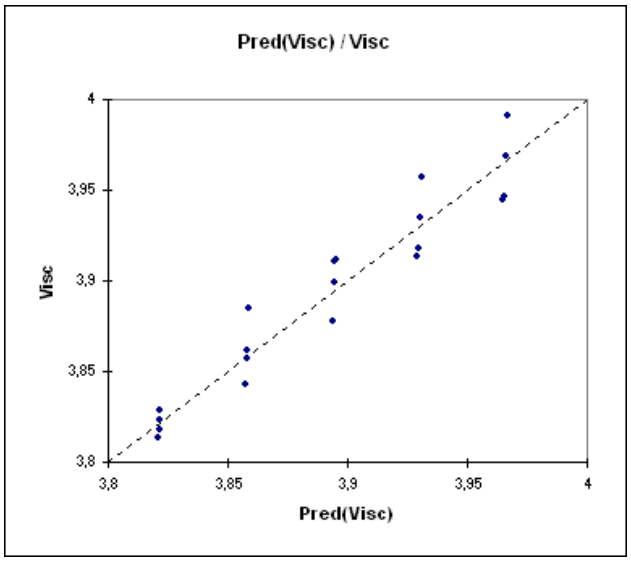

Fig. 5. Multiple regression

3. RESULTS AND DISCUSSION

In Table 1, the parameters and hardnessof hardened specimens. We mark specimens from P1 to P21. Parameter X1 presents the parameter of temperature [°C], X2 presents the hardening speed [mm/s] and X3 presents the fractal dimension estimating with new method. The last parameter Y is the martensite structure in (%) of the laser-hardened robot specimens. In Table 1, we can see that specimen P15 has the largest fractal dimension, 2.408. Thus specimen P15 is the most complex. Specimen P6 has the most martensite stucture after hardening, that is 61%. In table 2, the experimental and prediction data are presented. Column 1 present name of specimens, column 2 present experimental data and column 3 present predicted data of multiple regression. Prediction with multiple regression are presented in columns 3. The measured and predicted martensite structure of laser-hardened robot specimens is shown in the graph in Fig. 6. The regression model presents a 14.21% deviation from the measured data.

Model Regression

$$Y=5.724788459\times10^{-3}\times X1-1.296365336\times X2+3.987427179\times X3+35.07017084$$

S	X1	X2	X3	Y
P1	1000	2	2.304	38
P2	1000	3	2.264	42
P3	1000	4	2.258	45
P4	1000	5	2.341	37
P5	1400	2	2.222	52
P6	1400	3	2.388	61
P7	1400	4	2.250	39
P8	1400	5	2.286	44
P9	1000	2	2.178	53
P10	1000	3	2.183	60
P11	1000	4	2.408	35
P12	1000	5	2.210	41
P13	1400	2	2.257	36
P14	1400	3	2.265	40
P15	1400	4	2.433	58
P16	1400	5	2.289	59
P17	800	0	2.232	46
P18	1400	0	2.235	57
P19	2000	0	2.261	51
P20	950	0	2.282	50
P21	850	0	2.319	55

Table 1. Parameters and hardness of hardened specimens

S	ED	R
P1	38	47.38926085
P2	42	45.93339843
P3	45	44.61310853
P4	37	43.64769965
P5	52	49.35220721
P6	61	48.71775478
P7	39	46.8711245
P8	44	45.71830654
P9	53	46.88684503
P10	60	45.61041683
P11	35	45.21122261
P12	41	43.12534669
P13	36	49.49176716
P14	40	48.22730124
P15	58	47.60082367
P16	59	45.73026882
P17	46	48.54993907
P18	57	51.99677443
P19	51	55.53532061
P20	50	49.6080287
P21	55	49.18308466

Table 2. Experimental and prediction data

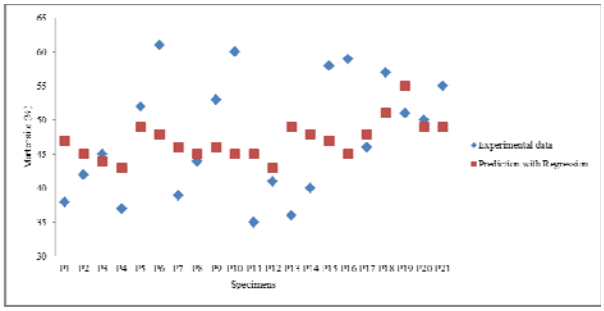

Fig. 6. Measured and predicted hardness of hardened specimens

The martensite structure of a material is an important mechanical property that affects the of materials. We cannot apply Euclidian geometry to describe the martensite structure of hardened specimens because hardness is very complex. Here we use fractal geometry to describe the martensite structure of robot laser-hardened specimens. The fractal approach is more appropriate in the characterization of complex and irregular surface microstructures observed in the martensite microstructure surface of robot laser hardened specimens and can be effectively utilized for predicting the properties of material from fractal dimensions of the microstructure. A statistically significant relationship was found between the roughness, parameters of the robot-laser cell and fractal dimension. In addition, image analysis of the *SEM* images of the robot-laser-hardened specimens is an interesting approach.

4. CONCLUSSION

In the paper we present new methof for determinating martensite microstructure of robot lser hardened specimens. We use method fractal geometry to analise complexity of the robot-laser-hardened specimens. The main findings can be summarised as follows:

1. We describe martensite structures of the hardened specimens by using fractal geometry.
2. We describe the relationship between martensite structure and the parameters of the robot-laser cell by using the fractal dimension. This finding is important with regard to certain alloys that are hard to mix because they have different melting temperatures; however, such alloys have better technical characteristics. By varying different parameters (e.g., temperature), the robot-laser cells produce different patterns with different fractal dimension.
3. To predict the (%) of the martensite structure of robot laser hardened specimens, we use multiple regression.
4. Using the presented intelligent system, we increase production of the robot laser hardening process by decreasing time of the process.

5. REFERENCING

[1] J. Grum, P. Žerovnik, R. Šturm: Measurement and Analysis of Residual Stresses after Laser Hardening and Laser Surface Melt Hardening on Flat Specimens; Proceedings of the Conference "Quenching ’96", Ohio, Cleveland, 1996.

[2] Verhoeven, John D. (2007). Steel Metallurgy for the Non-Metallurgist. American Society for Metals. pp. 26–31. ISBN 9780871708588.

[3] B. B. Mandelbrot, The fractal geometry of nature. New York: WH Freeman, 1982, p. 93

[4] Scott Patterson (13 July 2010). "'Artificial Intelligence' Gains Fans Among Investors - WSJ". WSJ. Retrieved 8 August 2015.

[5] Beverly Woolf, "Intelligent Tutoring Systems: A Survey," in Exploring Artificial Intelligence: Survey Talks from the National Conferences on Artificial Intelligence, ed. by Howard E. Shrobe and the American Association for Artificial Intelligence (San Mateo, CA.: Morgan Kaufmann, 1988), 1-43.

[6] Box, G. E. P. (1954). "Some Theorems on Quadratic Forms Applied in the Study of Analysis of Variance Problems, I. Effect of Inequality of Variance in the One-Way Classification". The Annals of Mathematical Statistics25 (2): 290. doi:10.1214/aoms/1177728786.

[7] BABIČ, Matej, KOKOL, Peter, GUID, Nikola, PANJAN, Peter. A new method for estimating the Hurst exponent H for 3D objects = Nova metoda za ocenjevanje Hurstovega eksponenta H za 3D-objekte. Materiali in tehnologije, ISSN 1580-2949. [Tiskana izd.], mar.-apr. 2014, letn. 48, št. 2, str. 203-208. http://mit.imt.si/Revija/

[8] Beverly Woolf, "Intelligent Tutoring Systems: A Survey," in *Exploring Artificial Intelligence: Survey Talks from the National Conferences on Artificial Intelligence*, ed. by Howard E. Shrobe and the American Association for Artificial Intelligence (San Mateo, CA.: Morgan Kaufmann, 1988), 1-43.

[9] Box, G. E. P. (1954). "Some Theorems on Quadratic Forms Applied in the Study of Analysis of Variance Problems, I. Effect of Inequality of Variance in the One-Way Classification". *The Annals of Mathematical Statistic s*25 (2): 290. doi:10.1214/aoms/1177728786.

[10] Lai, T.L.; Robbins; Wei; Robbins, H; Wei, C.Z. (1978). "Strong consistency of least squares estimates in multiple regression". *PNAS* 75 (7): 3034–3036. Bibcode:1978PNAS...75.3034L. doi:10.1073/pnas.75.7.3034. JSTOR 68164.

[11] Narula, Subhash C.; Wellington, John F. (1982). "The Minimum Sum of Absolute Errors Regression: A State of the Art Survey". *International Statistical Review* 50 (3): 317–326. doi:10.2307/1402501. JSTOR 1402501.

Author: Dr. Matej Babič, Bs. M.
Jožef Stefan Institute, Ljubljana, Slovenia
E-mail: babicster@gmail.com

Journal of Production Engineering
Vol.19 No.1
JPE (2016) Vol.19 (1) Preliminary Note
Senderská, K., Mareš, A., Ongyik, T.

MANUAL ASSEMBLY WORKSTATION DESIGN SUPPORTED BY ERGONOMICS SOFTWARE TOOLS

Received: 11 April 2016 / Accepted: 09 June 2016

Abstract: *Manual assembly workplaces need to be designed to take into account an ergonomic requirements resulting from the physical and psychological characteristics of human. In an effort to propose a workplaces that meet these requirements are very helpful software tools that allow you to insert into CAD model of workstation Manikin and perform directly at the design stage an ergonomic analysis. Article describes the design of manual workstation and using some software ergonomics analysis tools.*
Key words: *ergonomics, manual assembly, assembly workstation, CATIA*

Projektovanje pozicija ručne montaže pomoću ergonomskih softvera. *Pozicije ručne montaže treba da su projektovana na taj način da uzimaju u obzir ergonomske zahteve koji polaze od fizičkih i psiholoških osobina čoveka. U cilju postavljanja rešenja ovakvih radnih mesta od velike pomoći je i softver koji dozvoljava unošenje anatomsog CAD modela čovečjeg tela i na taj način omogućuje intervencije u fazi ergonomske analize. Rad opisuje projektovanje pozicije ručnog sklapanja korišćenjem nekih od ergonomsko analizirajućih softvera.*
***Ključne* reči:** *ergonomija, ručna montaža, montažno radno mesto, CATIA*

1. INTRODUCTION

Workstations, where the workers play a decisive role, whether the role of the management, supervision or performance have in manufacturing practices their unique place. In all these cases it is necessary to have a workplace designed so, that during the design was take into account ergonomic requirements of human activities. Failure to take into account of these requirements can lead to rapid fatigue of personnel and, consequently, to a decrease in productivity, errors and even accidents. The current status in the development of computer technology allows during workstation design use different software tools that, when are used correctly, it possible to achieve such a workplace proposal, that reflects the ergonomic aspects.

2. IMPORTANCE OF THE ERGONOMICS IN THE WORKPLACE DESIGN

As mentioned, ergonomically designed workstation is essential for the production process. Ergonomics as a discipline focused on the relationship between human and the working environment and working means integrates knowledge from various disciplines such as: anthropology, statistics, occupational hygiene, work organization, psychology, etc. This makes it a complex scientific discipline and it is difficult in terms of its application. When designing the new workstation there are increased demands on designers. Because not every designer is an expert in ergonomics, there was looked for ways, how to provide to designers an ergonomics research results. These results should be provided by such way, that they can be in a relatively simple form applied to solve workstation design. Some of these instruments were somatography templates and various tables with the recommended dimensions of the work tables, chairs and mutual distances of objects in the workplace and so on. With the gradual development of computer technology these tools were converted to a software form, either as a separate tools for specific ergonomic tasks, or as a comprehensive solutions. Since designers during development are using CAD systems, some manufacturers of CAD systems integrated ergonomic software tools into environment of developed CAD respectively PLM systems. These systems are different in number and type of tools for ergonomic analysis and possibility of correction of the proposed workstations. The basic element of these tools is the digital model of human.

3. DIGITAL MODEL OF HUMAN

Since 1960, when it was first human digital model developed were gradually developed a numbers of models of human. At present, we have routinely met with a 3D model of human also called as Manikin. Some models are only for illustrative purposes and it is not possible to do analysis with them, but some models are very sophisticated in detail, and offer a detailed handling with Manikin and ergonomic analysis. In Fig.1 shown are examples of 3D human models for various applications used in workstations 3D design. There are:

- Digital human model supplied by Autodesk in the design package called Autodesk Factory Design Suite. This model does not allow for positioning and ergonomic analysis, because these features are not supported in that software.
- V5 Human and V6 Human are human models used in the products of Dassault Systemes, such as CATIA and DELMIA. These models allow you to choose the

gender and change the physical dimensions, place the model in any position as well as create motion animation model and perform a variety of ergonomic analysis.

- PTC Creo Elements / Pro Manikin Extension - 3D human model used in applications Creo (formerly known as Pro/Engineer). Allows gender selection, adjust body size, detailed model positioning and creating of animations. Along with supplement PTC Creo Elements/Pro Manikin Analysis Extension enables the implementation of ergonomic analyzes.
- Tecnomatix Jack human model from Siemens is used in application Tecnomatix intended for design of digital production. It enables to choose the gender, change the physical dimensions and also the detailed positioning, model animation and detailed ergonomic analysis.
- Digital human model RAMSIS is model of the firm Human Solutions Group. This model is primarily focused on the ergonomic design of interior transport equipment (cars, trucks, buses, planes and helicopters as well as industrial vehicles - excavators, cranes, loaders, etc.). It allows you to change the dimensions of the model, positioning of the model in detail and to perform detailed ergonomic analysis.

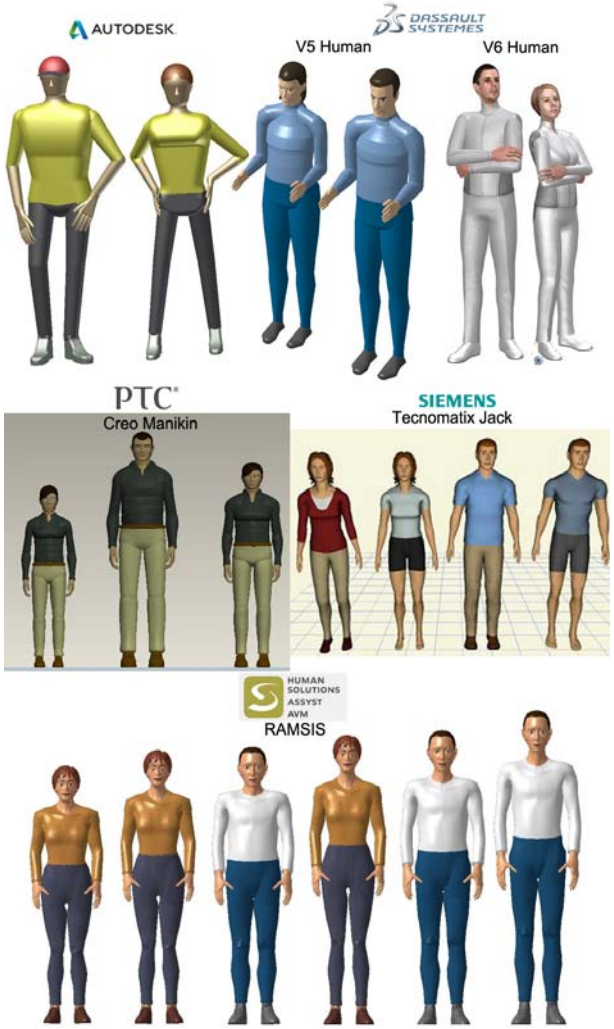

Fig. 1. Human digital models (image source: V6 Human [1], Creo Manikin [2], Tecnomatix Jack [3], Ramsis [4])

In addition to these software, there is also a range of others that are focused on ergonomic tasks. Some of them are standalone software applications and others are a supplement of CAD systems.

Whereas for solving the tasks described in the article were used ergonomic modules of CATIA in the next section just paid attention to CATIA ergonomics modules.

4. CATIA ERGONOMIC MODULES

In the CATIA are integrated four modules for ergonomic analyzes. There are: Human Activity Analysis, Human Builder, Human Measurements Editor and Human Posture Analysis. This modules allow you to create a 3D model of any human figure and make a various types of ergonomic analyzes, such as: RULA (Rapid Upper Limb Assessment), NIOSH (National Institute for Occupational Safety and Health), push-pull, Carry and Biomechanics analysis Single Action. Human Builder module allows you to quickly create a model based on the of gender and population percentile. There are data for American, Canadian, French, Japanese, Korean, German and Chinese (Taiwan) population. Human Measurements Editor module allows editing model dimensions according to the individual requirements, making it possible to create a model of any human. Human Posture Analysis modules quantitatively and qualitatively analyze all aspects of manikin posture. Human Activity Analysis module evaluates all elements of human performance from static posture analysis to complex task activities.

Mentioned modules where used to optimisation of assembly workstation.

5. MANUAL ASSEMBLY WORKSTATION

For the purpose of brake cylinder assembly was designed a manual assembly workstation. Brake cylinder is used in passenger as well as commercial vehicles equipped with drum brakes. It is a component which serves to hydraulically mashing brake shoes which provide braking of the wheel by friction on the brake drum, and consequently enables the car to stop. The effect is achieved by expansion of the hydraulic component - the brake cylinder which is fixed to the shield and located between the two braking jaws. Brake cylinder performs translational movement due to fluid pressure. Based on analysis of the brake cylinder 3D model which has been developed in CATIA (Fig. 2) was elaborated detailed technological process of assembly [5].

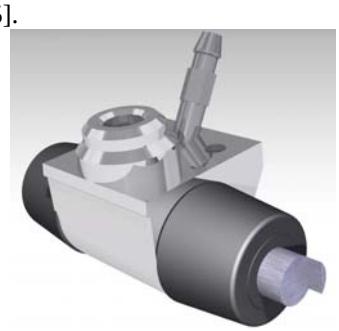

Fig. 2. 3D model of brake cylinder [1]

Subsequently, was in CATIA designed workstation for manual assembly. For workstation design were used standard modules of leading manufacturers of small modular assembly station (Fig. 3).

Fig. 3. 3D model of workstation [1]

For so designed workstation were sequentially carried out some ergonomic analysis.

6. MANUAL ASSEMBLY WORKSTATION ERGONOMICS ANALYSIS

The first task was by help of Human Builder modules and Human Measurement Editor to define a model of human. On this basis were performed pull-push, carry, lift/lower and RULA analysis.

6.1. Push/Pull analysis

The worker pushs or pulls rack on wheels in which are located 3 shelves. On the shelves there are placed either full containers of components, or empty containers returning from the assembly workstation. The worker so carry on the supply to assembly workstation. Worker brings the parts from the intermediate storage which is located approximately 10.5 meters from the assembly workstation. That operation is carried out once every two hours. As shown in Fig. 4 at the given parameters is the maximum allowable initial power of pushing 395.667N and continuous power 259.007 N. The forces for pulling are slightly smaller. These forces are not identical to the load weight. This represents at the maximum load 59.46 kg.

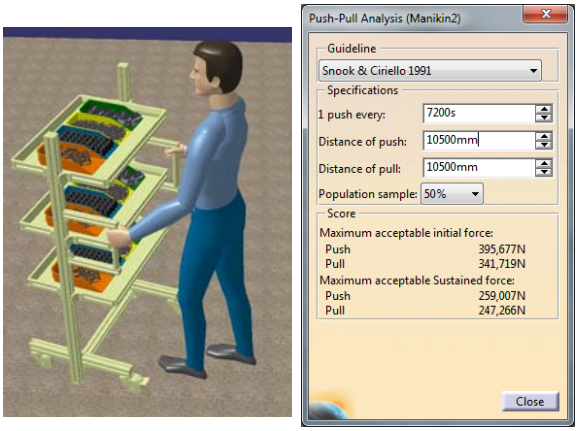

Fig. 4. Push/Pull analysis

6.2. Lift/Lower analysis

In this analysis it is determined the limit weight that the worker is able without difficulty to lift (or run down) during working time. In our case the worker lifts up the pallet with full containers. The total weight of the load is 5.4 kg.

It is possible to choose between three methods of evaluation: NIOSH 1981, NIOSH 1991 and Snook and Ciriello. For the actual analysis was used NIOSH 1991. For the analysis, it is necessary to define the so-called initial and final position of load lifting and lowering (see Fig. 5). The result of performed analysis is that the operation is in order, because the maximum recommended weight limit is 14.4 kg (Fig. 6).

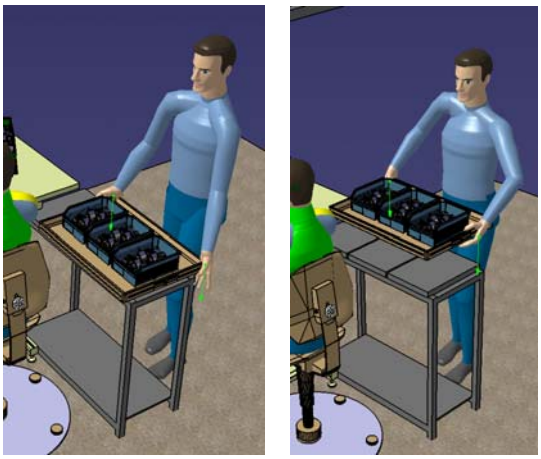

Fig. 5. Lift/Lower analysis
(left - initial posture, right -final posture)

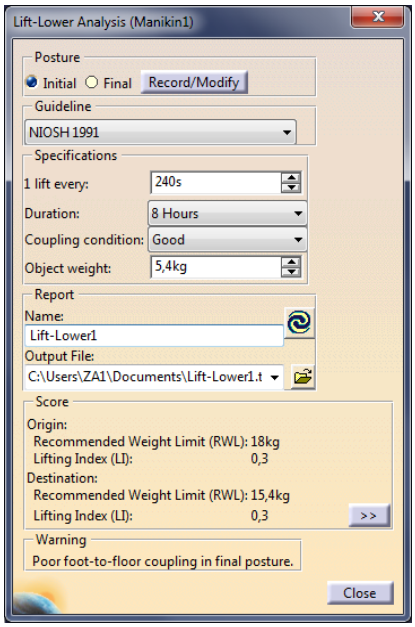

Fig. 6. Lift/Lower analysis dialog box

Another case when this analysis was applied was the pallet insertion into the rack. There was selected extreme case when it is necessary to insert the pallet to the highest place in the rack. In this case, the result - the recommended load in the top position is 0 kg. It follows that this operation is absolutely improper. This result was achieved also by the RULA analysis (see. Section 6.4).

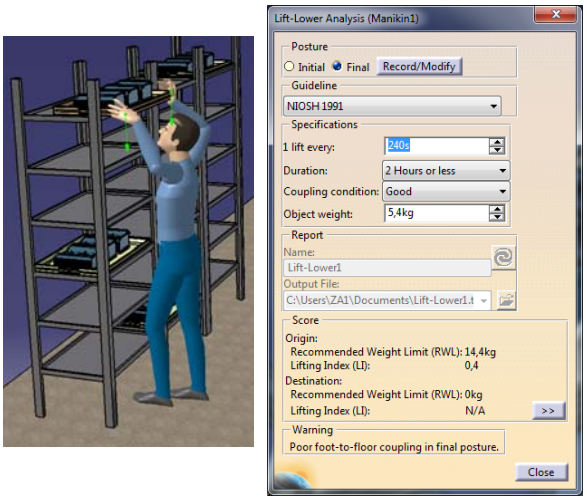

Fig. 7. Lift/Lower analysis

6.3. Carry analysis

Building on operation mentioned in previous chapter, when the worker lifts up a pallet with assembled components was performed the carry analysis. The worker carries finished components to the rack (Fig. 8). The load weight remains 5.4 kg. The maximum distance that has to go is 3300 mm. The maximum acceptable force applied to the worker and his hand is 297.111 N. Because the actual workload of the worker is about 540 N is the operation right.

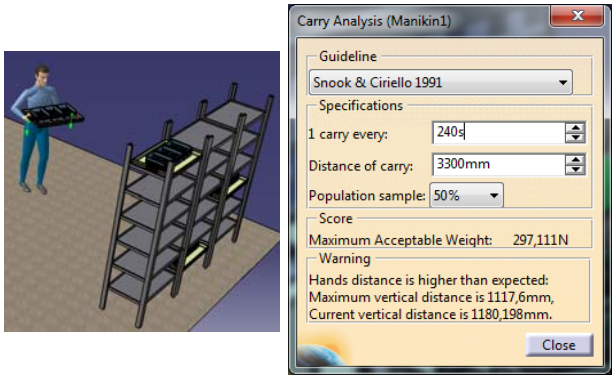

Fig. 8. Carry analysis

6.4. RULA analysis

As was mentioned by impose the pallet with assembled components into the rack, it was found unacceptable load. This operation was also analyzed by RULA analysis. The worker was arranged to the positions required for impose pallets in top placement of the rack (Fig. 9). Subsequently was started the RULA analysis as well as for right and left side of the body worker. The result for the left side is shown in Fig. 10. As can be seen, the resulting score is 7. This score means the worst-case. That load is totally unacceptable. For the right side of the worker body is the score the same. It follows that it is necessary to make changes of the workplace. One option is to modify the rack, it must be lower. The second option is to place stairs before the rack, which enable the worker to impose the pallet so way that he does not raise the hands so high, as it was in the original design of the workplace.

Fig. 9. Worker position by pallet storing

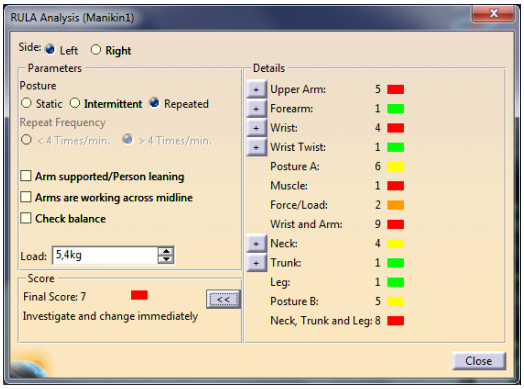

Fig. 10. Results of RULA analysis

7. CONCLUSION

On model of workstation were carried out further analyzes, but because of the scope of article could not be mentioned. The application of these analyzes proved to be very beneficial in the design of workstation, because help eliminate problems even before the build up of the workplace. This procedure will allow improving the working conditions and thus increasing productivity, quality and costs reducing.

8. REFERENCES

[1] http://www.cgw.com/images/issues/articles/feature_harm_2.jpg, (cit. 7.4.2016)
[2] http://communities.ptc.com/servlet/JiveServlet/downloadImage/38-1382-10171/450-389/people_size.jpg, (cit. 7.4.2016)
[3] http://images.vogel.de/vogelonline/bdb/397600/397662/4.jpg, (cit. 7.4.2016)
[4] https://www.lfe.mw.tum.de/en/research/methods-and-lab-equipment/ramsis-3d-human-model-for-cad-applications/ , (cit. 7.4.2016)
[5] Ongyik, T.: *Ergonomické moduly CATIE a ich aplikácia. (CATIA ergomomic modules application).* Diploma thesis, SjF TU v Košiciach, 2012

ACKNOWLEDGEMENTS: This contribution is the result of the project VEGA 2/0113/16 and project establishing lean knowledge and laboratories HUSK 1101/1.6.1/0161.

Authors: Ing. Katarína Senderská, PhD., Ing. Albert Mareš, PhD., Ing. Tomáš Ongyik, Technical University of Košice, Faculty of Mechanical Engineering, Department of Automobile Production, Masiarska 74, 04001 Košice, Slovakia.
E-mail: katarina.senderska@tuke.sk
albert.mares@tuke.sk, tomas.ongyik@gmail.com

Journal of Production Engineering
Vol.19 No.1
JPE (2016) Vol.19 (1) Preliminary Note

Tamás, P.

APPLICATION OF SIMULATION MODELING FOR FORMATION OF PULL-PRINCIPLED PRODUCTION CONTROL SYSTEM

Received: 04 April 2016 / Accepted: 07 June 2016

Abstract: *Firstly the lean philosophy has spread in the field of the production systems, however it also appeared in the service areas in the last decade as well. One of the philosophy's priority questions is realization of the push principle, namely the push systems' transformation into pull systems. The pull system enables the more flexible satisfaction of the customer needs and the more efficient process improvement as well. The transformation's process from push system into pull system has been already determined clearly, however we can increase this process's efficiency with use of the simulation modeling. Basically this paper presents these efficiency improvement possibilities.*

Key words: *lean philosophy, push principle, process improvement*

Primena modela simulacije formacije pul principa proizvodnog kontrolnog sistema. *Najpre se lean filozofija proširila u polje proizvodnih sistema, međutim u poslednjoj decenije je prisutna i u sferi servisa. Jedan od prioriteta ove filozofije je realizacija push principa, čime se konkretno misli na pretvaranje pul sistem u push sistem. Pul sistem omogućava fleksibilnost satisfakcije klijentovih potreba i efikasnije unapređenja procesa. Transformacija od push sistema u pul sistem je već tačno definisana, ali postoji mogućnost povećanja efikasnosti ovog procesa pomoću simulacijskog modelovanja. U ovom radu su predstavljena ova efikasna unapređenja mogućnosti.*

Ključne reči: *lean filozofija , push princip, poboljšanje procesa*

1. INTRODUCTION

In practical life the strengthening of the market competition demands the continuous reduction of the wastes. Those companies which are not able to reduce their wastes quickly and dynamically will become uncompetitive and their market role will reduce. The lean philosophy's device and rule system enable the reduction of the wastes, as a result of these the companies' competitiveness will increase. If we would like to determine the lean philosophy's essence, in our opinion the best definition is the reduction of the duration between the order and the payment with the elimination of the wastes [1]. The philosophy distinguishes 3 kinds of MU, namely the Muri (overburden), the Mura (unevenness) and the Muda (waste). The Muri and the Mura result in Muda, consequently most companies only speak about the Muda's elimination. We can distinguish 8 types of the wastes namely the overproduction, unnecessary inventory, transportation, unnecessary motion, waiting over-processing, defects. We can achieve these wastes' elimination with use of the lean philosophy's devices [1]. The lean determines 5 kinds of principles, which principles are able to realize the wastes' elimination efficiently. These principles are the following [1]:

- determination of the value,
- elaboration of the value stream,
- creation of the continuous flow,
- creation of the pull principle,
- continuous improvement.

We can tell that realization of the above steps will result in significant wastes reduction in the case of the ideal production systems, however, there are some cases when the mentioned principles' realization is not possible perfectly (e. g. we can't create continuous flow in the case of the heat treatment because of this equipment has a significant capacity, …, etc.) [2]. We will examine one of the priority principles, namely the transformation process which takes from the push-principled production system into the pull-principled production system. This paper will also introduce the simulation investigational possibilities in connection with this process.

2. EXPLANATION OF THE PUSH-PRINCIPLED AND THE PULL-PRINCIPLED PRODUCTION CONTROL PHILOSOPHY

The push-principled and pull-principled production control systems differ from each other therein that the push system is based on the forecast of the customer's needs however the pull system is based on the effective customer's needs. Consequently we can get overproduction and/or stock shortage in the case of the push system, however this can't occur in the case of the pull system.

E. g. If we use the push principle for the car's refueling then we have to determine the refueling's amount on the basis of the expected running distance in the other case (pull system) we will refuel if we reach a given fuel level. We can establish that the pull system gives us more security.

Push-principled production control philosophy	Pull-principled production control philosophy
Production on the basis of the customer's needs	Production on the basis of the effective customer's needs.
Longer production lead time	Shorter production lead time
Higher work in processes	Lower work in processes
Ad hoc effort for the elimination of the wastes.	Systematic effort for the elimination of the wastes
The workers realize simple workflows.	The workers realize complex workflows.
Utilization of the available resources (human, machine) is lower	Utilization of the available resources (human, machine) is higher
Bigger area need	Lower area need
Bigger batch sizes	Smaller batch sizes

Table 1. Comaprison of the push- and pull-principled production control philosophy

We can find the same at the production processes. One important objective of the pull system is the reduction of the production lead time. We do not have to keep WIP and finished goods if the production lead time is less than the order lead time. The figure 1 presents the differences between the push- and pull-principled production control systems.

3. PROCESS OF THE FORMATION OF THE PULL-PRINCIPLED PRODUCTION CONTROL SYSTEM

The transformation of the production logistics processes from the push system into pull system can be realized in two kinds of versions. In the first version the assigned total process will be transformed „simultaneously" (version A on the figure 1). In the second version the transformation will be realized in more steps, consequently we can use the realized process' working experiences at the next process step's realization (version B on the figure 1).

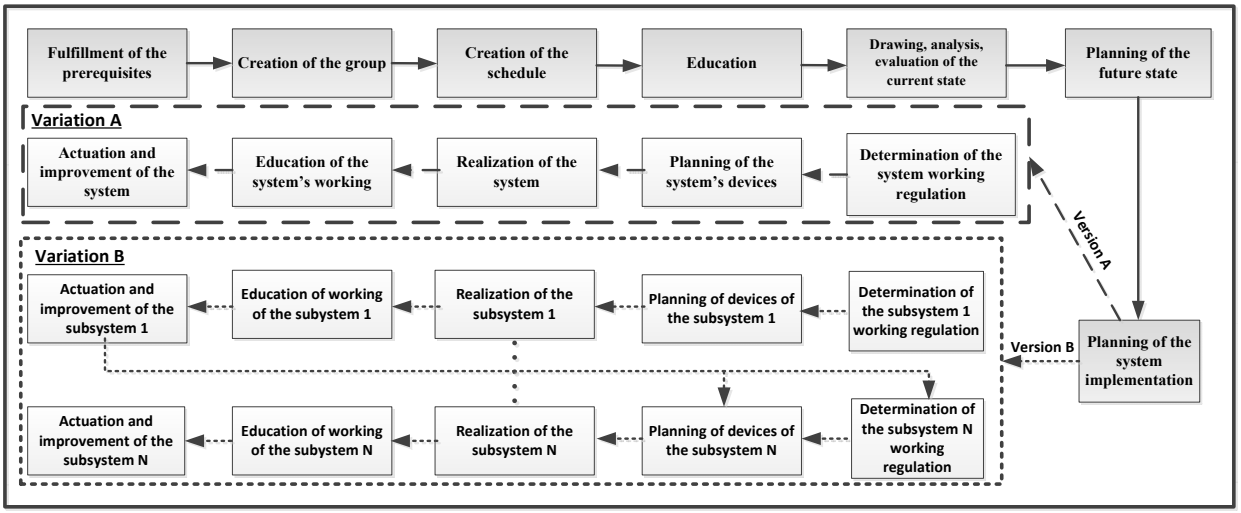

Figure 1. Transformation process from push system into pull system
[Source: Edited by me]

More important steps of the transformation process are the following [3]:

Fulfillment of the prerequisites: We have to realize the next lean devices before the pull-principled production control system's creation:

- visual management,
- proposals system,
- 5S,
- standardization,
- creation of the company culture in the interests of the more efficient process improvement,
- kaizen.

Creation of the group: We have to create a group which will plan and coordinate the pull-principled production control system's realization. We need to collect those company areas's representatives in this group who will be touched in the transformation. It is very important to be at least one person in the group who has experience in the pull system's realization.

Creation of the schedule: Determination of the implementation process' more important milestones and their deadline.

Education: In this step we have to keep some training for members of the group in connection with the creation and actuation of the push-principled production control systems.

Drawing, analysis, evaluation of the current state: We suggest the value stream mapping's method [4] for mapping of the current state of process to be transformed. This method enables the current state's understanding and objective evaluation.

Planning of the future state: Actually the planning of the future state means creation of the future state mapping [4] which is realized on the basis of more variations' evaluation and the adequate variation's selection. The map defines the principles of the working of the system, namely that where and what

kinds of device we need to locate, respectively how will the material- and information flow realize.

Planning of the system implementation*:* In this step we have to make a table with the followings data:

- tasks to be performed,
- period of the fulfillment (Gantt-diagram),
- indicators to be fulfilled,
- concerned persons (RASIC chart).

The scheduling of the implementation of the system can be realized during short lead time regarding the total examined process (variation A on the figure 1), respectively in more steps [4] (variation B on the figure 1). In the case of the variation B we can gain a lot of experience from the realized process steps which is usable at the next process step's realization.

Determination of the system working regulation: In this step we have to determine the exact work instructions of the working persons in the case of different conditions (e. g. mode of the process improvement, regulation of the stock level in the case of different customer needs, …, etc.).

Planning of the system's device: We have to determine the standard and the special kanban cards (e. g. pool kanban, express kanban, …, etc.), the heijunka boards, the supermarkets and/or FIFO lanes, the kanban storage areas, milkrun trains, …, etc.

Realization of the system: We have to realize the pull-principled production control system on the basis of the system's implementation plan.

Education of the system's working: In this step we need to keep some training for the workers in connection with the elaborated work instruction and the total system working. After these trainings we have to check the appropriate skills at the production area.

Actuation and improvement of the system: We have to actuate the system after the realization of the system and the workers' training, which may result in several failures in the beginning. We also need to realize process improvement during the actuation of the system, consequently we can use the gained experiences at the next process step's realization.

4. APPLICATION POSSIBILITIES OF THE SIMULATION MODELING FOR FORMATION OF THE PULL-PRINCIPLED PRODUCTION CONTROL SYSTEMS

If we would like to explain the simulation modeling's term, then basically this is such a method which is able to make a model for the real/planned processes/systems. Consequently we can examine the status changes of the processes/systems beside different settings [5]. We can realize the optimization of the real or planned logistics system with use of the simulation modelling's method [6]. The simulation modelling as a method is applied in a lot of cases e. g. optimization of the production scheduling [5], elimination of the planning failures [7], comparison of the different planning variation, examination of the stochastic processes, …, etc.. The transformation from push-principled production control system into pull-principled production control system is a very complex process which is realized in a lot of cases without use of the simulation modeling. This chapter presents the efficiency improvement possibilities with use of the simulation modeling's method. We highlighted those areas (thicker line) in figure 2 where the simulation investigational possibilities can result in efficiency improvement. In addition we will introduce these areas.

Drawing, analysis, evaluation of the current state: We can understand and evaluate the examined system with simulation modeling of the current state efficiently because in this case we can gain more information (we can use this information for the planning of the future state) [8].

Planning of the future state: We can create and examine more system variations rapidly with use of the simulation modeling. Thus we can make an objective decision on the basis of the assigned investigational aspects (area need, lead time, kanban cards's amount, workers' number, …, etc) [9].

Determination of the system working regulation: We can determine the action plans more efficiently with use of the simulation modeling in the case of different customer needs [10].

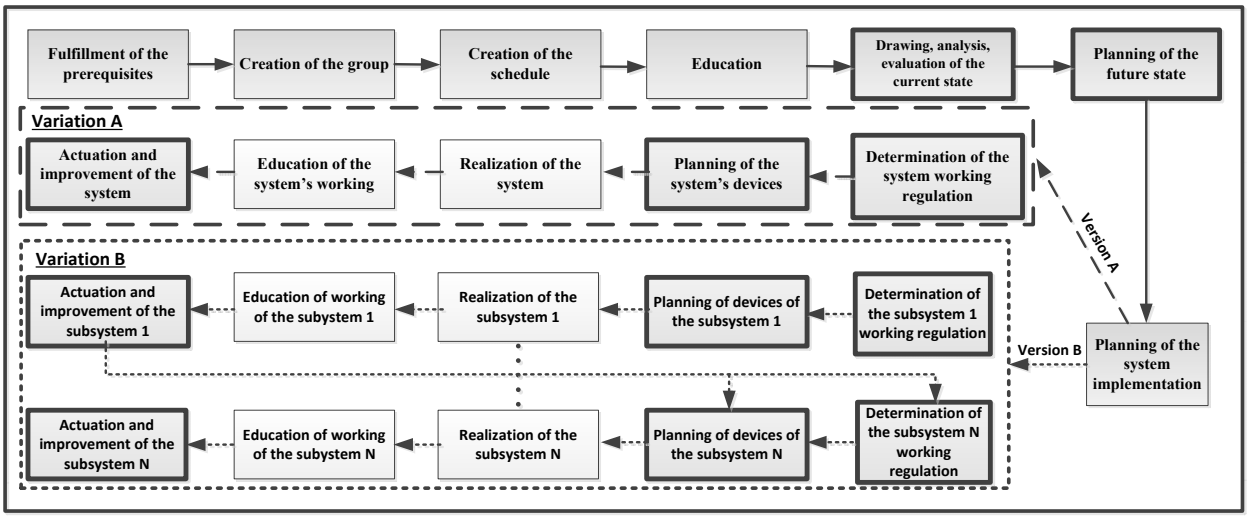

Figure 2. Simulation investigational possibilities in the process of the transformation from the push system into pull system

The kanban stock levels can also be determined more accurately, because we can take into consideration the stochastic effects with the simulation modeling. We can also define the production process's work instruction more efficiently, thus the utilization of the human- and machine resources can be increased.

Planning of the system's device: We can determine the necessary milkrun train's types and their number, kanban cards' types and their number, storage devices' types and their number with higher precision if we use the simulation modeling. This application possibility can result in significant savings for the companies.

Actuation and improvement of the system: The realized system's continuous improvement is necessary in the interest of the holding/increase of the competitiveness. We need to use simulation modeling in those cases when more value stream cross each other because in this case a failure process improvement decision can result in significant wastes (for example: purchasing of the lower performance equipment than it is necessary for the efficient production, …, etc.).

5. APPLICATION POSSIBILITIES OF THE SIMULATION MODELING FOR FORMATION OF THE PULL-PRINCIPLED PRODUCTION CONTROL SYSTEMS

One of the most important milestones of application of the lean philosophy is the formation of the pull-principled production control system. This system can increase the flexibility of satisfaction of the customer needs, respectively it enables more efficient improvement of the logistics processes as well. This system can be created with transformation of the push system into pull system at most companies. This paper presented this transformation's process, as well as its improvement possibilities with the simulation modeling. All in all, we can tell, that the simulation modeling can decrease the planning failure, as well as can increase the utilization of the human and machine resources at the formation of the pull-principled production control systems.

6. REFERENCES

[1] J. P. Womack, D. T. Jones: Lean thinking, Simon & Schuster Inc., 2008.

[2] J. Cselényi, B. Illés: Planning and controlling of material flow systems. Textbook, Miskolci Egyetemi Kiadó, 2006.

[3] Kosztolányi János, Schwahofer Gábor: Kanban, KAIZENPRO Kft., 2012.

[4] M. Rother, J. Shook: Learning to See: Value Stream Mapping to Add Value and Eliminate Muda, Lean Enterprise Institute, 2003.

[5] P. Tamás, B. Illés, S. Tollár: Simulation of a flexible manufacturing system. Advanced Logistic System Theory and practice, Volume 6. (2012), HU ISSN 1789-2198, pp. 25-33.

[6] P. Košťál, K. Velíšek: Flexible manufacturing system (Scopus) In: World Academy of Science, Engineering and Technology. - ISSN 2010-376X. - Vol. 77 (2011), pp. 825-829

[7] D. Leriche, M. Oudani, A. Cabani, G. Hoblos, J. Mouzna, J. Boukachour, A. El Hilali Alaoui: Simulating new logistics system of Le Havre Port, IFAC-PapersOnLine, Volume 48, Issue 3, 2015, pp. 418-423

[8] Dr. Tamás Péter: Application of value stream mapping at flexible manufacturing systems, KEY ENGINEERING MATERIALS 686: pp. 168-173. (2016)

[9] M.P. Fanti, G. Iacobellis, W. Ukovich, V. Boschian, G. Georgoulas, C. Stylios: A simulation based Decision Support System for logistics management, Journal of Computational Science, Volume 10, September 2015, pp. 86-96

[10] Gubán Ákos: Szervezéstechnológia, E-learning tananyag, TÁMOP 4.2.1/A (2014)

ACKNOWLEDMENTS

"This project has received funding from the European Union's Horizon 2020 research and innovation programme under grant agreement No 691942". „This research was (partially) carried out in the framework of the Center of Excellence of Mechatronics and Logistics at the University of Miskolc"

Author: **Dr. Péter Tamás (assistant professor)**, University of Miskolc, Faculty of Mechanical Engineering and Informatics, Institute of Logistics, H-3515, Miskolc-Egyetemváros

E-mail: alttpeti@gmail.com

Journal of Production Engineering
Vol.19 No.1
JPE (2016) Vol.19 (1) Preliminary Note
Pawar, P., Ballav, R., Kumar, A.

FINITE ELEMENT METHOD ANALYSIS OF STRESS INTENSITY FACTOR IN I CHANNEL SECTION

Received: 03 March 2016 / Accepted: 18 April 2016

Abstract: *In this research, a I channel section containing an semi-elliptical crack has been modeled and investigated using finite element method. The stress intensity factor of mode I and J-Integral have been calculated and analyzed.*
Key words: *Finite element method, Semi elliptical crack, stress intensity factor*

Analiza faktora intenziteta napona kod i profila metodom konačnih elemenata. *U okviru ovog istraživanja je izvršena analiza i modelovanja metodom konačnih elemenata I profila sa polu-eliptičnom pukotinom. Faktor intenziteta napona I i J integrala je izračunat i analiziran.*
Ključne reči: *Metoda konačnih elemenata, Polu eliptična pukotina, faktor intenziteta napona*

1. INTRODUCTION

Fracture mechanics are often utilized to characterize such failure. For linear elastic materials, it is satisfactory to use Stress Intensity Factor (SIF) to investigate the crack behavior [1]. The stress intensity factor accomplished a highest value near the corner point and then declined to zero at the point is approached [2]. The thickness as well as the initial surface cracks length have a major role on fatigue life up for failure in cyclic loading [3] The stress intensity factor is dependent on elastic-plastic properties of material and fracture toughness [4]. The stress intensity factors were amplified when the values of relative depth of crack ratio amplified [5]. In fracture mechanics, SIF and J-integral is essential in order to calculate the consistency of crack structures. Recently, mode I SIFs has agreed more priority since its effect is considerable compared with other types of SIFs for example mode II and III [6]. *J*-integral firstly introduced by Rice and it is defined as an arbitrary curve around the crack tip and it is estimated counter-clock wise [7]. In this research, the stress intensity factor of mode 1 and J-Intergral has been analyzed using ANSYS with 31 nodes isoparametric three-dimensional stainless steel NL solid elements.

2. METHODOLOGY

The Geometric modelling of I channel section was done using ANSYS workbench. Meshing was done by using a tetrahedron type of element in ANSYS mesh tool. Loading and boundary conditions were applied to I channel section to ascertain the critical region or crack zone of I channel section shown in fig.1. Further, crack was introduced in the critical region of I channel section. Semi-elliptical crack geometry in the crack zone for various crack lengths was initiated till stress intensity factor for mode I and J-Integral condition.

Crack shape semi elliptical with major radius of $4.e^{-0.003}$ m and minor radius of $4.e^{-0.003}$ m. Circumferential divisions are 8 and mesh contours are 5.

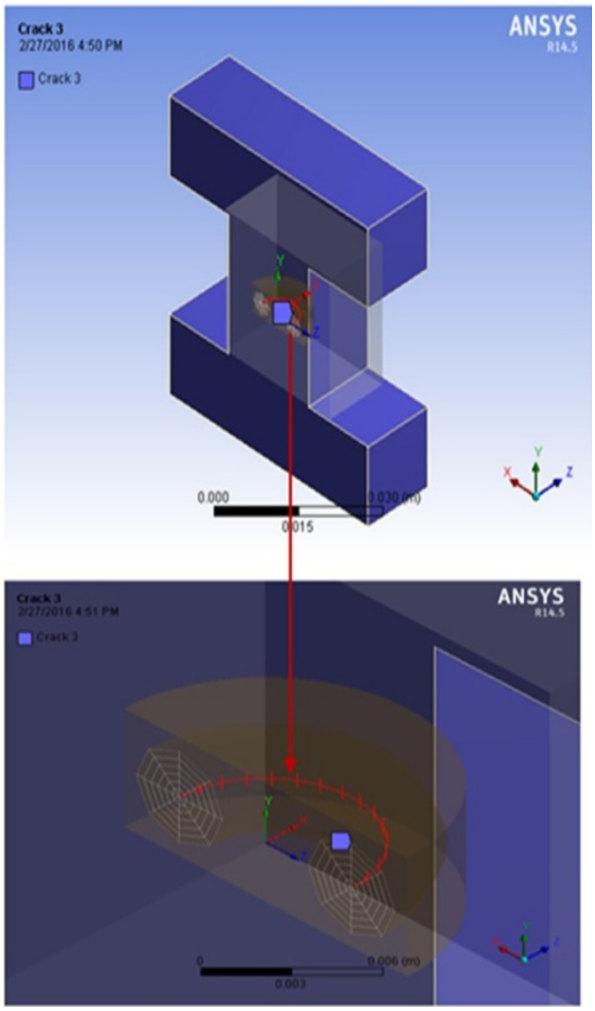

Fig. 1. FE Model with benchmarking of problem.

3. BENCHMARKING PROBLEM

The assumptions were considered to obtain stress intensity factor solution solved by using a fracture module in ANSYS. The analysis of stainless steel NL solid elements of I channel section specimen having a length of 56.08mm, width of 50mm and thickness of 30mm is conducted on ANSYS. The applied pressure magnitude of 500pa. from top side and bottom side is applied fixed support. The density of material 7750 kg. m^{-3}, Specific heat 80J. kg^{-1}. C^{-1}, Young's Modulus is 1.93E11Pa, Poisson's Ratio is 0.31, and Yield Strength is 2.1E8 Pa. The total numbers of nodes are 24406 and elements are 14780.

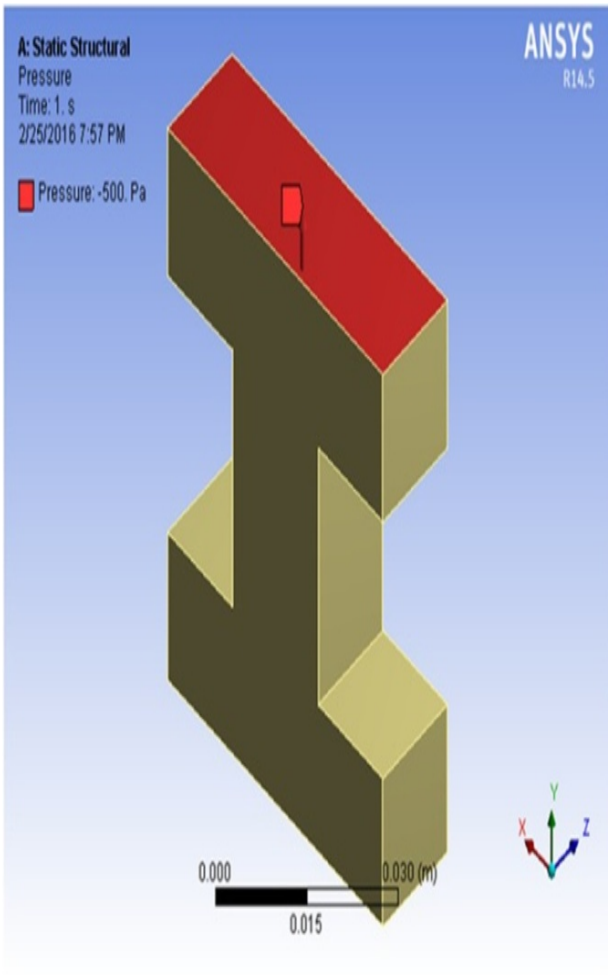

Fig. 2. Static structure of I channel section.

4. FINITE ELEMENT MODEL

Finite element modelling is identified as the analyst's choice of material models, finite elements meshes, constraint equations, pre and post processing options, governing matrix equations and their solution techniques available in a chosen commercial FEA program for the intended analysis [8]. The proposed finite element model involves a fine mesh of isoparametric tetrahedron solid elements. While introducing the crack, the most important region is the region between top and bottom portion I channel section of the crack.

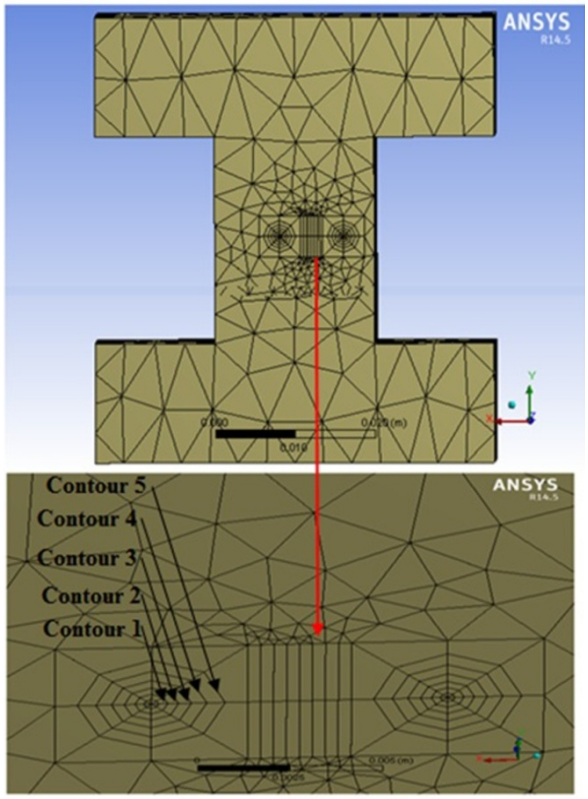

Fig. 3. Meshed model of I channel section.

5. TOTAL DEFORMATION

The fig. 4. Shows that total deformation obtained with respect to its crack lengths. The maximum total deformation obtained is 5.8614e^{-10}m.

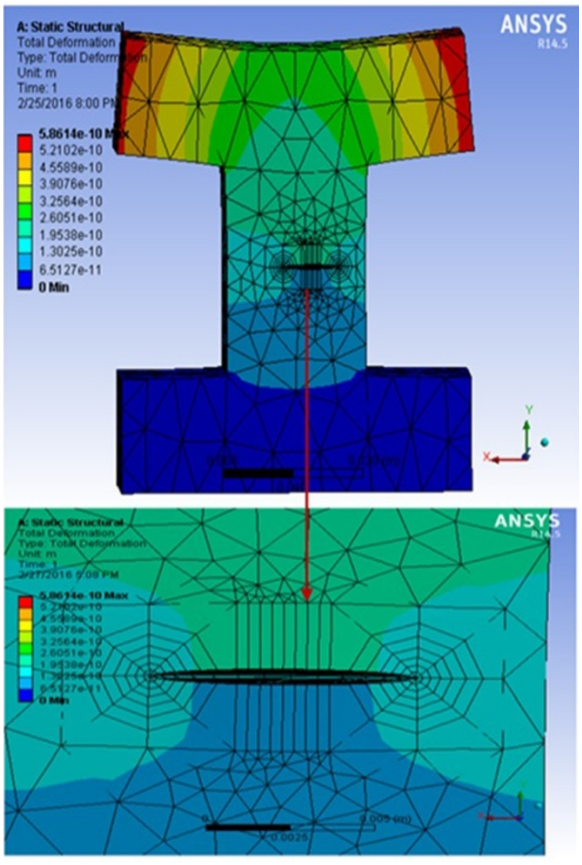

Fig. 4. Total deformation of I Channel Section.

6. STRESS INTENSITY FACTOR

The fracture tool is used to calculate the stress intensity factor mode I and J-Integral the following steps are followed

1) Define a local crack front with X-axis parallel to crack face and Y-axis perpendicular to crack face
2) Define crack front divisions and mesh contours
3) Obtain stress intensity factor of mode 1 and J-Integral

7. RESULTS OF STRESS INTENSITY FACTOR MODE 1

The The table 1 shows that values obtained by using ANSYS software. The tabulated values show that stress intensity factor for mode I with their each contour of semi elliptical crack with respect to their length of each cracks.

Sr. No	Length	Stress Intensity Factor mode I				
		Counter 1	Counter 2	Counter 3	Counter 4	Counter 5
1	0	107.3	112.6	112.3	112.0	111.8
2	4.19e-4	107.4	112.5	112.2	111.9	111.8
3	8.37e-4	104.7	110.6	110.2	109.7	109.4
4	1.26e-3	102.3	107.7	107.3	106.9	106.5
5	1.67e-3	100.4	106.4	106.2	105.9	105.5
6	2.09e-3	98.94	104.3	104.2	104.0	103.7
7	2.51e-3	97.76	103.6	103.7	103.5	103.2
8	2.93e-3	96.76	102.1	102.2	102.1	101.9
9	3.35e-3	96.02	101.9	102.0	101.9	101.8
10	3.77e-3	95.40	100.7	100.8	100.8	100.8
11	4.19e-3	94.95	100.8	100.9	101.0	100.9
12	4.61e-3	94.60	99.93	100.1	100.1	100.2
13	5.02e-3	94.40	100.2	100.4	100.5	100.8
14	5.44e-3	94.29	99.62	99.85	99.95	100.0
15	5.86e-3	94.28	100.1	100.3	100.4	100.5
16	6.28e-3	94.35	99.68	99.92	100.0	100.1
17	6.70e-3	94.5	100.3	100.5	100.6	100.7
18	7.12e-3	94.76	100.0	100.2	100.3	100.4
19	7.54e-3	95.04	100.9	101.1	101.1	101.1
20	7.96e-3	95.45	100.8	101	101.0	101.0
21	8.37e-3	96.01	101.9	102.0	102.0	101.9
22	8.79e-3	96.65	102.0	102.1	102.1	101.9
23	9.21e-3	97.42	103.3	103.4	103.3	103.1
24	9.63e-3	98.30	103.7	103.8	103.6	103.4
25	1.00e-2	99.41	105.4	105.4	105.2	104.9
26	1.05e-2	100.7	106.2	106.1	105.8	105.6
27	1.09e-2	102.4	108.5	108.3	108.0	107.6
28	1.13e-2	104.5	110.0	109.6	109.2	108.9
29	1.17e-2	107.2	113.2	112.8	112.4	112.1
30	1.21e-2	110.3	115.5	115.1	114.9	114.8
31	1.26e-2	110.3	115.7	115.4	115.1	114.8

Table 1. Stress intensity factor mode 1

Various iterations were carried out for different crack lengths and depths and it was found that stress intensity factor for mode 1 is minimum of 100.04Pa·$m^{0.5}$ and maximum at 114.87Pa·$m^{0.5}$

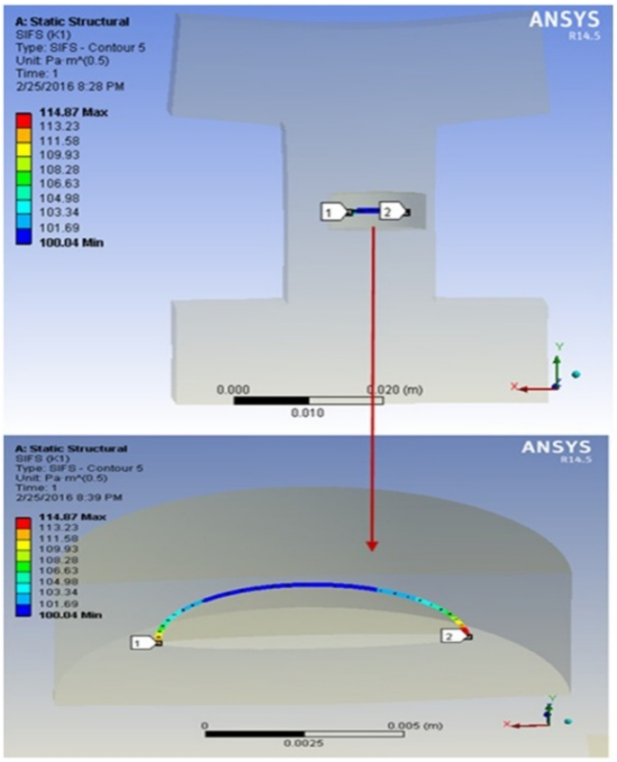

Fig. 5. Profile of the critical crack of SIF mode 1

SIF for J-Integral was evaluated for different crack lengths. The plot below shows the stress intensity factor for J-Integral with their 5 numbers of contour verses length of cracks.

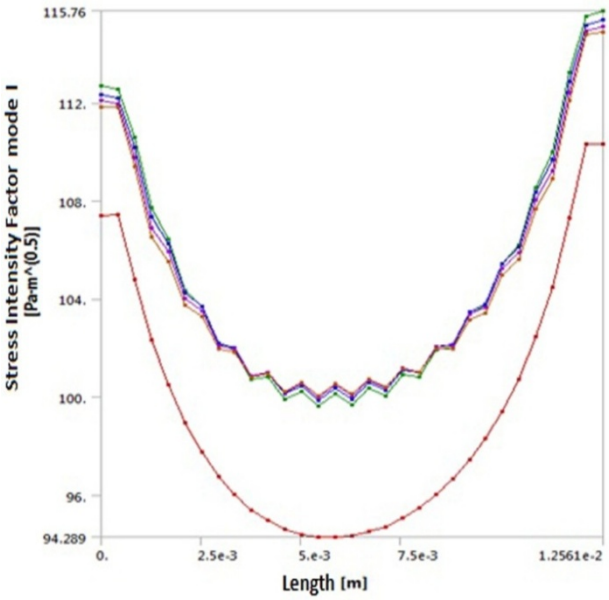

Fig.6. SIF for various contours for mode 1 verses crack length

8. RESULTS OF STRESS INTENSITY FACTOR J-INTEGRAL

The table 2 shows that values obtained by using ANSYS software. The tabulated values show that stress intensity factor for J-Integral with their each contour of semi-elliptical crack with respect to their length of each cracks.

Sr. No.	Length	Stress Intensity Factor J-Integral				
		Counter 1	Counter 2	Counter 3	Counter 4	Counter 5
1	0	5.9e-8	6.1e-8	6.1e-8	6.1e-8	6.1. e-8
2	4.1e-0	5.8e-8	6.e-8	6.3e-8	6.0e-8	6.0. e-8
3	8.3e-4	5.5e-8	5.7e-8	5.7e-8	5.7e-8	5.7. e-8
4	1.2e-3	5.2e-8	5.4e-8	5.4e-8	5.4e-8	5.4. e-8
5	1.6e-3	5.0e-8	5.2e-8	5.2e-8	5.2e-8	5.2. e-8
6	2.0e-3	4.9e-8	5.0e-8	5.0e-8	5.8e-8	5.0. e-8
7	2.5e-3	4.7e-8	4.9e-8	4.9e-8	4.9e-8	4.9. e-8
8	2.9e-3	4.7e-8	4.8e-8	4.8e-8	4.8e-8	4.8. e-8
9	3.3e-3	4.6e-8	4.7e-8	4.7e-8	4.7e-8	4.7. e-8
10	3.7e-3	4.5e-8	4.7e-8	4.7e-8	4.7e-8	4.7. e-8
11	4.1e-3	4.5e-8	4.6e-8	4.6e-8	4.6e-8	4.6. e-8
12	4.6e-3	4.4e-8	4.6e-8	4.6e-8	4.6e-8	4.6. e-8
13	5.0e-3	4.4e-8	4.6e-8	4.6e-8	4.6e-8	4.6. e-8
14	5.4e-3	4.4e-8	4.5e-8	4.6e-8	4.6e-8	4.6. e-8
15	5.8e-3	4.4e-8	4.5e-8	4.5e-8	4.6e-8	4.6. e-8
16	6.2e-3	4.4e-8	4.6e-8	4.6e-8	4.6e-8	4.6. e-8
17	6.7e-3	4.4e-8	4.6e-8	4.6e-8	4.6e-8	4.6. e-8
18	7.1e-3	4.5e-8	4.6e-8	4.6e-8	4.6e-8	4.6. e-8
19	7.5e-3	4.5e-8	4.6e-8	4.6e-8	4.6e-8	4.6. e-8
20	7.9e-3	4.5e-8	4.7e-8	4.7e-8	4.7e-8	4.7. e-8
21	8.3e-3	4.6e-8	4.7e-8	4.7e-8	4.7e-8	4.7. e-8
22	8.7e-3	4.6e-8	4.8e-8	4.8e-8	4.8e-8	4.8. e-8
23	9.2e-3	4.7e-8	4.9e-8	4.9e-8	4.9e-8	4.9. e-8
24	9.6e-3	4.8e-8	4.9e-8	5.0e-8	5.0e-8	5.1. e-8
25	1.0e-2	4.9e-8	5.1e-8	5.1e-8	5.1e-8	5.1. e-8
26	1.0e-2	5.0e-8	5.2e-8	5.2e-8	5.2e-8	5.2. e-8
27	1.0e-2	5.2e-8	5.4e-8	5.4e-8	5.4e-8	5.4. e-8
28	1.1e-2	5.5e-8	5.6e-8	5.6e-8	5.6e-8	5.6. e-8
29	1.1e-2	5.8e-8	5.9e-8	5.9e-8	6.0e-8	6.0. e-8
30	1.2e-2	6.1e-8	6.3e-8	6.3e-8	6.3e-8	6.4. e-8
31	1.2e-2	6.2e-8	6.4e-8	6.4e-8	6.4e-8	6.4. e-8

Table 2. Stress intensity factor J-Integral

Various iterations were carried out for different crack lengths and depths and it was found that stress intensity factor for J-Integral is minimum at $4.5959e^{-8}$ J/m² and maximum at $6.4487e^{-8}$ J/m². Various iterations were carried out for different crack

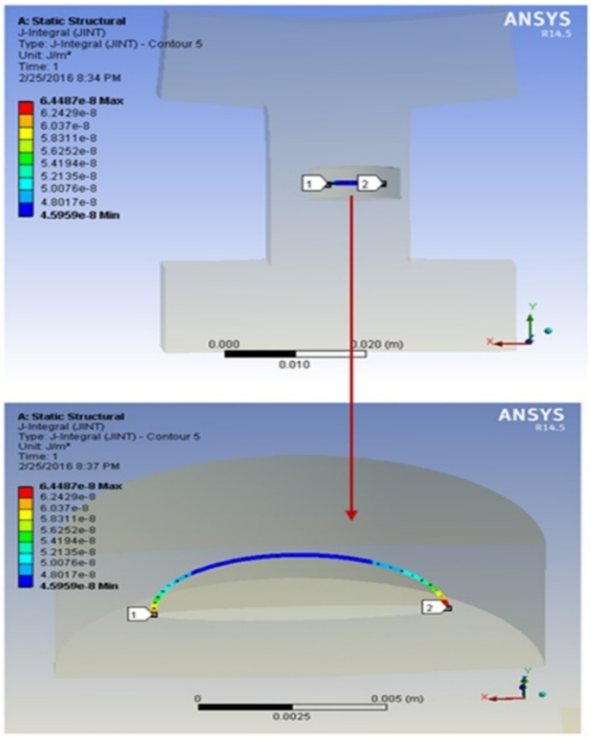

Fig. 7. Profile of the critical crack of SIF J-Integral

SIF for J-Integral was evaluated for different crack lengths. The plot below shows the stress intensity factor for J-Integral with their 5 numbers of contour verses length of cracks

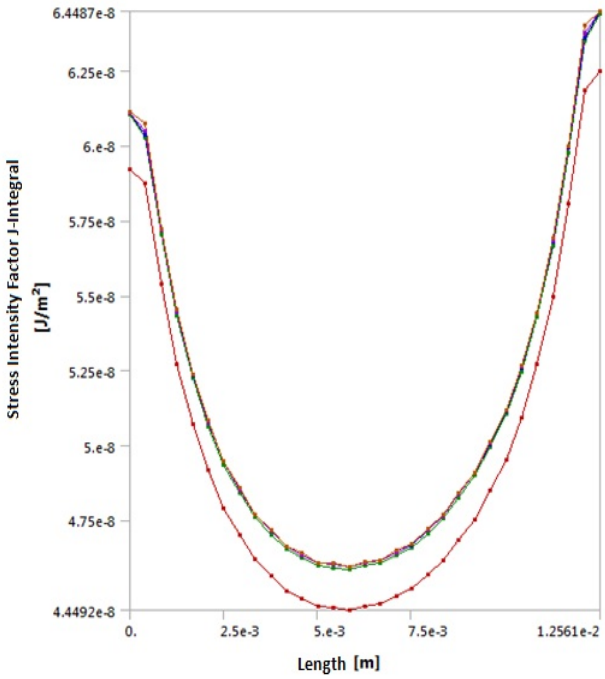

Fig. 8. SIF for various contours for J-Integrals verses crack length

9. CONCLUSION

1) Static stress analysis for the operating conditions on was performed. Crack zone in the I channel section was identified middle of section of the channel, maximum stress of 500MPa occurred in this region.
2) The stress intensity factor (SIF) is found to have the maximum value of the middle part of the channel.
3) Stress intensity factor for mode 1 is minimum of 100.04Pa·$m^{0.5}$ and maximum of 114.87Pa·$m^{0.5}$
4) It is found that the stress intensity factor for J-Integral minimum of 4.5959e^{-8} J/m² and maximum of 6.4487e^{-8} J/m².

10. REFERENCES

[1] Ismail, A.E., Ariffin, A.K., Abdullah, S. and Ghazali, M.J.: *J-Integral Evaluation of Surface Cracks in Round Bar under Mode III Loadings*, Research Journal of Applied Sciences, Engineering and Technology, 7(10), pp. 1985-1993, 2014.

[2] Hayashi, K., Abe, H.: *Stress intensity factors for a semi-ellip surface of a semi-infinite solid,* International journal of fracture. Vol.16, No.-3, 1980, pp. 275-285.

[3] Boljanovic, S.: *Fatigue Strength Analysis of a Semi-Elliptical Surface Crack*, Scientific Technical Review, Vol.62 ,No.1, pp.10-16, 2012

[4] Sharma, R.K., Shrivastava, S.K., Dixit, P.M., Basu, S.: *On the problem of an axial semi-elliptical crack in a hollow ductile cylinder,* International journal of fracture, 140, pp. 269-275, 2006.

[5] Nami, M.R., and Eskandari, H.: *Stress Intensity Factors in a Rotating Impeller Containing Semi-Elliptical Surface Crack,* Mechanics Based Design of Structures and Machines: An International Journal, 40: 1–18, 2012

[6] Raju, I.S., and Newman, J.C.: *Stress-intensity factor for internal and external surface cracks in cylindrical vessels,* Int. J. Pressure Vessels Technol., 104, pp. 293-301, 1982.

[7] Rice, J.R.: *A path independent integral and the approximate analysis of strain concentration by notches and cracks*, J. Appl. Mech., 35, pp.379-386, 1968.

[8] Sharma, R.S., Ranganath, B., Vikyath Monnappa, B.M., Vinay Sagar, N.B.: *Evaluation of Stress Intensity Factor and fatigue life for Mixed-Mode crack propagation in Drive Shaft of an All-Terrain Vehicle*, International Journal of Engineering Research & Technology, Vol. 2, Issue 11, 2013.

ACKNOWLEDGEMENT

The author would like to acknowledge the financial support from the TEQIP II and Department of Manufacturing Engineering, National Institute of Technology, Jamshedpur, India. Author would also like to acknowledge the continous motivational support from Dr. Raj Ballav and Dr. Amaresh Kumar.

Authors: **Mr. Pravin Pawar, Ph.D. Research Scholar**, Manufacturing Engineering Department, National Institute of Technology, Jamshedpur, Jharkhand, India, Phone.: +918 863 082-001

Dr. Raj Ballav, Associate Professor, Manufacturing Engineering Department, National Institute of Technology, Jamshedpur, Jharkhand, India, Phone.: +91-657-237-4133.

Dr. Amaresh Kumar, Head of Department and Associate Professor, Manufacturing Engineering Department, National Institute of Technology, Jamshedpur, Jharkhand, India, Phone.: +91-657-2374129

E-mail: 2013rsprod004@nitjsr.ac.in
rballav.prod@nitjsr.ac.in
akumar.prod@nitjsr.ac.in

INSTRUCTIONS FOR CONTRIBUTORS

No. of pages:	4 DIN A4 pages
Margins:	left: 2,5 cm
	right: 2 cm
	top: 2 cm
	bottom: 2 cm
Font:	Times New Roman
Title:	Bold 12, capitals
Abstract:	Italic 10
Headings:	Bold 10, capitals
Subheadings:	Bold 10, small letters
Text:	Regular 10
Columns:	Equal column width with 0,7 cm spacing
Spacing:	Single line spacing
Formulae:	Centered and numerated from 1 in ascending order. Equations must be typed in Equation Editor, with following settings: Style>Math – Times New Roman Size>Full 12pt, Subscript/Superscript 7pt, Symbol 18 pt
Figures:	High quality, numerated from 1 in ascending order (e.g.: Fig.1, Fig. 2 etc.); Figures and tables can spread over both two columns, please avoid photographs and color prints
Tables:	Numerated from 1 in ascending order (e.g..: Tab. 1, Tab. 2, etc.)
References:	Numerated from [1] in ascending order; cited papers should be marked by the number from the reference list (e.g. [1], [2, 3] ...)
Submission:	**Papers prepared in MS Word format should be e-mailed to: pkovac@uns.ac.rs, savkovic@uns.ac.rs**
Notice:	**Papers are to be printed in Journal of Production Engineering** Sample paper with detailed instructions can be found at: **http://www.jpe.ftn.uns.ac.rs/**

FOR MORE INFORMATION, PLEASE CONTACT:

Prof. Pavel Kovač, PhD, MEng.
Assist. Prof. Borislav Savković, PhD, MEng.
FACULTY OF TECHNICAL SCIENCES
Department for Production Engineering
Trg Dositeja Obradovica 6
21000 Novi Sad
Serbia

Tel.: (+381 21) 485 23 24; 485 23 20 ; 450 366;
Fax: (+381 21) 454 495
E-mail: pkovac@uns.ac.rs, savkovic@uns.ac.rs
http://www.jpe.ftn.uns.ac.rs/